

# Design and characterization of gold and selenium nanoparticles as potential delivery systems of levodopa and dopamine

---

Kalčec, Nikolina

Doctoral thesis / Disertacija

2023

Degree Grantor / Ustanova koja je dodijelila akademski / stručni stupanj: **University of Zagreb, Faculty of Science / Sveučilište u Zagrebu, Prirodoslovno-matematički fakultet**

Permanent link / Trajna poveznica: <https://um.nsk.hr/um:nbn:hr:217:400256>

Rights / Prava: [In copyright](#) / [Zaštićeno autorskim pravom.](#)

Download date / Datum preuzimanja: **2024-05-21**



Repository / Repozitorij:

[Repository of the Faculty of Science - University of Zagreb](#)





Sveučilište u Zagrebu  
FACULTY OF SCIENCE

Nikolina Kalčec

**DESIGN AND CHARACTERIZATION OF  
GOLD AND SELENIUM NANOPARTICLES  
AS POTENTIAL DELIVERY SYSTEMS OF  
LEVODOPA AND DOPAMINE**

DOCTORAL DISSERTATION

Zagreb, 2023



University of Zagreb  
FACULTY OF SCIENCE

Nikolina Kalčec

# **DESIGN AND CHARACTERIZATION OF GOLD AND SELENIUM NANOPARTICLES AS POTENTIAL DELIVERY SYSTEMS OF LEVODOPA AND DOPAMINE**

DOCTORAL DISSERTATION

Supervisors:

Dr. Ivana Vinković Vrček, Titular Associate Professor

Dr. Frances Separovic, Professor Emeritus

Zagreb, 2023



Sveučilište u Zagrebu  
PRIRODOSLOVNO-MATEMATIČKI FAKULTET

Nikolina Kalčec

**DIZAJN I KARAKTERIZACIJA  
NANOČESTICA ZLATA I SELENA KAO  
POTENCIJANIH SUSTAVA ZA DOSTAVU  
LEVODOPE I DOPAMINA**

DOKTORSKI RAD

Mentori:

nasl. izv. prof. dr. sc. Ivana Vinković Vrček, zn. savj.  
prof. emer. Frances Separovic

Zagreb, 2023.

This doctoral thesis was carried out at the Institute for Medical Research and Occupational Health, Zagreb, Croatia and Bio21 Institute, Melbourne, Australia, under the supervision of Dr. Ivana Vinković Vrček, Titular Associate Professor and Dr. Frances Separovic, Professor Emeritus as a part of the Doctoral Program in Chemistry at the University of Zagreb, Faculty of Science, Department of Chemistry. This doctoral thesis has been fully supported by the project “Safe-by-Design Approach for Development of Nano-Enabled-Delivery Systems to Target the Brain – SENDER” (HRZZ-PZS-2019-02-4323) financed by the “Research Cooperability” Program of the Croatian Science Foundation and funded by the European Union from the European Social Fund under the Operational Programme Efficient Human Resources 2014–2020.

## Acknowledgements

*Above all, I would like to express my sincere gratitude to my mentor Assoc. Prof. Ivana Vinković Vrček, for giving me the opportunity to join her group and to participate in her projects. I am thankful for all the help, for encouraging me to be independent from the start, for introducing me to all the great scientists with whom I have collaborated, for all the conferences, short stays abroad and for the friendly atmosphere at work. Thank you for believing in me from the start!*

*I would also like to thank my second mentor Prof. Emer. Frances Separovic for all scientific discussions and helpful advice; for the help with writing my papers and all the hospitality during my stay in Australia. Thank you for including me to the AUS-NZ Croatian Women in Leadership community and for introducing me to Nevenka, Cindy and Kate. Because of you all, I felt at home so far away from home.*

*I am also very grateful to have had a chance to work with Dr. Marc-Antoine Sani. Your expertise in solid-state NMR is extraordinary and I could not be more thankful to work with you. Thank you for being there for me during my stay in Melbourne and thank you and Prof. Nicola D'Amelio for making a great atmosphere in the lab.*

*I also thank Prof. Valerije Vrček who helped me to perform NMR measurements and all the advice he gave me resulted in publishing the paper of which I am the proudest. Thanks to Assoc. Prof. Sabrina Pricl and her team for performing MD simulations and upgraded this work to a higher level.*

*I am thankful to Dr. Ruža Frkanec who was there during the whole of my Ph.D. journey, for providing all the compounds that I needed, and for all the kind words. Thanks to Assoc. Prof. Marija Ćurlin for the help with TEM and for believing in me that I could do measurements independently.*

*Thanks to all members of the Laboratory for biocolloids and surface chemistry, RBI, for all the help with nanomaterials characterization. Thanks to Christopher R. Hall and Trevor A. Smith for performing time-resolved measurements. I am very grateful for the help.*

*I am greatly thankful to my colleagues who became friends: Bare, Em, Kruno, Lucija, Maja, Mamić, Nike, Rinea (Rinea, don't worry, this is in alphabetical order!). Thanks for all the help in the lab and for being there for me on both tough days and days full of laughter. This Ph.D. would not be the same without you!*

*Thanks to my lifelong friends (Ana, Anđela, Kika, Roso) for always being by my side. I am extremely happy to have you in my life!*

*Najveće hvala mojoj obitelji na ogromnoj podršci tijekom cijelog života, vjerovanju da ja to mogu od samog početka. Mojim roditeljima želim zahvaliti na ogromnoj ljubavi, pažnji i strpljenju. Mojim bakama na svakom ručku i što ste uvijek uz mene. Mom didi, kojem posvećujem ovaj doktorat, jer znam da bi bio najviše ponosan na mene.*

## Contents

<b>ABSTRACT .....</b>	<b>IX</b>
<b>SAŽETAK.....</b>	<b>X</b>
<b>PROŠIRENI SAŽETAK.....</b>	<b>XI</b>
<b>§ 1. INTRODUCTION .....</b>	<b>1</b>
<b>§ 2. LITERATURE OVERVIEW .....</b>	<b>3</b>
<b>2.1. Parkinson's disease .....</b>	<b>3</b>
2.1.1. <i>Obstacles in the treatment of PD .....</i>	<i>5</i>
<b>2.2. Nanotherapeutic strategies for the treatment of PD .....</b>	<b>6</b>
<b>2.3. AuNP and SeNP in the therapy and diagnosis of Parkinson's disease.....</b>	<b>8</b>
<b>2.4. Synthesis of AuNP and SeNP .....</b>	<b>10</b>
2.4.1. <i>Chemical synthesis.....</i>	<i>11</i>
2.4.2. <i>Physical synthesis .....</i>	<i>13</i>
2.4.3. <i>Biological synthesis.....</i>	<i>14</i>
<b>2.5. Stabilization and functionalization of AuNP and SeNP .....</b>	<b>15</b>
2.5.1. <i>AuNP and SeNP stabilization approaches.....</i>	<i>15</i>
2.5.2. <i>Functionalization of AuNP and SeNP with BBB targeting ability.....</i>	<i>16</i>
<b>2.6. Conjugation strategies of AuNP and SeNP with drugs .....</b>	<b>19</b>
<b>2.7. Crossing the BBB with AuNP and SeNP.....</b>	<b>20</b>
2.7.1. <i>Cellular uptake mechanism of AuNP and SeNP .....</i>	<i>20</i>
2.7.2. <i>In vitro BBB models for permeability of AuNP and SeNP.....</i>	<i>21</i>
<b>§ 3. MATERIALS AND METHODS .....</b>	<b>23</b>
<b>3.1. Materials .....</b>	<b>23</b>
3.1.1. <i>Materials used for NP synthesis.....</i>	<i>23</i>
3.1.2. <i>Materials used for examination of the interaction between NP and proteins.....</i>	<i>23</i>
3.1.3. <i>Materials used for NMR experiments .....</i>	<i>24</i>
3.1.4. <i>Other materials .....</i>	<i>24</i>
<b>3.2. Synthesis of AuNP and SeNP .....</b>	<b>24</b>
3.2.1. <i>Preparation of differently coated AuNP .....</i>	<i>24</i>
3.2.2. <i>Seed-mediated preparation of AuNP .....</i>	<i>25</i>
3.2.3. <i>Preparation of SeNP .....</i>	<i>26</i>
<b>3.3. Characterization of AuNP and SeNP .....</b>	<b>26</b>
<b>3.4. Calculation of NP concentration.....</b>	<b>29</b>



<b>3.5. Determination of the binding mechanism of levodopa and dopamine to differently coated AuNP and SeNP .....</b>	<b>30</b>
3.5.1. <i>Steady-state fluorescence measurement.....</i>	30
3.5.2. <i>Time-resolved fluorescence measurements.....</i>	33
3.5.3. <i>DLS and ELS measurements .....</i>	34
3.5.4. <i>UV-Vis measurements .....</i>	34
<b>3.6. Calculation of drug-loading efficiency of differently coated AuNP and SeNP .....</b>	<b>34</b>
<b>3.7. Investigation of levodopa and dopamine stability during AuNP formation.....</b>	<b>35</b>
3.7.1. <i>NMR experiments.....</i>	35
3.7.2. <i>Density functional theory calculations.....</i>	37
3.7.3. <i>Molecular dynamics simulations.....</i>	38
<b>3.8. Evaluation of the ability of different AuNP and SeNP to cross BBB artificial models.....</b>	<b>40</b>
3.8.1. <i>BBB specific parallel artificial membrane permeability assay (PAMPA-BBB) .....</i>	40
3.8.2. <i>In vitro BBB endothelial transwell permeability assay.....</i>	42
<b>3.9. Statistical analysis .....</b>	<b>44</b>
<b>§ 4. RESULTS AND DISCUSSION .....</b>	<b>45</b>
<b>4.1. Physicochemical characteristics of AuNP and SeNP .....</b>	<b>45</b>
<b>4.2. Interactions of levodopa and dopamine with differently coated AuNP and SeNP .....</b>	<b>50</b>
4.2.1. <i>Steady-state and time-resolved fluorescence measurements .....</i>	50
4.2.2. <i>The influence of serum proteins on AuNP and SeNP interactions with catcehol .....</i>	63
4.2.3. <i>Changes in <math>d_H</math>, <math>\zeta</math> potential and SPR peak of AuNP and SeNP after interaction with fluorophores.....</i>	65
<b>4.3. Drug-loading efficiency of differently coated AuNP and SeNP .....</b>	<b>68</b>
<b>4.4. Transformation of levodopa and dopamine on the surface of AuNP .....</b>	<b>69</b>
4.4.1. <i>NMR study.....</i>	70
4.4.2. <i>DFT calculations.....</i>	75
4.4.3. <i>MD simulations.....</i>	78
<b>4.5. Permeability of AuNP and SeNP through BBB.....</b>	<b>79</b>
4.5.1. <i>Evaluation of AuNP and SeNP permeability using BBB-PAMPA model .....</i>	79
4.5.2. <i>Evaluation of AuNP and SeNP permeability using transwell assay .....</i>	81
<b>§ 5. CONCLUSIONS .....</b>	<b>87</b>
<b>§ 6. LIST OF ABBREVIATIONS AND SYMBOLS .....</b>	<b>89</b>
<b>§ 7. REFERENCES.....</b>	<b>91</b>
<b>§ 8. APPENDICES .....</b>	<b>XXVII</b>
<b>§ 9. CURRICULUM VITAE.....</b>	<b>XL</b>



University of Zagreb

Faculty of Science

**Department of Chemistry**

Doctoral Thesis

## ABSTRACT

### DESIGN AND CHARACTERIZATION OF GOLD AND SELENIUM NANOPARTICLES AS POTENTIAL DELIVERY SYSTEMS OF LEVODOPA AND DOPAMINE

Nikolina Kalčec

Ksaverska cesta 2, 10 000 Zagreb, Croatia

The development of new approaches in the treatment of Parkinson's disease presents a challenge due to the presence of the blood-brain barrier, which hinders effective drug delivery to the brain. Due to their unique physicochemical properties, nanoparticles have the potential to improve conventional therapeutic approaches and enable targeted drug delivery across the blood-brain barrier.

The main goal of this doctoral thesis was to synthesize and characterize differently functionalized gold and selenium nanoparticles and to examine their interaction with catechols (levodopa and dopamine) in order to design more effective and safer therapeutic systems for Parkinson's disease. The process of drug binding to the nano-surface was investigated using various spectroscopic, laser and microscopic methods, while the blood-brain barrier permeability of prepared nano-systems was tested under in vitro settings.

The obtained results have provided a better understanding of the processes that occur during the binding of catechol drugs to gold and selenium nanoparticles. This will potentially enable the development of a nano-formulation with targeted drug delivery to the brain with the aim of improving the therapy of Parkinson's disease.

(141 pages, 28 figures, 14 tables, 268 references, original in English)

Thesis deposited in Central Chemical Library, Horvatovac 102A, Zagreb, Croatia and National and University Library, Hrvatske bratske zajednice 4, Zagreb, Croatia.

Keywords: binding processes/ dopamine/ drug-delivery nanosystems/ gold nanoparticles/ levodopa/ Parkinson's disease/ selenium nanoparticles

Supervisors: Dr. Ivana Vinković Vrček, Titular Associate Professor and Dr. Frances Separovic, Professor Emeritus

Thesis accepted: May 3, 2023

Reviewers:

Dr. Snežana Miljanić, Full Professor

Dr. Maja Dutour Sikirić, Titular Associate Professor

Dr. Marko Močibob, Assistant Professor



Sveučilište u Zagrebu

Prirodoslovno-matematički fakultet

**Kemijski odsjek**

Doktorska disertacija

## SAŽETAK

### DIZAJN I KARAKTERIZACIJA NANOČESTICA ZLATA I SELENA KAO POTENCIJANIH SUSTAVA ZA DOSTAVU LEVODOPE I DOPAMINA

Nikolina Kalčec

Ksaverska cesta 2, 10 000 Zagreb, Croatia

Razvoj novih pristupa u liječenju Parkinsonove bolesti predstavlja izazov zbog prisutnosti krvno-moždane barijere koja otežava učinkovitu dostavu lijekova u mozak. Zahvaljujući jedinstvenim fizikalno-kemijskim svojstvima, nanočestice imaju potencijal poboljšati konvencionalne terapijske pristupe i omogućiti ciljanu isporuku lijekova preko krvno-moždane barijere.

Glavni cilj ovog doktorskog rada bio je sintetizirati i karakterizirati različito funkcionalizirane nanočestice zlata i selen te ispitati njihovo međudjelovanje s kateholima (levodopa i dopamin) u svrhu dizajniranja učinkovitijih i sigurnijih terapijskih sustava za liječenje Parkinsonove bolesti. Proces vezanja lijekova na nano-površinu ispitivao se pomoću različitih spektroskopskih, laserskih i mikroskopskih metoda, a zatim su se provela istraživanja propusnosti krvno-moždane barijere za novopripravljene nanosustave u in vitro uvjetima.

Dobiveni rezultati omogućili su bolje razumijevanje procesa koji se događaju prilikom vezanja lijekova kateholne strukture i novih nanočestica zlata i selen. Na taj način potiče se razvoj nano-formulacija s ciljanom isporukom lijekova u mozak s ciljem poboljšanja terapije za Parkinsonovu bolest.

(141 stranica, 28 slika, 14 tablica, 268 literaturnih navoda, jezik izvornika: engleski)

Rad je pohranjen u Središnjoj kemijskoj knjižnici, Horvatovac 102a, Zagreb i Nacionalnoj i sveučilišnoj knjižnici, Hrvatske bratske zajednice 4, Zagreb.

Ključne riječi: dopamin/ levodopa/ nanočestice selen/ nanočestice zlata/ nanosustavi za dostavu lijekova / Parkinsonova bolest/ procesi vezanja

Mentori: nasl. izv. prof. dr. sc. Ivana Vinković Vrček, zn. savj. i prof. emer. Frances Separovic

Rad prihvaćen: 3. svibnja 2023.

Ocjenitelji:

prof. dr. sc. Snežana Miljnić

nasl. izv. prof. dr. sc. Maja Dutour Sikirić, v. zn. sur.

doc. dr. sc. Marko Močibob



Sveučilište u Zagrebu  
Prirodoslovno-matematički fakultet  
**Kemijski odsjek**

Doktorska disertacija

## PROŠIRENI SAŽETAK

### Uvod

Parkinsonova bolest (eng. *Parkinson's disease*, PD) druga je najčešća neurodegenerativna bolest nakon Alzheimerove bolesti koja pogađa više od 8,5 milijuna ljudi s prevalencijom u starijoj populaciji.<sup>I-III</sup> Patološki, PD je karakterizirana degeneracijom ili gubitkom dopaminergičkih neurona te prisutnošću agregata  $\alpha$ -sinukleina, što dovodi do smanjene koncentracije dopamina u dijelu mozga koji se naziva *substantia nigra pars compacta*. PD se prvenstveno očituje u poremećajima kretanja kao što su bradikinezija, rigidnost i tremor, te nemotoričkim komplikacijama koje uključuju stanja poput depresije i demencije.<sup>II,IV</sup> PD terapija uglavnom se temelji na povećanju koncentracije dopamina u mozgu. S obzirom da dopamin ne može proći krvno-moždanu barijeru, u terapiji se koristi prekursor dopamina, levodopa, koja prolazi krvno-moždanu barijeru pomoću prijenosnika L-aminokiselina 1 (engl. *L-type amino acid transporter*, LAT1). Jednom kad se levodopa nađe u mozgu, dekarboksilacijom prelazi u dopamin pomoću dekarboksilaze aromatskih L-aminokiselina, čime se obnavljaju razine dopamina u preživjelim neuronima.<sup>II,IV-VI</sup> Međutim, dugoročna terapijska primjena levodope može uzrokovati oksidativno oštećenje na mjestu djelovanja i nastanak ozbiljnih nuspojava.<sup>II,VII</sup>

- 
- I. <https://www.who.int/news-room/fact-sheets/detail/parkinson-disease/> (pristupano 2. prosinca 2022.).
  - II. C.A. Davie, *Br. Med. Bull.* **86** (2008) 109–127.
  - III. A.C. Kaushik, S. Bharadwaj, S. Kumar, and D.Q. Wei, *Sci. Rep.* **8** (2018) 1–8.
  - IV. P.A. Serra, G. Esposito, P. Enrico, M.A. Mura, R. Migheli, M.R. Delogu, M. Miele, M.S. Desole, G. Grella, and E. Miele, *Br. J. Pharmacol.* **130** (2000) 937–945.
  - V. F. Haddad, M. Sawalha, Y. Khawaja, A. Najjar, and R. Karaman, *Molecules* **23** (2017) 40.
  - VI. T. Müller, *Expert Opin. Drug Metab. Toxicol.* **16** (2020) 403–414.
  - VII. J. Dorszewska, M. Kowalska, M. Prendecki, T. Piekut, J. Kozłowska, and W. Kozubski, *Neural Regen. Res.* **16** (2021) 1383.

Osim toga, prisutnost krvno-moždane barijere (eng. *blood-brain barrier*, BBB) predstavlja veliki izazov prilikom dostave lijekova u mozak zbog svoje zaštitne uloge koja omogućuje prolazak samo određenim tvarima kao što su hranjive tvari i voda te sprječava ulazak štetnih tvari i mikroorganizama u mozak.<sup>VIII</sup> Ta uloga ograničava i transport terapeutika u mozak. Zbog svih navedenih prepreka dizajn učinkovitog i sigurnog sustava za ciljanu isporuku lijekova i dalje predstavlja izazov u liječenju PD.

Glavni cilj ove doktorske disertacije je razvoj novih formulacija lijekova s većom sposobnošću prolaska kroz BBB pomoću nanotehnoloških metoda.

Primjena nanotehnologije posljednjih je godina doživjela ogroman interes te ponudila nova rješenja u liječenju neurodegenerativnih bolesti. Nanomaterijali zbog svoje male veličine na nanoskali pokazuju značajno poboljšanje u usporedbi s odgovarajućim materijalima na makroskali zbog povećanja omjera površine i volumena. Velika površina daje im mogućnost adsorpcije, nošenja i isporuke mnogobrojnih molekula kao što su lijekovi, proteini i dr. Nanomaterijali se također mogu koristiti u terapiji neurodegenerativnih bolesti zbog svoje sposobnosti prolaska kroz BBB i dostave lijekova specifično na ciljano mjesto. Ta svojstva nanomaterijala posebno su važna za rano dijagnosticiranje te dostavu lijekova kod bolesti središnjeg živčanog sustava. Nanomaterijali korišteni za dostavu lijekova obično sadrže dvije komponente, nanonosac koji služi kao dostavljač te aktivnu terapijsku komponentu. Nanomaterijali mogu prodrijeti kroz BBB pasivno i aktivno ovisno o veličini čestica i modifikaciji svojstava površine. Nadalje, isporuka specifična za ciljano mjesto može se postići modulacijom nanopovršine. Lijekovi se mogu lako vezati za nanopovršinu ili ugraditi u nanosustave bez ikakvih kemijskih reakcija, čime je očuvana aktivnost lijeka. Štoviše, kontrolirano i kontinuirano otpuštanje lijeka na određenom mjestu može povećati unos slabo topivih lijekova povećavajući njihovu bioraspoloživost. Na taj način poboljšava se terapijska učinkovitost pojedinog lijeka uz smanjenje njegovih nuspojava.<sup>IX</sup>

---

VIII. N. Poovaiah, Z. Davoudi, H. Peng, B. Schlichtmann, S. Mallapragada, B. Narasimhan, and Q. Wang, *Nanoscale* **10** (2018) 16962–16983.

IX. C. Spuch, O. Saida, and C. Navarro, *Recent Pat. Drug Deliv. Formul.* **6** (2012) 2–18.

Među različitim vrstama nanomaterijala, nanočestice zlata (AuNP) i selen (SeNP) pokazale su veliki potencijal za primjenu u području neurodegenerativnih bolesti zbog svojih antioksidativnih i neuroprotektivnih učinaka.<sup>X,XI</sup> Trenutno se koriste u razvoju sustava za isporuku gena ili lijekova, biosenzorima, biooslikavanju i dijagnostici zbog svojih izvanrednih svojstva kao što su stabilnost, netoksičnost, visoka biokompatibilnost i visok afinitet za različite molekule.<sup>X,XII,XIII</sup> Mogućnost funkcionaliziranja i stabiliziranja njihove površine omogućuje vezanje malih molekula lijekova kao i velikih biomolekula poput DNA, RNA i proteina te njihovu isporuku do ciljanog mjesta.<sup>XIV,XV</sup> Sva ta svojstva čine ih idealnim kandidatima za prolazak kroz BBB te u usporedbi s drugim nanomaterijalima imaju potencijalne prednosti u pripravi sustava za isporuku terapeutika u mozak.

U ovom doktorskom radu AuNP i SeNP korišteni su kao potencijalni nanonosaci za poboljšanu dopremu levodope odnosno dopamina na ciljano mjesto u mozgu te su istraženi procesi koji se odvijaju na sučelju lijek-nanočestica kako bi se potaknuo dizajn i razvoj novih terapijskih sustava za liječenje PD.

- 
- X. P.C.L. Silveira, M. Venâncio, P.S. Souza, E.G. Victor, F. De Souza Notoya, C.S. Paganini, E.L. Streck, L. Da Silva, R.A. Pinho, and M.M.S. Paula, *Mater. Sci. Eng. C* **44** (2014) 380–385.
- XI. M. Nazıroğlu, S. Muhamad, and L. Pecze, *Expert Rev. Clin. Pharmacol.* **10** (2017) 773–782.
- XII. A. Chowdhury, S. Kunjiappan, T. Panneerselvam, B. Somasundaram, and C. Bhattacharjee, *Int. Nano Lett.* **7** (2017) 91–122.
- XIII. I. Vinković Vrček, in: B. Michalke (Ed.), *Selenium*, Springer International Publishing, Cham, 2018, pp. 393–413.
- XIV. K. Hu, X. Chen, W. Chen, L. Zhang, J. Li, J. Ye, Y. Zhang, L. Zhang, C.H. Li, L. Yin, and Y.Q. Guan, *Nanomedicine Nanotechnology, Biol. Med.* **14** (2018) 1123–1136.
- XV. Y. Xia, Y. Chen, L. Hua, M. Zhao, T. Xu, C. Wang, Y. Li, and B. Zhu, *Int. J. Nanomedicine* **13** (2018) 6929–6939.

## Hipoteze i ciljevi

Postavljena hipoteza glasi: sposobnost vezanja levodope i dopamina na površinu AuNP i SeNP ovisi o površinskoj funkcionalizaciji nanočestica te o procesima koji se odvijaju na sučelju lijek-nanočestica.

Kako bi se postavljena hipoteza ispitala, postavljena su 4 glavna cilja:

1. Dizajnirati, pripremiti i karakterizirati različito funkcionalizirane AuNP i SeNP.
2. Odrediti jakost vezanja levodope i dopamina za različite AuNP i SeNP u ili bez prisutnosti proteina iz seruma.
3. Odrediti prirodu vezanja levodope odnosno dopamina za različite AuNP i SeNP.
4. Odrediti stabilnost levodope i dopamina s obzirom na njihovu potencijalnu oksidaciju tijekom međudjelovanja s nano-površinom.
5. Procijeniti mogućnost prolaska različitih AuNP i SeNP kroz krvno-moždanu barijeru primjenom umjetnih acelularnih i celularnih modela.

## Materijali i metode

Jedan od glavnih ciljeva ove doktorske disertacije bio je dizajnirati nove i učinkovite AuNP i SeNP kao sustave za isporuku levodope i dopamina. Za pripravu takvih sustava koristio se pristup pripreme nanočestica "od dolje prema gore" (engl. *bottom-up approach*) uz primjenu askorbinske kiseline, natrijevog borhidrida i natrijevog citrata kao reducirajućih sredstava, te soli zlata i selena (tetrakloroaurična kiselina,  $\text{HAuCl}_4$  i natrijev selenit,  $\text{Na}_2\text{SeO}_3$ ) kao prekursora.<sup>XVI,XVII</sup> Površina nanočestica funkcionalizirana je različitim ligandima u svrhu postizanja dugotrajne koloidne stabilnosti takvih sustava, te veće propusnosti nanoformulacija kroz BBB. Sintetski uvjeti optimizirali su se ispitivanjem različitih molarnih omjera reaktanata te mijenjanjem reakcijskih uvjeta (npr. temperatura, brzina i vrijeme miješanja, koncentracija reaktanata) s ciljem pripreme sferičnih i stabilnih nanočestica promjera manjeg od 100 nm.

---

XVI. J. Turkevich, P.C. Stevenson, and J. Hillier, *Discuss. Faraday Soc.* **11** (1951) 55–75.

XVII. M. Vahdati, and T. Tohidi Moghadam, *Sci. Rep.* **10** (2020) 1–10.

Kao površinski omotači korišteni su polietilen glikol (PEG) i polivinilpirolidon (PVP) te površinski-aktivna tvar polisorbat 20 (Tween 20), koji su odobreni od Američke agencije za hranu i lijekove (engl. *U.S. Food & Drug Administration*) za korištenje prilikom pripreme lijekova.<sup>XVIII</sup> Nadalje, za površinsku funkcionalizaciju nanočestica koristio se 1-adamantilamin (amantadin, Ad), 1-adamantilglicin (AdGly) i peptidoglikanski monomer GlcNAc-MurNAc-L-Ala-D-isoGln-mesoDAP( $\epsilon$ NH<sub>2</sub>)-D-Ala-D-Ala (PGM) zbog lipofilnosti, mogućnosti prolaska kroz BBB te boljeg vezanja lijekova.<sup>XIX,XX</sup> Ispitana je i primjena levodope i dopamina kao reducirajućih odnosno funkcionalizirajućih sredstava prilikom pripreme nanočestica.<sup>XXI,XXII</sup>

Sve pripravljene nanoformulacije karakterizirane su s obzirom na oblik, raspodjelu veličine čestica, zeta ( $\zeta$ ) potencijal, kemijski sastav, te površinska i optička svojstva.

Hidrodinamički promjer ( $d_H$ ) i  $\zeta$  potencijal određeni su metodama dinamičkog raspršenja svjetlosti (engl. *Dynamic Light Scattering*, DLS) odnosno elektroforetskog raspršenja svjetlosti (engl. *Electrophoretic Light Scattering*, ELS) dok su podatci o primarnoj veličini i obliku dobiveni pomoću transmisijske elektronske mikroskopije (TEM). Spektroskopija u vidljivom i ultraljubičastom području (UV/Vis spektroskopija) korištena je za određivanje signala površinske plazmonske rezonancije (engl. *surface plasmon resonance*, SPR) kod AuNP, jer je poznato da SPR signal ovisi o obliku i veličini nanočestica.<sup>XXIII</sup> Kemijski sastav i ukupna količina Au i Se u suspenzijama AuNP i SeNP određena je pomoću atomske apsorpcijske spektroskopije (engl. *atomic absorption spectroscopy*, AAS).

- 
- XVIII. Q. Yan, X. Chen, H. Gong, P. Qiu, X. Xiao, S. Dang, A. Hong, and Y. Ma, *FASEB J.* **32** (2018) 6948–6964.
- XIX. A. Štimac, M. Šekutor, K. Mlinarić-Majerski, L. Frkanec, and R. Frkanec, *Molecules* **22** (2017) 297.
- XX. M. McCully, M. Sanchez-Navarro, M. Teixido, and E. Giralt, *Curr. Pharm. Des.* **24** (2018) 1366–1376.
- XXI. Z.Y. Ong, S. Chen, E. Nabavi, A. Regoutz, D.J. Payne, D.S. Elson, D.T. Dexter, I.E. Dunlop, and A.E. Porter, *ACS Appl. Mater. Interfaces* **9** (2017) 39259–39270.
- XXII. M. Sajitha, A. Vindhyasarumi, A. Gopi, and K. Yoosaf, *RSC Adv.* **5** (2015) 98318–98324.
- XXIII. W. Haiss, N.T.K. Thanh, J. Aveyard, and D.G. Fernig, *Anal. Chem.* **79** (2007) 4215–4221.



Jakost i priroda vezanja levodope odnosno dopamina za novosintetizirane AuNP i SeNP ispitana je spektroskopskim (fluorescencijska i UV/Vis spektroskopija), te DLS i ELS metodama. Provedena su i mjerenja primjenom metoda vremenski razlučene fluorescencijske spektroskopije te fluorescencije u ustaljenom stanju kako bi se utvrdio mehanizam prigušivanja fluorofora (levodopa i dopamin) uslijed međudjelovanja s različito funkcionaliziranim nanočesticama. Dobiveni rezultati omogućili su određivanje Stern-Volmer konstante prigušivanja, koja se koristila za računanje konstante jakosti vezanja. Priroda istraživanih međudjelovanja definirana je nakon termodinamičke analize, dok je DLS i ELS mjerenjima procijenjena stabilnost nanočestica nakon međudjelovanja s levodopom odnosno dopaminom. S obzirom da svako međudjelovanje nanočestica s biološkim sustavom dovodi do stvaranja proteinskog omotača na nano-površini, tzv. biomolekulske korone (engl. *corona*), ispitan je i utjecaj proteina iz seruma. U tu svrhu ispitano je djelovanje proteina ljudskog transferina (engl. *human transferrin*, hTF) i albumina iz seruma goveda (engl. *bovine serum albumin*, BSA) na vezanje lijekova za različito funkcionalizirane AuNP i SeNP.<sup>XXIV,XXV</sup>

Stabilnost i potencijalne promjene levodope i dopamina tijekom međudjelovanja i vezanja za nano-površinu ispitane su zbog njihove sklonosti oksidacijskim procesima.<sup>XXII</sup> Derivati nastali oksidacijom nemaju poznato farmaceutsko značenje, a mogu negativno utjecati na stabilnost, ponašanje i sigurnost nanočestica. Stoga je bilo važno razumjeti mehanizam međudjelovanja levodope i dopamina s nanočesticama uslijed mogućeg nastajanja različitih oksidacijskih produkata, poput kinona, čime se posljedično mijenjaju i farmakološka svojstva takvih sustava.<sup>XXVI</sup> Takva međudjelovanja istražena su nuklearnom magnetskom rezonancijom (NMR) i računalnim tehnikama. Zbog potencijalne nestabilnosti i moguće oksidacije levodope i dopamina, <sup>1</sup>H i <sup>13</sup>C NMR spektri snimani su u različitim vremenskim intervalima tijekom nastajanja AuNP kako bi se identificirali potencijalni oksidacijski produkti (npr. dopakinon, dopakrom, leukodopakrom, dopaminkinon, leukoaminokrom) na nano-površini.

---

XXIV. A.O. Luby, E.K. Breitner, and K.K. Comfort, *Appl. Nanosci.* **6** (2016) 827–836.

XXV. K. Phopin, W. Ruankham, S. Prachayasittikul, V. Prachayasittikul, and T. Tantimongcolwat, *Int. J. Mol. Sci.* **21** (2019) 249.

XXVI. Y.Z. Zhou, R.G. Alany, V. Chuang, and J. Wen, *Chromatographia* **75** (2012) 597–606.

Dodatno je metodama računalne kemije provedena potpuna konformacijska analiza levodope i dopamina te njihovih potencijalnih oksidacijskih produkata, te analiza njihovog vezanja na Au<sub>n</sub> ( $n = 2, 4, 6$ ) klastere. Također je ispitan i utjecaj Au<sub>n</sub> klastera na kinetiku i termodinamiku ciklizacijskog koraka kinona. Koristeći teoriju funkcionala gustoće (engl. *density functional theory*, DFT), sve strukture su optimizirane te su provedeni frekvencijski računi na teorijskoj razini LANL2DZ/6-31+G(d,p). Nadalje, procijenjene su energetske barijere za reakciju ciklizacije kinona iz razlike energija između reaktanta najniže konformacijske energije i odgovarajuće strukture prijelaznog stanja. Računalna analiza provedena je u programskom paketu Gaussian uz korištenje vizualizacijskog programa GaussView. Dodatno su napravljeni i proračuni simulacije molekularne dinamike (MD) u programskom paketu Amber. Pri tome je ligand (leukodopakrom, dopakrom i tautomer dopakroma) postavljen u kutiju za MD simulaciju s Au nanopovršinama (111 kristalna struktura, 4 sloja, 748 atoma) i 2000 molekula vode. Ligand je bio smješten na udaljenosti 15 Å od površine, a simulacija je trajala 70 ns. Dobiveni rezultati korišteni su za izračunavanje slobodnih energija vezanja korištenjem MM-GBSA pristupa.

Za predviđanje pasivnog transporta AuNP i SeNP kroz BBB korišten je acelularni test propusnosti usporednih umjetnih membrana (engl. *Parallel Artificial Membrane Permeability Assay*, PAMPA) u kojem je polarni lipidni ekstrakt iz mozga svinje (eng. *Porcine Polar Brain Lipid Extract*, PBLE) dodan kako bi oponašao svojstva BBB. Dodatno je korišten i celularni model tzv. transwell assay za predviđanje propusnosti AuNP i SeNP kroz BBB uključujući pasivni i aktivni transport. U tom testu, korištena je cerebralna endotelijalna stanična linija hBEC-5i, kao reprezentativan uzorak moždanog tkiva. Propusnost nanočestica kroz primjenjene modele BBB određena je mjerenjem koncentracije Au ili Se u suspenziji nanočestica u donorskom i akceptorskom odjeljku pomoću AAS-a.

## Rezultati i rasprava

Različito funkcionalizirane AuNP i SeNP sintetizirane su metodom „odozdo prema gore“ te su dobivene stabilne i monodisperzne sferične nanočestice primarne veličine oko  $25,0 \pm 10,0$  nm u slučaju AuNP, dok je za PVP-SeNP i Tween-SeNP primarna veličina bila  $79,4 \pm 6,9$  odnosno  $52,4 \pm 6,7$  nm. Utvrđeno je da je hidrodinamička veličina svih AuNP-ova i SeNP-ova veća od njihove primarne veličine dobivene TEM-om zbog prisutnosti hidratacijske

ovojnice na površini, u rasponu od  $50,3 \pm 1,1$  do  $111,3 \pm 11,9$  nm za AuNP i od  $71,5 \pm 0,4$  do  $82,9 \pm 0,5$  nm za SeNP. Koloidna stabilnost svih testiranih NP-ova posljedica je elektrostatskog odbijanja što je potvrđeno negativnim vrijednostima  $\zeta$  potencijala, koje su za AuNP iznosile između  $-31,5 \pm 0,4$  i  $-18,8 \pm 0,2$  mV te  $-28,0 \pm 1,9$  za obje vrste SeNP.<sup>XXVII</sup> Koloidna stabilnost AuNP funkcionaliziranih kateholima (levodopom i dopaminom) ispitana je pri različitim molarnim omjerima reaktanata. TEM-vizualizacijom otkriveno je formiranje katehol-funkcionaliziranih AuNP-ova sferičnog oblika te oblika nalik na cvijet koji su imali primarnu veličinu u rasponu od  $81,8 \pm 3,9$  do  $94,0 \pm 5,1$  nm. Sferične AuNP nastale su samo kada je Au bio u molarnom suvišku u odnosu na dopamin. DLS mjerenjima učena je monomodalna distribucija veličine, s  $d_H$  vrijednostima u rasponu od  $97,4 \pm 0,6$  do  $139,1 \pm 0,9$  nm. Vrijednosti  $\zeta$  potencijala dobivene su u rasponu od  $-41,1 \pm 1,3$  do  $-29,6 \pm 0,6$  mV za [Au]:[levodopa], odnosno od  $-31,8 \pm 1,0$  do  $-21,5 \pm 0,4$  mV za [Au]:[dopamin], s negativnijim vrijednostima uočenim kod molarnog suviška Au u odnosu na katehole. Utvrđeno je da su molarni omjer [Au]:[katehol] = 1:6 i [Au]:[katehol] = 2:1 najstabilniji te su oni odabrani za NMR eksperimente.

Korištenjem fluorescencijske spektroskopije u ustaljnom stanju određene su konstante vezanja levodope i dopamina na različito funkcionalizirane AuNP i SeNP. Dodatkom različitih koncentracija AuNP i SeNP mjerena je intrinzična fluorescencija fluorofora (levodopa, dopamin, BSA/hTF) koja se gasila povećanje koncentracije NP-a za sve NP vrste. Primjer gašenja fluorescencije levodope prilikom dodavanja različitih koncentracija PGM-AuNP prikazan je na Slici Ia. Takav mehanizam gašenja fluorescencije bio je dokaz procesa vezanja fluorofora na nanopovršinu.

Pomoću Stern-Volmerovog modela (Slika Ib) određen je mehanizam prigušivanja fluorescencije. Iz Stern-Volmerovih konstanti ( $K_{sv}$ ) vidljivo je da njihove vrijednosti opadaju s porastom temperature za većinu ispitanih smjesa što ukazuje na primarnu ulogu statičkog mehanizma prigušivanja fluorescencije, budući da više temperature narušavaju formiranje kompleksa u osnovnom stanju.<sup>XXVIII,XXIX,XXX</sup>

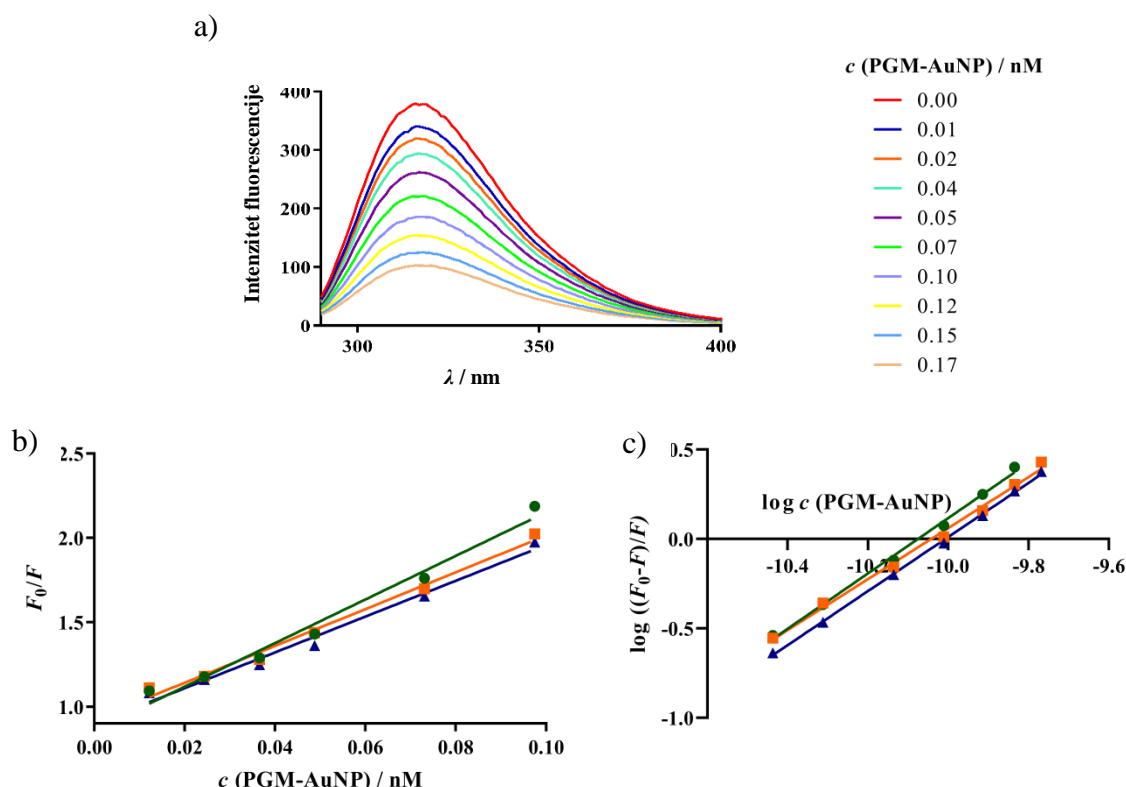
---

XXVII. E. Joseph, and G. Singhvi, in: A.M. Grumezescu (Ed.), *Nanomaterials for Drug Delivery and Therapy*, Elsevier, 2019, pp. 91–116.

XXVIII. A.T. Buddanavar, and S.T. Nandibewoor, *J. Pharm. Anal.* **7** (2017) 148–155.

XXIX. J.R. Lakowicz, *Princ. Fluoresc. Spectrosc.*, Springer US, Boston, MA, 2006, pp. 954.

XXX. G. Klebe, in: A.E. Scapin G., Patel D. (Ed.), *Multifaceted Roles of Crystallography in Modern Drug Discovery. NATO Science for Peace and Security Series A: Chemistry and Biology.*, Springer, Dordrecht, 2015, pp. 83–92.



**Slika I.** a) Fluorescencijski spektar emisije levodope u odsutnosti i prisutnosti različitih koncentracija PGM-AuNP u rasponu od 0,01 do 0,17 nM, b) Stern-Volmerov dijagram gašenja fluorescencije levodope i c) Hillov dijagram gašenja fluorescencije za levodopu nakon interakcije s PGM-AuNP na 288 K (zelena linija), 298 K (narančasta linija) i 308 K (plava linija).

Također, izračunate vrijednosti biomolekularnih konstanti gašenja ( $k_q$ ) bile su više od očekivane maksimalne vrijednosti za dinamički proces kontroliran difuzijom čime je potvrđena dominantna uloga statičkog procesa. Međutim, u slučaju PEG-AuNP,  $K_{sv}$  vrijednosti rastle su s temperaturom, sugerirajući da se gašenje fluorescencija odvija dinamički, no taj mehanizam bio je isključen nakon provedbe vremenski razlučenih fluorescencijskih mjerenja.

Iz konstanti vezanja ( $K$ ) dobivenih iz Hillovih grafova (Slika Ic) vidljivo je da AuNP pokazuju najveći afinitet za fluorofore kad im je površina funkcionalizirana s PGM-om. Također za tu vrstu nanočestica određena je najveća količina vezanih katehola (više od 80%), što je u skladu s određenim afinitetima vezanja. Prisutnost PGM-a na nanopovršini može

doprinijeti stvaranju vodikovih veza i elektrostatskim interakcijama s biomolekulama kao što su aminokiseline i proteini.<sup>xxxix</sup> Osim toga, ta vrsta AuNP-ova odlikuje se pozitivnijom vrijednošću  $\zeta$  potencijala u usporedbi s ostalim AuNP-ovima što može dodatno olakšati međudjelovanja s negativno nabijenim molekulama kao što su BSA i levodopa. Međutim, u usporedbi s levodopom i BSA, dopamin je pokazao najveći afinitet vezanja za PGM-AuNP, potencijalno zbog dodatne elektrostatske interakcije između negativno nabijene nanopovršine i pozitivno nabijene amino skupine dopamina. Ispitivanjem vezanja levodope, dopamina i hTF-a za SeNP, vidljivo je da levodopa ima najveći afinitet vezanja, dok je dopamin pokazao najslabiji afinitet. Uzimajući u obzir utjecaj površinskih omotača na konstante vezanja, utvrđeno je da se levodopa i dopamin jače vežu za PVP-SeNP u odnosu na Tween-SeNP.

Značajno smanjenje  $K$  vrijednosti s porastom temperature ukazuje na to da su primarne veze između fluorofora i AuNP/SeNP bile nekovalentne interakcije. Termodinamički parametri, uključujući promjenu entalpije ( $\Delta H^0$ ), promjenu entropije ( $\Delta S^0$ ) i Gibbsovu slobodnu energiju ( $\Delta G^0$ ), dali su uvid u primarne veze koje nastaju tijekom međudjelovanja između AuNP/SeNP i fluorofora.  $\Delta G^0$  imale su negativne vrijednosti za sve ispitivane sustave ukazujući da su međudjelovanja spontana.

Nadalje, uočeno je da su vodikove veze imale značajnu ulogu u interakcijama levodope i dopamina s PEG-, Ad- i AdGly-AuNP, jer su vrijednosti  $\Delta S^0$  i  $\Delta H^0$  bile negativne. Takovo ponašanje utvrđeno je i za vezanje levodope na PGM-AuNP i dopamina na Tween-SeNP. Vodikove veze mogu nastati između hidroksilnih skupina levodope/dopamina kao donora vodika i atoma kisika ili dušika na nanopovršini kao akceptora vodika. U slučaju hidrofilnih nanopovršina funkcionaliziranih s  $\text{NH}_2$ , vodikove veze mogu nastati s kateholnim skupinama ili kation- $\pi$  interakcijama s površinom.<sup>xxxix,xxxii</sup> Štoviše, vodikove veze najčešće pokreću međudjelovanja između proteina i metalnih nanočestica.<sup>xxxiii,xxxiv</sup> To je potvrđeno i u ovom istraživanju budući da su BSA i hTF u gotovo svim slučajevima vodikovom vezom vezani za AuNP i SeNP.

---

XXXI. W. Zhang, H. Yang, F. Liu, T. Chen, G. Hu, D. Guo, Q. Hou, X. Wu, Y. Su, and J. Wang, *RSC Adv.* **7** (2017) 32518–32527.

XXXII. H.C. Yang, R.Z. Waldman, M.B. Wu, J. Hou, L. Chen, S.B. Darling, and Z.K. Xu, *Adv. Funct. Mater.* **28** (2018) 1–14.

XXXIII. B. Meesaragandla, I. García, D. Biedenweg, J. Toro-Mendoza, I. Coluzza, L.M. Liz-Marzán, and M. Delcea, *Phys. Chem. Chem. Phys.* **22** (2020) 4490–4500.

XXXIV. Y. Bu, and S.W. Lee, *Int. J. Nanomedicine* **10** (2015) 47–54.

Dopamin se na PGM-AuNP i BSA na Ad-AuNP veže elektrostatskim međudjelovanjima. Takva priroda vezanja dodatno je potvrđena u međudjelovanjima između levodope i obje vrste SeNP-a. Kako su se reakcije odvijale pri pH vrijednosti  $4.9 \pm 1.3$ , levodopa je postojala kao zwitterion što je uzrokovalo elektrostatska međudjelovanja. Dopamin se elektrostatski veže i na PVP-SeNP, što se može pripisati međudjelovanju između pozitivno nabijene amino skupine dopamina, koja je N-protonirana u reakciji koja se odvijala pri pH 4.2, i negativno nabijene nanopovršine selenena.<sup>xxxiv</sup>

Nadalje, dodatak proteina iz seruma (BSA i hTF) u binarnu smjesu uzrokovao je smanjenje afiniteta vezanja levodope/dopamina za sve testirane NP, pri čemu je veličina smanjenja ovisila o površinskoj funkcionalizaciji. *K* vrijednosti nakon dodatka BSA smanjivale su se u nizu  $\text{PEG-AuNP} \geq \text{AdGly-AuNP} > \text{Ad-AuNP} > \text{PGM-AuNP}$ . Utjecaj proteina na vezanje katehola na površinu PGM-AuNP bio je beznačajan, što je u skladu s najvećim afinitetom levodope i dopamina za PGM-AuNP, dok je vezanje BSA na tu vrstu NP bilo relativno slabije nego za ostale AuNP. Istraživanja na SeNP vrstama pokazala su suprotan učinak. Utvrđeno je da je smanjenje konstante vezanja levodope i dopamina nakon dodatka hTF bilo izraženije za PVP-funkcionalizirane SeNP-ove nego za Tween-funkcionalizirane SeNP-ove, iako su potonji imali znatno slabije afinitete vezanja za levodopu i dopamin.

Tijekom međudjelovanja,  $d_H$  i  $\zeta$  potencijal AuNP-ova i SeNP-ova ostali su praktički nepromijenjeni nakon interakcije s levodopom i dopaminom, što ukazuje na stvaranje vrlo stabilnog kompleksa.<sup>xxxv</sup> Povećanje prosječnih  $d_H$  vrijednosti te  $\zeta$  potencijala nakon interakcija s BSA i hTF ukazuje na promjenu stabilnosti NP-a.<sup>xxxvi,xxxvii</sup> Stabilizacijski agensi, kao što su PEG, PVP i Tween, prisutni na površini NP-a učinkovito su poboljšali stabilnost NP-a, budući da je uočeno da su promjene u  $d_H$  i  $\zeta$  potencijalu nakon dodavanja proteina u takve sustave mnogo manje u usporedbi s ostalim NP-ovima.

---

XXXV. E. Ferreira de Macedo, D.M. Ducatti Formaggio, N. Salles Santos, and D. Batista Tada, *Sensors* **17** (2017) 2765.

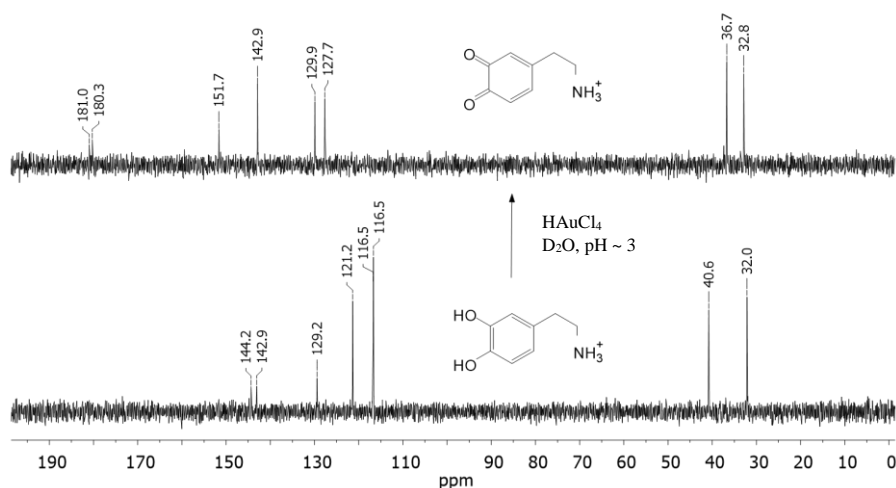
XXXVI. S.A. Alex, N. Chandrasekaran, and A. Mukherjee, *J. Mol. Liq.* **248** (2017) 703–712.

XXXVII. T. Zheng, P. Cherubin, L. Cilenti, K. Teter, and Q. Huo, *Analyst* **141** (2016) 934–938.

Dodatno, primijećene su značajne promjene u intenzitetu SPR pika Ad- i PGM-AuNP pri vezanju BSA i dopamina. Takve promjene dogodile su se zbog agregacije čestica u prisustvu BSA, što je rezultiralo crvenim pomakom i širenjem SPR pika. Nasuprot tome, dodavanjem dopamina došlo je do pojave novog pika na oko 665 nm zbog unakrsnog povezivanja susjednih kompleksa posredovano vodikovom vezom.<sup>XXXVIII</sup> Nažalost, promjene SPR-a pikova SeNP-a nakon međudjelovanja s fluoroforima nisu se mogle pratiti jer SPR pikovi za te vrste NP-a nisu dovoljno izraženi.

S obzirom na moguću oksidaciju katehola u kiselom pH prilikom pripreme AuNP, bilo je bitno ispitati njihovu stabilnost u takvim uvjetima.<sup>XXXIX</sup> NMR spektroskopijom praćene su strukturne promjene levodope odnosno dopamina tijekom njihovog međudjelovanja s nanopovršinom. Otkriveno je da produkt vezan za nanopovršinu odnosno opseg oksidacijske reakcije ovisi o molarnom omjeru reaktanata,  $\text{HAuCl}_4$  i katehola, odnosno omjeru  $[\text{Au}]:[\text{kateholi}]$ .

U slučaju viška Au, tj.  $[\text{Au}]:[\text{dopamin}] = 2:1$ ; sustav korišten za pripremu stabilnih sferičnih AuNP, dopamin je brzo i potpuno oksidiran u dopaminkinon, čija je struktura potvrđena  $^1\text{H}$  i  $^{13}\text{C}$  NMR spektrima (slika II). Nadalje, daljnja oksidacija nije uočena, odnosno dopaminkinona nije ciklizirao u leukoaminkrom.



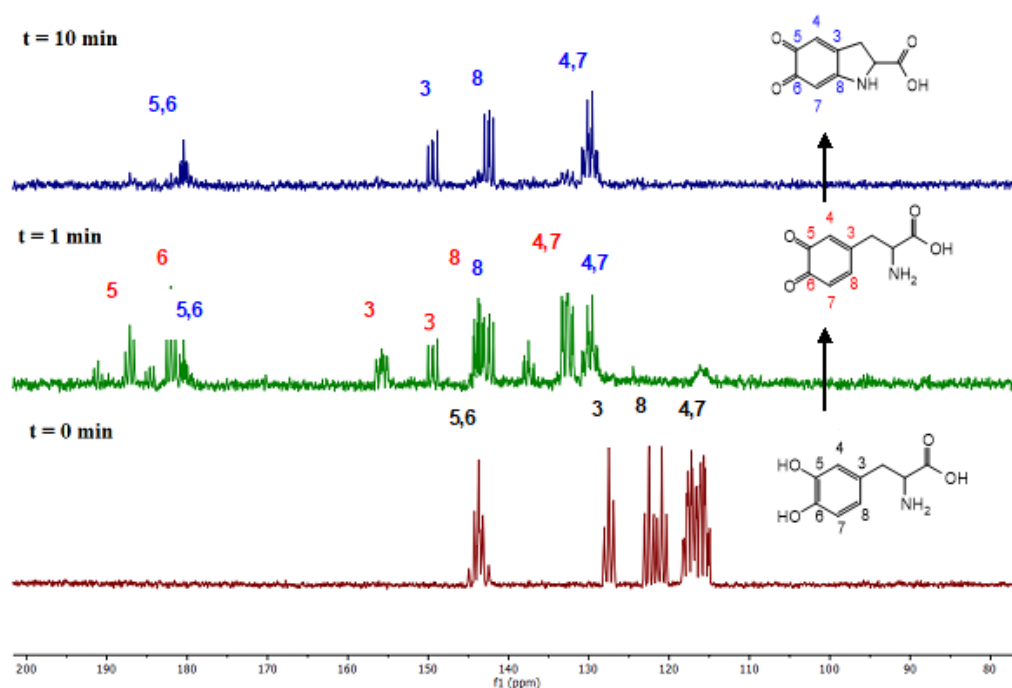
**Slika II.**  $^{13}\text{C}$  NMR spektri dopamina (10 mM) i produkta oksidacije dopamina (dopaminkinon) u  $\text{D}_2\text{O}$  ( $\text{pH} \approx 3$ ;  $[\text{Au}]:[\text{dopamin}] = 2:1$ ).

XXXVIII. A. Rostami, A. Hadjizadeh, and S. Mahshid, *J. Mater. Sci.* **55** (2020) 7969–7980.

XXXIX. M. Salomäki, L. Marttila, H. Kivelä, T. Ouvinen, and J. Lukkari, *J. Phys. Chem. B* **122** (2018) 6314–6327.

Nasuprot tome, kada je primijenjen omjer  $[Au]:[levodopa] = 2:1$ , sustav koji se koristi za formiranje stabilnih Au nanocvjetova, levodopa je trenutno oksidirana u dopakinon. Za razliku od dopaminkinona, dopakinon podliježe daljnoj intramolekularnoj ciklizaciji, što dovodi do stvaranja leukodopakroma/dopakroma, što je potvrđeno  $^1H$  i  $^{13}C$  NMR spektrima (Slika III). Leukodopakrom, dopakrom i njegov kinoidni tautomer mogu koegzistirati u brzom redoks ravnoteži, koju je teško razlikovati na vremenskoj skali NMR-a.

S druge strane, kada su kateholi korišteni u suvišku prilikom priprave AuNP-ova, nisu primijećeni oksidacijski produkti dopamina ili levodope. Stoga, kada je početni omjer reaktanata bio  $[Au]:[kateholi] = 1:6$ , pripremljene AuNP obložene su samo dopaminom ili levodopom. Nasuprot tome, kada je omjer reaktanata bio  $[Au]:[dopamin] = 2:1$ , površina pripremljenih AuNP-ova modificirana je dopaminkinonom, dok pri omjeru  $[Au]:[levodopa] = 2:1$  tri su različita produkta oksidacije mogla biti uključena u međudjelovanja s nanopovršinom: leukodopakrom, dopakrom ili njegov tautomerni oblik. Ta tri intermedijera ne mogu se razlikovati pomoću  $^1H$  NMR spektroskopije.



**Slika III.**  $^{13}C$  NMR spektri levodope (donji spektar, crni brojevi), njegovih oksidacijskih intermedijera dopakinon/dopakrom (srednji spektar, crveni/plavi brojevi) i dopakroma (gornji spektar, plavi brojevi) u  $D_2O$  ( $pH \approx 3$ ;  $[Au]:[levodopa] = 2:1$ ).



Nadalje, DFT izračunima pokušano je objasniti mehanizam oksidacijskih procesa katehola tijekom sinteze i funkcionalizacije AuNP-ova. Kako bi se procijenio utjecaj AuNP-ova na brzinu ciklizacije, reaktanti (dopakinon i dopaminkinon), prijelazna stanja i produkti (leukodopakrom i leukoaminokrom) kompleksirani su neutralnim klasterom  $Au_n$ , gdje je  $n = 2, 4$  ili  $6$ . Izračunate energetske barijere ( $\Delta G^\ddagger$ ) za sve  $Au_n$  potpomognute ciklizacije porasle su za približno 30-40 kJ/mol u odnosu na reakciju u odsutnosti metala ( $n = 0$ ). Unatoč ovom povećanju, predviđene brzine intramolekularnih Michaelovih  $N$ -adicija bile su slične za dopakinon i za dopaminkinon. Ipak, za razliku od dopaminkinona, intramolekularna ciklizacija dopakinona lakše se odvija zbog (veće) intrinzične kiselosti njegove nukleofilne amino skupine.<sup>XL,XLI</sup>

Stvaranje cikliziranih produkata vrlo je egzergono i termodinamički povoljnije, što znači da su leukodopakrom i leukoaminokrom stabilniji od dopakinona, odnosno dopaminkinona. Kao što je već rečeno, leukodopakrom lako oksidira u dopakrom, koji se nalazi u ravnoteži sa svojim kinoidnim tautomerom. Kako bi se odredilo koji se produkt oksidacije potencijalno veže za AuNP, provedene su klasične MD simulacije. Tim izračunima dobiveni su podatci o slobodnim energijama vezanja ( $\Delta G_{\text{bind}}$ ), pružajući uvid u međudjelovanja tih spojeva s površinom AuNP-ova. MD simulacije pokazale su da sve funkcionalne skupine doprinose interakciji s površinom Au. Rezultati su pokazali da dopakrom ima najveći afinitet prema Au nanopovršini ( $\Delta G_{\text{bind}} = -182,9$  kJ/ mol), a zatim leukodopakrom ( $\Delta G_{\text{bind}} = -160,9$  kJ/ mol ) i tautomer dopakroma ( $\Delta G_{\text{bind}} = -125,0$  kJ/ mol). Ti rezultati omogućili su identificiranje najprikladnijeg oksidacijskog intermedijera za funkcionalizaciju AuNP-ova.

Dodatno su provedeni pokusi predviđanja propusnosti različito funkcionaliziranih AuNP-ova i SeNP-ova koristeći acelularni i celularni test. Acelularni PAMPA model odabran je za procjenu pasivnog transporta samih SeNP-ova i AuNP-ova ili tih NP-ova u kombinaciji s levodopom kroz BBB. Za simulaciju BBB-a, polikarbonatna membrana obložena polarnim lipidnim ekstraktom iz mozga korištena je za odvajanje donorskog odjeljka koji sadrži spojeve od interesa od akceptorskog odjeljka.

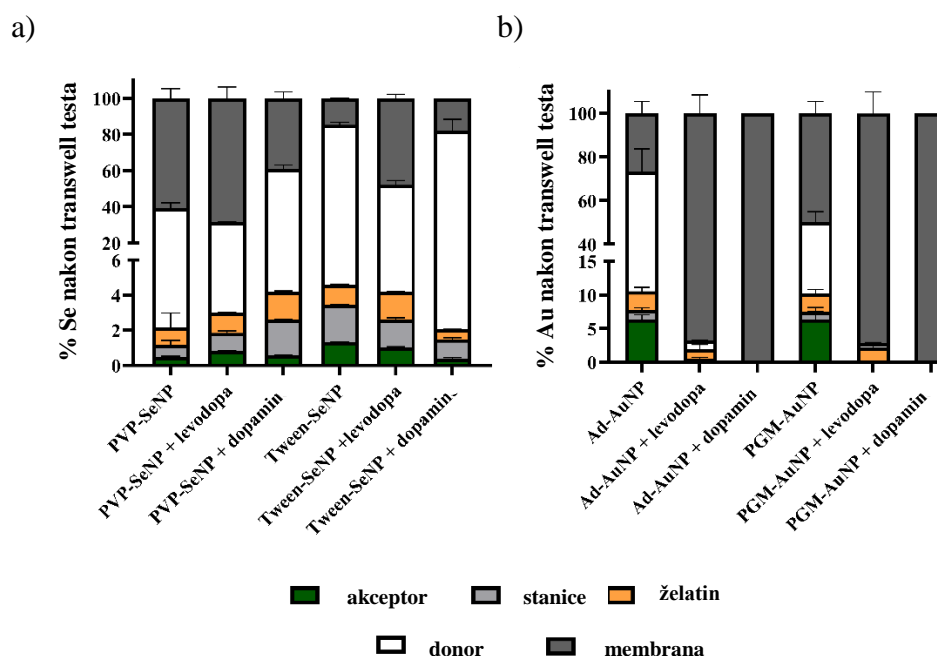
---

XL. M. Salomäki, L. Marttila, H. Kivelä, T. Ouvinen, and J. Lukkari, *J. Phys. Chem. B* **122** (2018) 6314–6327.

XLI. Y. Wang, H. Zhang, and M. Chen, *Anal. Chim. Acta* **1157** (2021) 338379.

Tween-SeNP i PEG-AuNP korišteni su u tom testu sami ili u kombinaciji s levodopom. Nakon 4-satnog perioda inkubacije, koncentracija levodope analizirana je korištenjem UV/Vis spektroskopije, dok je AAS korišten za određivanje koncentracija Au odnosno Se. Rezultati AAS-a pokazali su da je samo mala količina Tween-SeNP-ova identificirana u akceptorskom odjeljku nakon 4 sata inkubacije, dok se sadržaj Au nije mogao izmjeriti u akceptorskom odjeljku jer je bio ispod granice detekcije. Međutim, koncentracija Au u donorskom odjeljku ostala je ista kao i prije inkubacije, što ukazuje da AuNP ne prolazi kroz membranu u akceptorski odjeljak. Također, levodopa nije pronađena u akceptorskom odjeljku, što je u skladu sa prijašnjim saznanjima koja govore da levodopa ne prolazi BBB pasivnim već aktivnim transportom.<sup>V</sup>

Kao celularni model korišten je tzv. transwell assay uz staničnu liniju hBEC-5i za predviđanje propusnosti spojeva transportiranih putem pasivne difuzije ili aktivnim mehanizmom. AuNP-ovi i SeNP-ovi dodani su u donorski odjeljak, te je mjerena koncentracija Au odnosno Se koji su prošli kroz stanice, želatinu i membranu u akceptorski odjeljak, korištenjem AAS-a, a rezultati su izraženi kao postotak Se i Au, kao što je prikazano na slici IV.



**Slika IV.** Postoci a) Se i b) Au u različitim odjeljcima (akceptor, stanice, želatin, donor, membrana) transwell sustava izračunati iz mjerenja atomske apsorpcijske spektroskopije (AAS).

Rezultati pokazuju da je najveći dio primjenjene količine AuNP-a i SeNP-a ostao u donorskom odjeljku ili se adsorbirao na membrani nakon 3-satne inkubacije, s manje od 10% Au i Se u akceptorskom, želatinskom i staničnom odjeljku zajedno. Može se zaključiti da ti testovi nisu u potpunosti prikladni za proučavanje propusnosti NP-a. Izazovi poput agregacije i prijanjanja na membranu karakteristični su za NP, te su dodatno ispitani u ovom doktorskom radu za SeNP. Prvo, stabilnost SeNP-ova ispitana je u fosfatnom puferu (PBS) u kojem je rađen pokus. Rezultati DLS i ELS mjerenja pokazuju da je  $d_H$  za obje vrste SeNP-a povećana u fosfaPBS-u u usporedbi s ultra čistom vodom. Posljedično, takvi agregati mogu biti preveliki da prođu kroz membranu i mogu rezultirati eksperimentalnom greškom. Dodatno, potencijalna adsorpcija SeNP-ova na membranu ispitana je korištenjem membrane s istom veličinom pora (0,4  $\mu\text{m}$ ) kao što je korištena u transwell sustavu, ali bez stanica. Membrana je bila obložena želatinom kako bi oponašala BBB transwell assay. Rezultati su pokazali da je otprilike 80% Se bilo adsorbirano na takvoj membrani što je potencijalno moglo uzrokovati aglomeraciju SeNP-ova unutar pora membrane, ometajući transport nanočestica.

### **Zaključci:**

Različito funkcionalizirane nanočestice zlata i selena bile su sferične, te manje od 100 nm s negativnim vrijednostima  $\zeta$  potencijala. Nadalje, dobivenim rezultatima pokazano je da vezanje levodope odnosno dopamina na nanopovršinu zlata i selena kao i utjecaj proteina iz seruma na njihovo vezanje ovisi o površinskoj funkcionalizaciji te o vrsti nanočestica. Interakcije između katehola i ispitivanih nanočestica nekovalentnog su karaktera, te se mogu opisati elektrostatskim interakcijama ili van der Waalsovima i vodikovim vezama. NMR mjerenjima pokazano je da konačan oblik katehola na nanopovršini ovisi o načinu pripreme nano-susatva. Prilikom pripreme potrebno je da levodopa ili dopamin budu u suvišku u odnosu na zlato kako bi se površina AuNP funkcionalizirala s kateholima, a ne njihovim oksidacijskim produktima. Nadalje, transwell i PAMPA modelima za predviđanje propusnosti AuNP i SeNP utvrđena je zanemariva propusnost kroz BBB za sve ispitivane AuNP i SeNP vrste. Zbog agregiranja nanočestica te blokiranja pora membrane, može se zaključiti da ti modeli nisu najprikladniji za istraživanje propusnosti NP-ova.

## § 1. INTRODUCTION

The development of new strategies to treat brain diseases is one of the most challenging and expensive market niches for the pharmaceutical industry.<sup>1</sup> Nowadays, neurodegenerative diseases, like Parkinson's disease (PD), Alzheimer's disease, multiple sclerosis, and amyotrophic lateral sclerosis, are the fourth leading cause of death in the developed world after heart disease, cancer and stroke. They are the most debilitating disorders affecting thinking, skilled movements, feelings, cognition and memory. Despite the important differences in clinical manifestation, neurodegenerative disorders share common features such as their appearance late in life, extensive neuronal loss and synaptic abnormalities, increased oxidative stress, and the presence of cerebral deposits of misfolded protein aggregates.<sup>2</sup> Although over 10 million people globally suffer from neurodegenerative diseases each year, current therapeutic possibilities are limited by the lack of drug candidates that reaches the target. The reason for this may lie in the complexity of the brain, the liability of drugs to cause side effects, and their requirement to cross the blood-brain barrier (BBB), well-known as the best gatekeeper in the body, protecting the brain from possible threats within the blood by specific features of the brain capillaries.<sup>2,3</sup> For example, pharmacotherapy of PD has been limited by the BBB permeability.<sup>4</sup>

PD is characterized by the massive depletion of dopamine as a result of the degeneration of dopaminergic neurons.<sup>5</sup> Levodopa is the golden therapeutical standard for this disease as a source of dopamine and easily crosses the BBB. However, long-term treatment with levodopa or distribution of any anti-Parkinsonian drug in healthy tissues results in various side effects, such as psychiatric disturbances, dyskinesias, nausea and vomiting, which represent key challenges in the therapy of PD.<sup>5,6</sup>

Challenges in the treatment of PD may be overcome by nanotechnological approaches. Such approaches have already paved the way for the development of non-invasive drug delivery strategies to deliver pharmacologically active molecules close to their site of action, enhancing efficacy and limiting severe side effects. The specific properties of nanomaterials, such as small size, biocompatibility, prolonged blood circulation and non-toxicity, have been exploited for the creation of an emerging delivery platform that interacts with biological systems at the molecular level with a high degree of specificity.<sup>2</sup>

Despite significant progress in nanomedicine, only a small number of nanomaterials have reached a phase of clinical trials, and even fewer have entered clinical use.<sup>7</sup> The reason for disagreement between experimental discoveries and clinical outcomes may lie in the lack of knowledge and information about processes occurring at the nano-bio interface. Therefore, the main goal of this doctoral dissertation was to design and characterize different gold (AuNP) and selenium nanoparticles (SeNP) to obtain effective and neuroprotective nano-systems for the delivery of catechols (levodopa and dopamine) into the brain and to reveal the processes that occur at the nanoparticle-drug interface.

Along these lines, the set goal of the research leads to the following main hypothesis: “The binding ability of levodopa and dopamine to AuNP and SeNP depends on the nanosurface functionalization and processes occurring at the nanoparticle-drug interface.”

To examine this hypothesis, the processes that take place during catechol interactions with nanosurfaces were investigated to reveal the most favorable surface functionalization of investigated nanoparticles (NP) for more effective and safer drug delivery. Moreover, the potential formation of catechol oxidation products on the nanosurface was examined during their binding, as such products can influence the safety of nano-systems. For all nanoparticle-catechol systems, the possibility of passing through the BBB was tested using acellular and cellular models. Detailed characterization of the processes that occur during the interaction of catechol with nanosurface, and increasing the level of knowledge about the interaction of such systems with the BBB, will significantly improve the design of nano-formulations with the aim of achieving more efficient and safer therapies for the treatment of PD and other neurodegenerative diseases.

## § 2. LITERATURE OVERVIEW

### 2.1. Parkinson's disease

PD is the second most common neurodegenerative disease after Alzheimer's disease affecting over 8.5 million people with prevalence in the elderly population.<sup>5,8,9</sup> Pathologically, PD is characterized by degeneration or loss of dopaminergic neurons, which leads to a reduced concentration of dopamine in an area of the brain called *substantia nigra pars compacta* (Figure 1). Dopamine is produced in the dopaminergic neuron in two steps. First, levodopa is formed from the amino acid tyrosine (Tyr) in the presence of the enzyme tyrosine hydroxylase (TH). Then, levodopa is metabolised to dopamine by the enzyme aromatic amino acid decarboxylase (AADC).<sup>10</sup> Dopamine is released to bind to postsynaptic dopamine receptors and transmits a signal that is of great importance in movement. Therefore, PD is primarily manifested in movement disorders such as bradykinesia, rigidity and tremor. It is also important to mention non-motor complications of PD, which include mental health disorders such as depression and dementia. These symptoms are usually present when the disease progresses.<sup>5,11</sup>

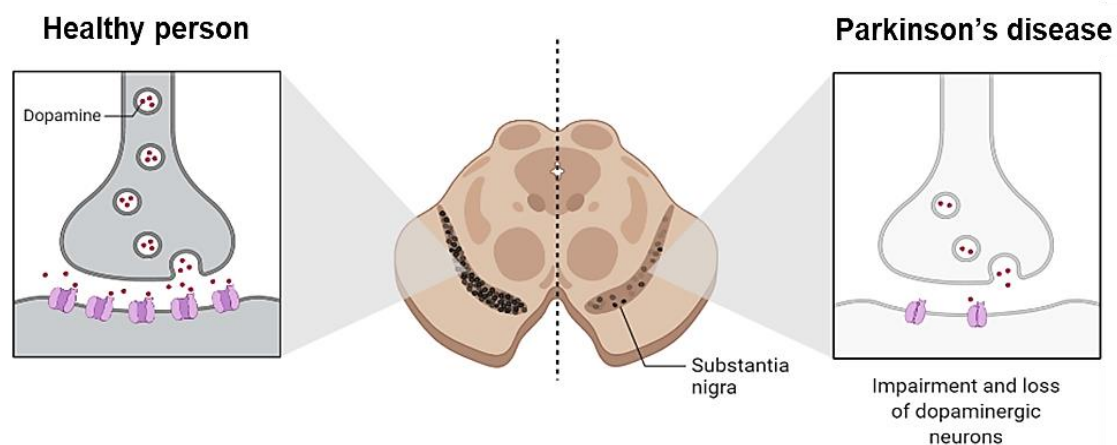


**Figure 1.** Schematic representation of pathological process present in PD (adapted from “Progression of Parkinson's Disease in the Substantia Nigra”, by BioRender.com (2023). Retrieved from <https://app.biorender.com/biorender-templates>).

An additional neuropathological hallmark of PD is the presence of Lewy bodies in the dopaminergic neurons of *substantia nigra pars compacta*. The protein predominantly detected

in the Lewy bodies is  $\alpha$ -synuclein, which is present in aggregated form. Mutations (such as A53T, A30P, and E46K) in the  $\alpha$ -synuclein gene (PARK1) are associated with PD in which Lewy bodies are also seen. Additionally, the parkin protein, known as an E3 ubiquitin ligase, facilitates the binding of ubiquitin (ubiquitination) to other proteins such as the  $\alpha$ -synuclein interacting protein synphilin-1 leading to the formation of Lewy bodies. Moreover, it is believed that the dementia symptom of PD is related to the formation of Lewy bodies.<sup>5,9</sup>

In addition to the mentioned pathological processes present in PD, recent studies indicate that neuroinflammation can also lead to the disturbance in the dopaminergic pathway as it was noticed that anti-inflammatory agents might slow the progression of the disease, especially the onset of dementia.<sup>12</sup> These studies also indicate that dopaminergic neurons can be damaged under stress conditions. Metabolism of dopamine and high iron content may generate reactive oxygen species (ROS) leading to dopaminergic neurons more susceptible to oxidative stress.<sup>10,13</sup> Moreover, mitochondrial dysfunctions including complex I impairment, mitochondrial DNA mutations and mitochondrial oxidative stress induced by the high concentration of  $\text{Ca}^{2+}$  ions in *substantia nigra pars compacta* lead to the degeneration of dopaminergic neurons. Additionally, MPTP (1-methyl-4-phenyl.1,2,3,6-tetrahydropyridine), a chemical precursor to the neurotoxin  $\text{MPP}^+$ , impairs dopaminergic neurons in the substantia nigra of the brain which leads to permanent PD symptoms.<sup>14</sup> Therefore, the therapy of PD may be directed towards targeting present pathological processes.

To date, PD is known as an incurable disease and, therefore, its therapy options are mainly based on relieving the symptoms.<sup>5</sup> L-dihydroxyphenylalanine (L-DOPA/levodopa) combined with a peripheral decarboxylase inhibitor (e.g. carbidopa or benserazide) has been a gold standard for the treatment of PD for decades. It is crucial to substitute for dopamine deficiency, but dopamine, as a small hydrophilic molecule, is unable to cross the BBB. Contrary, levodopa permeates the BBB easily via the large neutral amino acid transporter 1 (LAT-1). Once, it is inside the brain, levodopa is converted by neuronal aromatic L-amino acid decarboxylase into dopamine, hence restoring dopamine levels in surviving neurons.<sup>4,5, 11,15</sup>

Although levodopa may be considered as an initial treatment option in the early stage of PD, symptomatic therapy with monoamine oxidase type B (MAO-B) inhibitors, dopamine receptor agonists, catechol-O-methyltransferase (COMT) inhibitors, anticholinergics and

amantadine becomes necessary once motor complications become more severe.<sup>5,16</sup> On the other hand, symptoms related to mental illnesses are treated with antipsychotics.<sup>17</sup>

### *2.1.1. Obstacles in the treatment of PD*

The main obstacle in the treatment of central nervous system (CNS) related diseases is the presence of the BBB. The BBB is a highly selective barrier that separates the circulating blood from the brain and spinal cord, and it is composed of specialized cells called endothelial cells that tightly regulate the transport of molecules into the brain.<sup>18</sup> It also serves as a protective barrier allowing passage of certain substances such as nutrients and water and preventing the entrance of harmful agents and microorganisms into the brain.<sup>19</sup> On the other side, its protective role presents limitations concerning the transport of therapeutic agents into the brain. Despite strict transport regulations, there are still various mechanisms that are used for supplying the brain with essential molecules. These molecules can be transported passively or actively from the hydrophilic environment of blood, through the hydrophobic environment of lipophilic membranes of the BBB endothelial cells, into the brain.<sup>19,20</sup> Passively transported molecules move across the membrane through a concentration gradient without using cellular energy. However, they need to meet required physicochemical properties such as hydrophobicity and lipophilicity with molecular weight typically smaller than 600 Da.<sup>19,20</sup> Conversely, active transport needs cellular energy (e.g. ATP) to transport molecules against the concentration gradient. Active transport across the BBB can be adsorption-mediated (AMT), carrier-mediated (CMT), or receptor-mediated (RMT). These transport routes can be used for the delivery of therapeutic agents across BBB.<sup>7</sup>

However, PD therapy-related issues remain most troublesome. One would easily treat PD with dopamine but, as already mentioned, dopamine is restricted from entering the brain because of low lipid solubility and lack of specific transport carriers in the luminal membrane of the capillary endothelial cells.<sup>21</sup> On the other hand, levodopa can be easily transported into the brain and converted to dopamine but its long-term treatment might lead to serious side effects. It is known that long-term treatment with levodopa can induce dyskinesia, although the incidence is higher in younger patients. Moreover, levodopa with a half-life of 60-90 min can easily undergo auto-oxidation and induce oxidative stress.<sup>5,10</sup> Dopamine agonists have similar but more frequent side effects than levodopa, such as motor malfunction, hallucinations and confusion.<sup>22</sup> Nevertheless, the majority of potential therapeutic compounds



found to be neuroprotective *in vitro*, induces side effects when administered to animals. Such molecules usually suffer from limited stability due to fast degradation before reaching the site of action.<sup>23</sup> Therefore, the development of therapeutic alternatives is still demanding as conventional therapeutic approaches for PD treatment show a low level of efficacy with multiple side effects.

## 2.2. Nanotherapeutic strategies for the treatment of PD

The application of nanotechnology in the field of neurodegenerative diseases has attracted an unprecedented level of interest in recent years. Due to a lack of therapy options and poor diagnostic tools, the main goal was to find new formulations with the capability of delivering drugs to the specific site and producing biocompatible materials, which will lead to early diagnosis and successful treatment. NP showed exceptional properties that provide potential to be used in nanomedicine. Their size in the nanoscale range (1 to 100 nm) shows significant properties improvement in comparison with corresponding materials at the macroscale due to an enlargement in the surface-to-mass ratio. The large surface area gives them the possibility to adsorb, carry and deliver multiple molecules such as drugs, proteins and probes. NP can be also employed in the therapy of neurodegenerative diseases because of their ability to cross the BBB and deliver drugs specifically to the target site.<sup>2</sup> These NP's features are especially important for diagnostic and drug delivery opportunities for CNS diseases. NP made for these purposes usually contain two components, a nanovehicle which serves as the carrier agent, and a chemotherapeutic drug. Nanomaterials can penetrate the BBB passively and actively depending on particle size and modification of surface properties. Site-specific delivery can be achieved by modulating the nanosurface with targeting ligands. Drugs can be easily bound to the nanosurface or incorporated into the nanosystems without chemical reactions, thus preserving drug activity. Moreover, controlled and sustained drug release at the specific site might enhance the uptake of poorly soluble drugs, enhancing their bioavailability. In this way, the therapeutic efficacy of a particular drug can be improved with a reduction in its side effects.<sup>2</sup>

NP currently investigated for the potential therapy of PD can be classified according to the material of which they are composed (inorganic or organic) and the site of action with regard to target a particular pathological process. A generalized overview of some of the nanotechnology-based treatment solutions for PD is summarized in Table 1.

**Table 1.** Principle / Main nanotechnology devices used for the PD treatment.

Nanoparticles		Therapeutic/neuroprotective agent	Ref.
<b>ORGANIC NANOPARTICLES</b>	Polymeric nanoparticles	PLGA nanoparticles	Rasagilin, Selegiline, Levodopa, Puerarin, Rotigotine, Tolcapone, Superoxide dismutase, Nicotine, Dopamine 21,24–33
		PLA nanoparticles	Resveratrol 34
		Chitosan	Rotigotine, Ropinirole, Dopamine, Pramipexole, Levodopa, Selegiline 35–42
	Liposomes	Immunoliposomes	Antibodies (MAb against the transferrin BBB receptor (OX26MAb) and against $\alpha$ -synuclein (LB509MAb)). 43
	Solid-lipid nanoparticles		Citicoline, Apomorphine, Bromocriptine, Ropinirole 44–47
	Metal oxide nanoparticles	Cerium oxide nanoparticles	48
<b>INORGANIC NANOPARTICLES</b>	Metallic nanoparticles	Gold nanoparticles	Levodopa 49–52
		Ceria nanoparticles	53,54
		Silver nanoparticles	55,56
		Silica nanoparticles	Curcumin 57
	Magnetic nanoparticles	Fe <sub>3</sub> O <sub>4</sub>	Alpha-Synuclein RNAi Plasmid 58

PLGA - poly(lactic-co-glycolic acid); PLA - polylactic acid

As can be noted from Table 1, polymeric NP are the most investigated materials in nanomedicine because of their biocompatibility, biodegradation, and low toxicity. Among them, PLGA NP attracted the most attention because PLGA has been approved by U.S. Food and Drug Administration (FDA) and the European Medicine Agency (EMA) for use in drug-delivery systems. However, the lack of specificity and stability affects their efficacy.<sup>59</sup> On the other hand, inorganic NP have attracted interest due to their unique physicochemical properties, small size and surface plasmon properties. These features enable their use as therapeutic and diagnostic tools as well as their implementation in applications such as sensors and optic devices.<sup>2,60</sup>

Michael Faraday in 1857 first noticed the existence of inorganic NP in suspension. Since then, there has been a large increase in publications reporting the use of inorganic NP in the treatment of neurodegenerative diseases. Their size and shape can be easily modified by changing preparation protocols. The control of the size is crucial because sizes above 100 nm may lead to the clearance of NP by the mononuclear phagocyte system before reaching target cells. NP below 100 nm can have longer blood circulation time and consequently enhanced biodistribution and bioavailability. In comparison to organic NP, the surface of inorganic NP can be more easily modified by the binding of stabilizing or receptor-targeting ligands which makes them less toxic and more selective. Moreover, chemicals used for the preparation of inorganic NP are usually more affordable, providing cost-effective manufacturing processes.<sup>2,61</sup> Although there are many published papers on the use of NP in neurodegenerative disease, only a few have reached the clinical stage and their application in therapy needs to be considered comprehensively. Therefore, there is a need for further investigation of this relatively new nanotechnology-based approach. In this doctoral thesis, AuNP and SeNP were used to investigate new therapeutic options for PD.

### **2.3. AuNP and SeNP in the therapy and diagnosis of Parkinson's disease**

In addition to other inorganic NP, AuNP and SeNP have evoked tremendous expectations in the field of neurodegenerative disease due to their antioxidant and neuroprotective effects.<sup>62,63</sup> Recently, they have been employed in gene or drug delivery, biosensors, bioimaging, and diagnostic tools.<sup>63,64</sup> Colloidal gold which is mentioned for the first time in Indian traditional medicine (Ayurveda), in the last 50 years has been used as a food additive and in the treatment of inflammation, rheumatoid arthritis, tuberculosis and neoplastic diseases.<sup>60,63</sup> On

the other hand, selenium is known as an essential element for human health due to its exclusive properties and has been used for the treatment of inflammatory diseases, chronic lymphedema, rheumatoid arthritis and Crohn's disease.<sup>65</sup> In addition, Se has been found to participate in neurotransmission and dopaminergic pathways, and thus may serve as a biomarker in neurological diseases, while several selenoproteins have been shown to protect dopaminergic neurons and beneficially affect PD.<sup>65</sup> In their nano form, gold and selenium have shown outstanding properties such as stability, non-toxicity, high biocompatibility, and high affinity.<sup>60,66,67</sup> Moreover, the high surface area-to-volume ratio of AuNP and SeNP allows dense loading of functionalizing and stabilizing moieties that enable the binding of small drug molecules as well as large biomolecules like DNA, RNA, and proteins to deliver them to the target site.<sup>68,69</sup> All of these properties make them ideal candidates for BBB penetration and compared to other NP they have obvious advantages to deliver therapeutics to the brain and potentially as drug-delivery systems in the therapy of PD.<sup>70-72</sup> Besides, they could enhance the therapeutic potential of drugs and improve their pharmacokinetics, biodistribution and cellular uptake, which has been proven by Gonzalez-Carter *et al.* who showed that levodopa associated with AuNP diminished systemic toxicities of the drug while working synergistically to improve its efficiency.<sup>50</sup>

Moreover, AuNP and SeNP might be used for PD diagnosis since the development of biosensors has arisen due to their surface plasmon resonance (SPR) properties which influence their optical behavior.<sup>64,66</sup> AuNP have a higher potential in this application as their SPR property is greater than that of SeNP. Indeed, several nanobiosensors based on AuNP have been already developed to detect different biomarkers of PD such as dopamine,<sup>73-75</sup> alpha-synuclein protein,<sup>76-78</sup> and even PD-related genetic material.<sup>79,80</sup>

AuNP have been also used in PD animal models. Silva Córneo *et al.* showed that oxidative stress in a PD mouse model decreased after the treatment with AuNP while neurotrophic factors, important for neuron survival, improved together with motor symptoms.<sup>81</sup> Another study from Xue *et al.* showed results *in vitro* where AuNP efficiently scavenged the ROS and decreased the levels of inflammatory cytokines in microglial cells. In addition, *in vivo* results confirmed that AuNP treatment prevents dopaminergic neuroinflammation and increases the levels of dopamine, thereby protecting PD-induced mice from motor disorders.<sup>82</sup> Both studies demonstrated the efficient protective effect of AuNP on dopaminergic neurons without toxicity, producing side symptoms of the disease. On the other

hand, SeNP show exceptional antioxidant properties in comparison to commercial antioxidants, which are unable to cross BBB and scavenge high radical concentration effectively. Hence, these features can promote the use of SeNP in PD therapy. Yue *et al.* noticed that treatment with glycine nano-selenium can decrease oxidative stress induced by MPTP in the PD rat model. Additionally, it can reduce the loss of dopaminergic neurons and have a neuroprotective effect.<sup>83</sup>

## 2.4. Synthesis of AuNP and SeNP

For the preparation of NP, two main approaches are used, which are the “top-down” and “bottom-up” approaches (Figure 2). The top-down strategy includes the cleavage of bulk material to NP by using different synthesis routes such as laser ablation, ion sputtering, UV and IR irradiation and aerosol technology. On the contrary, the bottom-up approach implies the synthesis of NP from the atomic level and this usually includes the reduction of metal salts ( $\text{Au}^{3+}$  or  $\text{Se}^{4+/6+}$ ) to metal in oxidation state 0. Preparation approaches of AuNP and SeNP are generally divided into groups based on chemical, physical and biological methods.<sup>66</sup>

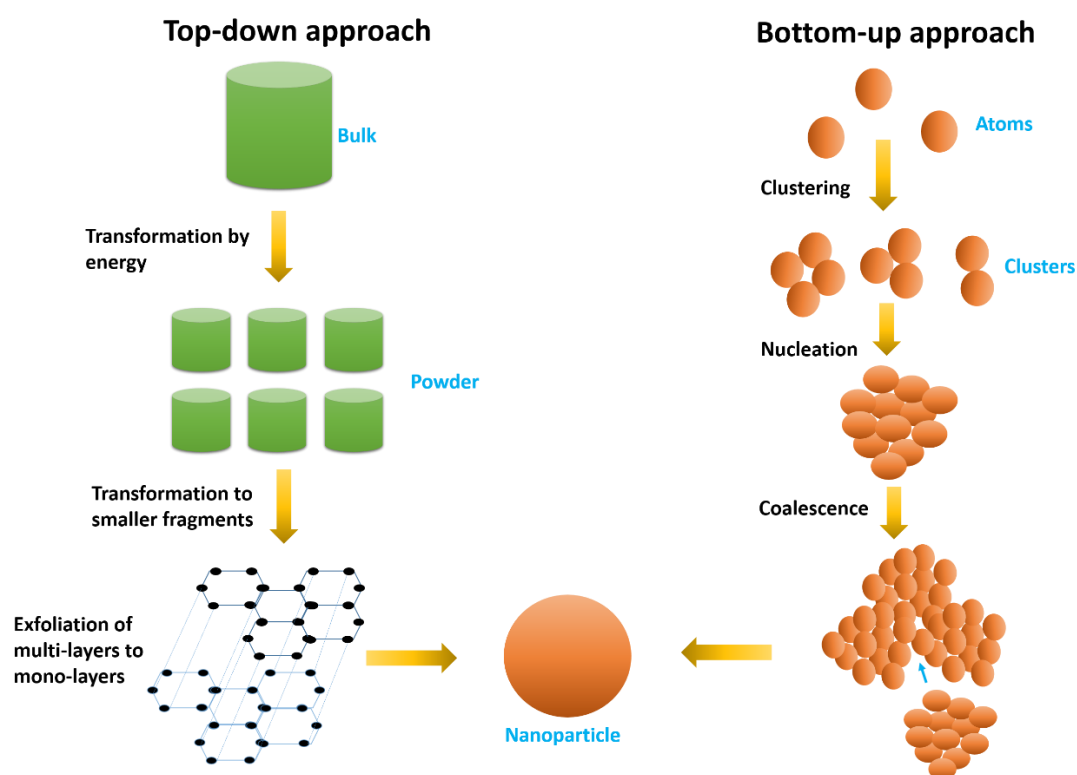


**Figure 2.** Schematic representation of the top-down and bottom-up approaches for the synthesis of NP (created based on Amina *et al.*<sup>66</sup> and Pem *et al.*<sup>84</sup>).

### 2.4.1. Chemical synthesis

Chemical synthesis includes a classic reduction reaction where the initial source of metal ions ( $\text{Au}^{3+}$  or  $\text{Se}^{4+/6+}$ ) is reduced first to  $\text{Au}^0$  and  $\text{Se}^0$  atoms, followed by their clustering, nucleation and growth (see Figure 2) to AuNP and SeNP, respectively. Reducing agents usually used to produce AuNP include sodium borohydride, amino acids, ascorbic acid, UV light, or citrate, while for the preparation of SeNP, the most commonly used reducing agent is ascorbic acid. Also, glutathione (GSH), glucose, acetic acid, pyruvic acid, benzoic acid and sodium borohydride have led to SeNP as well.<sup>65,66</sup> As a precursor, tetrachloroaurate in hydrate form ( $\text{HAuCl}_4 \times \text{H}_2\text{O}$ ) is most commonly used in AuNP synthesis. Apart from this, other precursors, such as  $\text{Au}(\text{NO}_3)_3$ , gold(III) acetate [ $\text{Au}(\text{CH}_3\text{COO})_3$ ], gold(I) bromide ( $\text{AuBr}$ ), and gold(III) hydroxide [ $\text{Au}(\text{OH})_3$ ], have been proposed as promising candidates.<sup>85</sup> On the other hand, in SeNP preparation protocols, the initial sources of Se ions usually come from sodium selenite, selenious acid, sodium selenate, sodium selenosulphate and selenium dioxide.<sup>86</sup>

In the past few decades, a wide range of chemical reduction methods has been developed for the synthesis of AuNP and SeNP depending on desired size, shape and surface functionality. The most famous method for the preparation of spherical AuNP was discovered by Turkovich *et al.* in 1951. They used citric acid to reduce  $\text{HAuCl}_4$  under boiling conditions, where citrate served for both, reduction and stabilization. Using this method, only AuNP with sizes 1-2 nm could be obtained.<sup>87</sup> In 1973, Frens improved the basic method by changing the gold-to-citrate ratio to extend the size range of synthesized particles.<sup>88</sup> Later, Brust and Schiffrin developed the breakthrough method for the preparation of highly stable and organic-soluble alkanethiol-stabilized AuNP through a two-phase reaction. In this reaction tetraoctylammonium bromide (TOAB) was used as the phase transfer reagent while sodium borohydride ( $\text{NaBH}_4$ ) was used as the reducing agent. Additionally, this method can be used as a starting point for further functionalization, as such prepared AuNP are highly stable due to the strong thiol-gold interactions and can be thoroughly dried and redispersed in solution without any aggregation.<sup>89</sup> In addition, there are many reported studies that described the preparation of spherical SeNP using reducing agents such as acetic acid, oxalic acid, aromatic acid (gallic acid), dithiothreitol,  $\beta$ -mercaptoethanol, L-cysteine, chitosan (CS), konjac glucomannan, acacia gum, carboxymethyl cellulose, ascorbic acid and GSH, with sodium selenite, sodium selenosulphate and selenious acid used as a source of Se. These methods yielded spherical SeNP in a range from 30 to 100 nm.<sup>90</sup>

Generally, it is known that spherical NP can be synthesized by isotropic growth on metal nuclei, whereas different shapes can be synthesized by anisotropic growth on metal nuclei. To obtain other shapes of AuNP, the seed-mediated growth technique is widely used and includes a two-step reaction. First, spherical Au seeds are prepared by reducing gold salts with strong reducing agents such as sodium borohydride. In the next step, prepared seeds are put in the solution containing the gold salt and a weak reducing agent like ascorbic acid. These seeds serve as a template on which newly synthesized AuNP deposit and form AuNP with larger sizes and different shapes. This approach may improve the monodispersity of AuNP by controlling nucleation and growth in solution.<sup>66</sup> Moreover, it has been reported that differently shaped AuNP can be synthesized by this method including shapes such as rods,<sup>91</sup> cubes,<sup>92</sup> flower- and urchin-like,<sup>93</sup> wires,<sup>94</sup> plates,<sup>95</sup> and stars.<sup>96</sup> It should be considered that the concentration of reactants, pH of the solution, reaction time and ratio between gold ions and capping agents influence the crystal-growth kinetics and, ultimately, the nanoparticle morphology.

At high gold ion concentrations, different shapes of AuNP (nanoplates) are generated. In this case, a capping (shape directing) agent is specifically adsorbed on the energetically favorable {111} crystal planes of the growing gold nuclei, thus blocking further growth along this plane. Therefore, the growth of NP occurs through the free facet, preferably {100} planes, resulting in the formation of nanoplates (triangular, pentagonal, hexagonal, or star-shaped). Contrarily, at low concentrations of gold ions, there is a high concentration of capping agents that are ready to be adsorbed on the gold nuclei, through specific and nonspecific adsorption. These molecules are bound to each plane of gold nuclei, causing their isotropic growth to the final nanosphere form. Additionally, urchin-shaped AuNP can be formed from spherical NP under a limited concentration of capping agents. Here, spherical AuNP specifically bound to the {100} planes of Au seeds, prevent further growth along this side and enable anisotropic growth along the {111} planes, which leads to the formation of the urchin-like AuNP. For the formation of 2D nanowires, first, the spherical agglomerates are formed from primarily formed spherical AuNP due to attractive van der Waals forces. Then, newly formed Au atoms deposit onto the concave surfaces of two connected particles which join together, finally resulting in the formation of long wires. When these wires undergo the process of Oswald ripening, it results in the formation of Au nanorods.<sup>66,97</sup> On the other hand, different shapes of SeNP can be obtained by following three steps involved in the growth of 1D SeNP. First,

amorphous Se particles need to be prepared. In the second step, seeds of trigonal SeNP are formed, using driving force, such as ultrasonication, abrupt cooling or aging. Finally, these seeds serve as a template for anisotropic crystal growth to build different shapes of SeNP. It has also been noted that capping agents can control crystal growth and consequently impact the final shape of SeNP. If shape-directing agents, such as carboxymethyl cellulose specifically adsorb on the energetically favorable {100} planes of Se crystal lattice and suppress the growth rates of these planes, further anisotropic growth will continue along the {001} planes and form Se nanorods.<sup>98</sup> Se nanowires can be synthesized by the reduction of selenium selenite with hydrazine at 100°C followed by growth along the [001] direction, while Se nanobelts have [101] preferred growth direction.<sup>99,100</sup> Interestingly, Se nanotubes can easily be generated by crystal growth along the c-axis without any templates or surfactants due to the exceptional anisotropy feature of Se.<sup>101</sup>

#### 2.4.2. *Physical synthesis*

Methods commonly employed in the physical synthesis of nanomaterials include microwave irradiation, pulsed laser ablation (PLA), hydrothermal methods and ultrasonication. Among these, PLA and ultrasonication are the most widespread methods.<sup>102,103</sup> PLA is an attractive approach for nanomaterial fabrication due to its simplicity and high product purity. The principle of the method is based on focusing a pulsed laser with high energy on the surface of bulk material whereupon its ablation, melting and crushing can quickly create high-quality NP without any chemical contamination. In PLA, the size of the formed nanoparticle is controlled by laser parameters like pulse duration, power density, wavelength, and ambient gas conditions such as pressure, flow rate, and nature of the gas.<sup>102,103</sup> Moreover, this method can be utilized in the synthesis of SeNP<sup>104</sup> and AuNP.<sup>105,106</sup> The second popular method is ultrasonication which can be also applied in the synthesis of AuNP and SeNP as well as for destroying nanoparticle agglomerates in the solution.<sup>107,108</sup> Additionally, microwave radiation can create high-frequency electric fields to facilitate chemical reactions between the precursors. This method yielded different Se nanostructures including nanotubes and nanorods.<sup>90</sup> In addition, Se nanorods and nanobelts can be prepared by PLA, while the hydrothermal method has been used to synthesize Se nanobelts and nanowires.<sup>101</sup>



### 2.4.3. Biological synthesis

Biological synthesis has recently attracted huge attention in the preparation of NP as it can overcome major issues for both chemical and physical synthesis such as environmental and biocompatibility concerns.<sup>103</sup> The use of certain chemicals in chemical synthesis can have adverse effects on the environment and pose risks when administered to living organisms, thereby restricting the range of biological applications for such nanoparticles, while physical methods face high cost, radiation exposure, high temperature and less productivity.<sup>66</sup> Contrarily, biological synthesis, also known as a green synthesis is harmless to the environment, non-toxic, biodegradable and cost-effective. In the biosynthesis of AuNP and SeNP, their precursor can be reduced and stabilized by compounds existing in plants, as well as microorganisms like bacteria, fungi and algae.<sup>66,103</sup>

Flavonoids, quinones, phenols, phytosterols and other compounds that are present in plants participate in the synthesis of AuNP and SeNP as reduction and stabilizing agents. Although almost every part of plants is full of biomolecules important for synthetic purposes, leaves are the most frequently used as they are the most abundant in such molecules. It was reported that leaves of *Justicia glauca*, *Terminalia arjuna*, *Cassia auriculata*, *Cassia auriculata* and *Mangifera indica* can be used for AuNP preparation. Apart from leaves, other parts of plants also facilitate AuNP synthesis, such as the fruit of *Citrus maxima*, flowers of *Lonicera Japonica* and *Moringa oleifera*, various types of roses, banana and mango peels, etc.<sup>66</sup> On the other hand, plant extracts also demonstrate potential in SeNP biosynthesis. Plant extracts reported for the use in SeNP synthesis include *Aloe vera* and *Clausena dentata* leaf extracts, extracts of *Allium sativum*, *Dillenia indica*, fresh citrus and lemon fruits, *Roselle* plant, *Cinnamomum zeylanicum* bark, *Prunus amygdalus* leaf, *Vitis vinifera* fruit extract, fruit extracts of *Embblica officinalis*, *Capsicum annuum* L. extract, garlic cloves (*Allium sativum*) and others.<sup>65,102,103</sup>

Moreover, microorganisms such as bacteria contain enzymes that are used for the synthesis of AuNP and SeNP. NADPH-dependent enzymes secreted by *Pseudomonas denitrifican* and *Rhodopseudomonas capsulate* promoted the synthesis of AuNP.<sup>66</sup> *Shewanella* species and *Bacillus cereus* were found to be useful in the synthesis of both AuNP and SeNP.<sup>66,90</sup> Other bacterial strains used for the preparation of AuNP include *Deinococcus radiodurans*, *Pseudomonas aeruginosa*, *Rhodopseudomonas capsulate*, *Rhodococcus*, *Marinobacter pelagius* and *Bacillus megaterium*. Additionally, there are many

published papers that describe the production of SeNP using bacteria such as *Escherichia coli*, *Aspergillus terreus*, *Thauera selenatis*, *Pseudomonas aeruginosa*, *Alternaria alternata*, *Klebsiella pneumonia*, *Pantoea agglomerans*, *Bacillus selenitireducens*, *Bacillus cereus*, *Shewanella*, *Pseudomonas stutzer*, *Sulfurospirillum barnesii* and *Selenihalanaerobacter shriftii*.<sup>90, 104, 109</sup> Moreover, microorganisms such as bacteria contain enzymes that are used for the synthesis of AuNP and SeNP. NADPH-dependent enzymes secreted by *Pseudomonas denitrificans* and *Rhodopseudomonas capsulate* promoted the synthesis of AuNP.<sup>66</sup> *Shewanella* species and *Bacillus cereus* were found to be useful in the synthesis of both AuNP and SeNP.<sup>66, 90</sup> Other bacterial strains used for the preparation of AuNP include *Deinococcus radiodurans*, *Pseudomonas aeruginosa*, *Rhodopseudomonas capsulate*, *Rhodococcus*, *Marinobacter Pelagius* and *Bacillus megaterium*. Additionally, there are many published papers that describe the production of SeNP using bacteria such as *Escherichia coli*, *Aspergillus terreus*, *Thauera selenatis*, *Pseudomonas aeruginosa*, *Saccharomyces cerevisiae*, *Alternaria alternata*, *Klebsiella pneumonia*, *Pantoea agglomerans*, *Bacillus selenitireducens*, *Bacillus cereus*, *Shewanella*, *Pseudomonas stutzer*, *Sulfurospirillum barnesii* and *Selenihalanaerobacter shriftii*.<sup>65, 90, 109</sup>

Apart from the mentioned biological species, fungi have also been investigated as a biological source for the synthesis of AuNP and SeNP. A fungal species, *Fusarium oxysporum*, and *Verticillium* have been used in the synthesis of AuNP while for the synthesis of SeNP *Alternaria alternate* was used.<sup>66, 109</sup>

Overall, plants are the preferred option among other biological approaches for synthesizing AuNP and SeNP due to multiple active components that accelerate the synthesis, they are safer and widely accessible, whereas maintaining and growing bacteria and fungi require specific conditions that are not necessary in the case of plants.<sup>65, 102</sup>

## 2.5. Stabilization and functionalization of AuNP and SeNP

### 2.5.1. AuNP and SeNP stabilization approaches

To produce ideal nanosystems for delivering drugs, manipulation of nanoparticle size and surface is crucial as the colloidal stability of NP in biological environments is usually compromised, resulting in their aggregation and clearance.<sup>110</sup> Under physiological conditions, NP can be cleared by the immune system (opsonization) since they can be recognized by the macrophages as threatening agents. Precisely, serum proteins can interact with NP and make a

protein layer around them that is called “protein corona”. This phenomenon can decrease the circulatory lifetime of NP in blood or inhibit their ability to bind to specific target receptors on cells and tissues.<sup>61</sup> In order to preserve the stability and, consequently, the bioactivity of NP, two main approaches are typically applied. The most common and simple method used for protecting NP from clearance is surface stabilization through electrostatic repulsion (e.g. citrate-mediated stabilization). Although this method may be useful in solutions with low ionic strength, in solutions with high ionic strength (e.g. biological media) it fails due to the inability to achieve particle-particle repulsion which leads to nanoparticle agglomeration. Another option is steric stabilization which includes NP coating with polymers or surfactants such as polyethylene glycol (PEG), poly (vinyl pyrrolidone) (PVP), polyethylene oxide, polyoxamer, poloxamine, polysorbate (Tween) 20/80, etc. It has been noted that hydrophobic NP are likely to be cleared due to a higher binding affinity to plasma proteins. Therefore, the goal was to modify nanosurfaces with hydrophilic polymers.<sup>61,110</sup>

Amongst other polymers, PEG has shown the best results in biological media, providing NP with colloidal stability and biocompatibility when attached to their surface. Its highly hydrophilic nature provides steric stabilization, while its short-range repulsive hydration layer enables long-term stability even under extreme conditions. Another reason for the preferential use of PEG as a stabilizing agent for NP is its ability to hinder nonspecific interactions between serum proteins and NP, thus, delaying the NP opsonization process while prolonging NP lifetime in blood circulation. This feature is very important when NP are used as drug-delivery systems since it enables drugs to reach the target site. Moreover, PEG can be easily functionalized with different molecules to improve selective binding.<sup>61,110</sup> In the case of AuNP, PEG-thiol is the first choice as the thiol group can be covalently grafted to the Au nanosurface.<sup>111,112</sup> Additionally, PEG is widely used to stabilize almost every kind of metallic NP, including SeNP.<sup>113,114</sup> Apart from PEG, several other compounds are used to stabilize AuNP and SeNP such as polymers like PVP<sup>115,116</sup> and Tween<sup>117,118</sup>, polysaccharides like chitosan<sup>67,119</sup> and gum arabic<sup>120,121</sup>, bovine serum albumin (BSA)<sup>122,123</sup> and many others.

### 2.5.2. Functionalization of AuNP and SeNP with BBB targeting ability

The functionalization of NP is a crucial aspect of developing nanocarriers for drug delivery purposes. There are various methods for nanocarrier functionalization, depending on the desired outcome. These methods include attaching biomolecules to the surface through

specific conjugation techniques. Targeting mechanisms can be either passive, such as Enhanced Permeability and Retention (EPR) effect, or active, using specific molecules to guide the nanocarriers to specific cells or tissues. Moreover, active targeting can increase the amount of drug delivered to the target site, leading to stronger therapeutic effects and fewer side effects. To facilitate their passage through the BBB and improve drug delivery to the brain, NP can be functionalized with BBB-targeting moieties, such as peptides, proteins, and antibodies (Figure 3). By functionalizing NP with such molecules, the particles can be directed to specific receptors on the endothelial cells of the BBB, thereby enhancing their ability to cross the barrier and reach their target in the brain. The ligands can be covalently or non-covalently bound to the surface of the nanoparticle, enabling selective binding to the receptors which need to be highly expressed and primarily found on the targeted cells. Such systems should likewise be stable enough to reach the target cells at a sufficient concentration.<sup>124</sup>

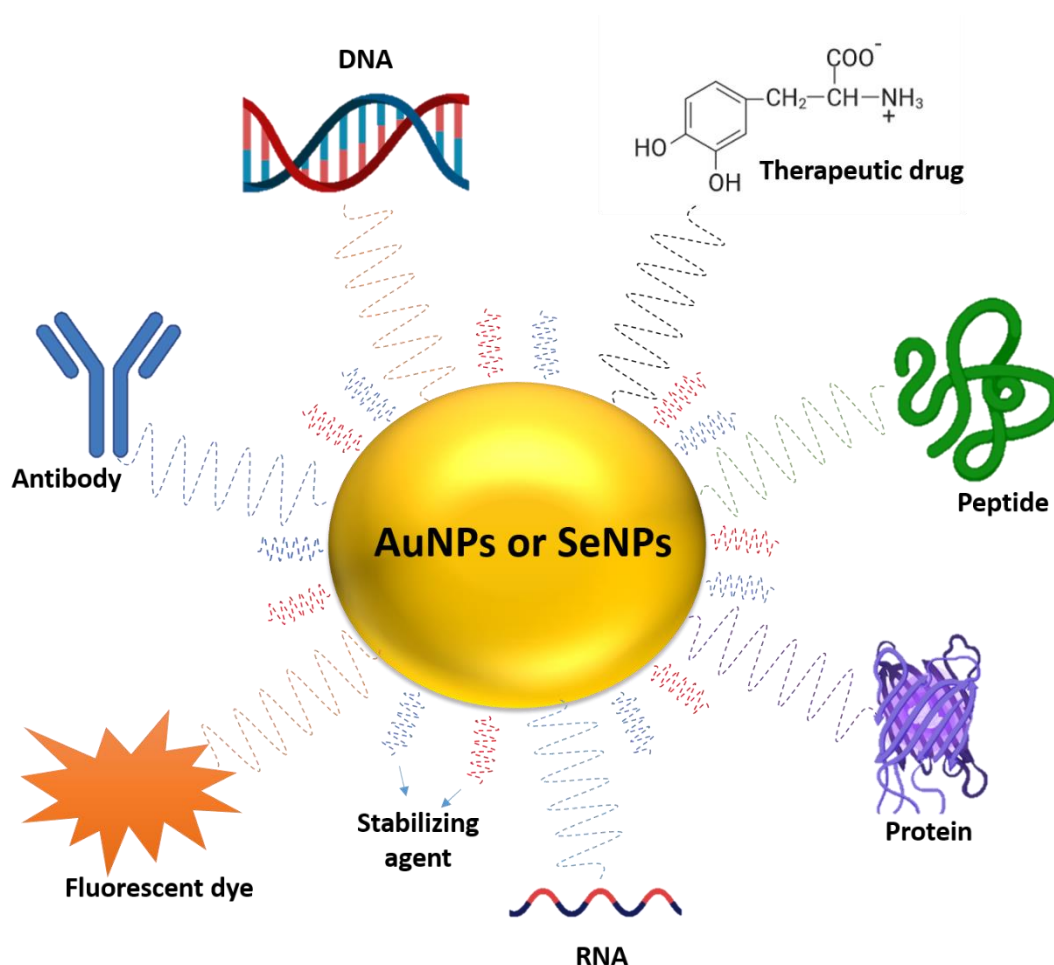


**Figure 3.** Functionalization strategies for AuNP and SeNP (created with BioRender.com).

Examples of BBB-targeting moieties that have been used to functionalize AuNP and SeNP include amphipathic peptide LPFFD directed against the transferrin receptor, which is highly expressed on the endothelial cells of the BBB.<sup>7,104</sup> The authors have additionally attached peptides, THRPPMWSPVWP and TGN, to improve transferrin receptor recognition and facilitate transcytosis of AuNP and SeNP through the BBB, respectively.<sup>7,104</sup> Basically, AuNP and SeNP could be functionalized with transferrin in order to target transferrin receptors, but this approach should be avoided for *in vivo* applications since high endogenous concentrations of transferrin in plasma can induce an overdose of iron. Moreover, the anti-transferrin receptor monoclonal antibody (OX26) on the surface of SeNP showed an improvement in targeted transport via transferrin receptor-mediated endocytosis and may also promote neuronal survival by targeting various cellular signaling pathways.<sup>104,125</sup> Although antibodies coupled to NP offer advantages such as ligand specificity and stability, they have limitations such as poor cell penetration due to their large size. Alternatively, NP can be functionalized in order to target other receptors present on the BBB. For instance, AuNP functionalized with insulin targeted insulin receptor or when functionalized with apolipoprotein E (ApoE) can be recognized by density lipoprotein (LDL) receptors and low-density lipoprotein receptor-related protein 1 (LRP-1), thereby facilitating their permeability through the BBB.<sup>7,126</sup> In order to prevent neuroinflammation, a characteristic malfunction in the majority of CNS diseases, a non-toxic diphtheria toxin mutant can be used as a targeting agent to inhibit diphtheria RMT which has been proven to be upregulated under such conditions. In addition, when NP are functionalized with cationic compounds, they can interact with negatively charged lipids of the BBB and promote AMT. For this purpose, cationized serum albumin was used to functionalize AuNP.<sup>7</sup> Alternatively, cell-penetrating peptides (CPP), like SynB vectors, penetratin, and TAT may help enhance BBB transport of NP using the AMT mechanism. These peptides are highly promising for diagnostic and therapeutic use due to their low toxicity and ability to carry a vast range of cargo. Normally, they enter the cells via clathrin-dependent endocytosis, caveolin-dependent endocytosis, or micropinocytosis.<sup>124</sup>

Despite these benefits, targeting specific brain receptors may not always be satisfactory due to the presence of the same or similar receptors in other parts of the body, which may potentially lead to off-target effects, toxicity and side effects. Additionally, it is difficult to achieve a high enough concentration of NP in the brain to have a therapeutic effect, and the BBB may also clear NP through efflux transporters. Therefore, more research

is needed to optimize the design of BBB-targeted NP and to develop more effective delivery strategies.

## 2.6. Conjugation strategies of AuNP and SeNP with drugs

The conjugation of AuNP and SeNP with drug molecules has the potential to enhance delivery efficacy, may be synergistic, and decrease their toxicity while overcoming severe adverse effects induced by conventional chemotherapeutic drugs on normal cells. Drug loading can either be achieved through covalent or non-covalent methods. Covalent methods use chemically bonded links, while non-covalent drug delivery encompasses most other methods including hydrophobic, electrostatic, hydrogen bonding, and steric immobilization. Additionally, these typical methods can be further categorized into surface-mediated or encapsulation techniques. Notwithstanding these classifications, both covalent and non-covalent drug binding require ideal loading sites on the nanosurface and a minimal impediment to diffusion from the nanocarriers upon reaching the target site. In the case of non-covalent drug loading, binding is influenced by the environment close to the NP, which is susceptible to physical forces, while the type of reaction during covalent binding is determined by the drug and nanosurface structure. In order to initiate covalent binding, linkers are required. For this purpose, the nanosurface can be modified with molecules that could promote chemical conjugation with certain drug moieties or vice versa, i.e., linkers that are prone to be bound to the nanosurface could be attached to drug molecules.<sup>127</sup>

AuNP and SeNP are usually functionalized with thiols or, to a lesser extent, amines, cyanides and hydroxyl groups. Therefore, amine-carboxyl, thiol-maleimide and thiol-thiol are the most common reactions used in the NP-drug chemical conjugation, generating amide, thioether or disulfide as covalent linkage.<sup>128</sup> For example, the anticancer drug, doxorubicin (DOX), was attached to AuNP through Au-disulfide interactions using a pH-sensitive linker. Additionally, drug molecules modified with thiol can be immobilized directly to gold nanosurface using a thiol-Au covalent interaction.<sup>129</sup> In general, when drug molecules are covalently bounded to metal NP, it is crucial but not particularly easy to break the strong covalent bond between them and enable the active site of the drug to be released and function efficiently. Additionally, a large number of enzymes found in blood serum may disrupt the covalent bond between a metal and a ligand. Consequently, for targeted therapy, the creation of drug-delivery nanosystems through noncovalent interaction might be the better choice, as

long as they possess sufficient stability to reach the targeted site after *in vivo* administration.<sup>130</sup> Indeed, non-covalent drug loading on NP is widely documented in the literature. Regarding AuNP and SeNP, anticancer therapeutics like phthalocyanine, tamoxifen, dexamethasone and penicillamine have been attached to the nanosurface mainly due to noncovalent interactions such as hydrophobic and electrostatic interactions while dopamine was bound primarily via hydrogen and van der Waals bonding.<sup>127,131–133</sup>

In order to provide efficient loading, the attachment of drugs to the NP carrier is a crucial step in both covalent and non-covalent drug loading methodologies. Accessible binding sites and drug diffusion are significant limiting factors for drug loading efficiency, but are not the only ones. For drugs that are covalently bound, the binding sites must be accessible and free of any potential barriers, such as high electrostatic repulsion or dense and rigid coatings with small pore sizes. By contrast, non-covalently bound drugs need to diffuse to the surface during loading while the target environment should be accessible both kinetically and thermodynamically during delivery. To determine loading efficiency, it is crucial to determine the ratio between free and bound drugs. Purifying the conjugates can present various challenges. For instance, it is widely recognized that AuNP and SeNP can effectively quench the fluorescence of drug molecules, and this has been utilized to determine not only the relative amount of bound drug by comparing absorption and fluorescence spectra but also to monitor drug release and also to reveal the nature of binding processes and thermodynamic parameters.<sup>127</sup> Localized surface plasmon resonance (LSPR) spectroscopy, dynamic light scattering (DLS), and isothermal titration calorimetry (ITC) are some additional techniques used to study the binding kinetics and affinity of NP towards small molecules conjugated to their surface.<sup>134</sup>

## 2.7. Crossing the BBB with AuNP and SeNP

### 2.7.1. Cellular uptake mechanism of AuNP and SeNP

Different strategies have been developed to enhance the passage of NP across the BBB by utilizing the various physiological mechanisms involved in this process. BBB passage using a paracellular pathway can be achieved by the disruption of the tight junctions between neighboring endothelial cells. To breach the tight junctions, various mechanisms such as the administration of osmotic solutions or the application of a physical stimulus such as ultrasound have been used. However, this method carries some risks as it could result in an

uncontrolled influx of many substances into the brain, compromising the BBB's homeostatic function and potentially causing cerebral toxicity. Another approach is the transcytosis pathway which enhances the binding of NP to the surface of endothelial cells through two distinct mechanisms (AMT and RMT). In both cases, the surface of NP needs to be decorated in a way to facilitate their binding to the luminal plasma membrane of endothelial cells. As mentioned above, AMT occurs more likely when NP are positively charged compared to neutral or negatively charged, as the plasma membrane of endothelial cells has a negative charge. On the other hand, RMT involves NP that are decorated with various ligands on their surface and can bind specific receptors, resulting in endocytosis. A variety of functionalizing options regarding AuNP and SeNP with BBB targeting have been described above (Section 2.6).

Transcytosis begins with the uptake of NP through endocytosis, a process in which endocytic vesicles are formed from invaginations of the plasma membrane, allowing the internalization of extracellular substances. It is a complicated mechanism that involves various components, including receptors and diverse signaling pathways. There are three primary paths for NP endocytosis: macropinocytosis, clathrin- and caveolae-mediated endocytosis. After entering the cell, clathrin-coated vesicles merge to form an early endosome, which matures into a late endosome as the intravesicular pH decreases, before eventually fusing with lysosomes, resulting in the degradation of its contents. In order to effectively deliver cargo, NPs must escape from the endosomes before they fuse with lysosomes, thus avoiding degradation. During caveolin-mediated endocytosis, caveolin vesicles fuse with other caveolin vesicles generating caveosomes, which can sometimes escape lysosomal degradation. However, at times transport into acidic lysosomes can serve as a foundation for designing nanotherapeutics that have acid-activated release properties. Macropinocytosis does not use lipid rafts or pit-forming proteins but forms a large vesicle (0.2–5  $\mu\text{m}$ ) that captures a significant amount of extracellular fluid. This process is nonspecific but it is important in the uptake of larger NPs that otherwise would not be possible to enter by the other two endocytosis processes.<sup>135,136</sup>

### 2.7.2. *In vitro* BBB models for permeability of AuNP and SeNP

Several *in vitro* models of both healthy and pathological human BBB have been developed in order to study and predict BBB permeability. Ideally *in vitro* BBB models should meet



various criteria, including simplicity, low cost, close approximation to *in vivo* conditions, and ability to function in high-throughput screening. The majority of BBB models in the current literature are based on *in vitro* monolayers of brain cells, such as endothelial cells.<sup>137</sup> Typically, transportation through cell monolayers has been conducted using transwell inserts, which are composed of an upper (apical) chamber, a cell-lined permeable membrane, and a lower (basolateral) chamber. By administering a treatment into the upper chamber, transportation can be measured from the apical to the basolateral direction. The treatment passes through the cell monolayer and porous membrane before being collected in the lower chamber for quantifying the transported materials. There are several methods to confirm the formation of a permeability barrier on transwells, such as the transendothelial electrical resistance (TEER) test and paracellular transport assays. Furthermore, the permeable filter on which the cells are grown can be taken out for imaging analysis (e.g. fluorescence, confocal, electron microscopy) to further validate the cell monolayer model and understand the transport mechanism.<sup>138</sup> Human brain microvascular endothelial cells (HBMECs) obtained from human brain tissue are primarily employed in such models. These cells are directly obtained from the target brain tissue and their protein expression specific to the cell type can be thoroughly analyzed. One disadvantage of using primary human brain cells is the uncertain long-term behavior of individual cells grown in a 2D culture and the lack of freezing protocols for extended use. To overcome these issues, immortalized cell lines have been created, especially for brain endothelial cells.<sup>139</sup> Amongst others, the bEnd3 immortalized mouse brain endothelial cell line has been widely used in *in vitro* BBB models, especially for the investigation of BBB crossing by SeNP and AuNP.<sup>72,140–142</sup> However, during the immortalization process, these cells may lose their barrier integrity, making them unsuitable for accurately reproducing the distinct characteristics of the BBB.<sup>139</sup> Moreover, the addition of other BBB cell types, such as astrocytes and pericytes, has led to the creation of co-culture transwell systems that showed stronger barrier properties, as indicated by higher TEER and lower permeability compared to single-cell transwell systems. There are also more sophisticated BBB models, such as spheroid or microfluidic models, that provide a more accurate representation of the *in vivo* environment.<sup>143</sup> In this work, both acellular and cellular *in vitro* BBB models were used to assess the permeation of functionalized NP.

## § 3. MATERIALS AND METHODS

### 3.1. Materials

#### 3.1.1. *Materials used for NP synthesis*

The following chemicals were used for NP synthesis: hydrogen tetrachloroaurate trihydrate ( $\text{HAuCl}_4 \times 3\text{H}_2\text{O}$ , Mr 393.83 g/mol, cat. no. 520918), 3,4-dihydroxy-L-phenylalanine (levodopa, Mr 197.19 mg/L, cat. no. D9628), dopamine hydrochloride (Mr 189.64 g/mol, cat. no. H8502), 1-adamantylamine hydrochloride (Ad, Mr 187.71, A1260), sodium selenite ( $\text{Na}_2\text{SeO}_3$ , Mr 172.94, cat. no. 214485), Tween 20 (cat. no. P1379), sodium dodecyl sulfate (SDS), and poly(ethylene glycol) methyl ether thiol (mPEGthiol, Mr 6 000, cat. no. 729159) were purchased from Sigma-Aldrich Chemie GmbH (Munich, Germany) while, L-(+)-ascorbic acid (Mr 176.12, cat.no. A15613) and trisodium citrate dihydrate (Mr 294.10, cat. No A12274) were purchased from Alfa Aesar (Kandel, Germany). Alpha-thio-omega-(propionic acid) octa(ethylene glycol) ( $\text{HS-EG}(8)\text{-(CH}_2\text{)}_2\text{-COOH}$ , Mr 458.57 g/mol, cat. no. 866889-02-3) was obtained from Iris Biotech GmbH (Germany) while poly (vinylpyrrolidone) (PVP, Mr 40,000 g/mol, cat. no. 5295), and sodium borohydride ( $\text{NaBH}_4$ , Mr 37.83 g/mol, cat. no. 806373) was purchased from Merck Suprapur (Darmstadt, Germany). Sodium hydroxide ( $\text{NaOH}$ , Mr 40.00 g/mol, cat. no. 1452506), hydrochloric acid ( $\text{HCl}$ , Mr 36.46 g/mol, cat. no. 182430), and nitric acid ( $\text{HNO}_3$ , Mr 36.01 g/mol, cat. no. 452201) were purchased from Kemika (Zagreb, Croatia). Peptidoglycan monomer GlcNAc-MurNAc-L-Ala-D-isoGln-mesoDAP( $\epsilon\text{NH}_2$ )-D-Ala-D-Ala (PGM) was prepared in PLIVA, Chemical and Pharmaceutical Works (Zagreb, Croatia) by the method described in the literature,<sup>144</sup> whereas 1-adamantyl-glycine (AdGly) was prepared in our laboratory according to previously described procedures.<sup>145</sup> Before use, all glassware was cleaned with aqua regia ( $\text{HCl}:\text{HNO}_3$ , 3:1 v/v) and rinsed with ultrapure water (UPW).

#### 3.1.2. *Materials used for examination of the interaction between NP and proteins*

BSA (Mr 66,000 g/mol, cat. no. A2153, lot SLBS1213V) was purchased from Sigma-Aldrich Chemie GmbH (Munich, Germany) while glycosylated transferrin isolated from human serum (hTF, Mr 77 000 g/mol, cat. no. pro-315-b, lot 518PHTF28) was purchased from ProSpec Bio (Rehovot, Israel). BSA and hTF were dissolved in 2 mL of UPW to a final concentration of 100  $\mu\text{M}$ . Then the protein solutions were aliquoted and stored at  $-20^\circ\text{C}$ . Before carrying out

the experiments in which the interactions between proteins and NPs were examined, the specified aliquots were dissolved and diluted with UPW to a certain concentration depending on the applied method.

### 3.1.3. Materials used for NMR experiments

Deuterium oxide ( $D_2O$ , Mr 20.03 g/mol, cat. no. 151882) and sodium deuterioxide 40% solution in  $D_2O$  ( $NaOD$ , Mr 41.00 g/mol, cat. no. 372072) were purchased from Sigma-Aldrich Chemie GmbH (Munich, Germany), while deuterium chloride 20% solution in  $D_2O$  (cat. no. 815016) was purchased from Merck Suprapur (Darmstadt, Germany).

### 3.1.4. Other materials

Plastic accessories were purchased from Sarstedt (Antwerpen, Belgium), and glass from Schott (Mainz, Germany). For all dilutions, UPW as ASTM Type I product water with an electrical conductivity of  $0.055 \mu S/cm$  was employed using Pure Water System OmniaTap 6 water purification system (Stakpure GmbH, Niederahr, Germany).

## 3.2. Synthesis of AuNP and SeNP

### 3.2.1. Preparation of differently coated AuNP

For both Ad-AuNP and AdGly-AuNP, the same synthetic procedure was employed. Initially, 1 mL of 10 mM  $HAuCl_4 \times 3H_2O$  and 20  $\mu L$  of 1.0 M NaOH were mixed to give **solution 1**. Then, 0.75 mL of **solution 1** and 1 mL of 0.83 mM 1-adamantylamine hydrochloride or 0.53 mM 1-adamantyl-glycine were added to 6.5 mL of UPW, respectively. A 0.5 mL aqueous solution of 15 mM  $NaBH_4$  was then added while stirring. After the addition of  $NaBH_4$ , the colour of the mixture turned from pale yellow to wine red. After allowing the mixture to stir at room temperature for 1.5 h, the synthesized Ad-AuNP were centrifuged twice at 8 000 rpm for 10 min, whereas AdGly-AuNP were centrifuged twice at 10 000 rpm for 20 min. The pellet was resuspended in UPW and stored in the dark at  $4^\circ C$ .

AuNP-PGM was prepared via the reduction of  $HAuCl_4 \times 3H_2O$  by  $NaBH_4$  and functionalized by PGM. Briefly, 1.5 mL of 10 mM  $HAuCl_4 \times 3H_2O$  and 1 mL of 0.12 mM PGM were added to 6.5 mL of UPW. A 0.5 mL aqueous solution of 15 mM  $NaBH_4$  was then added dropwise while stirring. After the addition of  $NaBH_4$ , the colour of the mixture turned from pale yellow to dark purple. After allowing the mixture to stir at room temperature for 20

min, the synthesized AuNP were centrifuged at 7 000 rpm 2 times for 10 min. The pellet was resuspended in UPW and stored in the dark at 4°C.

### 3.2.2. Seed-mediated preparation of AuNP

As outlined by Hernandez *et al.*<sup>146</sup>, the synthesis of PEG-coated AuNP was performed using a modified citrate reduction method. First, 79.5 mg of  $\text{HAuCl}_4 \times 3\text{H}_2\text{O}$  was dissolved in 183 mL of UPW and heated under constant stirring and reflux. When the solution started to boil, 5 mL of 164 mM sodium citrate dihydrate was added. The mixture was kept boiling for 30 min until the solution colour changed to wine red, whereupon the citrate-functionalized AuNP (citAuNP) were cooled down and kept at 4°C in the dark. Then, a mixture containing citAuNP (10 nM), SDS (0.028%), HS-EG(8)-COOH (52  $\mu\text{M}$ ), and NaOH (25 mM) was prepared in a total volume of 50 mL. The mixture was incubated for 16 h at room temperature. The excess PEG chains were removed by centrifugation at 14 000 rpm for 30 min at 4°C and the supernatant discarded. This washing process was repeated three times, the PEG-AuNP pellets were resuspended in UPW and kept at 4°C in the dark.

Catechol-functionalized AuNP were also prepared in two steps according to Ong *et al.*<sup>93</sup> with some modifications. First, 14 nm spherical citAuNP were prepared by chemical reduction of  $\text{HAuCl}_4$  with sodium citrate dihydrate at 100°C. Briefly, 11.8 mg of  $\text{HAuCl}_4 \times 3\text{H}_2\text{O}$  was dissolved in 100 mL UPW and heated under reflux and constant stirring. When the solution was brought to a boil, 300  $\mu\text{L}$  of 388 mM sodium citrate dihydrate was rapidly added. The reaction was allowed to proceed for 30 min until the solution attained a wine-red color and the citAuNP were then cooled down and kept at 4°C in the dark. Different molar ratios of catechols and  $\text{HAuCl}_4$  were tested to design catechol-functionalized AuNP using 100  $\mu\text{L}$  of 0.1 M  $\text{HAuCl}_4 \times 3\text{H}_2\text{O}$ , 144  $\mu\text{L}$  of 0.38 mM citAuNP, 400  $\mu\text{L}$  of 1.7 mM mPEG thiol, and 4 mL of various concentrations of catechols in a total volume of 50 mL under vigorous stirring. The concentration of  $\text{HAuCl}_4$  was kept constant, while the concentration of levodopa or dopamine was adjusted to obtain the following molar ratios:  $[\text{Au}]:[\text{catechol}]=1:6$ ;  $[\text{Au}]:[\text{catechol}]=1:1$ ;  $[\text{Au}]:[\text{catechol}]=2:1$ ;  $[\text{Au}]:[\text{catechol}]=6:1$ . After 2 hours of stirring, AuNP were pelleted by centrifugation at 800 g for 10 minutes and kept at 4°C in the dark.

### 3.2.3. Preparation of SeNP

SeNP were prepared using the classical reduction method with two different stabilizing agents, PVP and Tween 20. PVP-functionalized SeNP (PVP-SeNP) were prepared according to previously published papers with some modifications.<sup>147,148</sup> Initially, 10 mL of 1 wt. % aqueous solution of PVP was added to 77.9 mL of UPW and stirred at 500 rpm for 15 min. Then, 11 mL of 0.1 M L-ascorbic acid and 1.1 mL of 0.1 M sodium selenite were added under constant stirring. After the addition of sodium selenite dropwise, the colour of the mixture turned gradually from clear white to clear red. After stirring for 20 min, the mixture was centrifuged for 15 min two times at 10000 rpm. The pellet was resuspended in UPW and stored at 4°C.

Tween 20-functionalized SeNP (Tween-SeNP) were synthesized as previously described by Vahdati *et al.*<sup>117</sup> Briefly, 1.74 mL of 0.1 M sodium selenite solution was added to 90 mL of UPW. While stirring continuously, 10 mL of 56.7 mM L-ascorbic acid was added dropwise to the selenite solution. After each 2 mL of the ascorbic acid solution, 10 µL of Tween 20 was added. The colour of the reaction mixture turned from clear white to clear red after 20 min. Synthesized SeNP were then centrifuged twice at 12 000 rpm for 10 min. The pellet was then resuspended in UPW and stored at 4°C.

## 3.3. Characterization of AuNP and SeNP

AuNP and SeNP were characterized by determining their shape, size, size distribution, zeta ( $\zeta$ ) potential, optical properties, chemical composition and concentration in suspension.

Transmission electron microscopy (TEM) was used for the visualization of AuNP and SeNP and for the determination of their primary diameter ( $d_{\text{TEM}}$ ) and degree of aggregation/agglomeration. TEM is one of the most commonly used techniques in nanotechnology, and has been successfully applied to examine the properties of metal NP.<sup>149</sup> The sample preparation for this technique was carried out by diluting NP suspensions with UPW to a concentration of 10 mg metal/L. A volume of 5 µL of the suspension was dropped onto copper grids coated with Formvar® polymer (SPI Supplies, West Chester, USA), and allowed to air dry. After drying, the samples were imaged with a bright-field TEM (Carl Zeiss Meditec AG, Jena, Germany) at an accelerating voltage of 80 kV. Images were taken at magnifications of 50,000 to 140,000 times using a Canon PowerShot S50 camera connected to the instrument. In total, 100 particles were taken into consideration to measure the primary

diameter for each type of NP using the ImageJ software (National Institutes of Health, Bethesda USA).

Size distribution and NP stability were investigated using the DLS technique. The basic principle of this method relies on the random movement of the particles in the solution, which is called Brownian motion and depends on particle size. Small particles move quickly while large particles move slower. The particles scatter the light when they are illuminated by a light source (e.g. laser). The initial intensity trace is further used to generate a correlation function which can be used to calculate the size distribution.<sup>150</sup> This technique, unlike TEM, is non-destructive and does not require sample drying. However, it does not measure the actual NP diameter, but the hydrodynamic diameter ( $d_H$ ).  $d_H$  can be defined as the diameter that includes the NP size and the solvation shell formed around the particle in the medium, which moves with it as a whole.<sup>150</sup> It determines the diameter of a hypothetical sphere that diffuses at the same speed as the measured particle. Although it is not the actual size of the NP, its determination is essential as it reflects the behaviour of the NP in the medium. The samples for the measurement were diluted in UPW to a concentration of 10 mg metal/L. A volume of 1 mL of the sample was pipetted into a disposable plastic cuvette (Sarstedt, Nümbrecht, Germany). All measurements were performed on a Zetasizer Nano ZS instrument (Malvern Instruments, Malvern, UK), which was equipped with a green laser (532 nm), and the detection of scattered radiation was performed at an angle of 173° at a temperature of 25°C. DLS results were reported as the average values of the size-intensity distribution function of 6 consecutive measurements. Data processing was performed in Zetasizer software 6.32 (Malvern Instruments, Malvern, UK).

The electrophoretic light scattering (ELS) method, which is based on determining the electrophoretic mobility of the NP, was used to determine their  $\zeta$  potential. It can be defined as the potential on the shear plane between the particle and the solution. When a particle that has a surface charge is dispersed in a suspension, it attracts ions of the opposite charge to its surface, resulting in the formation of an electrical double layer. The double layer consists of a Stern layer and a diffusion layer. Inside the diffusion layer, there is an imaginary boundary, a shear plane or a sliding plane where the particle and ions form a stable unit. When the particle moves, the ions move along with it. The potential on that plane is called the  $\zeta$  potential and its value indicates the stability of the colloidal system, i.e., electrostatic stabilization.<sup>151</sup> NP that have a large absolute value of the  $\zeta$  potential (either positive or negative) will be repelled

during a collision and their aggregation or agglomeration will not occur. In general, NPs are declared electrostatically stabilized if their absolute value of  $\zeta$  potential is greater than 30 mV.<sup>152</sup> All NP samples were measured after dilution in the tested medium to a concentration of 10 mg metal/L. The samples were pipetted into special cuvettes for ELS measurements (Malvern Instruments, Malvern, UK) with a total volume of 1 mL. All measurements were performed on a Zetasizer Nano ZS instrument (Malvern Instruments, Malvern, UK). Henry's equation with the Smoluchowski approximation was used to calculate the  $\zeta$  potential. Data processing was performed using the Zetasizer program, version 6.32 (Malvern Instruments, Malvern, UK). The results are expressed as the average value of 3 consecutive measurements with standard deviation.

Metal concentration in AuNP and SeNP solution was determined by atomic absorption spectroscopy (AAS) and expressed as mg Au/L or mg Se/L. AAS is a standard method for elemental analysis, which is based on the property of atoms to absorb electromagnetic radiation of precisely defined wavelengths. Absorbance follows the Beer-Lambert law, i.e., it is linearly dependent on the concentration of atoms.<sup>153</sup> An AAnalyst 600 instrument (Perkin Elmer, Shelton, USA) with a graphite furnace was used for the measurements. Cathode lamps were used for Au and Se, at wavelengths of 268 nm and 196 nm, respectively. The metal concentration in each sample was calculated from the calibration curve showing the linear correlation between the concentration and the absorbance of the sample. The calibration curve was made at the beginning of each working day by determining the absorbance of standard Au or Se solutions of known concentration. Calibrators were prepared by diluting standard Au or Se solutions (1000 mg metal/L in 5% HNO<sub>3</sub>, Merck, Darmstadt, Germany) in 1% (v/v) HNO<sub>3</sub>, ranging in concentration from 50 to 500  $\mu$ g Au/L for AuNP or from 1 to 20  $\mu$ g Se/L for SeNP. The calibration curve was determined using 6 calibration points and was considered acceptable when the correlation coefficient  $R^2$  was  $> 0.995$ . The samples were prepared by diluting in 1% (v/v) HNO<sub>3</sub> 100 to 250 thousand times and pipetted into polystyrene cups with a volume of 1 mL. The measured metal concentrations in the samples were used to calculate the AuNP and SeNP concentrations, as described in the next chapter.

The optical features of metallic NPs rely on their SPR properties, which results from the oscillation of free electrons in the conduction band of the metal. Metal NPs absorb radiation whose wavelength corresponds to the oscillation frequency. The absorbance intensity and peak wavelength depend on the NP characteristics and the refractive index of the

medium.<sup>154</sup> The SPR for the tested NP was determined by the UV/Vis spectroscopic method on a CARY 300 spectrophotometer (Varian Inc., Melbourne, Australia), using a quartz cuvette with an optical path length of 1 cm, in the wavelength range of 200-800 nm. All measurements were performed at 25°C. The samples were diluted to a concentration of 10 mg metal/L in UPW.

All pH measurements were performed using a Thermo Scientific Orion Star A214 Benchtop pH/ISE Meter (Waltham, USA) equipped with a glass electrode and Ag-AgCl reference electrode. The pH meter and electrode were calibrated prior for each experiment using Orion™ pH buffer solutions (Lexington, USA) of pH 4.01, 7.01, and 10.01.

### 3.4. Calculation of NP concentration

From the obtained metal concentration in the NP suspensions, the NP molar concentrations were calculated using the following equation:

$$c(\text{NP}) = \frac{c(\text{metal}) \times Ar}{m(\text{NP}) \times N_A} \quad (1)$$

where  $c(\text{NP})$  is the molar concentration of NP,  $c(\text{metal})$  is the molar concentration of Au or Se obtained by AAS measurements as previously described,  $Ar$  is the atomic mass of Au (196.97 g/mol) or Se (78.96 g/mol),  $m(\text{NP})$  represents the mass of one NP and  $N_A$  is Avogadro's number ( $6.022 \times 10^{23} \text{ mol}^{-1}$ ).

The mass of one NP particle is obtained from the following equation:

$$m(\text{g}) = \rho(\text{g nm}^{-3}) \times V(\text{nm}^3) \quad (2)$$

where  $m(\text{NP})$  is the mass of one NP,  $\rho$  is the density of Au ( $1.93 \times 10^{-20} \text{ g/nm}^3$ ) or Se ( $4.79 \times 10^{-21} \text{ g/nm}^3$ ) and  $V(\text{NP})$  is the volume of one particle.

Considering the spherical shape of the NP, the volumes of NP were calculated based on the formula for the volume of a sphere using the following equation:

$$V = \frac{4 \times r^3 \times \pi}{3} \quad (3)$$

where  $V(\text{NP})$  is the volume of one NP,  $r$  represents the radius of the spherical NP calculated as half of the  $d_{\text{TEM}}$  obtained from TEM images.<sup>155</sup>



### 3.5. Determination of the binding mechanism of levodopa and dopamine to differently coated AuNP and SeNP

#### 3.5.1. Steady-state fluorescence measurement

Fluorescence spectroscopy is a type of luminescence that analyzes the fluorescence properties of molecules.<sup>156</sup> Before determining the binding constants ( $K$ ) between NPs and catechols/proteins, preliminary measurements were performed to define the optimal experimental conditions to avoid the inner-filter effect. This effect involves the absorption of excitation or emission radiation by the analyte in the sample and consequently affects the accuracy of the fluorescence results. Absorption of the excitation radiation is called primary, while absorption of the emission radiation is called the secondary effect of the inner-filter.<sup>157</sup> Absorbance of excited or emitted light causes spectral distortions, which lead to a non-linear relationship between fluorescence intensity and concentration. The test was performed in a way that the excitation and emission spectra of the NP themselves were measured in the concentration range mentioned in Table 2. The excitation and emission slit widths were set to 5.0 and 10.0 nm, respectively. The NP samples were pipetted into a quartz cuvette with an optical path length of 1 cm and a total volume of 2 mL. The emission spectra of NPs were recorded after excitation at a wavelength of 280 nm in the wavelength range from 200 to 450 nm. Excitation spectra of NPs were recorded in the range from 200 to 290 nm, with the emission wavelength set at 317 and 350 nm, respectively. After measuring the excitation and emission spectra, the fluorescence intensity of NPs at 280 nm (wavelength of levodopa, dopamine and proteins excitation), 317 nm (wavelength of maximum levodopa and dopamine fluorescence intensity) and 350 nm (wavelength of maximum protein fluorescence intensity) was read, and a curve of the relationship between these values and NP concentration was plotted. A value of the correlation coefficient ( $R^2$ ) greater than 0.95 was a condition for confirming the linearity of the relationship between fluorescence and concentration. When the observed fluorescence intensity was not linearly related to the concentration of NP or when fluorescence drops with concentration increase, an inner-filter correction<sup>158</sup> was made to the fluorescence intensities using the following equation:

$$F_{obs} = F_{corr} \times 10^{\frac{-A_{ex} \times d_{ex}}{2} - \frac{-A_{em} \times d_{em}}{2}} \quad (4)$$

where  $F_{\text{obs}}$  and  $F_{\text{corr}}$  present the observed and corrected fluorescence intensities, respectively;  $A_{\text{ex}}$  and  $A_{\text{em}}$  were the absorbance value of AuNP and SeNP at the excitation and emission wavelength, respectively;  $d_{\text{ex}}$  and  $d_{\text{em}}$  were the cuvette path length in the excitation and emission direction (in cm), respectively.<sup>159</sup>

During interactions between fluorophores (levodopa, dopamine, BSA and hTF) and NPs, fluorophore fluorescence is quenched depending on the concentration of NPs. Quenching of fluorescence in the equilibrium state (steady state fluorescence quenching) is a common method for determining binding constants between molecules.<sup>160</sup> There are different mechanisms of fluorophore fluorescence quenching in the presence of quenchers, among which static and dynamic quenching are the most common. Static quenching mechanism occurs as a result of the formation of a non-fluorescent ground-state complex between the fluorophore and quencher.<sup>160</sup> On the other hand, the dynamic mechanism results from diffusive encounters between the fluorophore and quencher during the lifetime of the excited state. By exciting the fluorophore using electromagnetic radiation of a certain wavelength, electrons in a higher energy state transfer part of the energy to the quencher. Such energy transfer is known as fluorescence resonance energy transfer (FRET), whereby a molecule that is excited transfers energy to another molecule in an excited state, which then emits a low-energy photon, or loses energy in the excited state through vibrational relaxation or in the form of heat.<sup>156,161</sup> Moreover, two quenching mechanisms can be distinguished by their differing dependence on temperature and viscosity, or preferably by time-resolved measurements (see in the next chapter).

The fluorescence quenching can be described by the Stern-Volmer equation, which provides information on the binding constants ( $K$ ) and the number of binding sites ( $n$ ), also called the Hill coefficient. The model is applied to examine interactions between NPs and fluorophores because it is simple and sensitive, and the principles of the method are well-known.<sup>162</sup>

Fluorescence spectra were recorded on Agilent Cary Eclipse fluorescence spectrophotometer (Agilent Technologies, Santa Clara, USA) using a quartz cuvette (Hellma Optician GmbH, Jena, Germany) with an optical path length of 1.0 cm. Quenching of levodopa and dopamine intrinsic fluorescence was evaluated after the addition of increasing concentrations of AuNP and SeNP, while the fluorophore concentration was kept constant (15  $\mu\text{M}$  levodopa, 25  $\mu\text{M}$  dopamine, 0.5  $\mu\text{M}$  BSA, and 2.5  $\mu\text{M}$  hTF), respectively. Additionally,

0.1  $\mu\text{M}$  BSA was added to evaluate its impact on levodopa or dopamine binding to different AuNP, while 0.5  $\mu\text{M}$  hTF was used to investigate the binding affinities of differently coated SeNPs with levodopa or dopamine. NP concentrations were selected in order to avoid the inner-filter effect and are listed in Table 2.

**Table 2.** Concentration range of NP used for fluorophore quenching measurements and for inner-filter effect testing.

NP type	Concentration range
<b>PEG-AuNP</b>	0.04-0.68 nM
<b>Ad-AuNP</b>	0.01-0.14 nM
<b>AdGly-AuNP</b>	0.01-0.08 nM
<b>PGM-AuNP</b>	0.01-0.17 nM (for levodopa and dopamine) 0.01-0.12 nM (for BSA)
<b>PVP-SeNP</b>	0.21-2.60 pM
<b>Tween-SeNP</b>	0.72-9.04 pM

The samples were pipetted into 2 mL tubes in the following order: UPW, NP solution and fluorophore solution, and the reaction mixture was incubated for 10 min at 288 K, 298 K, and 308 K. The excitation and emission slit widths were set to 5.0 and 10.0 nm, respectively. The fluorescence emission spectra were recorded in the range from 290 to 450 nm with the excitation wavelength set at 280 nm. The results were processed using the Stern-Volmer equation:

$$\frac{F_0}{F} = 1 + k_q \tau_0 c (\text{NP}) = 1 + K_{\text{SV}} c (\text{NP}) \quad (5)$$

where  $F_0$  and  $F$  are the fluorescence intensities in the absence and presence of NP, respectively;  $k_q$  is the bimolecular quenching constant;  $\tau_0$  is the lifetime of the fluorophore in the absence of NP,  $c (\text{NP})$  is the molar concentration of NP; and  $K_{\text{SV}}$  is the Stern-Volmer quenching constant.<sup>156,162</sup>  $c (\text{NP})$  was obtained from equation (1) as described in Chapter 3.4.

Moreover, the binding constant and the number of binding sites for fluorophore-NP interactions were calculated using the Hill equation<sup>131</sup>:

$$\log\left(\frac{F_0 - F}{F}\right) = \log K + n \log c(\text{NP}) \quad (6)$$

where  $F_0$  and  $F$  are the fluorescence intensities in the absence and presence of NP, respectively;  $K$  is the binding constant;  $n$  (Hill coefficient) is the number of binding sites, and  $c(\text{NP})$  is the molar concentration of NP.

The obtained  $K$  values at a corresponding temperature of  $T$  (K) can serve for calculating thermodynamic parameters, such as enthalpy change ( $\Delta H^0$ ) entropy change ( $\Delta S^0$ ) and Gibbs free energy change ( $\Delta G^0$ ) by using the van't Hoff's expression and Gibbs–Helmholtz equation as follows:

$$\ln K = -\frac{\Delta H^0}{RT} + \frac{\Delta S^0}{R} \quad (7)$$

and

$$\Delta H^0 = \Delta G^0 - T\Delta S^0$$

(8)

where  $R$  is the gas constant ( $8.31 \text{ JK}^{-1}\text{mol}^{-1}$ ).

### 3.5.2. Time-resolved fluorescence measurements

Time-resolved fluorescence measurements have been utilized to measure fluorescence intensity decay. The high-speed detection system records the intensity decay on an ns timescale. This method can precisely determine if quenching occurs due to diffusion in excited state or complex formation in the ground state of fluorophores and, thereby, is the most accurate technique for distinguishing the nature of quenching processes.<sup>156</sup> Fluorescence decay of fluorophores was recorded at an emission wavelength of 310 nm at 298 K with and without the addition of PEG-AuNP. Measurement conditions were taken from the protocol for steady-state measurements, as follows: fluorophore concentration (15  $\mu\text{M}$  levodopa, 25  $\mu\text{M}$  dopamine and 0.5  $\mu\text{M}$  BSA) was kept constant, while concentrations of PEG-AuNP were modulated in the range 0.04–0.68 nM. The time-resolved fluorescence measurements were performed using a conventional time-correlated single-photon counting (TCSPC) system equipped with an imaging spectrometer (Andor Kymera 193i spectrograph) and a single-photon hybrid detector (Becker and Hickl HPM-100-07-C). Timed photon events were

acquired using conventional timing electronics (Ortec model 457 time-to-amplitude converter and Ortec 9307 Picotiming constant fraction discriminator (FAST Commtec, MCA-3 multichannel analyzer)). The frequency tripled the output of a cavity-dumped, modelocked Ti:sapphire laser oscillator generated excitation pulses at 280 nm by producing ~100 fs duration pulses at a repetition rate of 5.4 MHz and a wavelength of 840 nm (Coherent Mira 900 with APE PulseSwitch cavity dumper). Spectroscopic data were analyzed by using nonlinear least square iterative reconvolution software (FAST, Edinburgh Instruments Ltd).

### 3.5.3. DLS and ELS measurements

Changes in size and  $\zeta$  potential were examined after interactions of PEG-AuNP, Ad-AuNP, AdGly-AuNP, PGM-AuNP, PVP-SeNP and Tween-SeNP with levodopa and dopamine as well as BSA and hTF, respectively, using DLS and ELS methods. By measuring the mentioned parameters, it is possible to determine the formation of a protein corona and changes in the physical and chemical properties of NP after their interaction with investigated fluorophores. The highest concentration of each NP used in fluorescence measurements was applied here and incubated with fluorophores at concentrations of 15  $\mu\text{M}$  levodopa, 25  $\mu\text{M}$  dopamine, 0.5  $\mu\text{M}$  BSA, and 2.5  $\mu\text{M}$  hTF for 10 minutes in UPW (pH = 5.68) at 298 K. DLS and ELS measurements were performed described in Chapter 3.3.

### 3.5.4. UV-Vis measurements

Changes in SPR peak upon the interaction of different AuNP with levodopa, dopamine and BSA were monitored, taking into consideration that the SPR peak of AuNP is dependent on their shape and size.<sup>163</sup> SeNP were not taken into consideration as their SPR is not as visible. The conditions were maintained as used for DLS and ELS measurements. Measurements were carried out on a CARY 300 spectrophotometer (Varian Inc., Melbourne, Australia), using a quartz cuvette with an optical path length of 1 cm, in the wavelength range of 200-800 nm. All measurements were performed at 285 K.

## 3.6. Calculation of drug-loading efficiency of differently coated AuNP and SeNP

To test the drug-loading efficiency (DLE), AuNP and SeNP were loaded with levodopa/dopamine by incubating three different concentrations of each AuNP and SeNP with a constant concentration of the levodopa (15  $\mu\text{M}$ ) and dopamine (25  $\mu\text{M}$ ). Concentrations of

AuNP and SeNP were recalculated according to their total surface area (SA) using the following equation:

$$\text{total NP SA} = d_{\text{TEM}}^2 \times \pi \times c(\text{NP}) \times N_A \quad (9)$$

where  $d_{\text{TEM}}$  is the diameter of NP obtained from TEM images,  $c(\text{NP})$  is the molar concentration of NP, and  $N_A$  is the Avogadro constant ( $6.022 \times 10^{23} \text{ mol}^{-1}$ ).

The total surface area needs to be the same for each type of NP in order to be able to compare results.

Levodopa and dopamine encapsulation efficiency were studied by separating NPs from the aqueous medium containing free drug by centrifugation through Amicon Ultra-15 Centrifugal Filter Unit (cut-off 50 kDa, Merck) at 5 000 g at room temperature for 20 min. The amount of free levodopa/dopamine was determined from the calibration curve using the Agilent Cary Eclipse fluorescence spectrophotometer (Santa Clara, USA) at the excitation wavelength of 280 nm. The DLE of different NP were calculated using the following equation:

$$DLE (\%) = \frac{(\text{total amount of drug} - \text{free drug})}{\text{total amount of drug}} \quad (10)$$

### 3.7. Investigation of levodopa and dopamine stability during AuNP formation

#### 3.7.1. NMR experiments

NMR is a method developed for examining the structure of compounds based on the magnetic properties of individual atoms, and it can be used to identify and quantify ligands on nanosurfaces, check the purity of coated NPs, detect interactions between NPs and ligands, determine binding affinity, monitor release, etc.<sup>164</sup> Monitoring the interactions of ligands with NPs is possible by NMR spectroscopy due to changes in the chemical environment of ligands when found at the interface of a solution and a solid substance. This can lead to the shift of individual signals, changes in linewidth of spectral lines or even the disappearance of signals.

The chemical shift can change due to binding to different sites and pairing of resonances with the electrons in a conduction band of the metal.<sup>165</sup>

Therefore, NMR spectroscopy offers the ability to monitor structural changes of levodopa and dopamine during their interaction with the gold nanosurface. Due to potential instability and susceptibility to oxidation of the NP, <sup>1</sup>H and <sup>13</sup>C NMR spectra at different time intervals were recorded during the AuNP formation to evaluate the possible formation of oxidation products (e.g. dopaquinone, leukodopachrome, dopaminequinone, leukoaminochrome) at the nanosurface.

Aliquots of reaction mixtures, as well as control solutions, were pipetted into Wilmad<sup>®</sup> NMR glass tubes with a diameter of 5 mm (intended for 400 MHz spectrometers, Sigma Aldrich, Darmstadt, Germany) and D<sub>2</sub>O was added to a final concentration of 10% (v/v). <sup>1</sup>H and <sup>13</sup>C spectra were recorded according to the pulse protocol available in the program package VnmrJ 4.2A. The levodopa and dopamine oxidation was investigated during formation of catechol-functionalized AuNP. <sup>1</sup>H NMR spectra were recorded at different time points after mixing the reagents and until AuNP formation ended (approximately 2 h). Later, the NP were purified by centrifugation, resuspended in D<sub>2</sub>O, and <sup>1</sup>H and <sup>13</sup>C spectra were recorded again to observe the final structural features of catechols bound to the AuNP surface. Contrary to dopamine, levodopa is very difficult to observe easily in <sup>13</sup>C NMR spectra, due to its poor solubility. Therefore, ring-<sup>13</sup>C<sub>6</sub>-labeled levodopa (Cambridge Isotope Laboratories GmbH, Radeberg, Germany) was used. Control spectra of 10 mM levodopa in D<sub>2</sub>O and 10 mM dopamine in D<sub>2</sub>O were used for signal assignment. The stability of both catechols was monitored in a 10 mM D<sub>2</sub>O solution (pD = 3) by recording the spectrum after 7 days. Additionally, the stability of 10 mM levodopa and dopamine was also checked when the pH was raised to 11 and 10 by alkalizing with NaOD, and the spectra were recorded up to 60 and 210 min, respectively. All NMR spectra were recorded at 25°C using a Varian INOVA 400 spectrometer (Varian, Palo Alto, USA) at 399.6 MHz (<sup>1</sup>H) and 100.5 MHz (<sup>13</sup>C). The chemical shifts were expressed in parts per million (ppm) and are referenced to the residual water signal (approximately 4.5 ppm). The WET and PRESAT pulse sequences, available in OpenVnmrJ software (v2.1revA, Inova Varian, Palo Alto, CA, USA), were used in order to suppress the solvent signal, where appropriate. The MestReNova 6.0.2 software package (Mestrelab Research SL, Santiago de Compostela, Spain) was used to process the spectra.

### 3.7.2. Density functional theory calculations

Quantum chemistry starts from the basic laws of quantum physics, i.e., based on solving the Schrödinger equation. The solution of the Schrödinger equation is a set of wave functions and their associated energies, which gives a complete description of the system.<sup>166</sup> One of the methods in quantum chemistry is density functional theory (DFT), which is not based on wave functions but on electron density, from which the physical properties of molecular systems are calculated.<sup>167</sup>

DFT methods were employed to examine the mechanism of catechol interaction with  $\text{Au}_n$  clusters ( $n = 2, 4, 6$ ). Full conformational analysis of levodopa, dopamine, dopaquinone, leukodopachrome, dopaminequinone, leukoaminochrome was conducted with the PC Model software<sup>168</sup> using MMX parameters. The resulting structures were subjected to geometric optimization and frequency calculation. Geometric optimization is the process of finding the structure of the molecule that has the lowest energy (the so-called stationary point on the potential energy surface). Stationary points obtained by geometric optimization were characterized by frequency calculation/vibrational analysis to confirm whether the structure is a minimum (no imaginary frequencies) or a first-order saddle point (one imaginary reference). Also, geometric optimization and frequency calculation together give the values of  $H_{298}$  and  $G_{298}$  for each molecule.<sup>169</sup> In this dissertation, thermal corrections for enthalpy ( $H_{\text{corr}}$ ) and Gibbs energy ( $G_{\text{corr}}$ ) were calculated using the rigid rotor/harmonic oscillator model, at a temperature of 298.15 K (25°C) and a pressure of 1 atm. Upon completion of the calculation, the most stable conformer (global minimum) and several local minima within an energy range of 25 kJ/mol from the global minimum were located and used in further calculations.

The most stable conformers of levodopa, dopamine and their oxidation products (dopaquinone, leukodopachrome, dopaminequinone, leukoaminochrome) were placed in proximity to Au clusters composed of 2, 4 or 6 atoms. The clusters are oriented in different positions and brought into spatial interaction (3 Å) with all functional groups of investigated ligands. For each ligand–cluster combination, about 200 structures were created and subjected to geometric optimization and frequency calculation. The obtained stable complexes were analyzed for the structure (orientation of the molecule in relation to the metal cluster) and their energies compared. The global minimum is considered the most likely complex at room



temperature. The configuration of the most stable complexes reveals the functional group of catechols that binds most strongly to the metal surface.

To gain insight into the cyclization step, an estimation of the energy barrier ( $\Delta G^\ddagger$ ) for the quinone cyclization reaction was obtained by calculating the energy difference between the lowest energy conformations of reactants and the corresponding transition state structures. The transition state (TS) connects two minima on the potential energy surface (PES) (reactant and product). The TS structure is defined by one imaginary frequency of vibration. To confirm the connection between TS and the minimum, the calculation of the intrinsic reaction coordinate (IRC) was conducted. The IRC calculation starts from the TS structure, and partially optimizes the structure along the reaction coordinate in both directions (toward reactant and product, i.e., reverse and forward direction).<sup>170,171</sup>

All calculations were performed using Gaussian 16 software package<sup>172</sup>, while the GaussView program<sup>173</sup> was used to visualize the structures. All geometric optimizations were performed in an implicit solvent using the Solvent Model based on Density (SMD model) with the dielectric constant of water ( $\epsilon = 78.3553$ ).<sup>174</sup> For geometry optimizations, the Minnesota 2006 local functional (M06L) and split basis set LANL2DZ/6-31+G(d,p) were used. Generally, Au atoms were optimized using LANL2DZ and C, H, N, and O atoms using a 6-31+G(d,p) basis set. Different assemblies of  $\text{Au}_n$  clusters placed around catechol molecules were generated using a modified stochastic method.<sup>175</sup>

### 3.7.3. Molecular dynamics simulations

Molecular dynamic (MD) simulations are a set of computational techniques that are based on the principles of classical physics, i.e., on Newton's laws. Due to less complexity and higher calculation speed, MD can be used for large chemical systems (many thousands of atoms). It is commonly used to simulate large biomolecules such as proteins, nucleic acids, lipids or polysaccharides. MD simulations enable the monitoring of processes such as conformer change, the interaction of multiple molecules or the movement of molecules in the medium in time.<sup>176</sup> By solving Newton's equations of motion, a set of coordinates and velocities of atoms is obtained for each point in time, i.e., the trajectory of the system.

Classical MD was performed using the AMBER 17 software package.<sup>177</sup> A simulation box with dimensions of 32 x 43 x 55 Å was created. A metal plate (Au), a ligand molecule (leukodopachrome, dopachrome, and quinoid tautomer of dopachrome) and 2000 water

molecules were added. Au (111) plates consisting of 748 atoms were arranged in 4 layers. The bottom three layers were restrained to maintain the integrity of the plate, while the top layer was unrestrained. Ligand molecules were placed at a distance of 15 Å above the plate. The force field used for the description of the metal was the InterfaceFF27 which was created and used previously for ligand-metal interaction studies.<sup>178</sup> The ligands were described using the standard GAFF force field found in Amber software, and the water molecules were described using the TIP3P model.<sup>179</sup> The Particle Mesh Ewald method was used for electrostatic energy calculations. The Ewald method was modified by Fourier transformation in order to speed up the calculations, resulting in the particle mesh Ewald (PME) method.<sup>180</sup>

In the first step, the energy of the system was minimized through 1000 cycles using the steepest descent algorithm, and then the temperature of the system was raised from 0 to 298 K in 100 ps. A Langevin thermostat with a collision frequency of 2 ps<sup>-1</sup> was used. The equilibration phase was performed for 20 ns in the NPT ensemble, using anisotropic pressure scaling and the Berendsen barostat to maintain 1 atm of pressure. Finally, 50 ns simulations were performed in the NVT ensemble. During all stages of the simulation, a threshold value for nonbonded interactions of 10 Å was used, and the SHAKE algorithm was used to fix the length of O–H bonds in water molecules. The time step was 1 fs. All images were prepared using the Visual Molecular Dynamics (VMD) program.<sup>181</sup>

The binding free energies ( $\Delta G_{\text{bind}}$ ) can be calculated using Molecular Mechanics-Generalized Born method (MM-GBSA) available in AmberTools.<sup>177,182</sup> This method has been successfully applied for the calculation of interactions between nanomaterials and organic molecules.<sup>183,184</sup> Calculations are performed based on trajectories created by MD simulations. The enthalpy contribution to the  $\Delta G_{\text{bind}}$  corresponds to the potential energy of the system in NpV conditions and is calculated by molecular mechanical (MM) methods, i.e., using a force field. The entropic contribution is calculated by normal mode analysis, which approximates the vibrational and rotational frequencies. The MM-GBSA calculation uses the generalized Born equation to analyze the solvation contributions. The non-polar contribution is determined from the solvent-accessible surface area (SASA). In this dissertation, 1000 time points were extracted from the production phase of each simulation (when the ligand was in contact with the metal) and the trajectories were used to calculate the  $\Delta G_{\text{bind}}$ .

### 3.8. Evaluation of the ability of different AuNP and SeNP to cross BBB artificial models

#### 3.8.1. BBB specific parallel artificial membrane permeability assay (PAMPA-BBB)

The PAMPA is acellular, high-throughput permeation model for predicting the passive diffusion of drug molecules across phospholipid membranes. It has been applied in the early phase of drug discovery for decades due to its cost-effectiveness, robustness, and good reproducibility. The original PAMPA model was composed of a phosphatidylcholine membrane. However, subsequent models have been developed that are specific to certain organs and can assess permeability through the gastrointestinal tract (GI), BBB, and skin barrier.<sup>185,186</sup> The PAMPA model is composed of donor wells, artificial (filter) membranes, and acceptor wells (Figure 4). The method is based on the principle of passive diffusion, where the substance movement follows the direction of the concentration gradient, i.e., from an area of higher concentration to an area of lower concentration, without using energy. In the PAMPA model, the compound of interest is put in the donor wells and permeates across the artificial membrane into the acceptor wells.<sup>185–188</sup>

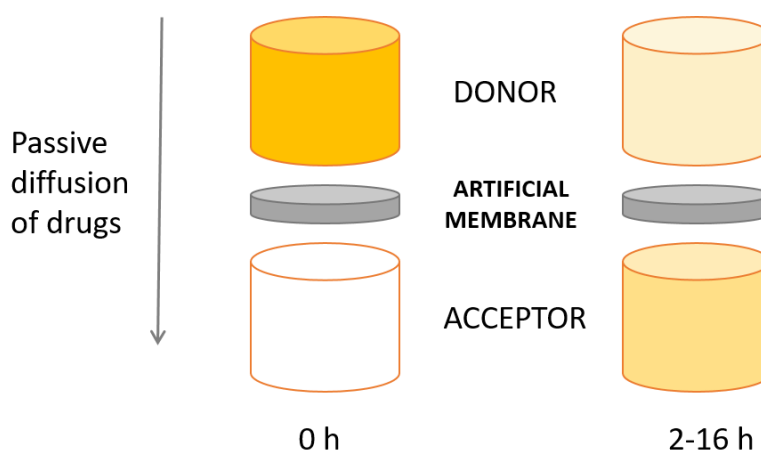


**Figure 4.** Schematic representation of the PAMPA model (downloaded and adapted from Sigma-Aldrich webpage<sup>189</sup>).

In this doctoral thesis, the PAMPA-BBB assay was carried out on 96-well plates where donor and acceptor plates were separated by polycarbonate membrane (PCTE) with a 0.4  $\mu\text{m}$  pore size (MultiScreen® Permeability Filter Plate, Sigma-Aldrich Chemie GmbH, Germany). To evaluate BBB permeability, the membrane was coated with Porcine Polar Brain Lipid Extract

(PBLE, Avanti Polar Lipids, Inc, USA). The lipid mixture was prepared by adding 10% w/v PBLE in a mixture of n-hexane:n-dodecane (3:1), where the mass of PBLE was calculated for the volume of dodecane since n-hexane evaporated more rapidly. 5  $\mu$ L of lipid mixture was added to coat each filter membrane on the donor plate. BBB-PAMPA assay was performed using two different concentrations of SeNP and AuNP: 20 mg Se or Au/L and 200 mg Se or Au/L. In addition, the permeability of NP mixtures with levodopa was also investigated by incubating different concentrations of Tween-SeNP and PEG-AuNP (20 mg Se/L and 200 mg Se/L, respectively) with a constant concentration of levodopa (200  $\mu$ M). Previously published results recommended levodopa concentrations in the PAMPA assay to be 200  $\mu$ M and, therefore, the same concentration was used here.<sup>187</sup> For positive control, carbamazepine (Sigma-Aldrich Chemie GmbH, Munich, Germany) was used at a concentration of 500  $\mu$ M as recommended in the literature.<sup>189</sup> Each compound in triplicate was put in the donor plate and the acceptor plate was filled with 270  $\mu$ L of UPW. The donor compartment comprised 150  $\mu$ L of test compound solutions and was covered with a lid to minimize evaporation during the incubation period of 4 h at RT. Samples from both the donor and acceptor wells were retrieved and metal concentrations were evaluated using AAS, whereas carbamazepine and levodopa concentrations in both compartments were obtained using UV/Vis spectroscopy (SpectraMax iD3 plate reader, Molecular Devices, LLC., San Jose, USA). The apparent permeability ( $P_{app}$ ) of samples that can passively diffuse was determined using the following formula:

$$P_{app} = \frac{-\ln\left(1 - \left[\frac{c_A(t)}{c_{eq}}\right]\right)}{A \times \left(\frac{1}{V_D} + \frac{1}{V_A}\right) \times t} \quad (11)$$

where concentration of the compound in the equilibrium ( $c_{eq}$ ) is:

$$c_{eq} = \left[ \frac{c_D(t) \times V_D + c_A(t) \times V_A}{V_D + V_A} \right] \quad (12)$$

and  $V_D$  and  $V_A$  are the volumes of the donor and acceptor compartments, respectively,  $A$  is the surface area of the membrane multiplied by the porosity,  $t$  is the incubation time,  $c_D(t)$  is the concentration (mol/cm<sup>3</sup>) of the compound in the donor compartment at time  $t$ ,  $c_A(t)$  is the concentration (mol/cm<sup>3</sup>) of the compound in the acceptor compartment at time  $t$ .

### 3.8.2. *In vitro* BBB endothelial transwell permeability assay

To assess transport across the BBB, the conventional method involves using a transwell system. This system comprises an upper (apical) chamber and a lower (basolateral) chamber separated by a permeable, porous membrane. Cells are grown on the membrane and form a tight monolayer, creating a barrier. To measure the transport of a molecule or NP through the barrier, the substance is administered to the upper chamber, and the resulting transport through the cell monolayer and the porous membrane is quantified by collecting the medium from the lower chamber.

Here, Corning transwell inserts were placed in a clear 24-well acceptor plate (both purchased from Merck Millipore, USA) and the membrane was coated with 0.1% w/v gelatin solution. Cerebral microvascular endothelial cell line hBEC-5i were seeded on coated inserts at 20 000 cells/well density in the following cell culture medium: DMEM/F-12 medium supplemented with 10% v/v Fetal Bovine Serum, 1% v/v PenStrep, and 40 mg/mL of Endothelial Cell Growth Supplement (ECGS) (all materials purchased from Sigma Aldrich, St Louis, USA) and incubated for 3 days at 37°C and 5% CO<sub>2</sub>. Throughout the incubation period, cell confluence was assessed daily with Epithelial Volt/Ohm Meter 3 (EVOM3, World Precision Instruments, Sarasota, USA). When cells were determined to be 100% confluent, cell culture medium in donor and acceptor compartments was replaced with phosphate-buffered saline (PBS), and cells were treated with NP in 1 mg Se/L and 10 mg Au/L concentration alone or in a combination with levodopa/dopamine (10 µM). After 3 h incubation at 37°C and 5% CO<sub>2</sub>, phosphate buffer solution containing NP and/or levodopa/dopamine from donor and acceptor compartments was collected in separate 2 mL tubes (Eppendorf, Germany). In order to determine the amount of SeNP, AuNP, levodopa and dopamine remaining in cells, UPW was added to transwell inserts, which were then incubated for 10 min at 37°C in order to lyse cells and release remaining intracellular SeNP and AuNP. After the cells were removed, Trypsin-EDTA solution (Sigma Aldrich, USA) was added to inserts in order to dissolve gelatin on which cells were seeded and collect SeNP and AuNP that passed through the cell layer but not into the acceptor compartment. After trypsin addition, inserts were incubated for 10 min at 37°C, and the solution containing gelatin, and remaining compounds (AuNP, SeNP, levodopa, dopamine) was collected into 2 mL tubes (Eppendorf, Germany). Total Se and Au concentrations in samples from four compartments (donor, acceptor, cell and gelatin fraction) were analyzed using AAS, while levodopa and

dopamine concentration was determined by commercial ELISA assays (MyBioSource, Inc., San Diego, USA).

In addition to transwell assays, acellular experiments were conducted using the same PCTE membrane (0.4  $\mu\text{m}$  pore size) and concentration of SeNP (1 mg Se/L) as was used for the transwell permeability assay in order to evaluate the permeability of SeNP without the cells. In these experiments, PCTE membranes were coated with 0.1% (w/v) gelatin or maintained bare. After incubation of 3 h, Se concentrations in samples from each compartment were evaluated using AAS.

Prior to the assay, it was crucial to consider the concentration of NP that will be applied. Thus, flow cytometry analysis was performed according to the following protocol: hBEC-5i cells were seeded as described before but on a gelatin-coated T75 flask (Eppendorf, Hamburg, Germany). Cell culture medium was removed from the 12-well plates and 900  $\mu\text{L}$  of fresh medium was added. Nanoparticle suspensions for cell treatment were prepared in 10 and 100 mg Se/L and 100 mg Au/L concentration in UPW. Then, these suspensions were added (100  $\mu\text{L}$ /well) to cells to obtain final treatment concentrations of 1 and 10 mg Se/L and 10 mg Au/L. Negative controls were cells treated with 100  $\mu\text{L}$  of sterile  $\text{H}_2\text{O}$  while positive control cells were treated with 10% (v/v) DMSO (Kemika, Zagreb, Croatia). Plates were incubated for 24 h at 37° C and 5%  $\text{CO}_2$ . Following the incubation, media containing detached dead cells were collected into 2 mL centrifuge tubes (Eppendorf, Germany). Cells remaining in wells were washed twice with sterile PBS and detached by adding Trypsin-EDTA solution (Sigma Aldrich, USA), followed by 3 min incubation at 37°C and 5%  $\text{CO}_2$ . Detached cells were added to corresponding 2 mL tubes containing dead cells from the same treatment. Samples were prepared for flow cytometry measurements by staining with Annexin V-FITC Kit (Bio Rad, Hercules, USA) according to the manufacturer's instructions in order to determine the percentage of live, dead, and apoptotic cells. Cells stained by Annexin V-FITC were categorized as Early apoptotic, PI-stained cells were categorized as Dead/Late apoptotic, and non-stained cells were considered Live intact cells. Samples were acquired on an Attune® acoustic focusing flow cytometer (Applied Biosystems, Foster City, USA) equipped with a 488 nm laser. Results were analyzed using FlowJo software (FlowJo LLC, Ashland, USA). Results obtained from 3 independent experiments (with duplicates for each treatment) are expressed as mean % values of apoptotic, dead/late apoptotic or live cells.

### 3.9. Statistical analysis

All obtained results were statistically processed by calculating the arithmetic mean as a measure of centrality and the standard deviation as a measure of dispersion. The results obtained by the DLS, ELS, TEM, fluorescence and UV-Vis spectroscopy, were processed using descriptive procedures (graphics and tables). In order for better evaluation of the correlation between binding affinities and drug loading efficiencies and to clarify the impact of BSA on interactions of AuNP and levodopa or dopamine, data were analyzed using Pearson correlation coefficient ( $r$ ) and the level of significance ( $p$ ). The whole set of data was analyzed including that for levodopa, dopamine, and all types of AuNP. Moreover, statistical significance for data obtained for treated cells compared to negative controls was determined with one-way ANOVA, followed by Dunnett's Multiple Comparison test where all treatment values were compared to control cell values. Only  $p$  values less than 0.05 were considered statistically significant. All statistical analyses were performed in GraphPad Prism 6 (GraphPad Software, San Diego, USA).

## § 4. RESULTS AND DISCUSSION

### 4.1. Physicochemical characteristics of AuNP and SeNP

To synthesize differently coated AuNP and SeNP, a bottom-up approach was utilized wherein  $\text{Au}^{3+}$  and  $\text{Se}^{4+}$  were reduced using  $\text{NaBH}_4$  and L-ascorbic acid, respectively. The synthetic procedures were optimized by conducting a series of experiments, whereby various reaction conditions such as temperature, mixing time and speed, and reactant concentrations were systematically tested. The objective was to obtain stable NP with primary sizes smaller than 100 nm. To assess the stability of AuNP and SeNP,  $d_{\text{TEM}}$ ,  $d_{\text{H}}$  and  $\zeta$  potential values were determined by conducting TEM, DLS and ELS measurements in UPW, as shown in Table 3. The  $d_{\text{H}}$  values of all AuNP and SeNP was found to be larger than their primary size obtained by TEM, ranging from 50.3 to 111.3 nm for AuNP and 71.5 to 82.9 nm for SeNP, due to the presence of a hydration shell on the surface. The observed polydispersity index (PDI) values indicated a formation of monodisperse NP, with values near zero for both SeNP, while PDI values in the range from 0.27 to 0.40 indicated a limited size distribution of AuNP.<sup>152,190,191</sup> Good colloidal stability of all tested NP was aided by electrostatic repulsion forces, as evidenced by negative  $\zeta$  potential values in the range between -31.5 and -18.8 mV.<sup>152</sup> Moreover, TEM was used to characterize the morphology of AuNP and SeNP, as shown in Figure 5.

The synthetic protocols outlined in Sections 3.2.1. and 3.2.3. for preparation of differently coated AuNP and SeNP resulted in monodisperse and homogeneous spherical particles structures with primary size close to 25 nm in the case of AuNP (Figure 5, Table 3), while PVP-SeNP and Tween-SeNP presented spherical structures with primary diameters of 79.4 and 52.4 nm (Figure 6, Table 3), respectively. Moreover, PEG-AuNP prepared by seed-mediated synthetic protocol also yielded spherical NP but with a smaller primary size than other AuNP. Further characterization of NPs was carried out by UV/Vis spectroscopy. As shown in Figure 6, an SPR peak was observed for all AuNP but not for SeNP.<sup>163</sup> Ad-AuNP and PGM-AuNP showed an SPR peak at 530 nm (Figure 7(a)), suggesting that these two types of AuNP were of similar size as SPR depends on the shape and size of the NP. Conversely, AdGly-AuNP and PEG-AuNP exhibited an SPR peak located at 535 nm and 520 nm, respectively. Moreover, SeNP-Tween and SeNP-PVP showed their characteristic maximum absorbance peak at 260 nm (Figure 7(b)).



**Table 3.** The hydrodynamic diameter ( $d_H$ ) and polydispersity index (PDI) obtained from the size intensity-weighted distribution ( $n = 6$ ) using the dynamic light scattering method (DLS), zeta ( $\zeta$ ) potential ( $n = 3$ ) obtained using the electrophoretic light scattering method (ELS) and primary diameter ( $d_{TEM}$ ) obtained from TEM images ( $n = 100$ ) of different types of AuNP and SeNP. All measurements were done at 25°C in UPW and NP concentration of 100 mg Au or Se/L.

NP type	$d_{TEM} / \text{nm}$	$d_H / \text{nm}$	PDI	$\zeta / \text{mV}$
PEG-AuNP	$15.2 \pm 1.7$	$50.3 \pm 1.1$	0.39	$-26.8 \pm 2.9$
Ad-AuNP	$23.8 \pm 3.3$	$87.9 \pm 2.0$	0.27	$-31.5 \pm 0.4$
AdGly-AuNP	$30.2 \pm 4.2$	$111.3 \pm 11.9$	0.40	$-31.0 \pm 0.5$
PGM-AuNP	$23.7 \pm 2.2$	$86.0 \pm 10.3$	0.32	$-18.8 \pm 0.2$
PVP-SeNP	$79.4 \pm 6.9$	$82.9 \pm 0.5$	0.04	$-28.0 \pm 1.9$
Tween-SeNP	$52.4 \pm 6.7$	$71.5 \pm 0.4$	0.05	$-28.4 \pm 1.0$

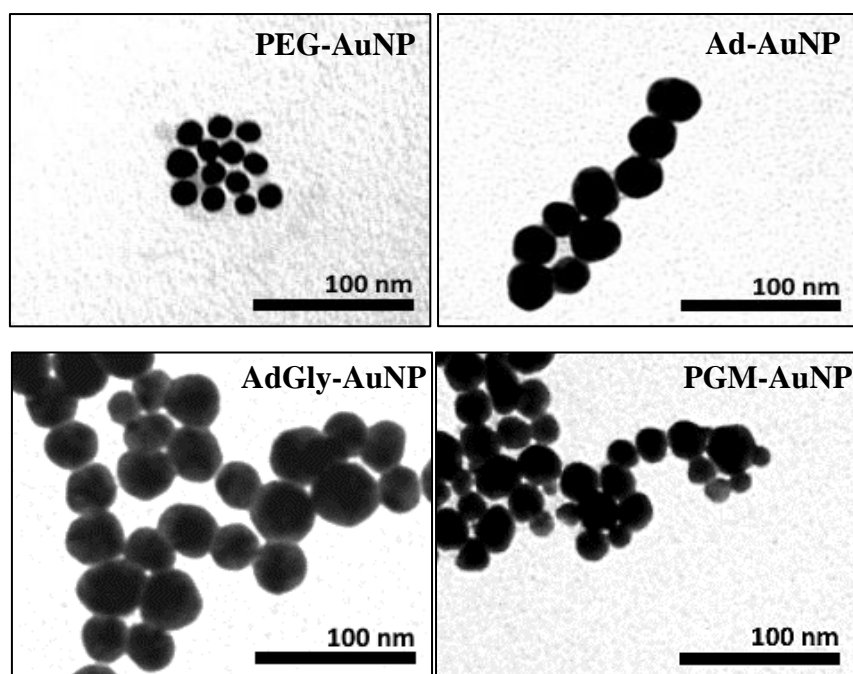


**Figure 5.** Transmission electron microscopy (TEM) images of PEG-AuNP, Ad-AuNP, AdGly-AuNP, and PGM-AuNP.

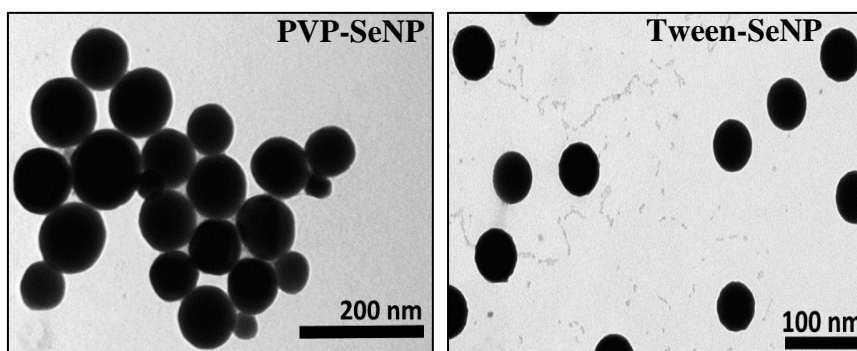


**Figure 6.** Transmission electron microscopy (TEM) images of PVP-SeNP and Tween-SeNP.

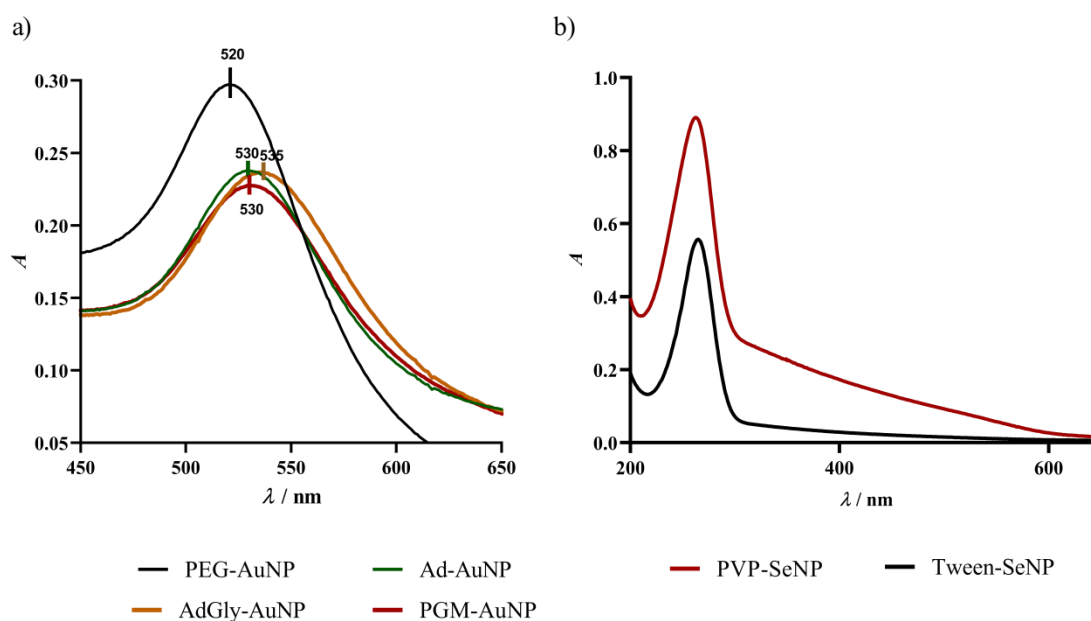


**Figure 7.** Ultraviolet/visible (UV/Vis) absorption spectra of different: a) AuNP, and b) SeNP, dispersed in UPW at a concentration of 10 mg Au or Se/L and 298 K.

Additionally, to ensure the stability of the catechol-functionalized AuNP throughout the NMR experiments, it was necessary to optimize the reaction conditions to obtain small and stable NPs that would not precipitate. To achieve this, various molar ratios of reactants, including Au salt and catechol, were employed for optimization. The resulting AuNP were monitored using several methods such as visual observation of precipitation, as well as TEM, DLS, and ELS measurements (Table 4). The primary sizes of all the different types of tested AuNP were near 100 nm. DLS measurements showed a monomodal size distribution, with  $d_H$  values ranging from 97.4 to 139.1 nm. The functionalization of AuNP with different catechol types

or with different [Au]:[catechol] ratios did not significantly affect the size distribution. The  $\zeta$  potential values ranged from -41.1 to -21.5 mV, with more negative values observed for the molar excess of Au over catechols. The obtained values of  $d_{\text{TEM}}$ ,  $d_{\text{H}}$ , and  $\zeta$  potential for AuNP synthesized at [Au]:[catechol] = 1:6 molar ratio were consistent with the original protocol.<sup>93</sup> Overall, all tested AuNP were found to be colloiddally stable throughout our experiments, except in the case where there was 6-fold molar excess of [Au]. Instead, a 2-fold molar excess of [Au] was found to be the ideal amount for successful AuNP preparation. As a result, the molar ratios of [Au]:[catechol] = 1:6 and [Au]:[catechol] = 2:1 were chosen for NMR experiments (bold frames in Table 4). Although some other molar ratios also produced stable AuNP, they were not considered since they did not demonstrate significant differences from the chosen ratios.

**Table 4.** The hydrodynamic diameter ( $d_{\text{H}}$ ) obtained from the size intensity-weighted distribution ( $n = 6$ ) using the dynamic light scattering method (DLS), zeta ( $\zeta$ ) potential ( $n = 3$ ) obtained using the electrophoretic light scattering method (ELS), primary diameter ( $d_{\text{TEM}}$ ) obtained from TEM images ( $n = 100$ ) and visual characteristic of catechol-functionalized AuNP obtained at different molar ratios of Au and catechols. All measurements were done at 25°C in UPW and NP concentration of 100 mg Au /L.

Catechol	[Au]:[catechol]	$d_{\text{TEM}} / \text{nm}$	$d_{\text{H}} / \text{nm}$	$\zeta / \text{mV}$	Visual characteristics (color/stability/shape)
<b>levodopa</b>	<b>1:6</b>	<b><math>88.3 \pm 4.5</math></b>	<b><math>116.8 \pm 0.6</math></b>	<b><math>-31.3 \pm 0.9</math></b>	<b>blue/stable/flower-like</b>
levodopa	1:1	$101.4 \pm 3.2$	$139.1 \pm 0.9$	$-29.6 \pm 0.6$	blue/stable/flower-like
<b>levodopa</b>	<b>2:1</b>	<b><math>94.0 \pm 5.1</math></b>	<b><math>119.9 \pm 0.4</math></b>	<b><math>-41.1 \pm 1.3</math></b>	<b>blue/stable/flower-like</b>
levodopa	6:1	*n.a.	*n.a.	*n.a.	dark gray/unstable/*n.a
<b>dopamine</b>	<b>1:6</b>	<b><math>93.2 \pm 4.5</math></b>	<b><math>117.6 \pm 1.1</math></b>	<b><math>-25.3 \pm 1.2</math></b>	<b>blue/stable/flower-like</b>
dopamine	1:1	$87.9 \pm 4.4$	$119.9 \pm 0.4$	$-21.5 \pm 0.4$	blue/stable/flower-like
<b>dopamine</b>	<b>2:1</b>	<b><math>81.8 \pm 3.9</math></b>	<b><math>97.4 \pm 0.6</math></b>	<b><math>-31.8 \pm 1.0</math></b>	<b>red-brown/stable/sphere</b>
dopamine	6:1	*n.a.	*n.a.	*n.a.	dark gray, unstable

\*not applicable

Moreover, TEM visualization (Figure 8) revealed the formation of spherical and flower-like AuNP. However, spherical AuNP were only produced when Au was in molar excess over dopamine. The observation of different AuNP shapes that result from various molar ratios of reactants was previously noted by Sajitha *et al.*<sup>192</sup> When reducing agents are in excess ( $[\text{Au}]:[\text{catechol}] = 1:6$ ), they lead to the formation of only flower-shaped particles, as shown in Figure 8(a,c). On the other hand, at lower molar ratios of reducing agents ( $[\text{Au}]:[\text{catechol}] = 2:1$ ), excess of  $\text{AuCl}_4^-$  ions adsorb on Au seeds, promoting NP aggregation.<sup>193</sup> Under this condition, spherical AuNP larger than Au seeds are typically formed.<sup>192,194,195</sup> Interestingly, when levodopa is used as a reducing agent, flower-shaped AuNP are obtained (Figure 8(d)), whereas dopamine leads to the formation of spherical AuNP (Figure 8(b)). This difference can be attributed to the distinct oxidation processes of levodopa and dopamine. Although using the same molar ratio, levodopa undergoes one additional oxidation step, releasing two extra electrons compared to dopamine's two-electron oxidation to the quinone form. As a result, levodopa exhibits a stronger ability to reduce  $\text{Au}^{3+}$  ions with four electrons, increasing the reaction rate and promoting the rapid deposition of  $\text{Au}^0$  onto the (111) planes. This is crucial for the formation of multibranched nanocrystals, such as flower-like NP.<sup>196</sup>

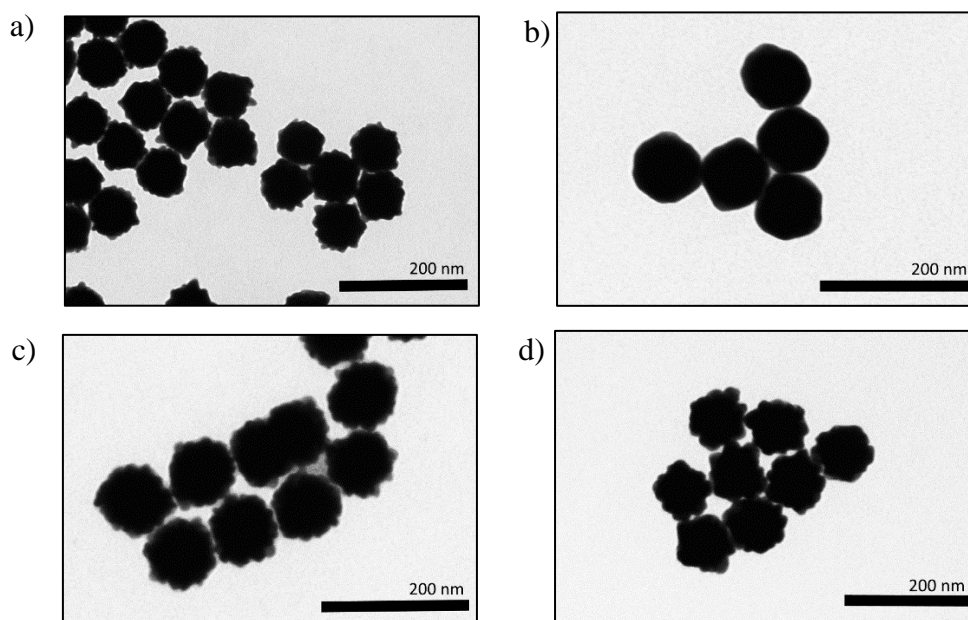


**Figure 8.** Transmission electron microscopy (TEM) images of catechol-functionalized AuNP obtained at different molar ratios of Au to catechols: a)  $[\text{Au}]:[\text{dopamine}] = 1:6$ , b)  $[\text{Au}]:[\text{dopamine}] = 2:1$ , c)  $[\text{Au}]:[\text{levodopa}] = 1:6$ , and d)  $[\text{Au}]:[\text{levodopa}] = 2:1$ .

The UV-Vis spectra confirmed the shape of catechol-functionalized AuNP (Figure 9) showing that AuNP nanoflowers exhibited an SPR peak at wavelengths above 600 nm, as expected for flower-like NP.<sup>93,197</sup> Meanwhile, dopamine-functionalized spherical AuNP showed an SPR peak at 575 nm, consistent with the literature for spherical AuNP.<sup>194</sup> AuNP functionalized with levodopa exhibited a redshift in the SPR peak compared to dopamine, which can be attributed to an increase in AuNP size, as confirmed by TEM and DLS measurements.<sup>193</sup>

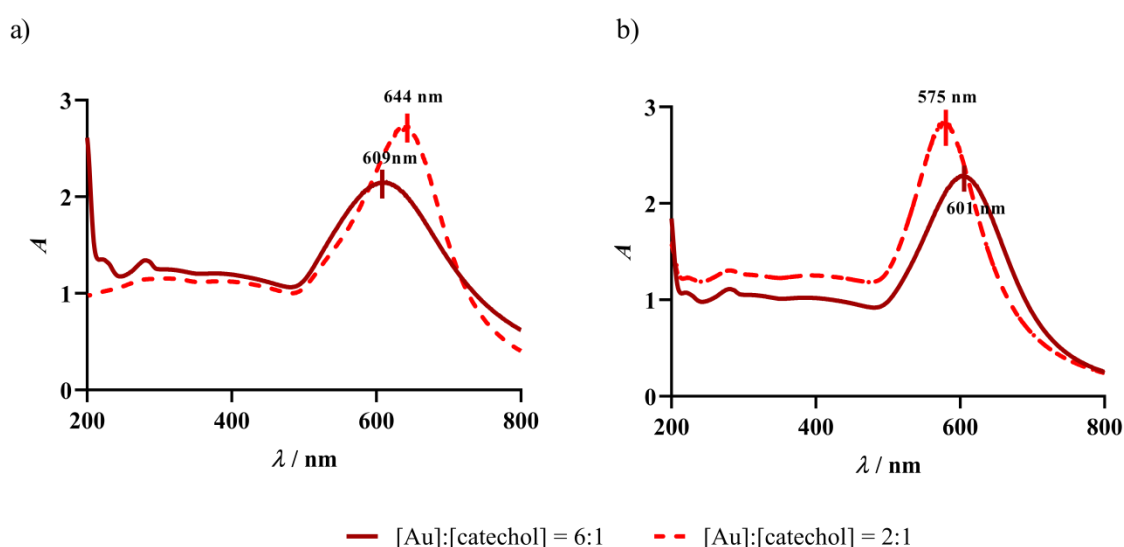


**Figure 9.** Ultraviolet/visible (UV/Vis) absorption spectra of catechol-functionalized AuNP obtained at different molar ratios between Au and catechols: a) [Au]:[levodopa], and b) [Au]:[dopamine].

## 4.2. Interactions of levodopa and dopamine with differently coated AuNP and SeNP

### 4.2.1. Steady-state and time-resolved fluorescence measurements

Before determining the binding constants using the fluorescence spectroscopy method, it was necessary to determine the inner-filter effect, which occurs as a consequence of NP absorption at emission and excitation wavelengths. Since NP have a certain fluorescence, by monitoring the dependence of fluorescence on the concentration of the NP themselves, it is possible to establish the absorption effect of NP on fluorescence. If the relationship between fluorescence and concentration is linear, absorbance is negligible.<sup>157</sup> Linearity was checked at different concentration ranges depending on the type of NP. According to the results, there was a linear

relationship with fluorescence for all tested NP in certain concentration ranges (Table 2) since the  $r^2$  value was greater than 0.95, except for PEG-AuNP where fluorescence dropped with increase in concentrations and, therefore, was corrected using Eq 4. After conducting these preliminary measurements and determining the NP concentration at which the effect of the inner filter can be minimized, interactions between NP and fluorophores were examined.

As an effective method, steady-state fluorescence spectroscopy is widely used to study biomolecule-NP interactions, providing information on fluorescence quenching mechanisms.<sup>131, 159,198,199</sup> Thus, this method was used to determine the binding affinities of levodopa and dopamine to the differently coated AuNP and SeNP. To the best of our knowledge, investigations on the molecular interactions of levodopa and dopamine with SeNP are not available in the literature, while there are only a few papers that focus on interactions of AuNP with dopamine.<sup>131</sup> Additionally, interactions of AuNP and SeNP with proteins (BSA and hTF) were included in these experiments to provide data for subsequent evaluation of the impact of serum proteins on drug-binding affinities. PEG-AuNP were chosen to compare our data with those in the literature as this type of AuNP has been well studied for interactions with BSA.<sup>200–202</sup> Moreover, there are few published papers on the interaction of SeNP with serum albumin<sup>203–205</sup>, while interactions with hTF have not been previously investigated.

The maximum fluorescence peak of levodopa and dopamine was found to be at the excitation wavelength of 280 nm, as their structure derives from phenylalanine.<sup>206,207</sup> On the other hand, tryptophans (Trp) and tyrosines (Tyr) are the main amino acids that contribute to the intrinsic fluorescence of hTF and BSA when excited at 280 nm.<sup>208,209</sup> When excited at 280 nm, levodopa and dopamine showed strong fluorescence emission maxima at 317 nm, while the emission of hTF and BSA exhibited an emission spectrum typical for the majority of proteins, with a maximum peak at 345 nm. Upon addition of various concentrations of AuNP and SeNP the fluorophore's intrinsic fluorescence decreased. Such fluorescence quenching mechanism is evidence of binding processes occurring at the nanosurface. As an example of fluorescence quenching, Figure 10 shows emission spectra of levodopa, dopamine, and BSA upon exposure to various concentrations of PGM-AuNP. Similar decrease in fluorescence was observed in the emission spectra of fluorophores with all types of NPs studied.

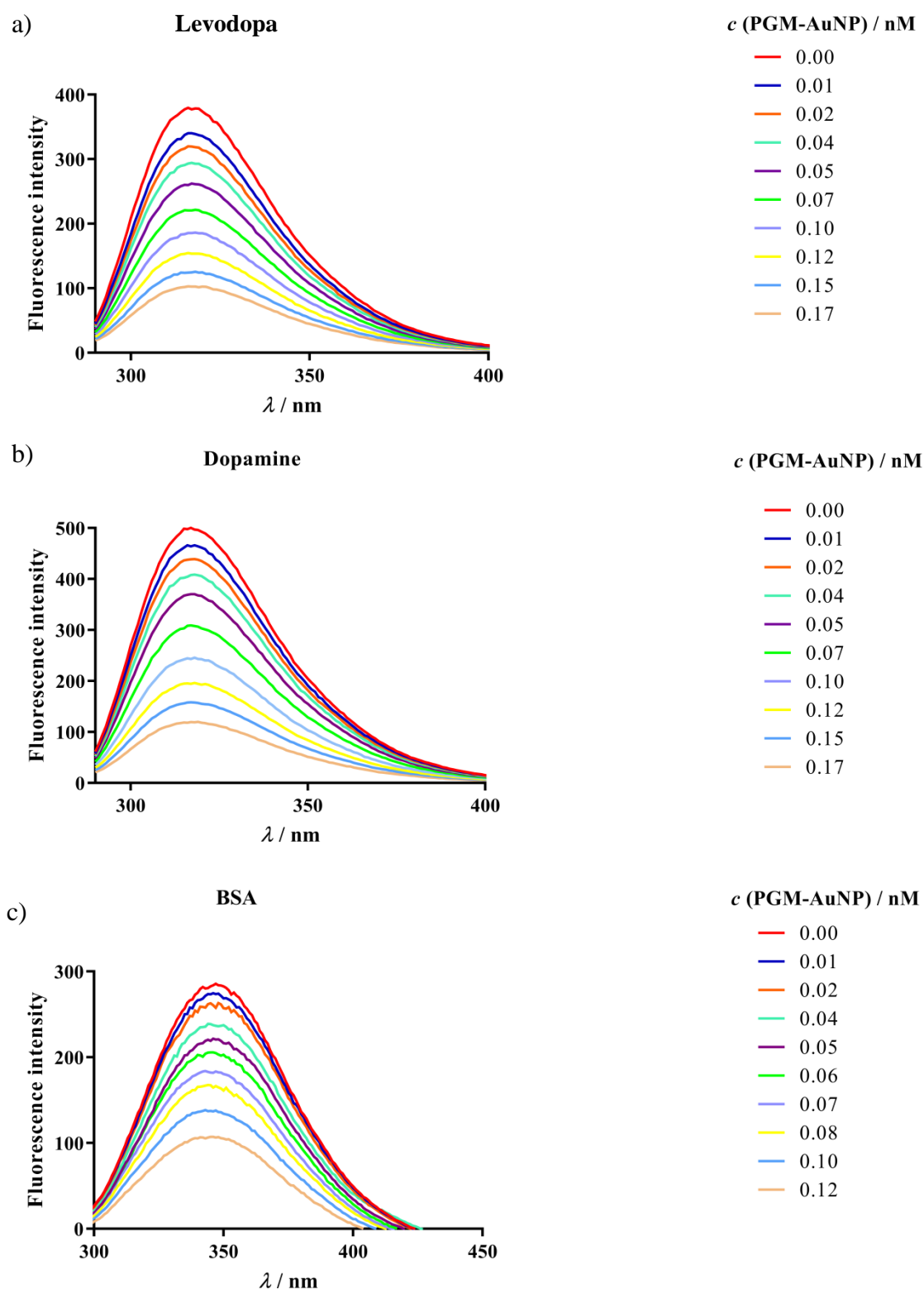


**Figure 10.** Fluorescence quenching spectra of: a) 0.15  $\mu\text{M}$  levodopa, b) 0.25  $\mu\text{M}$  dopamine, and c) 0.5  $\mu\text{M}$  BSA upon addition of different concentrations of PGM-AuNP at 298 K.

Using the Stern-Volmer equation (Eq 5), Stern-Volmer plots were created to distinguish dynamic from static quenching mechanism. Examples of Stern-Volmer plots of levodopa, dopamine, and BSA with different concentrations of PGM-AuNP are shown in Figure 11(a,c,e).

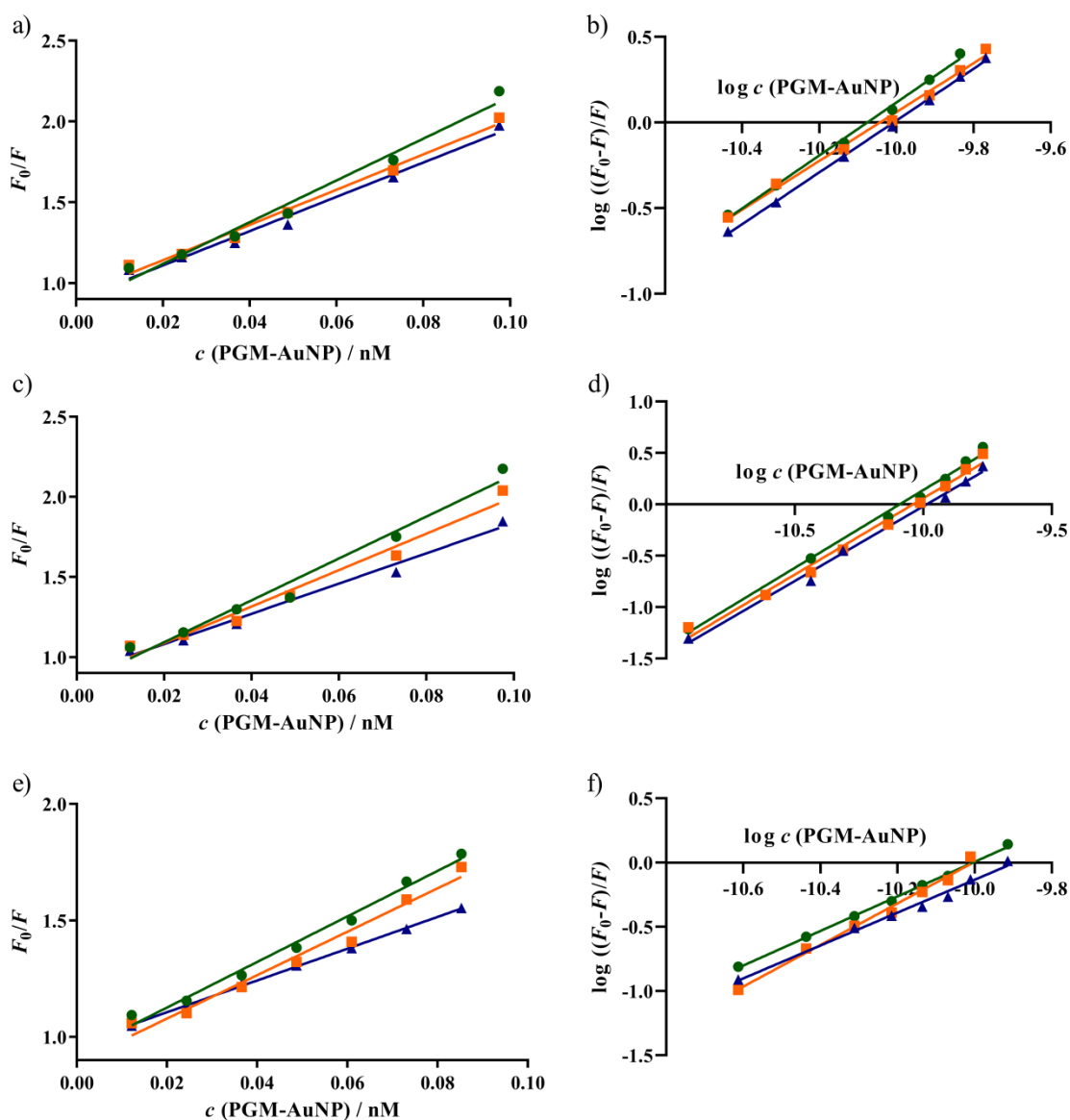


**Figure 11.** Temperature-dependent Stern-Volmer plots for the fluorescence quenching of: a) levodopa, c) dopamine, and e) BSA; and corresponding Hill plots of fluorescence quenching for: b) levodopa d) dopamine, and f) BSA upon interaction with PGM-AuNP at 288 (green line), 298 (orange line), and 308 K (blue line).



The interactions were governed by either the dynamic or static quenching mechanism, as the Stern-Volmer plots were well-matched with a linear Stern-Volmer equation at three different temperatures (308, 298, and 288 K), indicating a single quenching mechanism. The  $K_{SV}$  obtained using linear regression fit of Eq 5, together with the  $k_q$  obtained from time-resolved fluorescence measurements at 298 K, are presented in Table 5. The decrease in  $K_{SV}$  values with increasing temperature for most of the mixtures indicates the primary role of the static quenching process, as higher temperatures disturb the ground-state complex formation.<sup>156,206,210</sup> Moreover, as the calculated values of  $k_q$  were significantly higher than the expected maximum value for the diffusion-controlled quenching process, which is typically around  $1.0 \times 10^{10} \text{ M}^{-1} \text{ s}^{-1}$ , then the main fluorescence quenching mechanism of the complexes between differently coated AuNP and SeNP and fluorophores was not initiated by dynamic collision but rather by the static quenching mechanism.<sup>211</sup> However, in the case of PEG-AuNP, the Stern-Volmer constants increased with temperature, suggesting a dynamic quenching process even though  $k_q$  for these interactions was higher than  $10^{10} \text{ M}^{-1} \text{ s}^{-1}$ .<sup>159,212</sup>

Average fluorescence lifetime values ( $\tau$ ) of all fluorophores were measured using time-resolved fluorescence measurements in order to calculate  $k_q$  (Table 5) according to Eq 5. The fluorescence decay curves of levodopa and dopamine were adequately described by single-exponential functions. However, the fluorescence decay of BSA and hTF was bi-exponential, thereby mean (average) lifetimes for such systems were calculated using the following equation:

$$\tau = \frac{(\alpha_1\tau_1 + \alpha_2\tau_2)}{(\alpha_1 + \alpha_2)} \quad (13)$$

where  $\alpha_1$  and  $\alpha_2$  are pre-exponential factors.

The  $\tau$  values for free levodopa, dopamine, BSA and hTF were determined to be  $1.04 \pm 0.01$  ns,  $0.85 \pm 0.01$  ns,  $4.78 \pm 0.02$  ns, and  $2.05 \pm 0.05$ , respectively. The  $\tau$  values for dopamine and BSA were consistent with previously reported values of 0.8 ns and 5.45 ns, respectively.<sup>213,214</sup>

Additionally, time-resolved measurements were applied in order to investigate the nature of the quenching mechanism for interactions of fluorophores with PEG-AuNP.<sup>215</sup> Specifically,  $\tau$  values of fluorophores (levodopa, dopamine and BSA) were measured in the presence of PEG-AuNP. Upon the addition of PEG-AuNP, there was no significant decrease in the  $\tau$  values for any of the tested fluorophores (levodopa, dopamine and BSA), which

suggested that the dominant quenching mechanism was static. Additionally, plots of  $F_0/F$  vs.  $c$  (PEG-AuNP) did not align with plots of  $\tau_0/\tau$  vs.  $c$  (PEG-AuNP) for all tested fluorophores (Figure 12). Moreover,  $\tau_0/\tau$  values were found to be close to 1, which provided further confirmation of a static quenching mechanism for the interaction between PEG-AuNP and the selected fluorophores.<sup>156</sup>

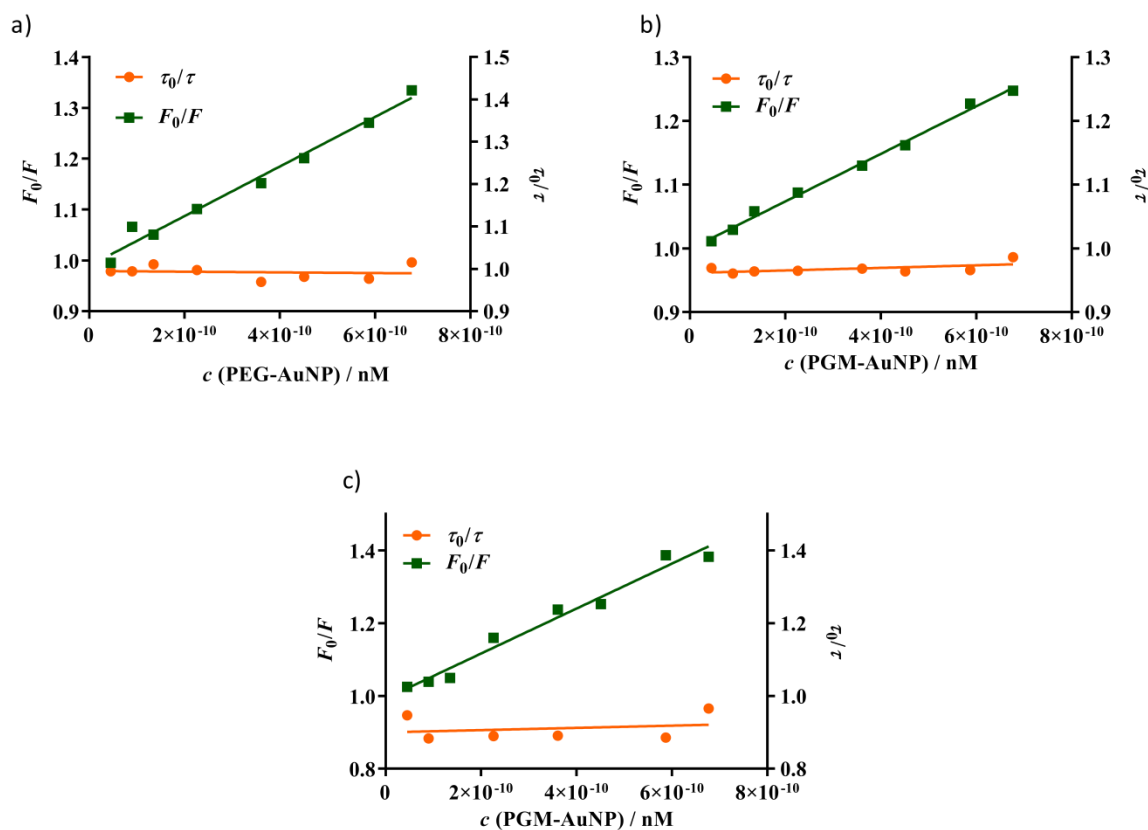


**Figure 12.** Comparison of  $F_0/F$  vs.  $c$  (PEG-AuNP) and  $\tau_0/\tau$  vs.  $c$  (PEG-AuNP) plots obtained by time-resolved fluorescence measurements of the interaction between PEG-AuNP and: a) levodopa, b) dopamine, and c) BSA at 298 K.

**Table 5.** The Stern-Volmer constant ( $K_{SV}$ ) and bimolecular quenching constant ( $k_q$ ) values calculated for the interaction of differently coated AuNP and SeNP with levodopa, dopamine, and BSA/hTF at three different temperatures (288, 298 and 308 K). Results are presented as the mean of  $K_{SV}$  and  $k_q$  values obtained from three independent measurements with standard deviations.

NP type	Fluorophore	288 K	298 K		308 K
		$K_{SV}$	$K_{SV}$	$k_q$	$K_{SV}$
		$\times 10^9 / \text{M}^{-1}$	$\times 10^9 / \text{M}^{-1}$	$\times 10^{17} / \text{M}^{-1}$	$\times 10^9 / \text{M}^{-1}$
PEG-AuNP	Levodopa	$0.39 \pm 0.01$	$0.46 \pm 0.01$	$4.44 \pm 0.05$	$0.50 \pm 0.01$
Ad-AuNP		$7.75 \pm 0.05$	$7.30 \pm 0.04$	$70.20 \pm 0.40$	$6.99 \pm 0.08$
AdGly-AuNP		$11.00 \pm 0.12$	$10.70 \pm 0.00$	$103.00 \pm 1.00$	$9.97 \pm 0.04$
PGM-AuNP		$13.00 \pm 0.60$	$11.30 \pm 0.38$	$109.00 \pm 3.66$	$10.80 \pm 0.00$
PVP-SeNP		$133.00 \pm 2.80$	$164.00 \pm 2.50$	$1590.00 \pm 10.20$	$203.00 \pm 4.20$
Tween-SeNP		$34.30 \pm 1.50$	$32.80 \pm 0.90$	$320.00 \pm 2.90$	$31.80 \pm 0.60$
PEG-AuNP	Dopamine	$0.30 \pm 0.00$	$0.36 \pm 0.00$	$4.28 \pm 0.01$	$0.48 \pm 0.01$
Ad-AuNP		$6.25 \pm 0.11$	$6.14 \pm 0.03$	$72.20 \pm 0.34$	$6.02 \pm 0.14$
AdGly-AuNP		$9.87 \pm 0.05$	$9.57 \pm 0.02$	$112.00 \pm 0.30$	$9.23 \pm 0.06$
PGM-AuNP		$13.20 \pm 0.12$	$11.40 \pm 0.06$	$134.00 \pm 0.68$	$10.50 \pm 0.14$
PVP-SeNP		$175.00 \pm 4.20$	$171.00 \pm 4.70$	$2010.00 \pm 12.3$	$162.00 \pm 0.70$
Tween-SeNP		$44.60 \pm 3.30$	$37.30 \pm 1.30$	$440.00 \pm 5.10$	$29.50 \pm 0.10$
PEG-AuNP	BSA	$0.47 \pm 0.00$	$0.59 \pm 0.01$	$1.24 \pm 0.02$	$0.70 \pm 0.00$
Ad-AuNP		$8.58 \pm 0.16$	$8.35 \pm 0.02$	$17.50 \pm 0.03$	$7.93 \pm 0.52$
AdGly-AuNP		$11.30 \pm 0.23$	$9.32 \pm 0.03$	$19.50 \pm 0.07$	$5.81 \pm 0.06$
PGM-AuNP		$10.40 \pm 0.07$	$9.17 \pm 0.56$	$19.20 \pm 1.16$	$7.01 \pm 0.15$
PVP-SeNP	hTF	$125.00 \pm 4.20$	$111.00 \pm 2.30$	$540.00 \pm 1.20$	$104.00 \pm 0.70$
Tween-SeNP		$40.90 \pm 0.80$	$38.90 \pm 0.10$	$190.00 \pm 3.20$	$36.40 \pm 0.50$

Using Eq 6, Hill plots were generated, and examples are shown for interactions of levodopa, dopamine and BSA with PGM-AuNP (Figure 11(b,d,f)). From the slope and intercept (the antilog of the y-intercept) of the Hill plots  $\log((F_0-F)/F)$  vs.  $\log c$  (SeNP/AuNP), the values of  $n$  and  $K$  at three different temperatures (288, 298, and 308 K) were obtained and are listed in Table 6 and 7, respectively.

**Table 6.** The number of binding sites ( $n$ ) values obtained from the interaction of differently coated AuNP and SeNP with levodopa, dopamine, and BSA/hTF at three different temperatures (288, 298, and 308 K). The results are presented as the mean of  $n$  values with corresponding standard deviations calculated from 3 independent measurements.

NP type	Fluorophore	$n$		
		288 K	298 K	308 K
PEG-AuNP	Levodopa	$1.20 \pm 0.01$	$1.14 \pm 0.01$	$1.08 \pm 0.01$
Ad-AuNP		$1.11 \pm 0.01$	$1.08 \pm 0.01$	$1.03 \pm 0.01$
AdGly-AuNP		$1.05 \pm 0.01$	$0.99 \pm 0.01$	$0.95 \pm 0.01$
PGM-AuNP		$1.48 \pm 0.01$	$1.43 \pm 0.01$	$1.37 \pm 0.01$
PVP-SeNP		$1.17 \pm 0.00$	$1.13 \pm 0.05$	$1.08 \pm 0.01$
Tween-SeNP		$1.03 \pm 0.02$	$1.01 \pm 0.01$	$0.98 \pm 0.00$
PEG-AuNP	Dopamine	$1.22 \pm 0.01$	$1.12 \pm 0.06$	$1.11 \pm 0.01$
Ad-AuNP		$1.10 \pm 0.01$	$1.07 \pm 0.01$	$1.02 \pm 0.01$
AdGly-AuNP		$1.05 \pm 0.01$	$0.99 \pm 0.01$	$0.93 \pm 0.02$
PGM-AuNP		$1.51 \pm 0.01$	$1.48 \pm 0.01$	$1.46 \pm 0.01$
PVP-SeNP		$1.13 \pm 0.01$	$1.10 \pm 0.02$	$1.08 \pm 0.00$
Tween-SeNP		$1.02 \pm 0.01$	$0.95 \pm 0.01$	$0.92 \pm 0.00$
PEG-AuNP	BSA	$1.25 \pm 0.01$	$1.19 \pm 0.01$	$1.12 \pm 0.01$
Ad-AuNP		$1.28 \pm 0.01$	$1.24 \pm 0.01$	$1.18 \pm 0.01$
AdGly-AuNP		$1.17 \pm 0.01$	$1.10 \pm 0.01$	$1.08 \pm 0.01$
PGM-AuNP		$1.34 \pm 0.01$	$1.28 \pm 0.01$	$1.23 \pm 0.01$
PVP-SeNP	hTF	$1.07 \pm 0.01$	$1.03 \pm 0.00$	$0.99 \pm 0.01$
Tween-SeNP		$1.17 \pm 0.01$	$1.06 \pm 0.00$	$0.94 \pm 0.00$

**Table 7.** The binding constant ( $K$ ) values obtained from the interaction of differently coated AuNP and SeNP with levodopa, dopamine, and BSA/hTF at three different temperatures (288, 298 and 308 K). The results are presented as the mean of  $K$  values and their corresponding SD values obtained from three independent measurements.

NPs type	Fluorophore	$K \times 10^{10} / \text{M}^{-1}$		
		288 K	298 K	308 K
PEG-AuNP	Levodopa	$2.43 \pm 0.17$	$0.96 \pm 0.20$	$0.24 \pm 0.03$
Ad-AuNP		$8.40 \pm 0.35$	$3.92 \pm 0.29$	$1.34 \pm 0.13$
AdGly-AuNP		$3.51 \pm 0.54$	$0.85 \pm 0.03$	$0.29 \pm 0.03$
PGM-AuNP		$75200.00 \pm 1040.00$	$23700.00 \pm 4780.00$	$5760.00 \pm 285.00$
PVP-SeNP		$1110.00 \pm 79.40$	$480.00 \pm 102.00$	$178.00 \pm 16.20$
Tween-SeNP		$8.24 \pm 3.96$	$3.81 \pm 0.25$	$2.03 \pm 0.13$
PEG-AuNP	Dopamine	$3.25 \pm 0.38$	$1.07 \pm 0.19$	$0.44 \pm 0.02$
Ad-AuNP		$5.56 \pm 0.02$	$2.62 \pm 0.36$	$0.92 \pm 0.07$
AdGly-AuNP		$3.06 \pm 0.54$	$0.64 \pm 0.02$	$0.29 \pm 0.03$
PGM-AuNP		$176000.00 \pm 12000.00$	$76200.00 \pm 3620.00$	$38200.00 \pm 7120.00$
PVP-SeNP		$515.00 \pm 86.40$	$250.00 \pm 51.60$	$144.00 \pm 3.72$
Tween-SeNP		$7.01 \pm 0.93$	$1.21 \pm 0.11$	$0.35 \pm 0.04$
PEG-AuNP	BSA	$11.80 \pm 1.64$	$2.85 \pm 0.46$	$0.93 \pm 0.02$
Ad-AuNP		$414.00 \pm 38.70$	$186.00 \pm 21.50$	$66.30 \pm 7.50$
AdGly-AuNP		$37.10 \pm 0.95$	$10.30 \pm 1.70$	$3.80 \pm 0.33$
PGM-AuNP		$2570.00 \pm 381.00$	$476.00 \pm 36.50$	$148.00 \pm 10.40$
PVP-SeNP	hTF	$73.20 \pm 11.40$	$23.20 \pm 2.29$	$10.30 \pm 0.71$
Tween-SeNP		$294.00 \pm 47.60$	$16.50 \pm 0.51$	$0.91 \pm 0.04$

The  $n$  values indicate the average number of binding sites for the fluorophore-AuNP/SeNP complexes. These coefficients are commonly used to assess the level of cooperativity involved in ligand binding. A value of  $n = 1$  implies that no interaction occurs between the binding sites, resulting in non-cooperative binding. On the other hand, if  $n$  values fall below or exceed 1, this suggests negative or positive cooperativity in binding, respectively.<sup>216</sup> All interactions exhibited a slight decline in their  $n$  values as temperature increased (Table 6). The binding of levodopa and dopamine to PEG-, Ad- and PGM-AuNP and PVP-SeNP was characterized by the increase in affinity of a binding site after binding of a fluorophore to another site, resulting in  $n$  values greater than 1 at all tested temperatures. Positive cooperativity was also observed for interactions of AdGly-AuNP and Tween-SeNP with levodopa and dopamine at 288 K. However, non-cooperativity and negative cooperativity for these reactions were observed at 298 K and 308 K, respectively. The binding of BSA with all AuNP displayed positive cooperativity, which is consistent with earlier studies.<sup>200,217</sup> Interactions of hTF with PVP-SeNP resulted in non-cooperative binding ( $n$  close to 1), while binding of hTF with Tween-SeNP exhibited positive cooperativity at 288 K, non-cooperativity at 298 K and negative cooperativity at 308 K.

The gold nanosurface exhibited the highest affinity for fluorophores when functionalized with PGM (Table 7). The presence of PGM on the surface of AuNP may enhance the formation of hydrogen bonds and electrostatic interactions with biomolecules such as amino acids and proteins.<sup>218</sup> Additionally, this type of AuNP is distinguished by a more positive  $\zeta$  potential value in comparison to the other tested AuNP, which can further facilitate interactions with negatively charged molecules such as BSA and levodopa. However, in comparison to levodopa and BSA, dopamine exhibited the highest binding affinity to PGM-AuNP, potentially due to the additional electrostatic interaction between the negatively charged nanosurface and the positively charged amino group of dopamine. This amino group was N-protonated under acidic conditions as the pH of the reaction mixture was 4.52.<sup>219</sup> When considering Ad-AuNP, levodopa exhibited greater attraction than dopamine. However, their affinities to PEG- and AdGly-functionalized AuNP were relatively similar, and  $K$  values reduced as the temperature increased. On the other hand, BSA demonstrated various levels of affinities for different types of AuNP, with PGM-AuNP exhibiting the highest affinity, followed by Ad-AuNP, AdGly-AuNP, and PEG-AuNP. Notably, BSA had stronger bonds with PEG-, Ad-, and AdGly-functionalized AuNP compared to levodopa and

dopamine. However, the opposite trend was observed for PGM-functionalized AuNP. The lower  $K$  values observed for the binding of BSA with PEG-AuNP may not only be due to the presence of PEG, a commonly used polymer for preventing protein adsorption on surfaces but also due to the particle size, as PEG-AuNP had the smallest  $d$  and  $d_H$  compared to other AuNP. These findings align with earlier studies on the binding of BSA to PEG-functionalized AuNP.<sup>200</sup>

When examining the binding of levodopa, dopamine, and hTF to SeNP, it was evident that levodopa had the highest affinity, whereas dopamine displayed the weakest. Taking into account the impact of surface coatings on binding constants, the PVP-SeNP exhibited stronger attraction to levodopa and dopamine. Nevertheless, lower  $K$  values observed in the binding of levodopa and dopamine to Tween-SeNP might be due to their smaller size compared to PVP-SeNP. While such a correlation has been noted for the interactions of some biomolecules with AuNP, the opposite trend has been reported for AgNPs.<sup>155,220</sup> Thus, we cannot claim that effect is broadly related to SeNP since there was no distinct correlation between the binding affinities and the size of the NP. Additionally, even if there were a trend of increasing binding constants with the size of the NP, it becomes insignificant when the diameter exceeds approximately 60 nm.<sup>220</sup>

The significant decrease in  $K$  values with the increase in temperature (Table 7) indicates that the primary interactions between fluorophores and AuNP/SeNP were non-covalent. In contrast to covalent interactions, weak non-covalent interactions are destabilized with increasing temperature, which disrupted AuNP/SeNP-fluorophore complexes, as reported previously.<sup>221,222</sup> The thermodynamic parameters, including the  $\Delta H^0$ ,  $\Delta S^0$  and  $\Delta G^0$ , provide insight into the underlying forces between AuNP/SeNP and fluorophores that occur during their interaction. Thermodynamic parameters were calculated from the van't Hoff plots using Eq. 7 and 8 at three different temperatures and are listed in Table 8. Examples of van't Hoff plots for interactions between PGM-AuNP and fluorophores (levodopa, dopamine and BSA) are shown in Figure 13.  $\Delta G^0$  had negative values for all investigated interactions, which suggest that the binding occurred spontaneously. Based on the Ross and Subramanian categorization, hydrogen bonds and van der Waals interactions are the dominant interaction forces when both  $\Delta S^0$  and  $\Delta H^0$  are negative. Conversely, electrostatic interactions prevail when  $\Delta S^0$  is positive and  $\Delta H^0$  is negative.<sup>223</sup> It was observed that hydrogen bonds played a significant role in the interactions of levodopa and dopamine with PEG-, Ad- and AdGly-

AuNP, as values of  $\Delta S^0$  and  $\Delta H^0$  were both negative. The same was found for the binding of levodopa to PGM-AuNP and dopamine to Tween-SeNP.

These interactions may result from hydrogen bonding between the hydroxyl groups of levodopa/dopamine as hydrogen donors and oxygen or nitrogen atoms on the nanosurface as hydrogen acceptors. In the case of hydrophilic  $\text{NH}_2$ -terminated nanosurfaces, interactions may also arise through hydrogen bonding with catechol groups or cation- $\pi$  interactions with the surface.<sup>224,225</sup> Moreover, hydrogen bonds are the most common forces that initiate interactions between proteins and metal NP.<sup>226</sup> This also was confirmed here since almost all AuNP and SeNP interact with BSA and hTF through hydrogen bonding. Regarding Au nanosurface electrostatic interactions were observed only in the case of dopamine binding to PGM-AuNP and BSA to Ad-AuNP. Additionally electrostatic nature was found as a dominant force in interactions between levodopa and both types of SeNP. As the reactions occurred at  $\text{pH } 4.9 \pm 1.3$ , levodopa was a zwitterion with both positive and negative charges in this pH range.<sup>227</sup> Zwitterionic molecules exhibit a strong affinity to metal surfaces through electrostatic interactions.<sup>228</sup> Therefore, this could be the reason for the higher affinity of levodopa to selenium nanosurfaces in comparison to other fluorophores. The same mechanism was observed in the binding of dopamine to PVP-SeNP, which may be attributed to the interaction between the positively charged amino group of dopamine (which is N-protonated in an acidic environment ( $\text{pH} = 4.2$ )) and the negatively charged selenium nanosurface.<sup>219</sup> From these results, it can be concluded that the surface structure, i.e., the selection of the coating agents on the surface of the NP, plays an important role in nano-interactions.

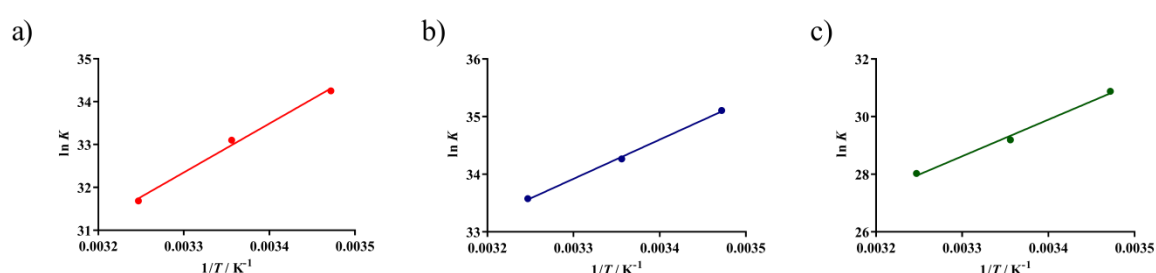


**Figure 13.** Van't Hoff plots for the interaction between PGM-AuNP and: a) levodopa, b) dopamine, and c) BSA.



**Table 8.** Thermodynamic parameters obtained for the interaction of levodopa, dopamine, and BSA/hTF with differently coated AuNP and SeNP.

NP type	Fluorophore	$\Delta H^0 \times 10^4$	$\Delta S^0$	$\Delta G^0 \times 10^4 / \text{kJmol}^{-1}$		
		/ $\text{kJmol}^{-1}$	/ $\text{Jmol}^{-1}\text{K}^{-1}$	288 K	298 K	308 K
PEG-AuNP	Levodopa	-8.44	-93.40	-5.75	-5.65	-5.56
Ad-AuNP		-6.76	-25.10	-6.04	-6.01	-5.99
AdGly-AuNP		-9.17	-117.00	-5.80	-5.69	-5.57
PGM-AuNP		-9.46	-43.10	-8.22	-8.17	-8.13
PVP-SeNP		-6.80	15.50	-7.20	-7.22	-7.23
Tween-SeNP		-5.20	29.50	-6.88	-6.38	-5.88
PEG-AuNP	Dopamine	-7.38	-55.10	-5.79	-5.73	-5.68
Ad-AuNP		-6.63	-24.00	-5.94	-5.91	-5.89
AdGly-AuNP		-11.00	-183.00	-5.78	-5.60	-5.41
PGM-AuNP		-5.64	95.90	-8.40	-8.50	-8.59
PVP-SeNP		-4.70	80.00	-7.00	-7.08	-7.16
Tween-SeNP		-11.10	-177.00	-5.96	-5.79	-5.61
PEG-AuNP	BSA	-9.36	-114.00	-6.10	-5.98	-5.87
Ad-AuNP		-6.74	7.93	-6.97	-6.98	-6.98
AdGly-AuNP		-8.42	-71.10	-6.37	-6.30	-6.23
PGM-AuNP		-10.50	-110.00	-7.38	-7.27	-7.16
PVP-SeNP	hTF	-7.20	-24.5	-6.53	-6.51	-6.48
Tween-SeNP		-21.30	-500.0	-6.88	-6.38	-5.88

#### 4.2.2. *The influence of serum proteins on AuNP and SeNP interactions with catcehol*

An estimate of the influence of proteins present in biological media on the binding affinities was examined. When NP interact with serum proteins, they can form a protein corona around the surface of the nanoparticle, which can significantly impact the efficacy of drug binding.<sup>229,230</sup> BSA and hTF were selected as representatives of serum proteins due to their longer persistence time in the blood and ability to form a protein corona on the surface of the nanoparticle.<sup>206,231</sup> To assess the impact of BSA and hTF on the binding of levodopa and dopamine to AuNP and SeNP, respectively, fluorescence titration measurements were repeated while incorporating BSA or hTF. The obtained results were compared to the binding affinities acquired in the absence of proteins (Table 7) in order to determine the reduction in the binding constant (Figure 14).

The addition of proteins disrupted the balance of the initial binary systems, and the competitive binding led to a decrease in the binding affinities of levodopa/dopamine with the tested NPs. However, the percentage reduction varied depending on the functionalizing agents present on the nanosurface. The reduction in binding constants after the addition of BSA followed the sequence  $\text{PEG-AuNP} \geq \text{AdGly-AuNP} > \text{Ad-AuNP} > \text{PGM-AuNP}$ . These findings were consistent with the binding affinities observed for binary mixtures (Table 7), where levodopa/dopamine-AuNP complexes with lower binding constants exhibited a greater reduction after the addition of BSA. Moreover, the decrease was greater for those AuNP that displayed a higher binding affinity for BSA than for levodopa or dopamine. To explain this phenomenon, levodopa and dopamine had a stronger binding affinity to PGM-AuNP, while BSA binding was comparatively weaker. Consequently, levodopa and dopamine molecules that had already attached to the nanosurface were not easily displaced and substituted by BSA<sup>232,233</sup>, and thus, the effect of protein on the drug binding to PGM-AuNP was insignificant.

On the contrary, investigation of SeNP revealed the opposite effect. Specifically, the decrease in the binding constant for levodopa and dopamine after the addition of hTF was more pronounced for PVP-SeNP than for Tween-SeNP, even though the latter had considerably weaker binding affinities for levodopa and dopamine. Under the experimental conditions used to examine the influence of hTF ( $T = 298 \text{ K}$ ), it was observed that hTF had a slightly stronger binding affinity to PVP-SeNP as opposed to Tween-SeNP. This could potentially disrupt the binding of levodopa/dopamine to PVP-SeNP and cause a greater

reduction in the binding constant of such a system. Consequently, Tween-SeNP might be a preferable choice for use as a drug-delivery system owing to their greater resilience to proteins in biological fluids. Overall, functionalization of AuNP with PGM and SeNP with Tween may enhance the stability of the particles in biological fluids and maintain their drug loading integrity by preventing non-specific interactions with proteins. As a result, it can be inferred that PGM and Tween may enhance the drug-loading capacity of AuNP and SeNP, respectively, and prolong their circulation time in the bloodstream, thus increasing the likelihood of reaching the central nervous system. Additionally, PGM may serve as a promising peptide shuttle with the ability to target the brain with minimal toxicity and disruption.<sup>234</sup> Previous reports have demonstrated that peptidoglycans (PGN) can cross the BBB through the recognition of specific pattern-recognition receptors (PRRs) of the innate immune system, such as PGN-recognition proteins (Pglyrp2) and NOD-like receptors, with high expression of PGN transporter PepT1.<sup>235</sup> Therefore, PGM-AuNP could potentially be employed as a delivery system for dopamine and levodopa to facilitate their BBB crossing and delivery to the targeted CNS areas.

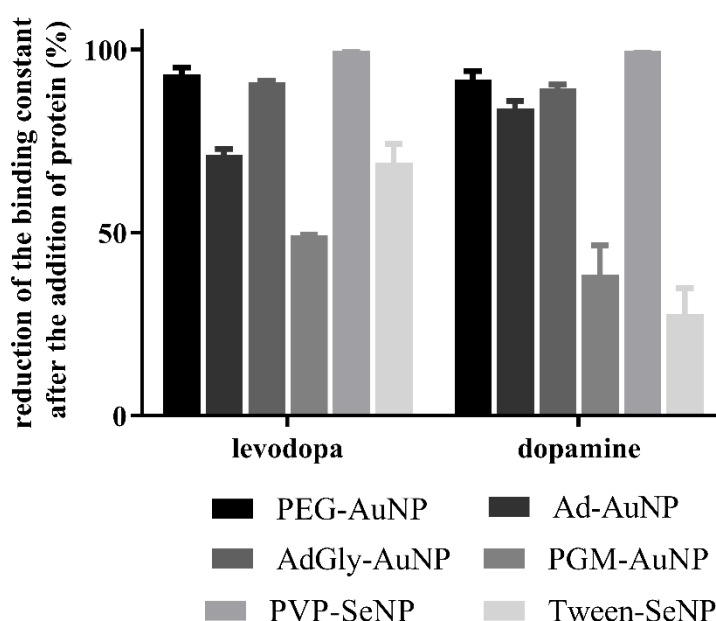


**Figure 14.** Reduction (%) of binding constant ( $K$ ) values for the interaction of levodopa or dopamine with differently coated AuNP and SeNP after the addition of BSA and hTF at 298 K, respectively.

#### 4.2.3. *Changes in $d_H$ , $\zeta$ potential and SPR peak of AuNP and SeNP after interaction with fluorophores*

When AuNP and SeNP were exposed to levodopa, dopamine, and BSA/hTF, alterations in the  $d_H$ ,  $\zeta$  potential, and SPR peak intensity were observed and are shown in Figures 15 and 16. The size and  $\zeta$  potential of the AuNP and SeNP remained practically unchanged after interaction with levodopa and dopamine, respectively, indicating the formation of a highly stable complex between them.<sup>236</sup> An increase in average  $d_H$  values (Figure 15(a)) after interactions with BSA and hTF indicates NP aggregation.<sup>237,238</sup> Moreover, protein binding to almost all NP led to a change in  $\zeta$  potential towards more positive values due to the masking of the charge on the nanosurface (Figure 15(b)). Stabilizing agents such as PEG, PVP and Tween present on the surface of NP improved their stability, as changes in the  $d_H$  and  $\zeta$  potential upon the addition of proteins to such AuNP and SeNP were much smaller compared to differently functionalized NPs. In contrast, PGM- and Ad-AuNP showed a significant increase in average  $d_H$  and  $\zeta$  potential after interaction with BSA, which was possibly caused by the aggregation of these NPs. These results correlate with results obtained for binding constants (Table 7), as BSA showed higher affinities towards PGM- and Ad-AuNP compared to other AuNP. Moreover, BSA adsorption to NP is known to be influenced by the solution pH, and the strongest association between nanoparticle-protein occurs at or near the protein's isoelectric point (pI). In the case of BSA, its pI is within the pH range of 4.5-5.0, which was the pH range used in this study.<sup>239</sup> When BSA is dissolved in water, its hydrophilic surface can interact with negatively charged nanosurfaces through electrostatic or hydrogen bonds, as indicated by thermodynamic analysis. However, binding processes can induce changes in protein conformation and reorientation. Thus, hydrophobic moieties of BSA can be exposed for interactions which can consequently cause aggregation of NPs.<sup>240</sup> Interestingly, when levodopa and dopamine were bound to PGM-AuNP, BSA could hardly approach the nanosurface, which was confirmed by the lowest reduction in binding constants for the interactions of levodopa and dopamine with PGM-AuNP after the addition of BSA. Therefore, it can be concluded that levodopa and dopamine prevent PGM-AuNP from binding to proteins.

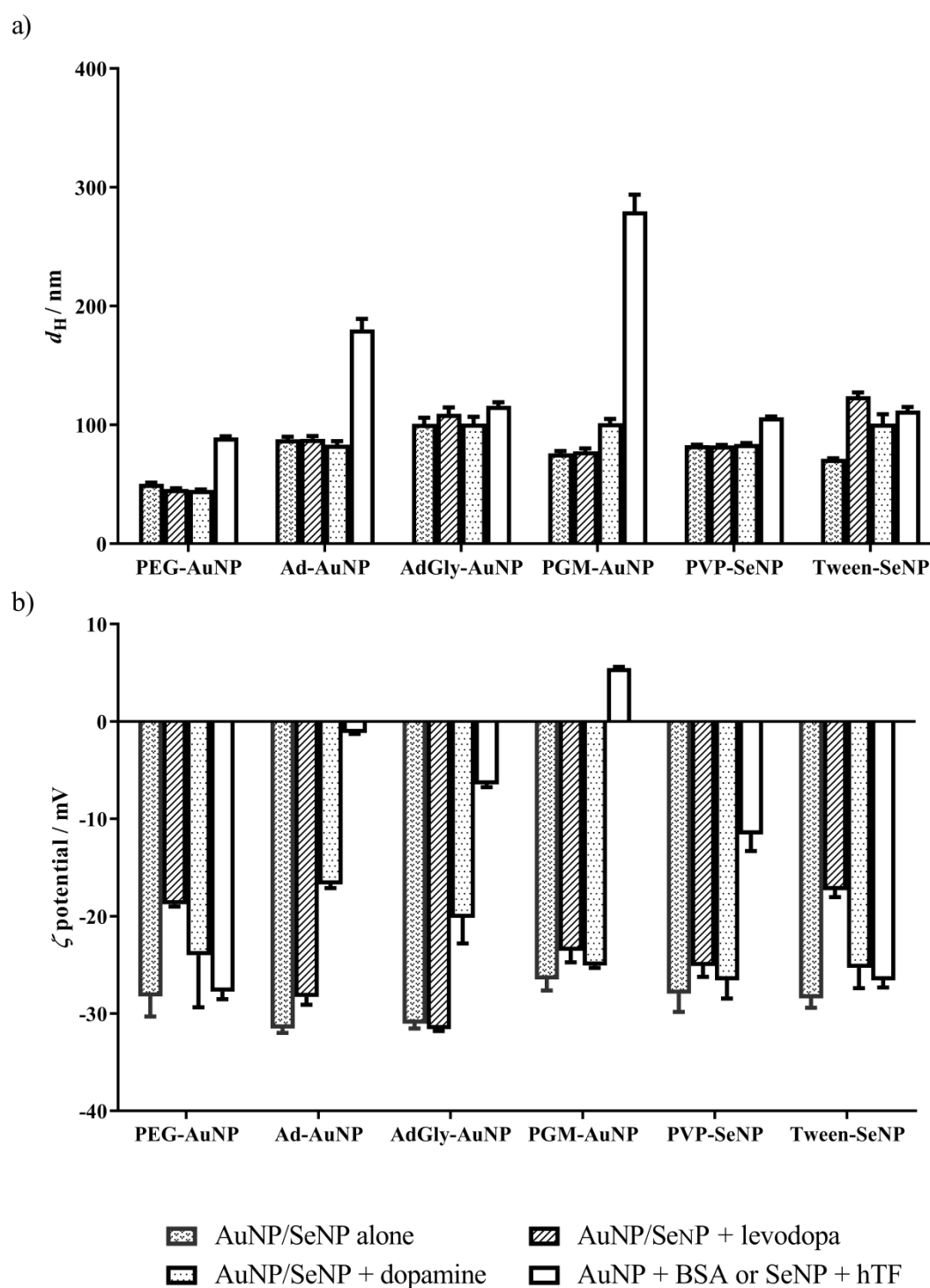


**Figure 15.** Changes in: a) hydrodynamic diameters ( $d_H$ ), and b) zeta ( $\zeta$ ) potentials for differently coated AuNP and SeNP following interaction with levodopa, dopamine or BSA/hTF, measured by dynamic light scattering (DLS), and electrophoretic light scattering (ELS) techniques, respectively. All measurements were done at 25°C in UPW.

Additionally, significant changes in the SPR peak intensity were observed for the binding of BSA and dopamine with Ad- and PGM-AuNP, due to particle aggregation (Figure 16(b,d)) which is also visible from enlargement in  $d_H$  values (Figure 15(a)). In the case of BSA, plasmon coupling occurred within the AuNP aggregates, resulting in a red shift (25-45 nm) and broadening of the plasmon peak. Conversely, the addition of dopamine led to the appearance of a new peak at around 665 nm due to hydrogen-bond-mediated cross-linking between neighboring complexes.<sup>241–245</sup> The changes in SPR peak intensity of PEG- and AdGly-AuNP upon interaction with dopamine and BSA were almost negligible, indicating more stable complexes (Figure 16(a,c)). Additionally, the AuNP exhibited narrower SPR peaks after the addition of levodopa, indicating that the levodopa layer around the AuNP enhances their stability. PGM-AuNP showed a significant increase in absorbance and the most negative values of  $\zeta$  potential after interacting with levodopa, suggesting the formation of a highly stable complex between levodopa and PGM-AuNP. Unfortunately, the SPR changes of SeNP after interactions with fluorophores could not be monitored as SPR peaks for these types of NP are not sufficiently intense.

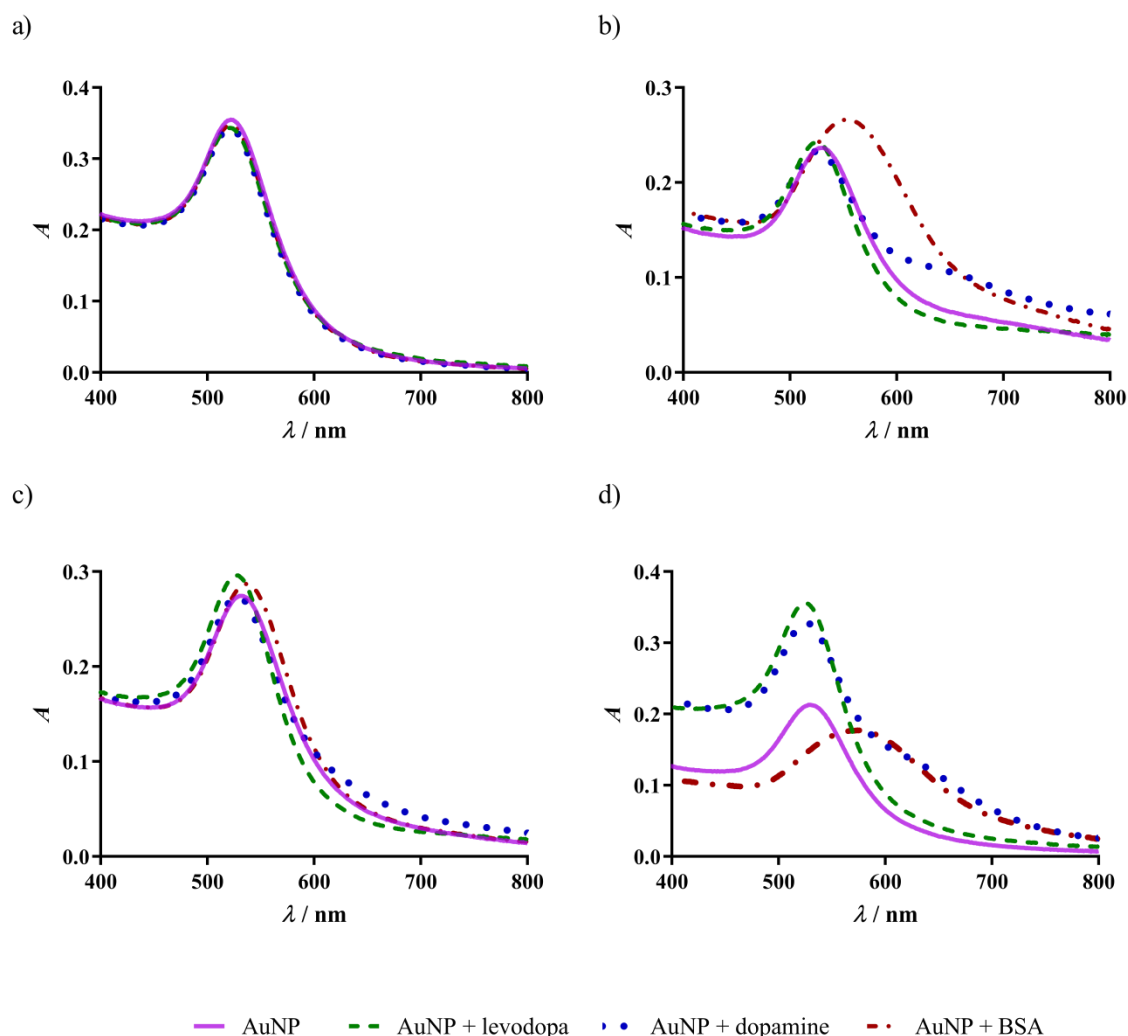


**Figure 16.** Changes in surface plasmon resonance (SPR) peaks of: a) PEG-AuNP, b) Ad-AuNP, c) AdGly-AuNP, and d) PGM-AuNP upon interaction with levodopa, dopamine or BSA.

### 4.3. Drug-loading efficiency of differently coated AuNP and SeNP

Drug loading experiments can help to determine the optimal nano-system for delivering a specific drug to its intended target. Figure 17 shows the DLE data, which exhibit dose-response patterns largely consistent with the observed  $K$  values presented in Table 7. The concentrations of AuNP used in these experiments matched those utilized for fluorescence measurements, with an additional condition featuring an AuNP concentration corresponding to SA of  $5 \times 10^{17} \text{ nm}^2/\text{L}$ . The results revealed that PGM-AuNP consistently showed the greatest amount of bound levodopa and dopamine with more than 80% surface coverage, which is in

accordance with the observed binding affinities. At lower concentrations, PGM-AuNP exhibited a greater affinity for levodopa than dopamine and were found to bind more of the former than Ad- and AdGly-AuNP. PEG-AuNP had the lowest drug amount, which is likely attributable to saturation effects. Ad- and AdGly-functionalized AuNP exhibited comparable drug loading results, even though the observed  $K$  values for Ad-AuNP were much greater than those for AdGly-AuNP. Moreover, the DLE of SeNP was not able to be calculated due to their strong adhesions to the filters used for the separation of NP from free drugs, thus blocking their passage.

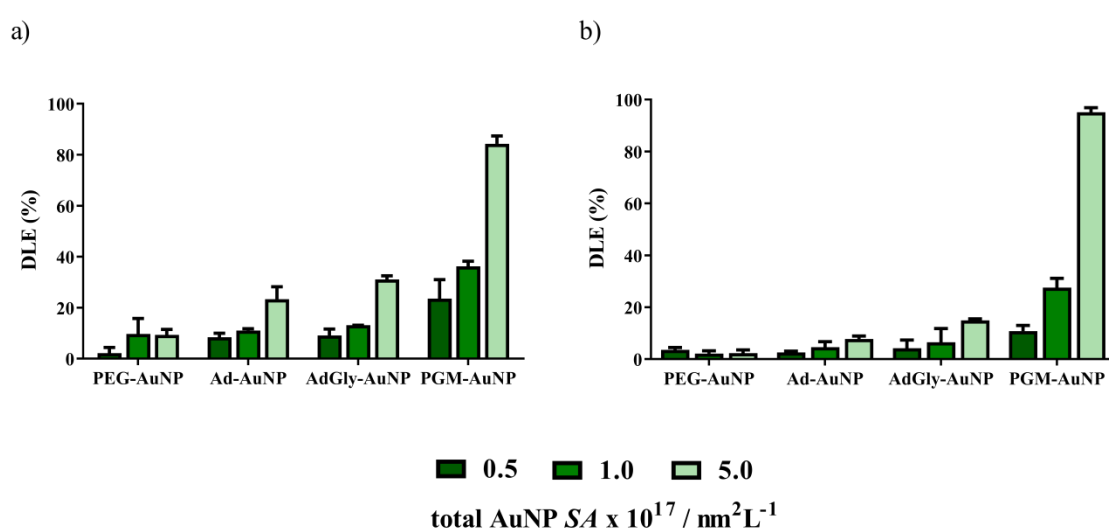


**Figure 17.** The drug-loading efficiency (DLE) of differently coated AuNP loaded with: a) 15  $\mu\text{M}$  levodopa, and b) 25  $\mu\text{M}$  dopamine. Three different surface area (SA) of AuNP were used ( $0.5$ ,  $1.0$ , and  $5.0 \times 10^{17} \text{ nm}^2/\text{L}$ ) and experiments were performed at 298 K.

#### 4.4. Transformation of levodopa and dopamine on the surface of AuNP

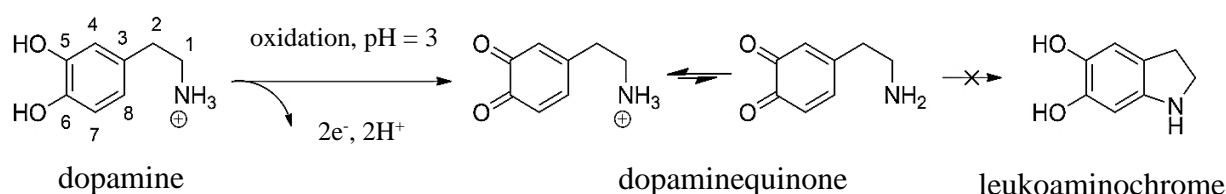
In both the reaction mixtures and purified catechol-functionalized AuNP suspensions, the pH ranged from 3.15 to 3.25. While there have been extensive studies on levodopa and dopamine autoxidation under alkaline and neutral conditions,<sup>246–252</sup> the oxidation of these catechols in an acidic environment has not been well documented. Due to the potential for transition-metal ions to facilitate their oxidation under mildly acidic pH, there has been growing interest in these processes.<sup>253</sup> Therefore, in this doctoral dissertation the aim was to investigate the



behavior of levodopa and dopamine upon interaction with a gold nanosurface in an acidic environment by using a combination of NMR spectroscopy and computational methods.

#### 4.4.1. NMR study

Levodopa and dopamine may be easily oxidized in the acidic medium in the presence of  $\text{HAuCl}_4$ . The extent of the oxidation reaction depends on the molar ratio of reactants  $\text{HAuCl}_4$  and catechols, i.e.,  $[\text{Au}]:[\text{catechols}]$  ratio, which also determines the shape, stability and colour of AuNP (Table 4 and Figure 8). In the case of Au excess, i.e.,  $[\text{Au}]:[\text{dopamine}] = 2:1$ ; as used for the preparation of stable spherical AuNP (Figure 8(b)), dopamine was rapidly and completely oxidized to dopaminequinone (Scheme 1), which remained stable for > 2 hours



**Scheme 1.** Schematic of dopamine oxidation in an acidic environment ( $\text{pH} \approx 3$ ).

The dopaminequinone structure was confirmed using  $^1\text{H}$  and  $^{13}\text{C}$  NMR spectra. Notably, the latter was recorded for the first time, as demonstrated in Figure 18(b). In the  $^1\text{H}$  spectrum (Figure 18(a)), three new signals emerged in the aromatic region and two new signals in the upfield region. In the  $^{13}\text{C}$  spectrum, all of the aromatic signals were shifted downfield, with the two carbonyl signals exhibiting the largest chemical shifts (180.96 and 180.27 ppm). These findings align with the structure of dopaminequinone that was formed during the AuNP formation process and are consistent with previous structural assignments of dopamine oxidation products.<sup>246</sup> Furthermore, the absence of proton signals corresponding to leukoaminochrome, aminochrome, and/or 5,6-dihydroxyindole confirms that cyclization of dopaminequinone did not occur.

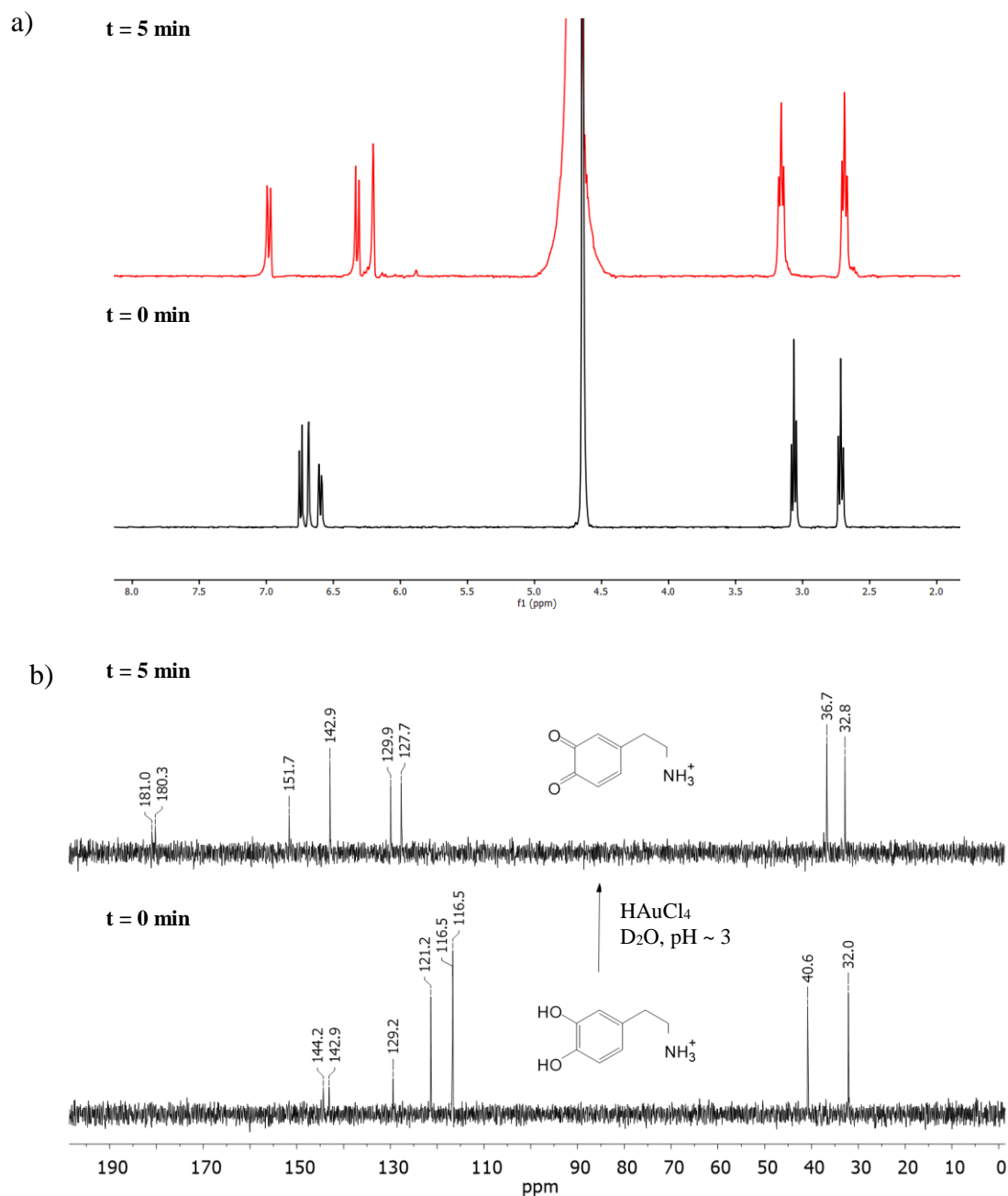


**Figure 18.** a)  $^1\text{H}$  NMR, and b)  $^{13}\text{C}$  NMR spectra of dopamine (10 mM) and dopamine oxidation product (dopaminequinone) in  $\text{D}_2\text{O}$  (pH  $\approx 3$ ;  $[\text{Au}]:[\text{dopamine}] = 2:1$ , as used for the preparation of stable spherical AuNP).

Previous studies have shown that cyclization of dopaminequinone can be triggered by various factors such as increased pH,<sup>253–255</sup> increased voltage in the electrochemical oxidation,<sup>256</sup> by hydrothermal methods,<sup>257</sup> or plasma-activated water.<sup>258</sup> However, it is important to note that

none of these procedures are applicable to the original protocol<sup>93</sup> used for functionalizing AuNP with dopamine.

Conversely, when a ratio of  $[\text{Au}]:[\text{levodopa}] = 2:1$  was applied, as used for the preparation of stable Au nanoflowers, all proton signals of levodopa vanished from the  $^1\text{H}$  NMR spectrum immediately, and three new signals appeared (green spectrum in Figure 19). These newly observed signals in the aromatic and upfield regions correspond to dopaquinone. This represents the first NMR evidence of the initial oxidation product of levodopa.

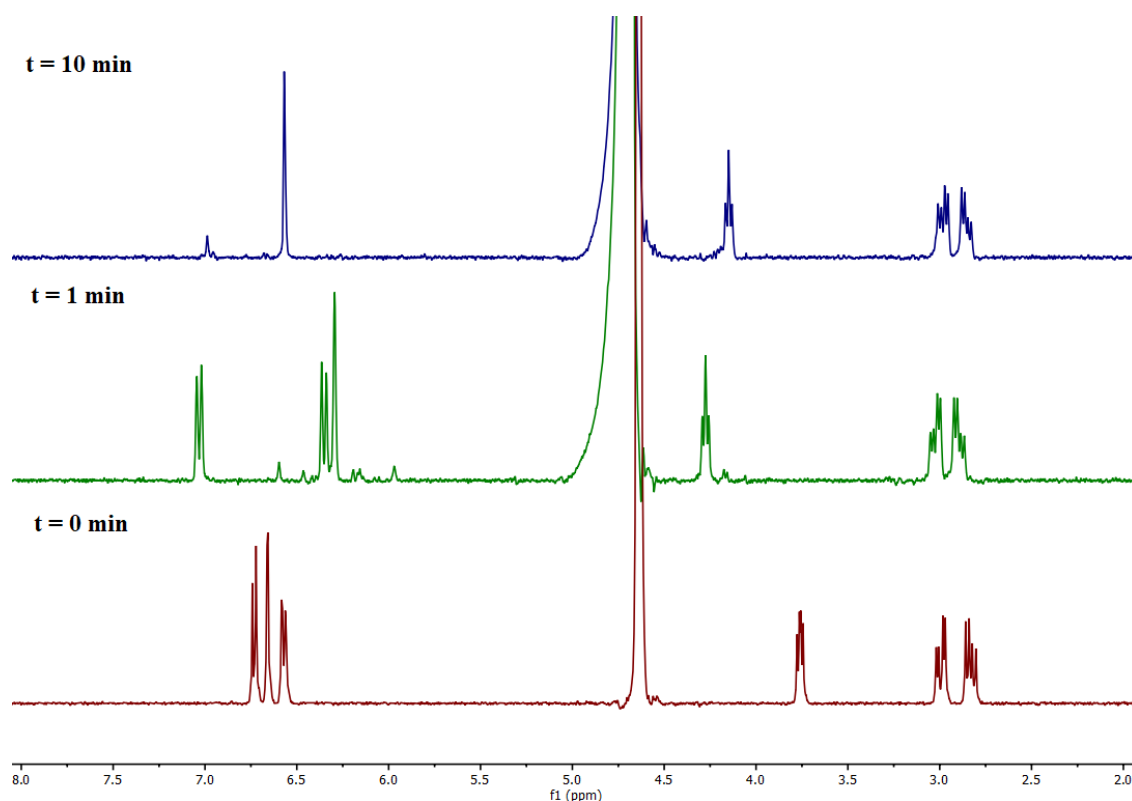


**Figure 19.**  $^1\text{H}$  NMR spectra of levodopa (bottom/red spectrum), its oxidation intermediates dopaquinone (middle/green spectrum), and dopachrome/leukodopachrome (top/blue spectrum) in  $\text{D}_2\text{O}$  ( $\text{pH} \approx 3$ ;  $[\text{Au}]:[\text{levodopa}] = 2:1$ , as used for the preparation of stable Au nanoflowers).

To facilitate a quick and convenient observation of all carbon signals in the aromatic region, the reaction was repeated using ring- $^{13}\text{C}6$ -labeled levodopa (Figure 20). However, the short lifetime of dopaquinone made it difficult to record a well-resolved  $^{13}\text{C}$  NMR spectrum.

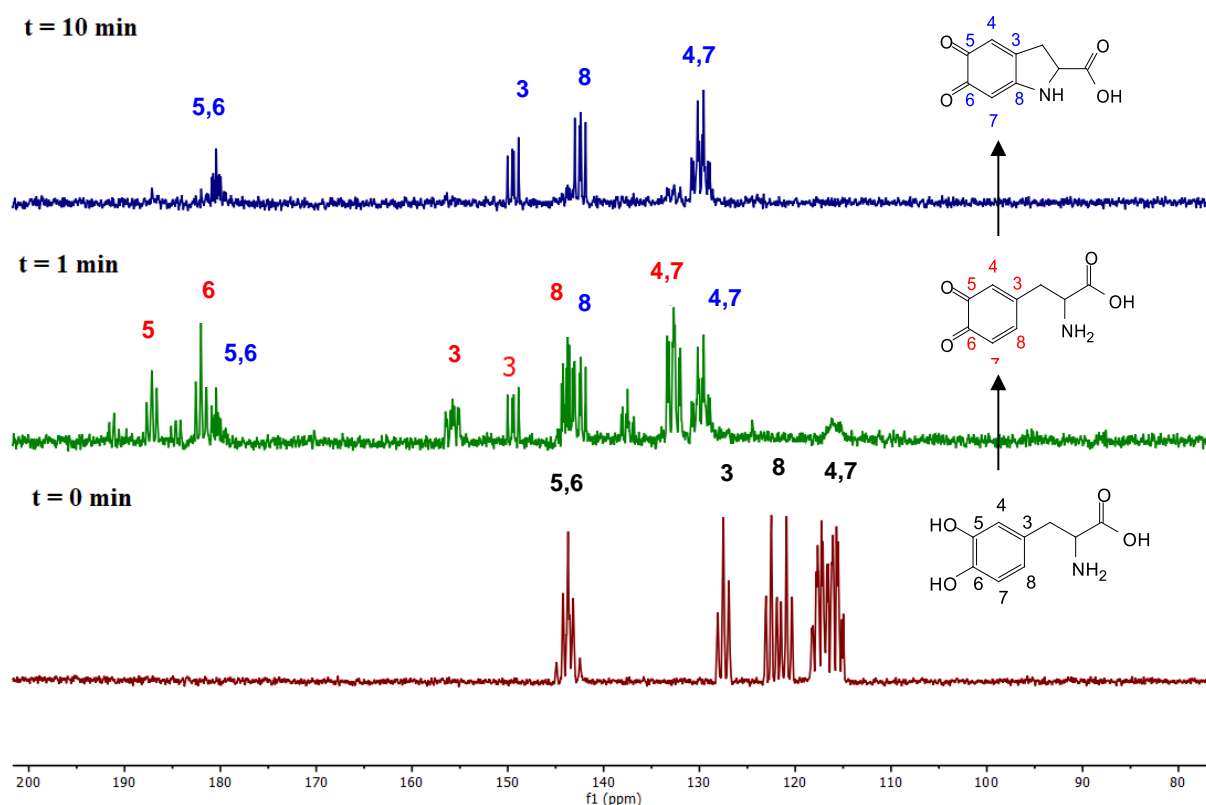
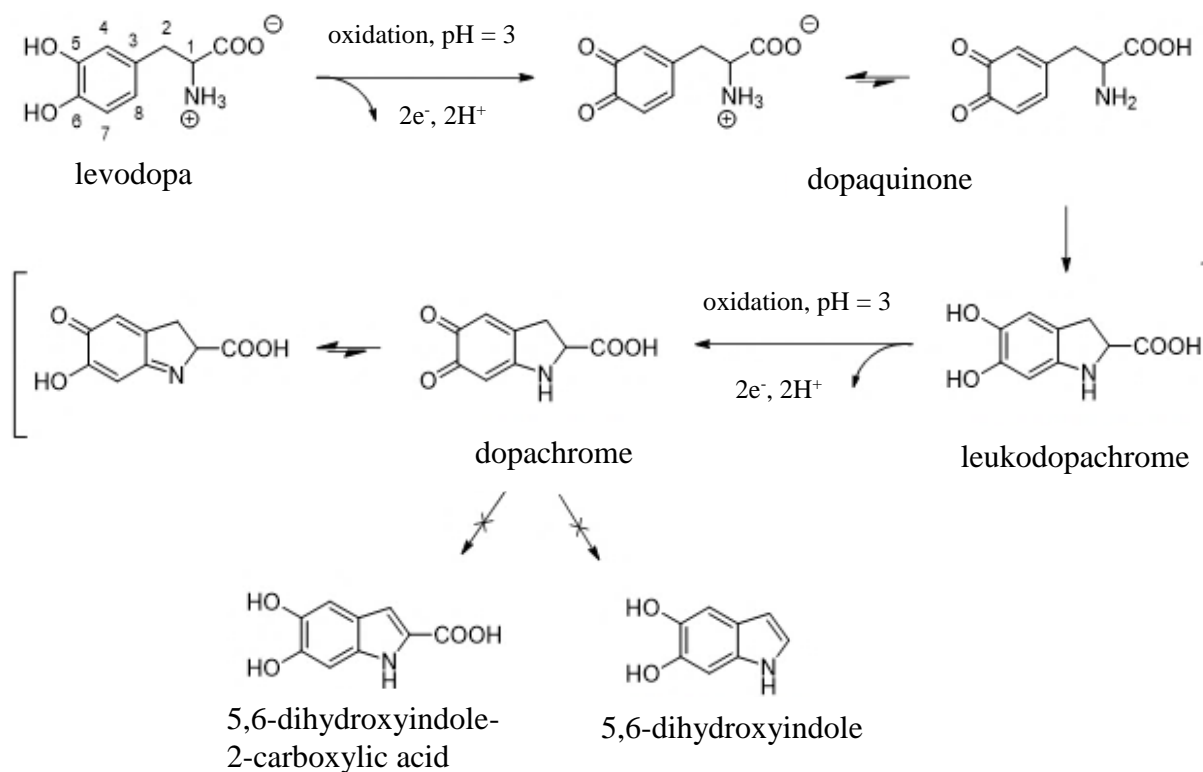


**Figure 20.**  $^{13}\text{C}$  NMR spectra of levodopa (bottom spectrum, black numbers), its oxidation intermediates dopaquinone/dopachrome (middle spectrum, red/blue numbers), and dopachrome (top spectrum, blue numbers) in  $\text{D}_2\text{O}$  ( $\text{pH} \approx 3$ ;  $[\text{Au}]:[\text{levodopa}] = 2:1$ , as used for the preparation of stable Au nanoflowers). All ring carbon atoms 3 – 8 are  $^{13}\text{C}$ -enriched.

It is apparent that dopaquinone undergoes intramolecular cyclization, leading to the formation of leukodopachrome/dopachrome, as illustrated in Scheme 2. In contrast to dopaminequinone, dopaquinone easily undergoes intramolecular cyclization or Michael addition reactions. In the  $^1\text{H}$  NMR spectrum (Figure 19, blue spectrum), two new signals emerged in the aromatic region that corresponds to leukodopachrome or its oxidized form, dopachrome. Both leukodopachrome and its oxidized form, dopachrome, may coexist in a rapid redox equilibrium, which is challenging to distinguish on the NMR time scale. Moreover, dopachrome can tautomerize to its isomeric quinoid structure, which is anticipated to exhibit a signal pattern in the  $^1\text{H}$  NMR spectrum that can be hardly distinguished from

leukodopachrome and/or dopachrome. Likewise, the  $^{13}\text{C}$  NMR spectrum faces a similar issue of spectral ambiguity.



**Scheme 2.** Schematic representation of levodopa oxidation in an acidic environment ( $\text{pH} \approx 3$ ). Structures in squared brackets could not be differentiated by  $^1\text{H}$  NMR spectroscopy (in  $\text{D}_2\text{O}$ ). All structures may exist in zwitterionic form.

From the  $^1\text{H}$  NMR spectrum (Figure 19) it was observed that all dopaquinone signals disappeared within 10 min, while subsequent intermediates (leukodopachrome/dopachrome) persisted in the reaction mixture for roughly 2 hours. This indicates that the rearrangement of dopachrome to 5,6-dihydroxyindole-2-carboxylic acid or its decarboxylation to 5,6-dihydroxyindole are slower processes compared to the cyclization of dopaquinone. Neither 5,6-dihydroxyindole-2-carboxylic acid nor 5,6-dihydroxyindole structures match the experimental chemical shifts observed in the  $^1\text{H}$  and/or  $^{13}\text{C}$  NMR spectra. The most definitive evidence arises from the  $^{13}\text{C}$  NMR spectrum, which detects two  $\text{sp}^3$ -hybridized carbon signals in the upfield region, effectively excluding 5,6-dihydroxyindole-2-carboxylic acid and 5,6-dihydroxyindole as possible oxidation products.

On the other hand, when a large excess of catechols was used in the preparation of stable AuNP, no oxidation product of dopamine or levodopa was observed. The ratio of [Au]:[catechols] appeared to control the products formed during the preparation of AuNP, indicating that the type of coating on the AuNP surface depends on the initial reaction conditions. The  $^1\text{H}$  NMR spectra of the isolated and purified AuNP supported this observation. When the initial ratio of reactants was [Au]:[catechols] = 1:6, the prepared AuNP were coated with dopamine or levodopa only. In contrast, when the ratio of reactants was [Au]:[dopamine] = 2:1, the surface of prepared AuNP was modified with dopaminequinone; while at the ratio of [Au]:[levodopa] = 2:1 three different oxidation products of levodopa may be involved in interactions with the AuNP surface: leukodopachrome, dopachrome or its tautomeric form. These three intermediates could not be differentiated by  $^1\text{H}$  NMR spectroscopy.

#### 4.4.2. DFT calculations

DFT calculations were carried out to gain a better understanding of the mechanism behind the oxidation processes in catechols during the synthesis and functionalization of AuNP. An important aspect of this analysis was to examine the reactivity of dopaquinone and dopaminequinone and their intramolecular cyclization. Upon initial oxidation, both levodopa and dopamine are transformed into their respective quinone forms, which have the potential to undergo intramolecular Michael addition as shown in Schemes 1 and 2. In this reaction, the amino group containing lone-pair electrons attacks the C5 position in the oxidized catechol ring. Previous studies have reported that the experimental barriers (at 298 K) for the intramolecular cyclization of dopaquinone ( $\Delta G^\ddagger = 62.3$  kJ/mol) and dopaminequinone ( $\Delta G^\ddagger = 64.8$  kJ/mol) are rather similar.<sup>259,260</sup>

The SMD-M06L/6-31+G(d,p)/LANL2DZ level of theory successfully reproduced the experimental results, as evidenced by the calculated  $\Delta G^\ddagger$  of 63.3 kJ/mol and 58.9 kJ/mol for dopaquinone and dopaminequinone, respectively. This indicates that the intrinsic rates of cyclization are similar and fairly rapid for both compounds. The rate-determining step of the cyclization involves the unprotonated form of the amino group, making the rate of reaction dependent on pH. In our particular scenario, in the presence of  $\text{HAuCl}_4$  at a relatively low pH, cyclization only occurred in the case of dopaquinone (as mentioned earlier). This distinct reactivity between dopaquinone and dopaminequinone has been attributed to the proportion of

neutral amino groups, as denoted by the pre-equilibrium acidity constant ( $K_a$ ). Previous studies have revealed that the  $pK_a$  value of the  $NH_3^+$  group in dopaquinone is approximately 2 units lower than in dopaminequinone, which results in a 10-fold difference in the cyclization rates.<sup>253,255</sup>

To evaluate the impact of AuNP on the cyclization rate, the reactants (dopaquinone and dopaminequinone), transition states, and products (leukodopachrome and leukoaminochrome) were complexed with the neutral cluster  $Au_n$ , where  $n$  equals 2, 4, or 6. Compared to the reaction in the absence of metal ( $n = 0$ ), the calculated  $\Delta G^\ddagger$  for all  $Au_n$ -assisted cyclizations increased by approximately 30-40 kJ/mol, as shown in Table 9. Despite this increase, the predicted rates for intramolecular Michael  $N$ -additions were still similar for both dopaquinone and dopaminequinone. Using the Eyring equation derived from transition state theory, the computed  $\Delta G^\ddagger = 91.7 - 101.9$  kJ/mol correspond to reaction rate constants  $k_{obs}$  of approximately  $5 \times 10^{-4} - 9 \times 10^{-6} s^{-1}$  ( $t_{1/2} \sim 0.4 - 20.8 h^{-1}$ ).

Previous research has been suggested that the effect of  $Au_n$  clusters on the  $pK_a$  value of the ionizable amino group is not significant.<sup>253</sup> Therefore, different rates of cyclization between dopaquinone and dopaminequinone observed in experiments was not caused by the presence of  $Au_n$  nanoclusters. In contrast to dopaminequinone, the intramolecular cyclization of dopaquinone occurs more easily due to the (greater) intrinsic acidity of its nucleophilic amino group. Based on calculations obtained in this study, the formation of cyclized products is highly exergonic, which means that leukodopachrome and leukoaminochrome are more stable than dopaquinone and dopaminequinone, respectively. For both metal-free and Au-assisted reactions, the cyclized products were found to be 25-75 kJ/mol more stable (Table 9), indicating that both reactions are thermodynamically favoured. The calculated  $\Delta G^\ddagger$  for Au-assisted reactions indicated that both reactions are potentially feasible ( $\Delta G^\ddagger \approx 100$  kJ/mol). However, because of the higher protonation state ( $NH_3^+$ ) of dopaminequinone, it cannot undergo nucleophilic Michael  $N$ -addition. Therefore, only the cyclized product of dopaquinone was observed.

Leukodopachrome may undergo oxidation to form dopachrome, which can exist in equilibrium with its quinoid tautomer (Scheme 2). It is difficult to identify the definitive form of the intermediate that accumulates in the presence of  $Au_n$  clusters, as evidenced by the NMR data. To determine which oxidation product could potentially serve as a coating candidate for AuNP, classical MD simulations were conducted. These calculations yielded

binding free energies (discussed below), providing insight into the interaction and stability of various species on the surface of AuNP.

**Table 9.** The relative energies ( $\Delta G^0$  in kJ/mol) of the stationary points that participate in the intramolecular cyclization of dopaquinone and dopaminequinone calculated using SMD-M06L/6-31+G(d,p)/LANL2DZ. These points include the reactant **R**, transition state **TS**, and product **P** (leukodopachrome and leucoaminochrome), which are complexed with a specific number of Au atoms denoted by  $n$ .

$\text{Au}_n$	Stationary point	$\Delta G^0 / \text{kJmol}^{-1}$	
		dopaquinone	dopaminequinone
$n = 0$	R	0.0	0.0
	TS	+63.3	+58.9
	P	-85.0	-74.1
$n = 2$	R	0.0	0.0
	TS	+94.1	+97.5
	P	-38.9	-26.4
$n = 4$	R	0.0	0.0
	TS	+101.9	+101.7
	P	-17.7	-25.9
$n = 6$	R	0.0	0.0
	TS	+91.6	+97.1
	P	-63.8	-47.2



#### 4.4.3. MD simulations

In order to compare the adsorption of different levodopa oxidation intermediates (leukodopachrome, dopachrome, and its quinoid tautomer) on AuNP, classical MD simulations with an Au nanosurface were employed. Since classical MD does not allow covalent bond formation, the simulations only considered physical interactions.<sup>261</sup> The results showed that, in all cases, the species moved downwards from their initial positions and attached to the Au plates within the first few nanoseconds (10 ns) of the simulation, where they persist for the entire duration of the MD simulations (50 ns). For each Au/ligand binding was strong enough to prevent desorption, but sufficiently weak to allow lateral diffusion. This is in accordance with previously published results.<sup>84,262–264</sup> The MD simulations indicate that all functional groups contribute to the interaction between levodopa oxidation products and the Au surface, as shown in Figure 21.

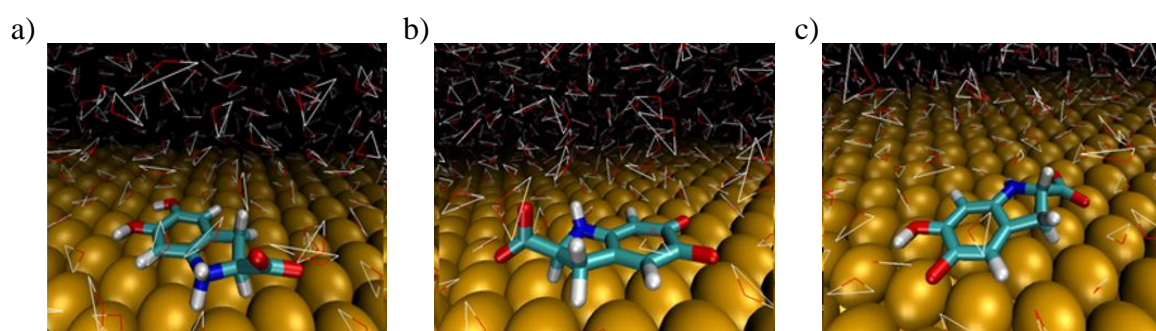


**Figure 21.** Close-up snapshots of the last frames of the production run from classical MD simulations of zwitterionic forms of: a) leukodopachrome, b) dopachrome, and c) dopachrome tautomer on Au(111) surface. Au atoms are shown as spheres of the corresponding van der Waals radius in orange, the ligand molecules are shown in Licorice mode, and the waters in Line mode as triangles due to the nature of the TIP3P water model. The binding free energies were calculated using the MM-GBSA protocol.

The MM-GBSA method was employed to compute the adsorption-free energy of each ligand onto the Au nanosurface. Although this computational approach is not entirely reliable for calculating absolute energies, it has been shown to be accurate in evaluating relative binding energies, so is widely used for comparing and ranking the affinities of similar ligands to a

particular receptor.<sup>265</sup> Collectively, the MM-GBSA outcomes at room temperature demonstrate that all three molecular adsorption processes are spontaneous from a thermodynamic perspective. Additionally, the results indicate that dopachrome exhibited the highest affinity to the Au nanosurface ( $\Delta G_{\text{bind}} = -182.9$  kJ/mol), followed by leukodopachrome ( $\Delta G_{\text{bind}} = -160.9$  kJ/mol) and dopachrome tautomer ( $\Delta G_{\text{bind}} = -125.0$  kJ/mol). These results aided in identifying the most suitable oxidation intermediate for functionalizing AuNP. In our study, the combination of MD simulations and NMR analysis (as mentioned earlier) confirmed that the dopachrome species exclusively modifies the surface of the synthesized AuNP when Au was used in excess, *i.e.*, [Au]:[levodopa] = 2:1.

## 4.5. Permeability of AuNP and SeNP through BBB

### 4.5.1. Evaluation of AuNP and SeNP permeability using BBB-PAMPA model

In this study, the BBB-PAMPA model was selected to assess the passive permeability of SeNP and AuNP alone or in combination with levodopa through the BBB. To simulate the BBB, a polycarbonate membrane coated with a polar brain lipid extract solution was used to separate the donor wells containing compounds of interest from the acceptor wells. To ensure the reliability of the PAMPA-BBB assay, a well-established FDA standard known as carbamazepine, was employed as a positive control, thus checking the consistency of the assay. This compound is recognized for its capability to passively diffuse through the cell membrane into the acceptor wells.<sup>266</sup> The substances selected for examination were Tween-SeNP and PEG-AuNP alone or in combination with levodopa. These compounds together with carbamazepine were placed in the donor compartments. The donor plate was then carefully placed on the acceptor plate so that the filters of all wells sit in the UPW previously added to the acceptor wells. The system was put on a shaker and left to incubate at room temperature for 4 hours since a longer period as recommended in the literature (18 hours) did not yield results.<sup>185,266</sup> After a 4-hour incubation period, concentrations of carbamazepine and levodopa were analyzed using UV/vis spectroscopy, while AAS was used to determine the content of Au and Se. The UV/Vis spectra were recorded at 280 nm as levodopa and carbamazepine demonstrate the highest absorbance values at this wavelength. Unlike levodopa, carbamazepine demonstrated the ability to effectively penetrate the artificial membrane. Using Equation 11, the  $\log(P_{\text{app}})$  value for carbamazepine was determined and the

resulting value of -4.46 matched the previously reported  $\log(P_{app})$  value of -4.54. This confirms the validity of the conducted experiments and accuracy of the obtained results.

Additionally, AAS results (Table 10) showed that only a small amount of Tween-SeNP was identified in the acceptor compartment after 4 hours of incubation, while Au content in the acceptor plate was not able to be measured as it was below the limit of quantification (LQ). However, the concentration of Au in the donor plate stayed the same as before the incubation, indicating that no AuNP permeated through the membrane to the acceptor plate. Higher Au and Se concentrations in the donor chamber when compared with the initial exposure concentration (20/200 mg Au or Se/L) could be due to some degree of evaporation of the media under the experimental conditions. These results are consistent with previously published research on AuNP,<sup>187</sup> leading us to conclude that investigated NP are not primarily transported across the BBB through passive diffusion.

**Table 10.** Se and Au concentrations in donor and acceptor compartments obtained from atomic absorption spectroscopy (AAS) measurements after blood-brain barrier specific parallel artificial membrane permeability assay (PAMPA-BBB).

ACCEPTOR PLATE				
	1	2	3	4
	PEG-AuNP	PEG-AuNP	PEG-AuNP	PEG-AuNP
A	(20 mg Au/L)	(200 mg Au/L)	(20 mg Au/L) + levodopa	(200 mg Au/L) + levodopa
	<LQ	<LQ	<LQ	<LQ
	Tween-SeNP	Tween-SeNP	Tween-SeNP	Tween-SeNP
B	(20 mg Se/L)	(200 mg Se/L)	(20 mg Se/L) + levodopa	(200 mg Se/L) + levodopa
	0.05 mg Se/L	0.09 mg Se/L	0.06 mg Se/L	0.06 mg Se/L
DONOR PLATE				
	1	2	3	4
	PEG-AuNP	PEG-AuNP	PEG-AuNP	PEG-AuNP
A	(20 mg Au/L)	(200 mg Au/L)	(20 mg Au/L) + levodopa	(200 mg Au/L) + levodopa
	19.39 mg Au/L	204.8 mg Au/L	18.98 mg Au/L	210.6 mg Au/L
	Tween-SeNP	Tween-SeNP	Tween-SeNP	Tween-SeNP
B	(20 mg Se/L)	(200 mg Se/L)	(20 mg Se/L) + levodopa	(200 mg Se/L) + levodopa
	25.74 mg Se/L	202 mg Se/L	25 mg Se/L	224.2 mg Se/L

#### 4.5.2. Evaluation of AuNP and SeNP permeability using transwell assay

In contrast to the PAMPA model, the cell-based transwell assay can predict the permeability of compounds that can pass through either passive diffusion or active mechanisms, and is considered more reliable due to the use of human cells.<sup>187</sup> This study utilized hBEC-5i cells, derived from the human cerebral cortex as a representative sample of brain tissue, which exhibit specific protein expression unique to the cell type.<sup>139</sup> Herein, hBEC-5i cells were grown on a porous membrane that was previously coated with 0.1% w/v gelatin solution. The monoculture model used in this study involved two compartments (donor and acceptor).

The concentration of AuNP and SeNP chosen for this experiment was determined by flow cytometry analysis (Figure 22). Moreover, the impact of the selected concentration of SeNP and AuNP (10 mg Se or Au/L) on both cell viability and apoptosis induction was investigated. After a 24-hour treatment, a decrease in cell viability was observed for SeNP (10 mg Se/L), while AuNP did not cause any negative effect on hBEC-5i cells under these conditions. Indeed, both types of AuNP caused a considerable rise in cell viability at this concentration (Figure 21(c)). To overcome the viability results with SeNP, an additional lower concentration (1 mg Se/L) was tested. The results revealed that this concentration of SeNP (1 mg Se/L) exhibited a greater proportion of viable cells and a lower proportion of cells undergoing apoptosis (Figure 22(b)). Concentrations that resulted in only a minimal reduction in the number of viable cells were chosen for further experiments. Therefore, for the transwell assay, a lower concentration of SeNP (1 mg Se/L) and an initial concentration of AuNP (10 mg Au/L) were selected as they were non-toxic.

Afterward, chosen concentrations of AuNP and SeNP were added into the donor compartment, and the number of NP that passed through cells, gelatin and membrane into the acceptor compartment was measured. To determine the number of AuNP and SeNP present in each compartment, AAS was employed, and the results were expressed as a percentage of Se and Au, as illustrated in Figure 23.

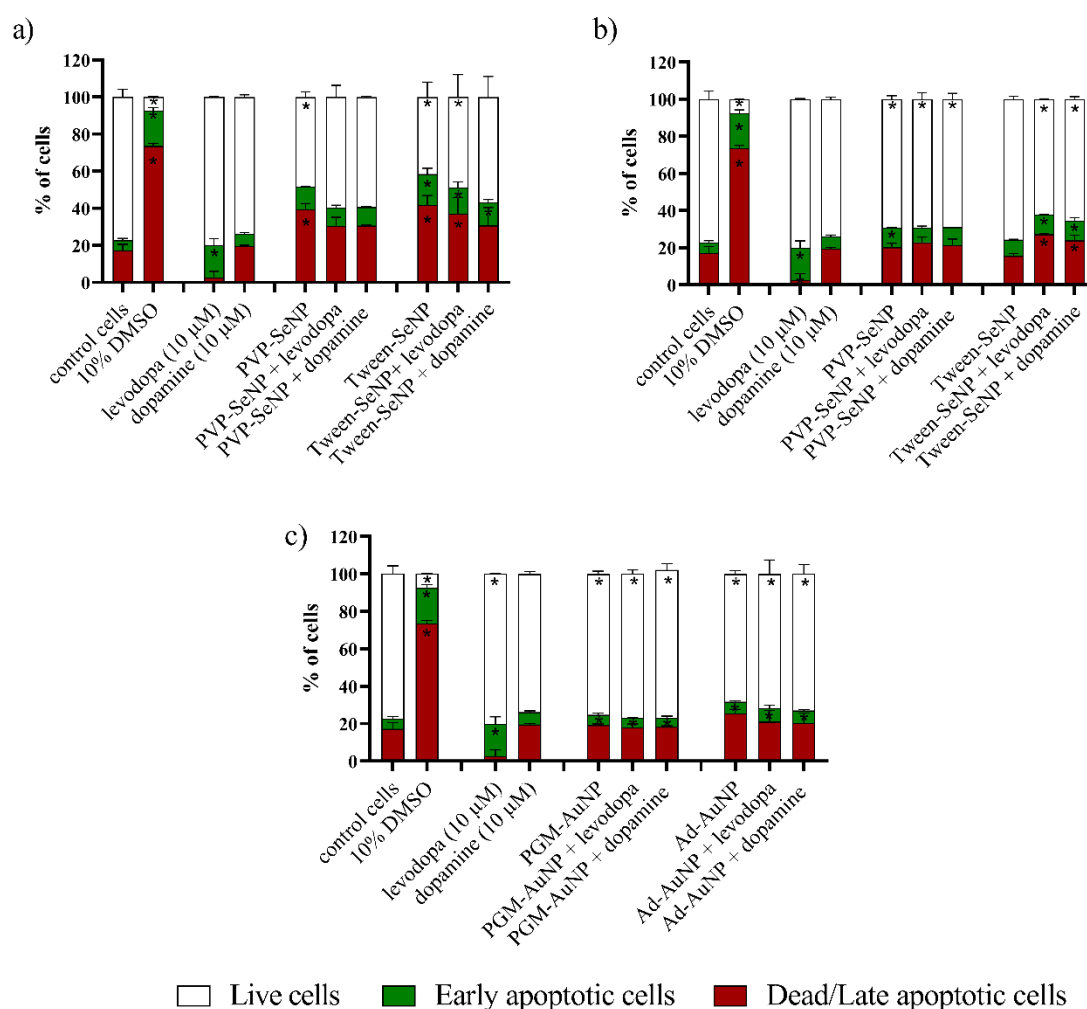


**Figure 22.** Flow cytometry results on viability and apoptosis induction in hBEC-5i cells treated with: a) 10 mg Se/L SeNP, b) 1 mg Se/L SeNP, and c) 10 mg Au/L AuNP for 24 h at 37°C and 5% CO<sub>2</sub>. Red – Dead/Late apoptotic cells, Green –Early apoptotic cells, White – Live cells. Non-treated cells were used as a negative control, while cells treated with 10% DMSO were used as a positive control. Results are presented as % of a number of cells and calculated as mean values obtained from 3 replicate experiments. Statistical significance was determined by one-way ANOVA with Dunnett’s multiple comparison test ( $p < 0.05$ ). Results significantly different compared to control cells are denoted with an asterisk (\*).

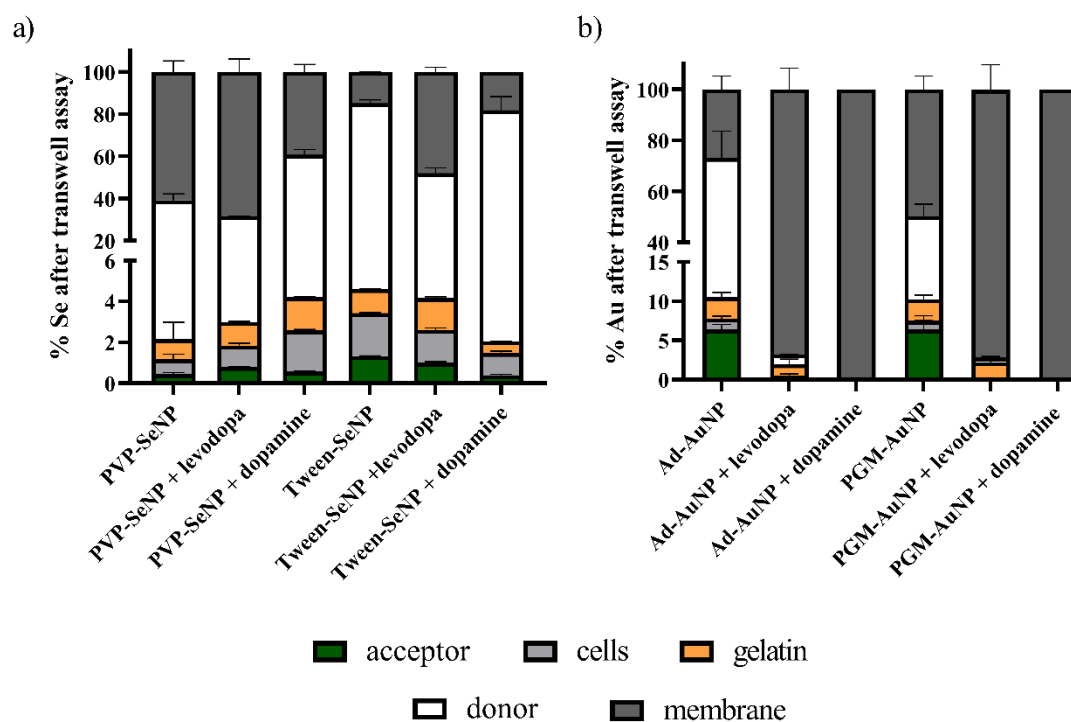


**Figure 23.** Percentages of: a) Se, and b) Au in different compartments (acceptor, cells, gelatin, donor, and membrane) of the transwell system calculated from atomic absorption spectroscopy (AAS) measurements.

The results revealed that the majority of AuNP and SeNP remained in the donor compartment or got stuck on the membrane after a 3-hour incubation period, with less than 10% of Au and Se detected in the acceptor, gelatin, and cell compartments together, respectively. When the transwell assay was treated with Tween-SeNP alone or in combination with levodopa and dopamine, approximately 1% of Se was detected in the acceptor compartment, while mixtures of PVP-SeNP showed even less amount of Se in this compartment. However, when levodopa or dopamine was bound to the PVP-SeNP, an increase in Se concentration was observed in all three compartments (acceptor, gelatin and cell). The opposite effect was observed in the case of Tween-SeNP. Moreover, the addition of levodopa caused an increase in the adherence of PVP-SeNP and Tween-SeNP to the membrane. The same effect was observed when Tween-SeNP were conjugated with dopamine, while dopamine lessened the attachment of PVP-SeNP to the membrane by 20% in comparison to PVP-SeNP alone. Regarding AuNP conjugated with dopamine, it was not possible to detect concentrations of Au in any compartment probably because the whole amount of AuNP was stuck on the membrane. Additionally,

when levodopa was bound to AuNP similar results were observed with only 3% of Au found in all compartments together. Such lack of permeability of *in vitro* model of BBB was found previously for other types of AuNP, such as citrate and 11-mercaptoundecanoic acid-coated AuNP.<sup>267</sup>

In addition to the results obtained by AAS, an ELISA kit was used to measure the concentrations of dopamine and levodopa in each compartment (Figure 24). However, the results were not reliable since levodopa and dopamine were detected in the donor and gelatin compartments after treatment only with NP. Additionally, levodopa was also detected in the donor compartment, while dopamine was found in cells and gelatin compartments of control cells. It can be concluded that the ELISA kit for both dopamine and levodopa was not sufficiently selective due to the presence of similar molecules in the systems. Although the cell medium was replaced with BSA to minimize the presence of molecules that might interfere with levodopa and dopamine detection, it was not possible to eliminate them completely as such molecules could originate from decomposed cells or gelatin. However, unlike dopamine, levodopa was found in the acceptor compartment but the increase in levodopa concentration when bound to the nanosurface in comparison to when alone was not observed. Interestingly, a mixture of both SeNP with dopamine showed their internalization in cells using AAS (Figure 22), while the ELISA method did not detect dopamine in this compartment (Figure 23). Possibly the ELISA kit could not detect such a small amount of dopamine or SeNP entering cells without dopamine which may have detached from the nanosurface before internalization. This could be caused by the lower binding affinity of dopamine to SeNP in comparison to levodopa.

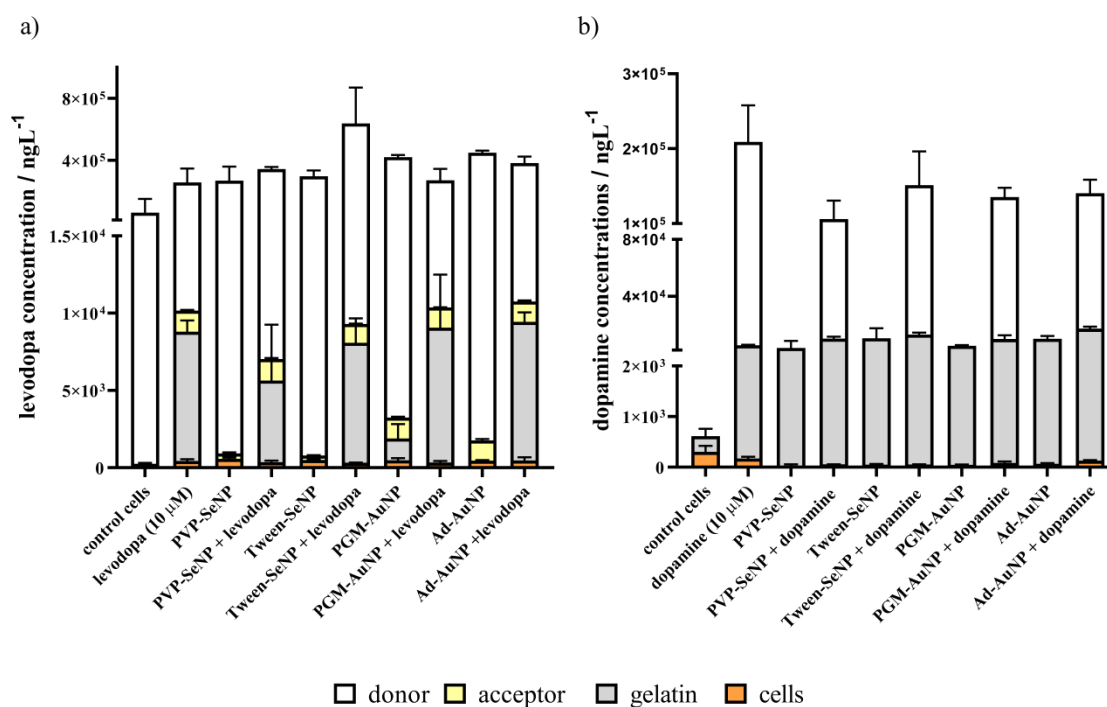


**Figure 24.** Concentrations of: a) levodopa, and b) dopamine in donor, acceptor, gelatin and cell compartments determined with a commercial ELISA kit after transwell assay.

Although the BBB transwell model is commonly used in the pharmaceutical industry for rapid drug permeability screening, it is not entirely suitable for studying NP permeability, as confirmed here. NPs can present additional challenges, such as self-agglomeration and adherence to the transwell membrane, which may exacerbate common transwell assay issues.<sup>139,268</sup> This study examined these issues for SeNP. First, the stability of SeNP in the medium (PBS) in which they are exposed to cells was tested. The results of DLS and ELS experiments indicated that both types of SeNP were enlarged in PBS compared to UPW (Table 11). Consequently, these larger SeNP reached the cells and influenced the transport process. Therefore, these agglomerates may be too large to pass through the membrane and may result in imprecise outcomes.



**Table 11.** The hydrodynamic diameter ( $d_H$ ) values of different types of SeNP in phosphate buffer saline (PBS) and ultrapure water (UPW) obtained from the size intensity-weighted distribution ( $n = 6$ ) using the dynamic light scattering (DLS) method. All measurements were done at 25°C in UPW and NP concentration of 100 mg Se/L.

NP type	PVP-SeNP		Tween-SeNP	
Medium	UPW	PBS	UPW	PBS
$d_H$ / nm	82.9 ± 0.5	132.2 ± 11.5	71.5 ± 0.4	101.9 ± 7.1
(% mean volume)	(100)	(100)	(100)	(100)

Additionally, the potential adherence of SeNP to the membrane was investigated by using a membrane with the same pore size (0.4  $\mu\text{m}$ ) as used for the transwell assay but without cells grown on it. The membrane was either coated with gelatine to mimic the BBB transwell assay or left bare. Se concentrations were measured using AAS. When the membrane was left bare, approximately half of PVP-SeNP adhered to the membrane, while Tween-SeNP did not adhere at all, but remained almost intact in the donor compartment (Table 12). In contrast, when the membrane was coated with gelatin, approximately 80% of Se was found adhered on the membrane. This result was in compliance with the results obtained using the transwell assay, where the gelatin compartment followed the donor compartment in terms of the amount of Se. Such interference could potentially cause agglomeration of SeNP inside the membrane pores, obstructing the transport of the NP.

**Table 12.** Percentage of Se in donor, acceptor and membrane compartment calculated from atomic absorbance spectroscopy (AAS) measurements using bare membrane and gelatin-coated membrane after acellular experiments, respectively.

NP type	Bare membrane			Gelatin-coated membrane		
	% Se in donor plate	% Se in acceptor plate	% Se adhered on the membrane	% Se in donor plate	% Se in acceptor plate	% Se adhered on the membrane
PVP-SeNP	$48.93 \pm 1.10$	$0.19 \pm 0.04$	$50.88 \pm 1.14$	$16.70 \pm 0.06$	$0.08 \pm 0.00$	$83.22 \pm 0.06$
Tween-SeNP	$99.37 \pm 2.16$	$0.63 \pm 0.15$	0	$22.08 \pm 0.93$	$0.29 \pm 0.14$	$77.63 \pm 1.07$

## § 5. CONCLUSIONS

Based on the results obtained in this thesis, the following conclusions are made:

- All spherical AuNP and SeNP synthesized in this doctoral study were smaller than 100 nm and had a negative  $\zeta$  potential.
- Steady-state fluorescence measurements revealed that differently coated AuNP and SeNP quenched levodopa, dopamine and BSA/hTF fluorescence which indicated the formation of binding complexes, while time-resolved measurements confirmed static quenching mechanisms for all the investigated systems.
- The  $K$  values and impact of serum proteins were dependent on the functionalizing agents on the nanosurface. Notably, PGM-AuNP and PVP-SeNP showed the strongest binding affinity and drug-loading efficiency toward levodopa and dopamine, respectively. BSA and hTF influence on drug binding was negligible for PGM-AuNP and Tween-SeNP.
- Thermodynamic analysis revealed that all binding processes were spontaneous and occurred mainly due to hydrogen bonding/van der Waals interactions and electrostatic interactions.
- Changes in  $d_H$  and  $\zeta$  potential upon interaction depended on surface functionalization. Serum proteins increased  $d_H$  and  $\zeta$  of AuNP and SeNP significantly, while stabilizing agents could minimize their binding to the nanosurface. PGM-AuNP showed a significant increase in SPR peak intensity and the most negative values of  $\zeta$  potential after interaction with levodopa, which suggested the formation of a highly stable complex.
- The stability of catechols during AuNP preparation was dependent on the molar ratio to Au. A large molar excess of levodopa or dopamine was needed for either to be present on the gold nanosurface in their original state. Conversely, a molar excess of Au promotes catechols oxidation.
- In comparison to dopaminequinone, dopaquinone underwent intramolecular cyclization in which additional oxidation products, leukodopachrome, dopachrome, or its tautomer, were formed. MD simulations revealed that of these three species, dopachrome is the most likely candidate for binding to AuNP.

- Transwell and PAMPA assays showed negligible permeability through the BBB for the investigated AuNP and SeNP. Overall, these model systems are not the most suitable for the investigation of the permeability of NP.

The obtained results confirmed the hypothesis that the binding ability of levodopa and dopamine to AuNP and SeNP depends on the nanosurface functionalization and processes that occur at the nanoparticle-drug interface. These results are essential for the development of new, safer and effective nanocarriers with efficient drug-loading, BBB-penetration, and CNS-targeting ability of levodopa or dopamine to potentially improve therapies for PD. Based on the results obtained, the most likely candidate for this purpose are PGM-functionalized gold NP. Therefore, this nanosystem will be the focus of further investigations.

## § 6. LIST OF ABBREVIATIONS AND SYMBOLS

<b>AAS</b>	atomic absorption spectroscopy	<b>ECGS</b>	endothelial cell growth supplement
<b>Ad</b>	1-adamantylamine hydrochloride	<b>ELS</b>	electrophoretic light scattering
<b>Ad-AuNP</b>	1-adamantylamine-functionalized AuNP	<b>EMA</b>	European Medicine Agency
<b>AdGly</b>	1-adamantyl-glycine	<b>EPR</b>	enhanced permeability and retention
<b>AdGly-AuNP</b>	1-adamantyl-glycine-functionalized AuNP	<b>FDA</b>	U.S. Food and Drug Administration
<b>AMT</b>	adsorption-mediated transcytosis	<b>FRET</b>	fluorescence resonance energy transfer
<b>ApoE</b>	apolipoprotein E	<b>hBEC-5i</b>	Cerebral microvascular endothelial cell line
<b>AuNP</b>	gold nanoparticles	<b>HBMECs</b>	human brain microvascular endothelial cells
<b>BBB</b>	blood-brain barrier	<b>hTF</b>	glycosylated transferrin isolated from human serum
<b>BSA</b>	bovine serum albumin	<b>IRC</b>	intrinsic reaction coordinate
<b>citAuNP</b>	citrate-functionalized AuNP	$k_q$	bimolecular quenching constant
<b>CMT</b>	carrier-mediated transcytosis	$K_{sv}$	Stern-Volmer quenching constant
<b>COMP</b>	catechol-O-methyltransferase	<b>LAT-1</b>	large neutral amino acid transporter 1
<b>CPP</b>	cell-penetrating peptides	<b>LDL</b>	density lipoprotein
<b>DFT</b>	density functional theory	<b>levodopa</b>	L-dihydroxyphenylalanine
$d_H$	hydrodynamic diameter	<b>LRP-1</b>	low-density lipoprotein receptor-related protein 1
<b>DLS</b>	dynamic light scattering	<b>LSPR</b>	localized surface plasmon resonance

<b>MAO-B</b>	monoamine oxidase type B	<b>PME</b>	particle mesh Ewald
<b>MD</b>	molecular dynamics	<b>PVP</b>	poly (vinyl pyrrolidone)
<b>MM-GBSA</b>	molecular mechanics with generalized Born and surface area solvation	<b>PVP-SeNP</b>	PVP-functionalized SeNP
<b>mPEGthiol</b>	poly(ethylene glycol) methyl ether thiol	<b><i>r</i></b>	Pearson correlation coefficient
<b>MPTP</b>	1-methyl-4-phenyl-1,2,3,6-tetrahydropyridine	<b>RMT</b>	receptor-mediated transcytosis
<b><i>N<sub>A</sub></i></b>	Avogadro constant	<b>SASA</b>	solvent-accessible surface area
<b>NMR</b>	nuclear magnetic resonance	<b>SeNP</b>	selenium nanoparticles
<b><i>p</i></b>	level of significance	<b>SMD model</b>	Solvent Model based on Density
<b>PAMPA</b>	Parallel Artificial Membrane Permeability Assay	<b>SPR</b>	surface plasmon resonance
<b><i>P<sub>app</sub></i></b>	apparent permeability	<b>TEER</b>	transendothelial electrical resistance
<b>PBLE</b>	Porcine Polar Brain Lipid Extract	<b>TEM</b>	transmission electron microscopy
<b>PBS</b>	phosphate-buffered saline	<b>Tween-SeNP</b>	Tween-functionalized SeNP
<b>PCTE</b>	polycarbonate membrane	<b>UPW</b>	ultrapure water
<b>PD</b>	Parkinson's disease	<b>UV-Vis</b>	ultraviolet-visible
<b>PDI</b>	polydispersity index	<b>VMD</b>	visual molecular dynamics
<b>PEG</b>	polyethylene glycol	<b><math>\Delta G^\circ</math></b>	Gibbs free energy change
<b>PEG-AuNP</b>	PEG-functionalized AuNP	<b><math>\Delta G^\ddagger</math></b>	energy barrier
<b>PES</b>	potential energy surface	<b><math>\Delta G_{\text{bind}}</math></b>	binding free energy
<b>PGM</b>	peptidoglycan monomer	<b><math>\Delta H^\circ</math></b>	enthalpy change
<b>PGM-AuNP</b>	peptidoglycan monomer-functionalized AuNP	<b><math>\Delta S^\circ</math></b>	entropy change
<b>PLA</b>	pulsed laser ablation	<b><math>\zeta</math> potential</b>	zeta potential

## § 7. REFERENCES

1. V.K. Gribkoff, and L.K. Kaczmarek, *Neuropharmacology* **120** (2017) 11–19.
2. C. Spuch, O. Saida, and C. Navarro, *Recent Pat. Drug Deliv. Formul.* **6** (2012) 2–18.
3. H. Aldewachi, R.N. Al-Zidan, M.T. Conner, and M.M. Salman, *Bioengineering* **8** (2021) 1–20.
4. F. Haddad, M. Sawalha, Y. Khawaja, A. Najjar, and R. Karaman, *Molecules* **23** (2017) 40.
5. C.A. Davie, *Br. Med. Bull.* **86** (2008) 109–127.
6. J. Dorszewska, M. Prendecki, M. Lianeri, and W. Kozubski, *Curr. Genomics* **15** (2014) 11–17.
7. C. Velasco-Aguirre, F. Morales, E. Gallardo-Toledo, S. Guerrero, E. Giralt, E. Araya, and M.J. Kogan, *Int. J. Nanomedicine* **10** (2015) 4919–4936.
8. <https://www.who.int/news-room/fact-sheets/detail/parkinson-disease/> (accessed December 2, 2022).
9. A.C. Kaushik, S. Bharadwaj, S. Kumar, and D.Q. Wei, *Sci. Rep.* **8** (2018) 1–8.
10. J. Dorszewska, M. Kowalska, M. Prendecki, T. Piekut, J. Kozłowska, and W. Kozubski, *Neural Regen. Res.* **16** (2021) 1383.
11. P.A. Serra, G. Esposito, P. Enrico, M.A. Mura, R. Migheli, M.R. Delogu, M. Miele, M.S. Desole, G. Grella, and E. Miele, *Br. J. Pharmacol.* **130** (2000) 937–945.
12. P.L. McGeer, and E.G. McGeer, *Parkinsonism Relat. Disord.* **10** (2004) S3–S7.
13. H. Li, P. Yang, W. Knight, Y. Guo, J.S. Perlmutter, T.L.S. Benzinger, J.C. Morris, and J. Xu, *J. Neurochem.* **152** (2020) 235–251.
14. S.R. Subramaniam, and M.F. Chesselet, *Prog. Neurobiol.* **106–107** (2013) 17–32.
15. T. Müller, *Expert Opin. Drug Metab. Toxicol.* **16** (2020) 403–414.
16. J. Jankovic, and W. Poewe, *Curr. Opin. Neurol.* **25** (2012) 433–447.
17. M. Rai, and A. Yadav, *Nanobiotechnology Neurodegener. Dis.*, Springer International Publishing, Cham, 2019, pp. 1–398.
18. J. Xie, Z. Shen, Y. Anraku, K. Kataoka, and X. Chen, *Biomaterials* **224** (2019) 119491.
19. N. Poovaiah, Z. Davoudi, H. Peng, B. Schlichtmann, S. Mallapragada, B. Narasimhan, and Q. Wang, *Nanoscale* **10** (2018) 16962–16983.
20. J.M. Koziara, P.R. Lockman, D.D. Allen, and R.J. Mumper, *J. Nanosci. Nanotechnol.* **6** (2006) 2712–2735.
21. R. Pahuja, K. Seth, A. Shukla, R.K. Shukla, P. Bhatnagar, L.K.S. Chauhan, P.N. Saxena, et al., *ACS Nano* **9** (2015) 4850–4871.
22. U. Lertxundi, R. Hernández, S. Domingo-Echaburu, J. Peral-Aguirregoitia, and J. Medrano, *Challenges Park. Dis.* (2016) 1–2.
23. N. Popovic, and P. Brundin, *Int. J. Pharm.* **314** (2006) 120–126.

24. N.R. Bali, and P.S. Salve, *Int. J. Biol. Macromol.* **164** (2020) 1006–1024.
25. P.Y. Gambaryan, I.G. Kondrasheva, E.S. Severin, A.A. Guseva, and A.A. Kamensky, *Exp. Neurobiol.* **23** (2014) 246–252.
26. N.R. Bali, and P.S. Salve, *J. Drug Deliv. Sci. Technol.* **54** (2019) 101299.
27. S. Arisoy, O. Sayiner, T. Comoglu, D. Onal, O. Atalay, and B. Pehlivanoglu, *Pharm. Dev. Technol.* **25** (2020) 735–747.
28. T. Chen, W. Liu, S. Xiong, D. Li, S. Fang, Z. Wu, Q. Wang, and X. Chen, *ACS Appl. Mater. Interfaces* **11** (2019) 45276–45289.
29. T. Nie, Z. He, J. Zhu, K. Chen, G.P. Howard, J. Pacheco-Torres, I. Minn, P. Zhao, Z.M. Bhujwalla, H.-Q. Mao, L. Liu, and Y. Chen, *Nano Res.* **14** (2021) 2749–2761.
30. C.C. Bi, A.P. Wang, Y.C. Chu, S. Liu, H.J. Mu, W.H. Liu, Z.M. Wu, K.X. Sun, and Y.X. Li, *Int. J. Nanomedicine* **11** (2016) 6547–6559.
31. Y. Casanova, S. Negro, K. Slowing, L. García-García, A. Fernández-Carballido, M. Rahmani, and E. Barcia, *Pharmaceutics* **14** (2022) 1080.
32. M.K. Reddy, L. Wu, W. Kou, A. Ghorpade, and V. Labhasetwar, *Appl. Biochem. Biotechnol.* **151** (2008) 565–577.
33. M.N. Tiwari, S. Agarwal, P. Bhatnagar, N.K. Singhal, S.K. Tiwari, P. Kumar, L.K.S. Chauhan, D.K. Patel, R.K. Chaturvedi, M.P. Singh, and K.C. Gupta, *Free Radic. Biol. Med.* **65** (2013) 704–718.
34. G. da Rocha Lindner, D. Bonfanti Santos, D. Colle, E.L. Gasnhar Moreira, R. Daniel Prediger, M. Farina, N.M. Khalil, and R. Mara Mainardes, *Nanomedicine* **10** (2015) 1127–1138.
35. S.K. Bhattamisra, A.T. Shak, L.W. Xi, N.H. Safian, H. Choudhury, W.M. Lim, N. Shahzad, N.A. Alhakamy, M.K. Anwer, A.K. Radhakrishnan, and S. Md, *Int. J. Pharm.* **579** (2020) 119148.
36. S. Ray, P. Sinha, B. Laha, S. Maiti, U.K. Bhattacharyya, and A.K. Nayak, *J. Drug Deliv. Sci. Technol.* **48** (2018) 21–29.
37. E. De Giglio, A. Trapani, D. Cafagna, L. Sabbatini, and S. Cometa, *Anal. Bioanal. Chem.* **400** (2011) 1997–2002.
38. A.S. Tzeyung, S. Md, S.K. Bhattamisra, T. Madheswaran, N.A. Alhakamy, H.M. Aldawsari, and A.K. Radhakrishnan, *Pharmaceutics* **11** (2019) 1–17.
39. R. Raj, S. Wairkar, V. Sridhar, and R. Gaud, *Int. J. Biol. Macromol.* **109** (2018) 27–35.
40. S. Sharma, S. Lohan, and R.S.R. Murthy, *Drug Dev. Ind. Pharm.* **40** (2014) 869–878.
41. V. Sridhar, R. Gaud, A. Bajaj, and S. Wairkar, *Nanomedicine Nanotechnology, Biol. Med.* **14** (2018) 2609–2618.
42. A. Trapani, E. De Giglio, D. Cafagna, N. Denora, G. Agrimi, T. Cassano, S. Gaetani, V.

- Cuomo, and G. Trapani, *Int. J. Pharm.* **419** (2011) 296–307.
43. J.A. Loureiro, B. Gomes, M.A. Coelho, M. do Carmo Pereira, and S. Rocha, *Futur. Sci. OA* **1** (2015).
44. A. Margari, A.G. Monteduro, S. Rizzato, L. Capobianco, A. Crestini, R. Rivabene, P. Piscopo, M. D’Onofrio, V. Manzini, G. Trapani, A. Quarta, G. Maruccio, C. Ventra, L. Lieto, and A. Trapani, *Pharmaceutics* **14** (2022) 1–17.
45. C. V. Pardeshi, P. V. Rajput, V.S. Belgamwar, A.R. Tekade, and S.J. Surana, *Drug Deliv.* **20** (2013) 47–56.
46. E. Esposito, M. Fantin, M. Marti, M. Drechsler, L. Paccamiccio, P. Mariani, E. Sivieri, F. Lain, E. Menegatti, M. Morari, and R. Cortesi, *Pharm. Res.* **25** (2008) 1521–1530.
47. M.-J. Tsai, Y.-B. Huang, P.-C. Wu, Y.-S. Fu, Y.-R. Kao, J.-Y. Fang, and Y.-H. Tsai, *J. Pharm. Sci.* **100** (2011) 547–557.
48. C.E. Dillon, M. Billings, K.S. Hockey, L. DeLaGarza, and B.A. Rzigalinski, *Tech. Proc. 2011 NSTI Nanotechnol. Conf. Expo, NSTI-Nanotech 2011* **3** (2011) 451–454.
49. K. Hu, X. Chen, W. Chen, L. Zhang, J. Li, J. Ye, Y. Zhang, L. Zhang, C.-H. Li, L. Yin, and Y.-Q. Guan, *Nanomedicine Nanotechnology, Biol. Med.* **14** (2018) 1123–1136.
50. D.A. Gonzalez-Carter, Z.Y. Ong, C.M. McGilvery, I.E. Dunlop, D.T. Dexter, and A.E. Porter, *Nanomedicine Nanotechnology, Biol. Med.* **15** (2019) 1–11.
51. G. Gao, R. Chen, M. He, J. Li, J. Li, L. Wang, and T. Sun, *Biomaterials* **194** (2019) 36–46.
52. Y.D. Álvarez, J.A. Fauerbach, J. V. Pellegrotti, T.M. Jovin, E.A. Jares-Erijman, and F.D. Stefani, *Nano Lett.* **13** (2013) 6156–6163.
53. H.J. Kwon, D. Kim, K. Seo, Y.G. Kim, S.I. Han, T. Kang, M. Soh, and T. Hyeon, *Angew. Chemie - Int. Ed.* **57** (2018) 9408–9412.
54. A. Pinna, L. Malfatti, G. Galleri, R. Manetti, S. Cossu, G. Rocchitta, R. Migheli, P.A. Serra, and P. Innocenzi, *RSC Adv.* **5** (2015) 20432–20439.
55. R.E. Sardjono, F. Khoerunnisa, I. Musthopa, N.S.M.M. Akasum, and R. Rachmawati, *J. Phys. Conf. Ser.* **1013** (2018) 012195.
56. S. Ma, Q. Yang, W. Zhang, G. Xiao, M. Wang, L. Cheng, X. Zhou, M. Zhao, J. Ji, J. Zhang, and Z. Yue, *Talanta* **219** (2020) 121290.
57. N. Taebnia, D. Morshedi, S. Yaghmaei, F. Aliakbari, F. Rahimi, and A. Arpanaei, *Langmuir* **32** (2016) 13394–13402.
58. S. Niu, L.K. Zhang, L. Zhang, S. Zhuang, X. Zhan, W.Y. Chen, S. Du, L. Yin, R. You, C.H. Li, and Y.Q. Guan, *Theranostics* **7** (2017) 344–356.
59. N. Poovaiah, Z. Davoudi, H. Peng, B. Schlichtmann, S. Mallapragada, B. Narasimhan, and Q. Wang, *Nanoscale* **10** (2018) 16962–16983.



60. A. Chowdhury, S. Kunjiappan, T. Panneerselvam, B. Somasundaram, and C. Bhattacharjee, *Int. Nano Lett.* **7** (2017) 91–122.
61. L. Guerrini, R. Alvarez-Puebla, and N. Pazos-Perez, *Materials (Basel)*. **11** (2018) 1154.
62. M. Nazıroğlu, S. Muhamad, and L. Pecze, *Expert Rev. Clin. Pharmacol.* **10** (2017) 773–782.
63. P.C.L. Silveira, M. Venâncio, P.S. Souza, E.G. Victor, F. De Souza Notoya, C.S. Paganini, E.L. Streck, L. Da Silva, R.A. Pinho, and M.M.S. Paula, *Mater. Sci. Eng. C* **44** (2014) 380–385.
64. I. Vinković Vrček, in: B. Michalke (Ed.), *Selenium*, Springer International Publishing, Cham, 2018, pp. 393–413.
65. C. Ferro, H.F. Florindo, and H.A. Santos, *Adv. Healthc. Mater.* **10** (2021) 1–50.
66. S.J. Amina, and B. Guo, *Int. J. Nanomedicine* **15** (2020) 9823–9857.
67. W. Cong, R. Bai, Y.F. Li, L. Wang, and C. Chen, *ACS Appl. Mater. Interfaces* **11** (2019) 34725–34735.
68. K. Hu, X. Chen, W. Chen, L. Zhang, J. Li, J. Ye, Y. Zhang, L. Zhang, C.H. Li, L. Yin, and Y.Q. Guan, *Nanomedicine Nanotechnology, Biol. Med.* **14** (2018) 1123–1136.
69. Y. Xia, Y. Chen, L. Hua, M. Zhao, T. Xu, C. Wang, Y. Li, and B. Zhu, *Int. J. Nanomedicine* **13** (2018) 6929–6939.
70. H. Sela, H. Cohen, P. Elia, R. Zach, Z. Karpas, and Y. Zeiri, *J. Nanobiotechnology* **13** (2015) 1–9.
71. B. Eltanameli, K. Sneed, and E. Pathak, *Biomed. J. Sci. Tech. Res.* **42** (2022) 33387–33396.
72. T. Yin, L. Yang, Y. Liu, X. Zhou, J. Sun, and J. Liu, *Acta Biomater.* **25** (2015) 172–183.
73. D.J. Park, J.H. Choi, W.J. Lee, S.H. Um, and B.K. Oh, *J. Nanosci. Nanotechnol.* **17** (2017) 8012–8018.
74. H.Y. Yue, H.J. Zhang, S. Huang, X.X. Lu, X. Gao, S.S. Song, Z. Wang, W.Q. Wang, and E.H. Guan, *Mater. Sci. Eng. C* **108** (2020) 110490.
75. S. Govindaraju, S.R. Ankireddy, B. Viswanath, J. Kim, and K. Yun, *Sci. Rep.* **7** (2017) 1–12.
76. D. Tao, Y. Gu, S. Song, E.P. Nguyen, J. Cheng, Q. Yuan, H. Pan, N. Jaffrezic-Renault, and Z. Guo, *Microchem. J.* **158** (2020) 105195.
77. X. You, S.C.B. Gopinath, T. Lakshmipriya, and D. Li, *J. Anal. Methods Chem.* **2019** (2019) 1–8.
78. M.N.S. Karaboğa, and M.K. Sezgintürk, *Analyst* **144** (2019) 611–621.
79. A.C. Bonoiu, S.D. Mahajan, H. Ding, I. Roy, K.T. Yong, R. Kumar, R. Hu, E.J. Bergey, S.A. Schwartz, and P.N. Prasad, *Proc. Natl. Acad. Sci. U. S. A.* **106** (2009) 5546–5550.
80. Z. Aghili, N. Nasirizadeh, A. Divsalar, S. Shoeibi, and P. Yaghmaei, *Artif. Cells, Nanomedicine Biotechnol.* **46** (2018) 32–40.

81. E. da Silva Córneo, G. de Bem Silveira, R. Scussel, M.E.A.B. Correa, J. da Silva Abel, G.P. Luiz, P.E. Feuser, P.C.L. Silveira, and R.A. Machado-de-Ávila, *Colloids Surfaces B Biointerfaces* **196** (2020) 111302.
82. J. Xue, T. Liu, Y. Liu, Y. Jiang, V.D.D. Seshadri, S.K. Mohan, and L. Ling, *J. Photochem. Photobiol. B Biol.* **200** (2019) 111635.
83. D. Yue, C. Zeng, S.K. Okyere, Z. Chen, and Y. Hu, *J. Trace Elem. Med. Biol.* **64** (2021) 126680.
84. B. Pem, M. Toma, V. Vrček, and I. Vinković Vrček, *Inorg. Chem.* **60** (2021) 4144–4161.
85. M. Shariq, B. Friedrich, B. Budic, N. Hodnik, F. Ruiz-Zepeda, P. Majerič, and R. Rudolf, *ChemistryOpen* **7** (2018) 533–542.
86. N. Bisht, P. Phalswal, and P.K. Khanna, *Mater. Adv.* **3** (2022) 1415–1431.
87. J. Turkevich, P.C. Stevenson, and J. Hillier, *Discuss. Faraday Soc.* **11** (1951) 55–75.
88. G. Frens, *Nat. Phys. Sci.* **241** (1973) 20–22.
89. Y.C. Yeh, B. Creran, and V.M. Rotello, *Nanoscale* **4** (2012) 1871–1880.
90. S. Chhabria, and K. Desai, *Encycl. Nanosci. Nanotechnol.* **20** (2016) 1–32.
91. J.G. Hinman, A.J. Stork, J.A. Varnell, A.A. Gewirth, and C.J. Murphy, *Faraday Discuss.* **191** (2016) 9–33.
92. H.L. Wu, C.H. Kuo, and M.H. Huang, *Langmuir* **26** (2010) 12307–12313.
93. Z.Y. Ong, S. Chen, E. Nabavi, A. Regoutz, D.J. Payne, D.S. Elson, D.T. Dexter, I.E. Dunlop, and A.E. Porter, *ACS Appl. Mater. Interfaces* **9** (2017) 39259–39270.
94. L. Wang, Y. Song, L. Sun, C. Guo, Y. Sun, and Z. Li, *Mater. Lett.* **62** (2008) 4124–4126.
95. C.S. Ah, Y.J. Yun, H.J. Park, W.J. Kim, D.H. Ha, and W.S. Yun, *Chem. Mater.* **17** (2005) 5558–5561.
96. L. Minati, F. Benetti, A. Chiappini, and G. Speranza, *Colloids Surfaces A Physicochem. Eng. Asp.* **441** (2014) 623–628.
97. S.K. Das, A.R. Das, and A.K. Guha, *Small* **6** (2010) 1012–1021.
98. Y. De Chiou, and Y.J. Hsu, *Appl. Catal. B Environ.* **105** (2011) 211–219.
99. Q. Lu, F. Gao, and S. Komarneni, *Chem. Mater.* **18** (2006) 159–163.
100. B. Gates, B. Mayers, B. Cattle, and Y. Xia, *Adv. Funct. Mater.* **12** (2002) 219–227.
101. W. Huang, M. Wang, L. Hu, C. Wang, Z. Xie, and H. Zhang, *Adv. Funct. Mater.* **30** (2020) 2003301.
102. D. K, and S. Venugopal, *Front. Nanotechnol.* **4** (2022) 1–12.
103. E.G. Varlamova, E.A. Turovsky, and E. V. Blinova, *Int. J. Mol. Sci.* **22** (2021) 10808.
104. C. Ferro, H.F. Florindo, and H.A. Santos, *Adv. Healthc. Mater.* **10** (2021) 2100598.
105. H. Naser, H.M. Shanshool, and K.I. Imhan, *Brazilian J. Phys.* **51** (2021) 878–898.

106. S. MacHmudah, M. Goto, Wahyudiono, Y. Kuwahara, and M. Sasaki, *Res. Chem. Intermed.* **37** (2011) 515–522.
107. N.S.M. Yusof, and M. Ashokkumar, *ChemPhysChem* **16** (2015) 775–781.
108. W. Cai, T. Hu, A.M. Bakry, Z. Zheng, Y. Xiao, and Q. Huang, *Ultrason. Sonochem.* **42** (2018) 823–831.
109. S. Rajeshkumar, L. Ganesh, and J. Santhoshkumar, in: M. Rai, A. Yadav (Eds.), *Nanobiotechnology in Neurodegenerative Diseases*, Springer International Publishing, Cham, 2019, pp. 209–224.
110. S.A.A. Rizvi, and A.M. Saleh, *Saudi Pharm. J.* **26** (2018) 64–70.
111. S. Al Shehab, R. El Kurdi, and D. Patra, *Microchem. J.* **153** (2020) 104382.
112. W. Wang, Q.Q. Wei, J. Wang, B.C. Wang, S. hui Zhang, and Z. Yuan, *J. Colloid Interface Sci.* **404** (2013) 223–229.
113. T.A. Mary, K. Shanthi, K. Vimala, and K. Soundarapandian, *RSC Adv.* **6** (2016) 22936–22949.
114. S. Zheng, X. Li, Y. Zhang, Q. Xie, Y.-S. Wong, W. Zheng, and T. Chen, *Int. J. Nanomedicine* **7** (2012) 3939.
115. E. Galić, K. Ilić, S. Hartl, C. Tetyczka, K. Kasemets, I. Kurvet, M. Milić, R. Barbir, B. Pem, I. Erceg, M. Dutour Sikirić, I. Pavičić, E. Roblegg, A. Kahru, and I. Vinković Vrček, *Food Chem. Toxicol.* **144** (2020) 111621.
116. A. Hitchman, G.H. Sambrook, Y. Ju-nam, M. Sterling, and J.R. Lead, *Chemosphere* **90** (2013) 410–416.
117. M. Vahdati, and T. Tohidi Moghadam, *Sci. Rep.* **10** (2020) 1–10.
118. K. Sivaji, and R.R. Kannan, *J. Clust. Sci.* **30** (2019) 897–906.
119. Y. Jin, Z. Li, L. Hu, X. Shi, W. Guan, and Y. Du, *Carbohydr. Polym.* **91** (2013) 152–156.
120. H. Kong, J. Yang, Y. Zhang, and Y. Fang, *Int. J. Biol. Macromol.* **65** (2014) 155–162.
121. C. Wu, and D. Chen, *Gold Bull.* **43** (2010) 234–240.
122. P.A. Tran, and T.J. Webster, *Int. J. Nanomedicine* **6** (2011) 1553–1558.
123. M. Jafari, J. Tashkhourian, and G. Absalan, *Spectrochim. Acta Part A Mol. Biomol. Spectrosc.* **185** (2017) 77–84.
124. M.J. Gomes, B. Mendes, S. Martins, and B. Sarmento, in: M. Aliofkhazraei (Ed.), *Handbook of Nanoparticles*, Springer International Publishing, Cham, 2016, pp. 941–959.
125. W. Chen, H. Cheng, and W. Xia, *Antioxidants* **11** (2022) 1965.
126. M. Schäffler, F. Sousa, A. Wenk, L. Sitia, S. Hirn, C. Schleh, N. Haberl, M. Violatto, M. Canovi, P. Andreozzi, M. Salmona, P. Bigini, W.G. Kreyling, and S. Krol, *Biomaterials* **35** (2014) 3455–3466.
127. T. Doane, and C. Burda, *Adv. Drug Deliv. Rev.* **65** (2013) 607–621.

128. A. Eras, D. Castillo, M. Suárez, N.S. Vispo, F. Albericio, and H. Rodriguez, *Front. Chem.* **10** (2022) 889083.
129. S. Aryal, R. B.K.C., N. Dharmaraj, N. Bhattarai, C.H. Kim, and H.Y. Kim, *Spectrochim. Acta Part A Mol. Biomol. Spectrosc.* **63** (2006) 160–163.
130. R. Bhattacharya, C.R. Patra, A. Earl, S. Wang, A. Katarya, L. Lu, J.N. Kizhakkedathu, M.J. Yaszemski, P.R. Greipp, D. Mukhopadhyay, and P. Mukherjee, *Nanomedicine Nanotechnology, Biol. Med.* **3** (2007) 224–238.
131. J. Rout, B.C. Swain, P.P. Mishra, and U. Tripathy, *J. Photochem. Photobiol. B Biol.* **203** (2020) 111770.
132. S. Moghimi, A. Morsali, and M.M. Heravi, *Indian J. Chem. -Section A* **59** (2020) 43–50.
133. I. Venditti, L. Fontana, I. Fratoddi, C. Battocchio, C. Cametti, S. Sennato, F. Mura, F. Sciubba, M. Delfini, and M.V. Russo, *J. Colloid Interface Sci.* **418** (2014) 52–60.
134. L. Li, Q. Mu, B. Zhang, and B. Yan, *Analyst* **135** (2010) 1519–1530.
135. S. Behzadi, V. Serpooshan, W. Tao, M.A. Hamaly, M.Y. Alkawareek, E.C. Dreaden, D. Brown, A.M. Alkilany, O.C. Farokhzad, and M. Mahmoudi, *Chem. Soc. Rev.* **46** (2017) 4218–4244.
136. V. Ceña, and P. Játiva, *Nanomedicine* **13** (2018) 1513–1516.
137. D. Guarnieri, O. Muscetti, and P.A. Netti, *Methods Mol. Biol.* **1141** (2014) 185–199.
138. R. Ghaffarian, and S. Muro, *J. Vis. Exp.* **80** (2013) 1–13.
139. C. Hajal, M. Campisi, C. Mattu, V. Chiono, and R.D. Kamm, *Biomicrofluidics* **12** (2018) 042213.
140. L. Yang, J. Sun, W. Xie, Y. Liu, and J. Liu, *J. Mater. Chem. B* **5** (2017) 5954–5967.
141. M. Shilo, A. Sharon, K. Baranes, M. Motiei, J.P.M. Lellouche, and R. Popovtzer, *J. Nanobiotechnology* **13** (2015) 1–7.
142. F.U. Rehman, J. Bao, P. Muhammad, W. He, S. Hanif, and M.A. Rauf, *Mater. Today Bio* **8** (2020) 100072.
143. N.L. Stone, T.J. England, and S.E. O’Sullivan, *Front. Cell. Neurosci.* **13** (2019) 1–11.
144. D. Keglević, B. Ladešić, J. Tomašić, Z. Valinger, and R. Naumski, *Biochim. Biophys. Acta - Gen. Subj.* **585** (1979) 273–281.
145. B. Gašpert, S. Hromadko, and B. Vranešić, *Croat. Chem. Acta* **48** (1976) 169–178.
146. Y. Hernandez, R. González-Pastor, C. Belmar-Lopez, G. Mendoza, J.M. De La Fuente, and P. Martin-Duque, *RSC Adv.* **9** (2019) 1327–1334.
147. E. Galić, K. Radić, N. Golub, D. Vitali Čepo, N. Kalčec, E. Vrčec, and T. Vinković, *Int. J. Mol. Sci.* **23** (2022) 9128.
148. A. Selmani, L. Ulm, K. Kasemets, I. Kurvet, I. Erceg, R. Barbir, B. Pem, P. Santini, I.D.

- Marion, T. Vinković, A. Krivohlavek, M.D. Sikirić, A. Kahru, and I. Vinković Vrček, *Chemosphere* **250** (2020) 126265.
149. M.A. Asadabad, and M.J. Eskandari, *Synth. React. Inorganic, Met. Nano-Metal Chem.* **45** (2015) 323–326.
150. R. Pecora, *J. Nanoparticle Res.* **2** (2000) 123–131.
151. T. Takagi, *Electrophoresis* **14** (1993) 1255–1256.
152. E. Joseph, and G. Singhvi, in: A.M. Grumezescu (Ed.), *Nanomaterials for Drug Delivery and Therapy*, Elsevier, 2019, pp. 91–116.
153. A. Zettner, *Adv. Clin. Chem.* **7** (1964) 1–62.
154. V. Amendola, and M. Meneghetti, *J. Phys. Chem. C* **113** (2009) 4277–4285.
155. R. Barbir, R.R. Jiménez, R. Martín-Rapún, V. Strasser, D. Domazet Jurašin, S. Dabelić, J.M. de la Fuente, and I. Vinković Vrček, *ACS Appl. Mater. Interfaces* **13** (2021) 27533–27547.
156. J.R. Lakowicz, *Princ. Fluoresc. Spectrosc.*, Springer US, Boston, MA, 2006, pp. 954.
157. T. Wang, L.-H. Zeng, and D.-L. Li, *Appl. Spectrosc. Rev.* **52** (2017) 883–908.
158. S.K. Panigrahi, and A.K. Mishra, *Photochem. Photobiol. Sci.* **18** (2019) 583–591.
159. C. Hao, G. Xu, Y. Feng, L. Lu, W. Sun, and R. Sun, *Spectrochim. Acta - Part A Mol. Biomol. Spectrosc.* **184** (2017) 191–197.
160. S. Bano, A. Mohd, A.A.P. Khan, and K.S. Siddiqi, *J. Chem. Eng. Data* **55** (2010) 5759–5765.
161. J.R. Albani, in: J.R. Albani (Ed.), *Structure and Dynamics of Macromolecules: Absorption and Fluorescence Studies*, Elsevier Science, Amsterdam, 2004, pp. 141–192.
162. A.A. Sousa, *J. Fluoresc.* **25** (2015) 1567–1575.
163. W. Haiss, N.T.K. Thanh, J. Aveyard, and D.G. Fernig, *Anal. Chem.* **79** (2007) 4215–4221.
164. R. López-Cebal, M. Martín-Pastor, B. Seijo, and A. Sanchez, *Prog. Nucl. Magn. Reson. Spectrosc.* **79** (2014) 1–13.
165. A.M. Smith, L.E. Marbella, K.A. Johnston, M.J. Hartmann, S.E. Crawford, L.M. Kozycz, D.S. Seferos, and J.E. Millstone, *Anal. Chem.* **87** (2015) 2771–2778.
166. P. Atkins, and R. Friedman, *Molecular Quantum mechanics*, Oxford University Press, Oxford, 2005, pp. 537.
167. T. Tsuneda, *Density Functional Theory in Quantum Chemistry*, Springer Japan, Tokyo, 2014, pp. 207.
168. K.E. Gilbert, *Pcmodel 10.0*, Serena Software, Bloomington, IN, USA, 2014.
169. W.J. Hehre, *A Guide to Molecular Mechanics and Quantum Chemical Calculations*, Wavefunction Inc., Irvine, 2003, pp. 816.
170. K. Fukui, *Acc. Chem. Res.* **14** (1981) 363–368.
171. H.P. Hratchian, and H.B. Schlegel, *J. Chem. Theory Comput.* **1** (2005) 61–69.

172. M.J. Frisch, G.W. Trucks, H.B. Schlegel, G.E. Scuseria, M.A. Robb, J.R. Cheeseman, G. Scalmani, et al., *Gaussian 16, Revision C.01*, Gaussian Inc., Wallingford CT, 2016.
173. R. Dennington, T.A. Keith, and J.M. Millam, *GaussView*, Semichem Inc., Shawnee Mission, KS, 2016.
174. A. V. Marenich, C.J. Cramer, and D.G. Truhlar, *J. Phys. Chem. B* **113** (2009) 6378–6396.
175. “KICK” stochastic search procedure code, <https://kick.science/KICK.html> (accessed February 1, 2022).
176. D.C. Rapaport, *The Art of Molecular Dynamics Simulation*, Cambridge University Press, New York, 2004, pp. 564.
177. D.A. Case, K. Belfon, I.Y. Ben-Shalom, S.R. Brozell, D.S. Cerutti, T.E. Cheatham, V.W.D. Cruzeiro, et al., *AMBER*, San Francisco: University of California, 2017.
178. H. Heinz, R.A. Vaia, B.L. Farmer, and R.R. Naik, *J. Phys. Chem. C* **112** (2008) 17281–17290.
179. M. Mahoney, *J. Chem. Phys.* **112** (2000) 28–32.
180. M.P. Allen, in: N. Attig, K. Binder, H. Grubmüller, K. Kremer (Eds.), *Computational Soft Matter: From Synthetic Polymers to Proteins, Lecture Notes*, John von Neumann Institute for Computing, Jülich, 2004, pp. 1–28.
181. W. Humphrey, A. Dalke, and K. Schulten, *J. Mol. Graph.* **14** (1996) 33–38.
182. P.A. Kollman, I. Massova, C. Reyes, B. Kuhn, S. Huo, L. Chong, M. Lee, T. Lee, Y. Duan, W. Wang, O. Donini, P. Cieplak, J. Srinivasan, D.A. Case, and T.E. Cheatham, *Acc. Chem. Res.* **33** (2000) 889–897.
183. M.L. Contreras, C. Torres, I. Villarroel, and R. Rozas, *Struct. Chem.* **30** (2019) 369–384.
184. C. Torres, I. Villarroel, R. Rozas, and L. Contreras, *Molecules* **24** (2019) 4281.
185. L. Di, E.H. Kerns, K. Fan, O.J. McConnell, and G.T. Carter, *Eur. J. Med. Chem.* **38** (2003) 223–232.
186. J. Müller, K. Ezzo, G. Dargó, Á. Könczöl, and G.T. Balogh, *Eur. J. Pharm. Sci.* **79** (2015) 53–60.
187. R. Prades, S. Guerrero, E. Araya, C. Molina, E. Salas, E. Zurita, J. Selva, G. Egea, C. López-Iglesias, M. Teixidó, M.J. Kogan, and E. Giralt, *Biomaterials* **33** (2012) 7194–7205.
188. H. Yu, Q. Wang, Y. Sun, M. Shen, H. Li, and Y. Duan, *PLoS One* **10** (2015) 1–13.
189. <https://www.sigmaaldrich.com/HR/en/technical-documents/technical-article/research-and-disease-areas/pharmacology-and-drug-discovery-research/evaluation-of-the-reproducibility-of-pampa> (accessed February 15, 2023).
190. G.S. El Hebeish A, *J. Nanomed. Nanotechnol.* **06** (2015) 1–8.
191. P. Eaton, P. Quaresma, C. Soares, C. Neves, M.P. de Almeida, E. Pereira, and P. West, *Ultramicroscopy* **182** (2017) 179–190.

192. M. Sajitha, A. Vindhyasarumi, A. Gopi, and K. Yoosaf, *RSC Adv.* **5** (2015) 98318–98324.
193. P. Qiu, and C. Mao, *J. Nanoparticle Res.* **11** (2009) 885–894.
194. X. Wang, D.P. Yang, P. Huang, M. Li, C. Li, D. Chen, and D. Cui, *Nanoscale* **4** (2012) 7766–7772.
195. S. Koepl, N. Ghielmetti, W. Caseri, and R. Spolenak, *J. Nanoparticle Res.* **15** (2013) 1471.
196. R.E. Darienzo, T. Mironava, and R. Tannenbaum, *J. Nanosci. Nanotechnol.* **19** (2019) 4740–4746.
197. A.L. Siegel, and G.A. Baker, *Nanoscale Adv.* **3** (2021) 3980–4004.
198. B. Hemmateenejad, and S. Yousefinejad, *J. Mol. Struct.* **1037** (2013) 317–322.
199. A. Bhogale, N. Patel, P. Sarpotdar, J. Mariam, P.M. Dongre, A. Miotello, and D.C. Kothari, *Colloids Surfaces B Biointerfaces* **102** (2013) 257–264.
200. S.P. Boulos, T.A. Davis, J.A. Yang, S.E. Lohse, A.M. Alkilany, L.A. Holland, and C.J. Murphy, *Langmuir* **29** (2013) 14984–14996.
201. R. Nicoară, M. Ilieș, A. Uifălean, C.A. Iuga, and F. Loghin, *Appl. Sci.* **9** (2019) 4789.
202. S. Dominguez-Medina, S. McDonough, P. Swanglap, C.F. Landes, and S. Link, *Langmuir* **28** (2012) 9131–9139.
203. A. V. Pansare, A.A. Shedge, and V.R. Patil, *Int. J. Biol. Macromol.* **107** (2018) 1982–1987.
204. S. Prasanth, and C. Sudarsanakumar, *New J. Chem.* **41** (2017) 9521–9530.
205. N. Shahabadi, S. Zendehcheshm, and F. Khademi, *Biotechnol. Reports* **30** (2021) e00615.
206. K. Phopin, W. Ruankham, S. Prachayasittikul, V. Prachayasittikul, and T. Tantimongcolwat, *Int. J. Mol. Sci.* **21** (2019) 249.
207. H.Y. Wang, Y. Sun, and B. Tang, *Talanta* **57** (2002) 899–907.
208. G. D’Andrea, G. Maurizi, A.M. D’Alessandro, M.L. Salucci, A. Impagnatiello, M.A. Saletti, and A. Oratore, *J. Protein Chem.* **11** (1992) 165–169.
209. U. Śliwińska-Hill, *Spectrochim. Acta Part A Mol. Biomol. Spectrosc.* **173** (2017) 468–475.
210. A.T. Buddanavar, and S.T. Nandibewoor, *J. Pharm. Anal.* **7** (2017) 148–155.
211. C.G. Chilom, N. Sandu, S. Iftimie, M. Bălăsoiu, A. Rogachev, O. Orelovich, and S. Stolyar, *Int. J. Mol. Sci.* **22** (2021) 7034.
212. M.B. Shahsavani, S. Ahmadi, M.D. Aseman, S.M. Nabavizadeh, M.M. Alavianmehr, and R. Yousefi, *J. Photochem. Photobiol. B Biol.* **164** (2016) 323–334.
213. M. Mabuchi, J. Shimada, K. Okamoto, Y. Kawakami, S. Fujita, and K. Matsushige, *Proc. SPIE* **4252** (2001) 140–148.
214. S.K. Pawar, and S. Jaldappagari, *J. Pharm. Anal.* **9** (2019) 274–283.
215. Z. Omidvar, A. Asoodeh, and J. Chamani, *J. Solution Chem.* **42** (2013) 1005–1017.
216. D.I. Cattoni, O. Chara, S.B. Kaufman, and F.L.G. Flecha, *PLoS One* **10** (2015) 1–14.

217. R. Barbir, B. Pem, N. Kalčec, S. Kastner, K. Podlesnaia, A. Csáki, W. Fritzsche, and I. Vinković Vrček, *Langmuir* **37** (2021) 1991–2000.
218. G. Klebe, in: A.E. Scapin G., Patel D. (Ed.), *Multifaceted Roles of Crystallography in Modern Drug Discovery. NATO Science for Peace and Security Series A: Chemistry and Biology.*, Springer, Dordrecht, 2015, pp. 83–92.
219. Y. Bu, and S.W. Lee, *Int. J. Nanomedicine* **10** (2015) 47–54.
220. S.H. De Paoli Lacerda, J.J. Park, C. Meuse, D. Pristinski, M.L. Becker, A. Karim, and J.F. Douglas, *ACS Nano* **4** (2010) 365–379.
221. S. Özdemir, and E. Biçer, *J. Chil. Chem. Soc.* **61** (2016) 2809–2815.
222. T.I. Mizan, P.E. Savage, and R.M. Ziff, *J. Phys. Chem.* **100** (1996) 403–408.
223. P.D. Ross, and S. Subramanian, *Biochemistry* **20** (1981) 3096–3102.
224. W. Zhang, H. Yang, F. Liu, T. Chen, G. Hu, D. Guo, Q. Hou, X. Wu, Y. Su, and J. Wang, *RSC Adv.* **7** (2017) 32518–32527.
225. H.C. Yang, R.Z. Waldman, M.B. Wu, J. Hou, L. Chen, S.B. Darling, and Z.K. Xu, *Adv. Funct. Mater.* **28** (2018) 1–14.
226. B. Meesaragandla, I. García, D. Biedenweg, J. Toro-Mendoza, I. Coluzza, L.M. Liz-Marzán, and M. Delcea, *Phys. Chem. Chem. Phys.* **22** (2020) 4490–4500.
227. X. Chen, J. Zhang, H. Zhai, X. Chen, and Z. Hu, *Food Chem.* **92** (2005) 381–386.
228. S.P. Schwaminger, P.F. García, G.K. Merck, F.A. Bodensteiner, S. Heissler, S. Günther, and S. Berensmeier, *J. Phys. Chem. C* **119** (2015) 23032–23041.
229. A.O. Luby, E.K. Breitner, and K.K. Comfort, *Appl. Nanosci.* **6** (2016) 827–836.
230. G.G.D. La Cruz, P. Rodríguez-Fragoso, J. Reyes-Esparza, A. Rodríguez-López, R. Gómez-Cansino, and L. Rodríguez-Fragoso, in: M.P. Sarria, A.C. Gomes (Eds.), *Unraveling the Safety Profile of Nanoscale Particles and Materials - From Biomedical to Environmental Applications*, InTech, 2018, pp. 37–59.
231. D. Chakraborty, P. Chauhan, S.A. Alex, S. Chaudhary, K.R. Ethiraj, N. Chandrasekaran, and A. Mukherjee, *J. Mol. Liq.* **268** (2018) 335–342.
232. X. Peng, W. Qi, R. Huang, R. Su, and Z. He, *PLoS One* **10** (2015) 1–23.
233. S.L. Hirsh, D.R. McKenzie, N.J. Nosworthy, J.A. Denman, O.U. Sezerman, and M.M.M. Bilek, *Colloids Surfaces B Biointerfaces* **103** (2013) 395–404.
234. M. McCully, M. Sanchez-Navarro, M. Teixido, and E. Giralt, *Curr. Pharm. Des.* **24** (2018) 1366–1376.
235. T. Arentsen, Y. Qian, S. Gkotzis, T. Femenia, T. Wang, K. Udekwu, H. Forssberg, and R. Diaz Heijtz, *Mol. Psychiatry* **22** (2017) 257–266.
236. E. Ferreira de Macedo, D.M. Ducatti Formaggio, N. Salles Santos, and D. Batista Tada,



- Sensors* **17** (2017) 2765.
237. S.A. Alex, N. Chandrasekaran, and A. Mukherjee, *J. Mol. Liq.* **248** (2017) 703–712.
238. T. Zheng, P. Cherubin, L. Cilenti, K. Teter, and Q. Huo, *Analyst* **141** (2016) 934–938.
239. H.T.M. Phan, S. Bartelt-Hunt, K.B. Rodenhausen, M. Schubert, and J.C. Bartz, *PLoS One* **10** (2015) e0141282.
240. G.P. Szekeres, and J. Kneipp, *Analyst* **143** (2018) 6061–6068.
241. A. Rostami, A. Hadjizadeh, and S. Mahshid, *J. Mater. Sci.* **55** (2020) 7969–7980.
242. Y. Zhang, B. Li, and X. Chen, *Microchim. Acta* **168** (2010) 107–113.
243. N. Mohseni, and M. Bahram, *Spectrochim. Acta - Part A Mol. Biomol. Spectrosc.* **193** (2018) 451–457.
244. Y. Bu, and S. Lee, *ACS Appl. Mater. Interfaces* **4** (2012) 3923–3931.
245. S. Dominguez-Medina, J. Blankenburg, J. Olson, C.F. Landes, and S. Link, *ACS Sustain. Chem. Eng.* **1** (2013) 833–842.
246. M. Bisaglia, S. Mammi, and L. Bubacco, *J. Biol. Chem.* **282** (2007) 15597–15605.
247. E. Herlinger, R.F. Jameson, and W. Linert, *J. Chem. Soc. Perkin Trans. 2* **2** (1995) 259.
248. F. Bernsmann, V. Ball, F. Addiego, A. Ponche, M. Michel, J.J. de A. Gracio, V. Toniazzi, and D. Ruch, *Langmuir* **27** (2011) 2819–2825.
249. R.P. Bacil, L. Chen, S.H.P. Serrano, and R.G. Compton, *Phys. Chem. Chem. Phys.* **22** (2020) 607–614.
250. T. Madrakian, A. Afkhami, M. Borazjani, and M. Bahram, *Bull. Korean Chem. Soc.* **25** (2004) 1764–1768.
251. H. Omotani, M. Yasuda, R. Ishii, T. Ikarashi, T. Fukuuchi, N. Yamaoka, K.I. Mawatari, K. Kaneko, and K. Nakagomi, *J. Pharm. Biomed. Anal.* **125** (2016) 22–26.
252. M.R. Hormozi-Nezhad, A. Moslehipour, and A. Bigdeli, *Sensors Actuators, B Chem.* **243** (2017) 715–720.
253. M. Salomäki, L. Marttila, H. Kivelä, T. Ouvinen, and J. Lukkari, *J. Phys. Chem. B* **122** (2018) 6314–6327.
254. N. Umek, B. Geršak, N. Vintar, M. Šoštarčič, and J. Mavri, *Front. Mol. Neurosci.* **11** (2018) 1–8.
255. Y. Wang, H. Zhang, and M. Chen, *Anal. Chim. Acta* **1157** (2021) 338379.
256. X.P. Zhang, W. Sun, S.H. Cao, W.L. Jiang, H. Peng, S.H. Cai, and Z. Chen, *Electrochemistry* **88** (2020) 200–204.
257. W. Zheng, H. Fan, L. Wang, and Z. Jin, *Langmuir* **31** (2015) 11671–11677.
258. T.P. Chen, T. Liu, T.L. Su, and J. Liang, *Langmuir* **33** (2017) 5863–5871.
259. T.E. Young, B.W. Babbitt, and L.A. Wolfe, *J. Org. Chem.* **45** (1980) 2899–2902.

- 
260. T.E. Young, and B.W. Babbitt, *J. Org. Chem.* **48** (1983) 5414.
261. S.A. Hollingsworth, and R.O. Dror, *Neuron* **99** (2018) 1129–1143.
262. E. Mateo-Martí, C. Rogero, C. Gonzalez, J.M. Sobrado, P.L. de Andrés, and J.A. Martin-Gago, *Langmuir* **26** (2010) 4113–4118.
263. S. Monti, V. Carravetta, and H. Ågren, *Nanoscale* **8** (2016) 12929–12938.
264. L. Yan, H. Chen, and C. Jing, *J. Phys. Chem. Lett.* **10** (2019) 898–903.
265. T. Hou, J. Wang, Y. Li, and W. Wang, *J. Chem. Inf. Model* **51** (2011) 69–82.
266. J. Mensch, A. Melis, C. Mackie, G. Verreck, M.E. Brewster, and P. Augustijns, *Eur. J. Pharm. Biopharm.* **74** (2010) 495–502.
267. M. Enea, M. Peixoto de Almeida, P. Eaton, D. Dias da Silva, E. Pereira, M.E. Soares, M. de L. Bastos, and H. Carmo, *Nanotoxicology* **13** (2019) 990–1004.
268. C. Åberg, *Tissue Barriers* **4** (2016) e1143545.

## § 8. APPENDICES

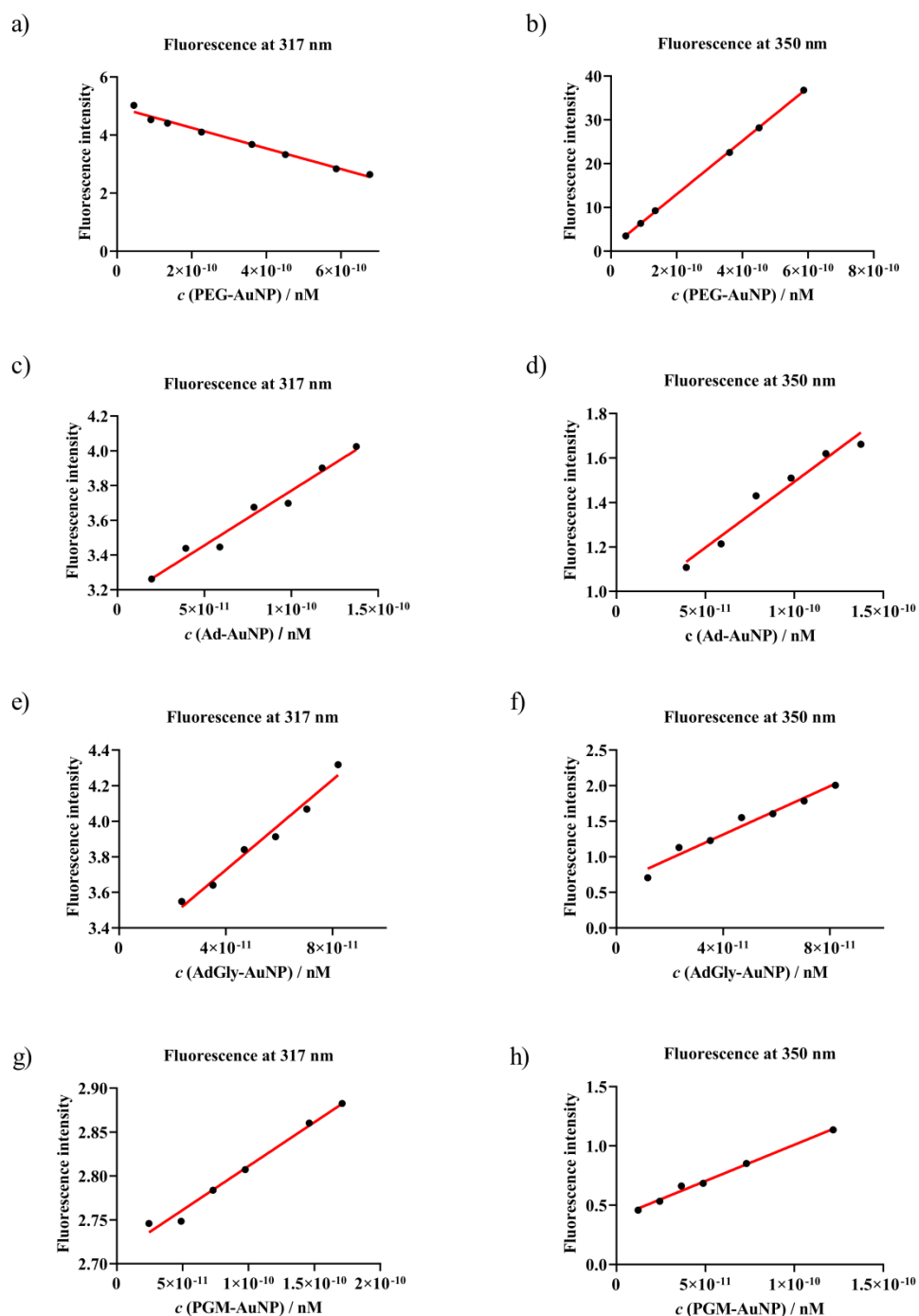


**Figure 25.** Fluorescence intensities of: a,b) PGM-AuNP, b,c) Ad-AuNP, e,f) Ad-Gly-AuNP, and g,h) PGM-AuNP at 317 and 350 nm vs. NP concentrations, respectively. Fluorescence spectra were recorded in UPW (pH = 5.68) at 25°C.

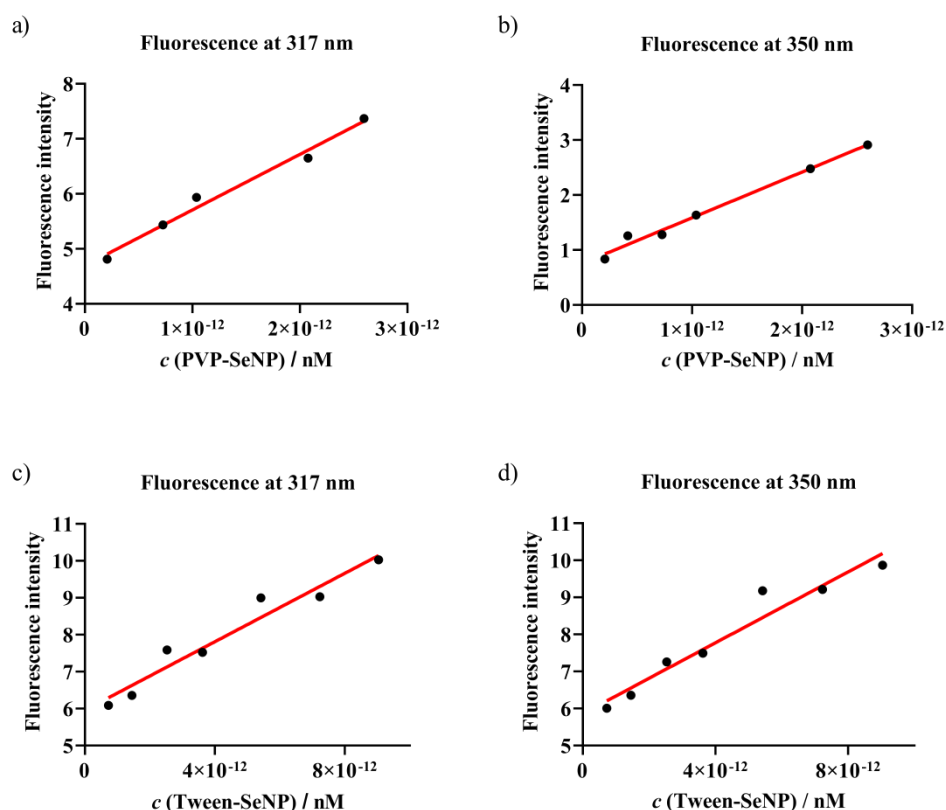


**Figure 26.** Fluorescence intensities of: a,b) PVP-SeNP, and c,d) Tween-SeNP at 317 and 350 nm vs. NP concentrations, respectively. Fluorescence spectra were recorded in UPW (pH = 5.68) at 25°C.

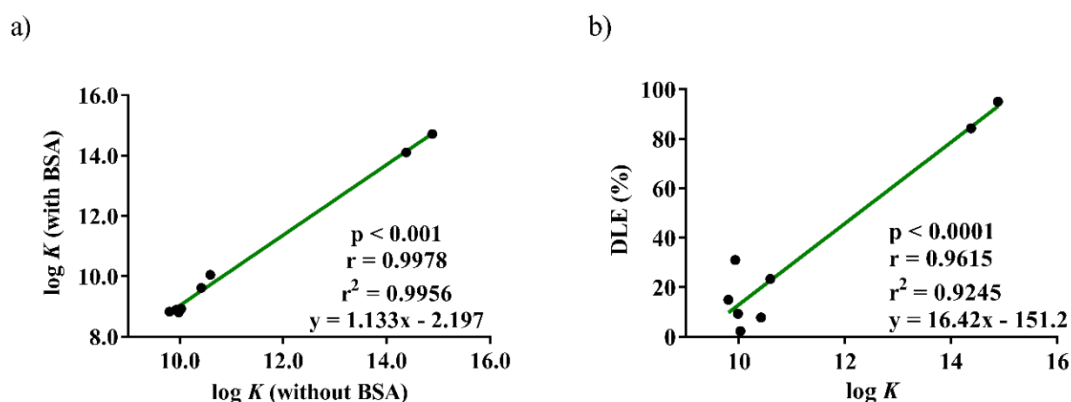


**Figure 27.** a) Correlation of  $\log K$  values for levodopa and dopamine interactions with different AuNP in the presence and the absence of BSA, and b) correlation between drug loading efficiency and  $\log K$  values for the highest AuNP concentration ( $5 \times 10^{17}$  nm<sup>2</sup>/L) after interaction with levodopa or dopamine.

**Table 13.**  $^1\text{H}$  and  $^{13}\text{C}$  NMR data for dopamine and dopaminequinone in the acidic aqueous medium (pH = 3).

NMR experiment	dopamine		dopaminequinone		
	$\delta$ / ppm	$J$ (H,H) / Hz	$\delta$ / ppm	$J$ (H,H) / Hz	Assignment <sup>a</sup>
$^1\text{H}$ NMR	6.75	d (8.1)	7.00	dd (10.2, 2.1)	H4
	6.69	d (2.1)	6.34	d (10.2)	H8
	6.60	dd (8.1, 2.1)	6.23	d (2.1)	H7
	3.07	t (7.3)	3.17	t (7.5)	H1
	2.72	t (7.3)	2.70	t (7.5)	H2
$^{13}\text{C}$ NMR	144.16	s	180.96	s	C5/C6
	142.93	s	180.27	s	C5/C6
	129.23	s	151.65	s	C3
	121.18	d	142.89	d	C8
	116.53	d	129.91	d	C4/C7
	116.49	d	127.66	d	C4/C7
	40.63	t	36.71	t	C1
	31.95	t	32.84	t	C2

<sup>a</sup> as denoted in Scheme 1.

**Table 14.**  $^1\text{H}$  and  $^{13}\text{C}$  NMR data for levodopa and its oxidized products dopaquinone and dopachrome in the acidic aqueous medium (pH = 3).

NMR exp.	levodopa		dopaquinone		dopachrome		Assignment <sup>a</sup>
	$\delta$ / ppm	$J$ (H,H) / Hz	$\delta$ / ppm	$J$ (H,H) / Hz	$\delta$ / ppm	$J$ (H,H) / Hz	
$^1\text{H}$ NMR	6.74	d (8.3)	7.02	dd (10.2, 1.8)	6.99	t (0.9)	H4
	6.66	d (1.2)	6.35	d (10.3)	-	-	H8
	6.58	dd (8.3, 1.2)	6.29	d (1.8)	6.57	s	H7
	3.78	dd (7.9, 5.9)	4.27	t (7.1)	4.15	t (7.0)	H1
	3.00	dd (5.9, 14.7)	3.02	dd (6.7, 15.0)	2.98	dd (7.0, 14.4)	H2
	2.84	dd (7.9, 14.7)	2.89	dd (7.6, 14.8)	2.86	dd (7.2, 14.0)	H2
$^{13}\text{C}$ NMR	173.91	s	-	-	-	-	
	143.78	m	187.1	m	180.9	m	C5/C6
	143.76	m	181.9	m	180.2	m	C5/C6
	127.57	m	155.8	m	149.5	m	C3
	121.78	m	143.6	m	142.4	m	C8
	116.72	m	133.2	m	130.6	m	C4/C7
	116.68	m	132.7	m	129.4	m	C4/C7
	56.00	s	-	-	-	-	C1
	35.50	d (45.0)	-	-	-	-	C2

<sup>a</sup> As denoted in Scheme 2.

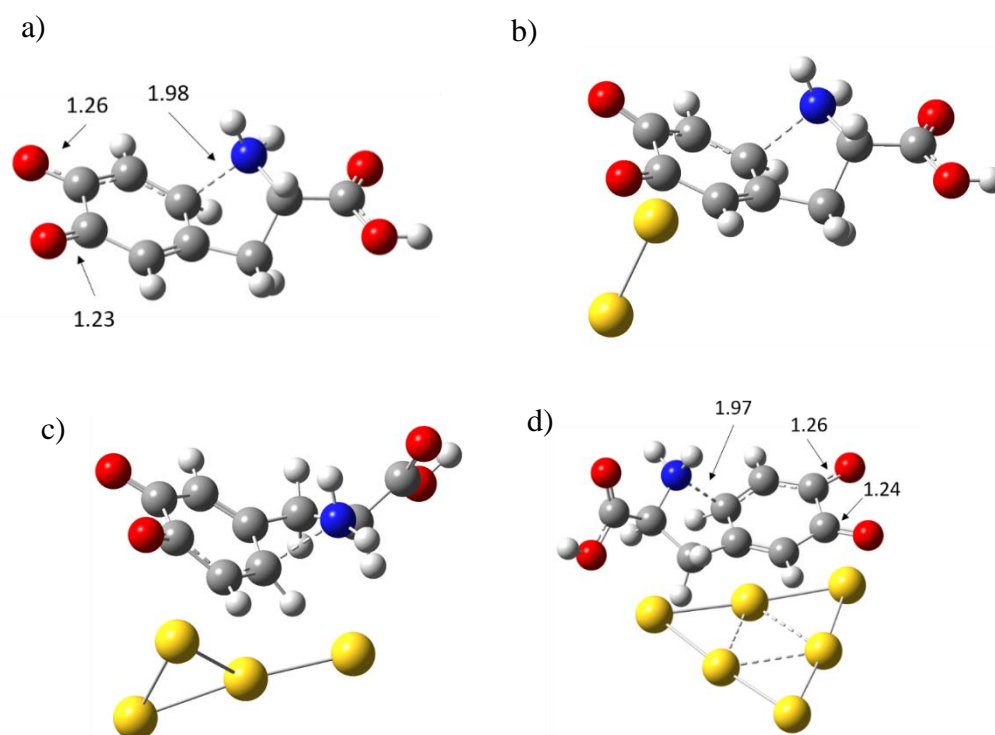


**Figure 28.** SMD-M06L/6-31+G(d,p)/LANL2DZ (solvent = water) optimized transition state structures for the intramolecular cyclization of dopaquinone in: a) metal-free process ( $n = 0$ ) and in the presence of  $\text{Au}_n$  clusters, where b)  $n = 2$ , c)  $n = 4$ , and d)  $n = 6$ . All distances are in Å.

### *XYZ coordinates of all structures from theoretical calculations*

SMD-M06L/6-31+G(d,p)/LANL2DZ calculated geometries (solvent = water) and  $G_{298}$  for all stationary points (**R** and **P**, NImag = 0; **TS**, NImag = 1) from Table 9.

### **Dopamine-quinone cyclization;**

**R** is reactant, **P** is product, **TS** is transition state structure,  $n$  is number of Au atoms included in the calculation

**R**,  $n = 0$  ( $G_{298} = -515.290072$  a.u.)

C,0,-2.0056758414,-0.7186650874,-0.1120140357  
C,0,-1.060208843,-1.5915392027,-0.7859571882  
C,0,0.2045367325,-1.1700827298,-1.0025661785  
C,0,0.6891564382,0.1529931194,-0.6033000125  
C,0,-0.1365506164,1.0274771237,0.0373048476

H,0,2.2205786032,1.9410040701,0.5837682024  
C,0,3.0164838328,-0.0282855009,0.0618903944  
H,0,3.4292780675,-0.4341069737,-0.8637926025  
N,0,2.1273676264,-1.0543609089,0.6194894101  
H,0,1.8398319308,-0.8637511905,1.5762253619  
H,0,2.4842821889,-2.0013364639,0.5423652798

C,0,-1.5051246454,0.6808049151,0.3274795928  
H,0,-1.40339043,-2.5733298363,-1.0964517813  
H,0,0.2151717163,2.0106881537,0.3393271618  
O,0,-2.298633455,1.4299788304,0.9044488166  
O,0,-3.1694331605,-1.0359382418,0.1282181043  
C,0,2.1235732253,0.4531558795,-0.8364616679  
H,0,2.4354526045,0.0534404765,-1.8083136066  
H,0,2.2942767216,1.5342222296,-0.8344903286  
C,0,3.0194052213,-0.1880711794,0.2504743226  
H,0,2.8486870559,-1.2689691212,0.2740686788  
N,0,2.8517619046,0.3411688903,1.5921269877  
H,0,1.8985902563,0.1777158618,1.9061382693  
H,0,2.9584346232,1.3518056152,1.5623017767  
H,0,0.9173359752,-1.8260869136,-1.4979253828  
H,0,4.0576115168,-0.040688783,-0.0589063761

**TS**,  $n = 0$  ( $G_{298} = -515.267970$  a.u.)

C,0,-1.7637198322,-0.7545436528,-0.0333910505  
C,0,-0.6083685676,-1.4128302967,-0.4867703197  
C,0,0.599130436,-0.7286038788,-0.6491917149  
C,0,0.7247189524,0.6992145443,-0.2848493617  
C,0,-0.361965354,1.3994620414,0.1027135034  
C,0,-1.6520293851,0.7481339602,0.2535683608  
H,0,-0.694775411,-2.4422503337,-0.8224538174  
H,0,-0.2840992302,2.4391076525,0.411790618  
O,0,-2.6467473551,1.362443638,0.6600906619  
O,0,-2.9053610401,-1.2793230208,0.0745771851  
C,0,2.1359214368,1.1947701275,-0.2104177255  
H,0,2.4309328054,1.69170761,-1.1411263981  
H,0,2.2205786032,1.9410040701,0.5837682024  
C,0,3.0164838328,-0.0282855009,0.0618903944  
H,0,3.4292780675,-0.4341069737,-0.8637926025  
N,0,2.1273676264,-1.0543609089,0.6194894101  
H,0,1.8398319308,-0.8637511905,1.5762253619  
H,0,2.4842821889,-2.0013364639,0.5423652798  
H,0,1.2698387246,-1.0695766361,-1.4370000972  
H,0,3.8514115707,0.1965262128,0.7297051097

**P**,  $n = 0$  ( $G_{298} = -515.318282$  a.u.)

C,0,-1.6349399474,-0.6688175209,-0.2098764781  
C,0,-0.4390676508,-1.3819034108,-0.0975332575  
C,0,0.751648802,-0.6672254249,0.0162116966  
C,0,0.7574592544,0.7318047787,0.0124375861  
C,0,-0.4375085495,1.4338632598,-0.0883828131  
C,0,-1.6394225378,0.7328612072,-0.2040691337  
H,0,-0.4596660965,-2.4688851284,-0.1044378861  
H,0,-0.4572898162,2.5217916121,-0.0891536667  
C,0,2.1750261088,1.1968368236,0.1923001759  
H,0,2.4526996358,2.0453462154,-0.4386093162  
H,0,2.3554067052,1.4981458731,1.2338128504

H,0,1.2698387246,-1.0695766361,-1.4370000972  
H,0,3.8514115707,0.1965262128,0.7297051097

**P**,  $n = 0$  ( $G_{298} = -515.318282$  a.u.)

C,0,-1.6349399474,-0.6688175209,-0.2098764781  
C,0,-0.4390676508,-1.3819034108,-0.0975332575  
C,0,0.751648802,-0.6672254249,0.0162116966  
C,0,0.7574592544,0.7318047787,0.0124375861  
C,0,-0.4375085495,1.4338632598,-0.0883828131  
C,0,-1.6394225378,0.7328612072,-0.2040691337  
H,0,-0.4596660965,-2.4688851284,-0.1044378861  
H,0,-0.4572898162,2.5217916121,-0.0891536667  
C,0,2.1750261088,1.1968368236,0.1923001759  
H,0,2.4526996358,2.0453462154,-0.4386093162  
H,0,2.3554067052,1.4981458731,1.2338128504  
C,0,2.9643722797,-0.0683608475,-0.1517086767  
H,0,3.1904504396,-0.0902100745,-1.2272829853  
N,0,2.050219733,-1.1735073686,0.2068258668  
H,0,2.2345297558,-2.0256775652,-0.309165283  
H,0,3.9072735021,-0.1518280422,0.392716679  
O,0,-2.8563292518,-1.292234785,-0.3384879592  
H,0,-2.7188329571,-2.2487590586,-0.3181112317  
O,0,-2.8687171798,1.3564637938,-0.3257011804  
H,0,-2.7300891694,2.3119779229,-0.2900600872

**R**,  $n = 2$  ( $G_{298} = -786.334590$  a.u.)

C,0,-1.2504454292,-2.3311761757,0.5006911842  
C,0,-0.68389823,-2.3352784793,-0.9302832726  
C,0,0.736339107,-2.1239834953,-1.0842855869  
C,0,-3.3383757051,-2.0463680241,1.3274218805  
C,0,-3.470312128,-2.7920627219,-0.0034559469  
H,0,-1.9004966251,0.3916038824,-2.2118805048  
H,0,-3.3699954393,0.644963779,2.5445373653  
H,0,-4.2548702258,-2.0860967804,1.9207378934  
H,0,-4.5048756008,-2.7490384426,-0.369295032  
H,0,-3.1768302511,-3.8414789034,0.0593026929  
H,0,-2.5372546412,-2.4835100787,1.9385906832  
N,0,-2.5750481724,-2.0529328146,-0.9146553222  
H,0,-2.7717327745,-2.1562782785,-1.902331116  
Au,0,0.21096142,0.0773648396,-0.5426195004  
Au,0,2.7069762432,-0.3301424412,-0.0592391348  
O,0,-2.6899402935,2.9320890362,1.5113863518  
H,0,-2.3768727951,3.6263463367,0.91381126  
O,0,-1.8432453708,2.8348049112,-1.0615724436  
H,0,-1.5202090391,2.6772240862,-1.9599647244

**R**,  $n = 4$  ( $G_{298} = -1057.397784$  a.u.)

C,0,1.7044758347,-2.3261820217,0.4200384251  
C,0,1.8247862813,-1.8245186678,-0.9217991564  
C,0,2.8098254857,-0.8462832507,-1.1676690082



C,0,2.9643722797,-0.0683608475,-0.1517086767  
 H,0,3.1904504396,-0.0902100745,-1.2272829853  
 N,0,2.050219733,-1.1735073686,0.2068258668  
 H,0,2.2345297558,-2.0256775652,-0.309165283  
 H,0,3.9072735021,-0.1518280422,0.392716679  
 O,0,-2.8563292518,-1.292234785,-0.3384879592  
 H,0,-2.7188329571,-2.2487590586,-0.3181112317  
 O,0,-2.8687171798,1.3564637938,-0.3257011804  
 H,0,-2.7300891694,2.3119779229,-0.2900600872

**R**,  $n = 2$  ( $G_{298} = -786.334590$  a.u.)

C,0,-1.2504454292,-2.3311761757,0.5006911842  
 C,0,-0.68389823,-2.3352784793,-0.9302832726  
 C,0,0.736339107,-2.1239834953,-1.0842855869  
 C,0,1.5590760634,-1.9326769328,-0.0095852929  
 C,0,1.0128645765,-1.9305391268,1.3383583206  
 C,0,-0.3121769271,-2.0653079626,1.587010388  
 H,0,1.1369569509,-2.1215253417,-2.0953120585  
 H,0,1.7035062246,-1.7987079982,2.1682611444  
 H,0,-0.706762574,-2.063190404,2.5989932962  
 O,0,-1.444475514,-2.5916207111,-1.878162964  
 O,0,-2.4190471035,-2.6974343042,0.6941930614  
 C,0,3.0356999799,-1.7227696282,-0.1832654599  
 H,0,3.5598062426,-2.5727444562,0.2731657962  
 H,0,3.2843347888,-1.7356000866,-1.2497613643  
 C,0,3.6046531053,-0.4675112404,0.4628800354  
 H,0,3.3486533228,-0.4210360573,1.5245798766  
 H,0,4.6971430018,-0.4980240815,0.3922481931  
 N,0,3.1031352739,0.7777296212,-0.1685134976  
 H,0,3.5448025855,1.5754896581,0.2811363858  
 H,0,3.3979614448,0.8014835453,-1.1426496657  
 Au,0,0.9195499902,0.93023557,-0.0818830574  
 Au,0,-1.6138218802,0.5054270872,0.063598538

**TS**,  $n = 2$  ( $G_{298} = -786.297466$  a.u.)

C,0,2.5928015725,1.9117871593,0.8187943892  
 C,0,2.6186661268,0.7660492449,1.6326419283  
 C,0,2.4060367066,-0.5187874498,1.1227989228  
 C,0,2.0877867756,-0.7338381597,-0.3118532273  
 C,0,2.0156657251,0.3661494085,-1.1637347778  
 C,0,2.3122434919,1.7140517173,-0.6723997373  
 H,0,2.7454715048,0.8975231634,2.7032338925  
 H,0,2.0139728932,0.2230731371,-2.2421964799  
 O,0,2.3884144374,2.6740496356,-1.4446973348  
 O,0,2.7342019039,3.0965634715,1.2241203398  
 C,0,2.3038916066,-2.1426365941,-0.8033179931  
 H,0,1.3636607978,-2.6969185458,-0.8759135606  
 H,0,2.7286035986,-2.105302146,-1.8099891509  
 C,0,3.2577976874,-2.8120624039,0.1865220713  
 H,0,2.7073548551,-3.340896368,0.9673726389

C,0,3.6809812659,-0.3745872218,-0.1819039743  
 C,0,3.639501669,-0.974920601,1.0835317146  
 C,0,2.6730151756,-1.9376084954,1.3659308273  
 H,0,2.8087770051,-0.3694962503,-2.1497507706  
 H,0,4.3191316015,-0.6389275826,1.8659203075  
 H,0,2.5825759539,-2.3418449713,2.3737578335  
 O,0,0.9399272003,-2.1611273514,-1.8713712496  
 O,0,0.6317551195,-3.0469614317,0.7974306569  
 C,0,4.4944097815,0.8689566341,-0.3994405431  
 H,0,5.530592756,0.7347957119,-0.0651478074  
 H,0,4.5368151644,1.1195080455,-1.4670560322  
 C,0,3.9386144218,2.0598486147,0.3716368965  
 H,0,3.8830978217,1.8289489038,1.4396257153  
 H,0,4.6089575464,2.9201202428,0.2546910371  
 N,0,2.5802326948,2.4570916211,-0.0742958539  
 H,0,2.3555593148,3.3498995923,0.3568179272  
 H,0,2.6141916283,2.6393581878,-1.0759844871  
 Au,0,-0.7261163872,-1.1891497998,1.113962534  
 Au,0,-1.9965027496,1.0501387567,0.2953790344  
 Au,0,-0.6995579209,-0.5222438616,-1.5663735107  
 Au,0,0.7649063356,1.2024611964,0.2225974841

**TS**,  $n = 4$  ( $G_{298} = -1057.359049$  a.u.)

C,0,2.7366025359,2.7566985705,-0.3782713687  
 C,0,1.6020907255,2.3179017847,-1.1527575164  
 C,0,0.3005868911,2.3598818961,-0.5792029136  
 C,0,0.1075384875,2.6461773566,0.8563690938  
 C,0,1.17201112,2.8677636466,1.6617092614  
 C,0,2.527376836,2.8958106957,1.1415792509  
 C,0,-4.5314784214,-0.0356145363,-0.2601188316  
 C,0,-4.2547326002,0.4182801007,1.0850926213  
 C,0,-3.4715621494,1.5037185576,1.3359280535  
 H,0,-4.1714362394,0.2836364065,-2.3439979202  
 H,0,-4.681774957,-0.1364671146,1.9172022502  
 H,0,-3.2846391632,1.8443279537,2.3507211401  
 O,0,-2.7923653881,2.5114887685,-2.1380343166  
 O,0,-2.5554501271,3.5006728616,0.434095906  
 C,0,-5.4371276915,-1.2187407357,-0.4592630115  
 H,0,-6.457160896,-0.9222219475,-0.1808136744  
 H,0,-5.4695345101,-1.4779018634,-1.5233449524  
 C,0,-5.0939390439,-2.4516371949,0.3574327598  
 H,0,-5.0343685303,-2.2158244591,1.4232194938  
 H,0,-5.8873578321,-3.197753367,0.2361898008  
 N,0,-3.7917032555,-3.0299198776,-0.0437180263  
 H,0,-3.6020291778,-3.8517804493,0.523313808  
 H,0,-3.8532269765,-3.3553570696,-1.0060815101  
 Au,0,-0.749732353,0.7215245023,0.0741025825  
 Au,0,0.6314436734,3.0492348196,0.0048429552  
 Au,0,-2.0623844895,-1.596871184,0.0653600532  
 Au,0,0.65319078,-1.7108977389,0.0074863573

N,0,3.9939455894,-1.7278817789,0.8407626637  
 H,0,4.6749783011,-1.2771963365,0.2344180164  
 H,0,4.4270897456,-1.9891472538,1.7208117309  
 H,0,2.0142845403,-1.2736085128,1.8019974178  
 H,0,3.9225599365,-3.5299657081,-0.3000782429  
 Au,0,-0.1156001692,-0.0651370479,-0.4548158316  
 Au,0,-2.582648627,-0.2365526322,0.2060533247

**P**,  $n = 2$  ( $G_{298} = -786.344659$  a.u.)

C,0,-2.9607461008,-0.6644514241,0.8764882243  
 C,0,-2.5048276105,-0.7499709284,-0.4470107832  
 C,0,-2.0235812108,0.3951331849,-1.13018828  
 C,0,-2.1457814106,1.6463889384,-0.4601419369  
 C,0,-2.6026202909,1.7201692715,0.8563050861  
 C,0,-3.006642118,0.559852502,1.5238127476  
 H,0,1.7069619238,2.2763029519,-2.2341216223  
 H,0,1.0346022125,3.1215568646,2.7097435061  
 O,0,3.5086022758,3.1151417627,1.8595877518  
 O,0,3.8659016526,2.9859679356,-0.8433979961  
 C,0,-1.3170760354,2.8656068288,1.2439768364  
 H,0,-1.8019205373,1.9069467855,1.4879237108  
 H,0,-1.3706631351,3.4986046553,2.1325834244  
 C,0,-2.0014217985,3.4987397048,0.0265221012  
 H,0,-2.5300878824,2.7315236353,-0.5517300519  
 N,0,-0.9371668915,4.0364335093,-0.8316034261  
 H,0,-0.5150156025,4.8853631505,-0.4643451943  
 H,0,-1.2160845685,4.1731207972,-1.7978237764  
 H,0,-0.5034295767,1.8332881292,-1.088498598  
 H,0,-2.7281231987,4.2652238521,0.308055139  
 Au,0,-3.2925843947,-0.0134639446,-0.0032089488  
 Au,0,-0.888137123,-1.0119415754,0.0959000088  
 Au,0,1.6164051414,0.1275759846,-0.5103143298  
 Au,0,1.4451529423,-2.4039149779,0.1950026578

**P**,  $n = 4$  ( $G_{298} = -1057.407648$  a.u.)

C,0,0.9995117329,-2.7661572714,-0.4190746181  
 C,0,-0.3036363445,-2.9192005037,-0.925313028  
 C,0,-1.4208666963,-3.0423305265,-0.0588434437  
 C,0,-1.1485728049,-3.152038822,1.3330784915  
 C,0,0.152136342,-3.0237087016,1.8226650172  
 C,0,1.2259805932,-2.8295444295,0.9460465519  
 C,0,1.9388099069,-2.6428893441,-1.5846490258  
 C,0,0.974701314,-2.3336305494,-2.7302089389  
 H,0,-2.3944703371,-3.3537358666,-0.4294013047  
 H,0,2.2280122141,-2.7225256976,1.3560173269  
 H,0,2.4731249279,-3.5866961592,-1.7586748351  
 H,0,1.3023870384,-2.7135605037,-3.6992603441  
 H,0,0.8328785449,-1.2411511318,-2.8090558073  
 H,0,2.6909516113,-1.8533384068,-1.4616832637  
 N,0,-0.2855125096,-2.9754759822,-2.310201034

Au,0,2.071734595,0.8060350913,0.0323387278  
 Au,0,3.356319399,-1.5494357469,0.0643059835

**TS**,  $n = 6$  ( $G_{298} = -1328.441005$  a.u.)

C,0,0.8453120778,1.5112009926,2.6557037002  
 C,0,2.1696773236,1.941520922,2.4560928415  
 C,0,3.2272711238,1.0284415947,2.3743180245  
 C,0,2.9764944096,-0.4268372654,2.3744513737  
 C,0,1.7319171677,-0.9000818225,2.5980694502  
 C,0,0.6105893458,0.0027357476,2.7932234592  
 H,0,2.3794505295,3.0065872292,2.506336099  
 H,0,1.5157715958,-1.9662814725,2.5548964161  
 O,0,-0.5294960883,-0.4156593761,3.0361280365  
 O,0,-0.1476034574,2.2686597885,2.8352060799  
 C,0,4.1255860819,-1.2680774352,1.9112045212  
 H,0,4.665993564,-1.7200517192,2.7501279608  
 H,0,3.7313947664,-2.0939075808,1.3044548709  
 C,0,5.0362290827,-0.3639001514,1.0799334906  
 H,0,5.8320825617,0.0713551711,1.6889897602  
 N,0,4.1905259857,0.7381548346,0.6164666877  
 H,0,3.4999610567,0.4469384081,-0.0841354367  
 H,0,4.6967246517,1.5617241536,0.3068806898  
 H,0,4.1951635983,1.3416839713,2.7635448061  
 H,0,5.5056785813,-0.8987113814,0.2489652745  
 Au,0,-3.0032668891,-1.4053859321,0.5762581551  
 Au,0,-1.6937665192,0.8850522513,0.0308358793  
 Au,0,-0.2424371523,3.0426205807,-0.7178999851  
 Au,0,1.0362398859,0.6879942749,-0.7830398123  
 H,0,1.1502452456,-1.393512504,3.1697741858  
 H,0,1.8735410841,0.7502316249,2.4701650339  
 H,0,1.980504405,1.0541593475,4.2181828356  
 H,0,0.5117412341,-0.7951230535,4.7042595049  
 N,0,0.2003448228,1.7706396017,3.294620911  
 H,0,0.4435096776,2.5298506203,2.6585227486  
 Au,0,1.2001154599,0.3554029406,0.0077958302  
 Au,0,1.4787062523,-2.3155011062,0.2930894533  
 Au,0,0.65448911,2.9992812504,-0.1128949764  
 Au,0,-1.2931575794,1.3355606692,-0.956226201  
 Au,0,-0.8801578592,-1.4623434628,-0.7162574886  
 Au,0,-3.18068077,-0.4395111346,-1.6650363229  
 O,0,-4.2784049516,1.0636445344,1.3376196035  
 H,0,-4.235476863,2.0088049874,1.136906963  
 O,0,-3.9007953632,-1.5963216017,1.6507984957  
 H,0,-4.5233687362,-1.1040539644,1.093858438

H,0,-1.1184543973,-2.6286707974,-2.7705005743  
Au,0,0.3910506115,1.0097722128,-0.8941274072  
Au,0,-2.1586064226,1.8408572257,-0.3449533007  
Au,0,2.9261392863,0.9917817518,-1.5056333002  
Au,0,-1.6696377213,-0.7286330033,-0.1540121141  
O,0,0.2879806903,-3.1030812054,3.1931491592  
H,0,1.2239096566,-3.0352193478,3.4237713253  
O,0,-2.1985188703,-3.3843340066,2.1713394744  
H,0,-1.8696076162,-3.3974414537,3.0834218338

**R**,  $n = 6$  ( $G_{298} = -1328.478114$  a.u.)

C,0,-2.9894511787,2.3450993925,0.2495526155  
C,0,-3.2035967157,1.832090466,-1.1730873102  
C,0,-3.9828497509,0.6273363644,-1.3290905554  
Au,0,-0.4408054861,-1.6777079192,-0.1905960979  
Au,0,2.1422912025,-1.7760638644,-0.9582722447

**P**,  $n = 6$  ( $G_{298} = -1328.496101$  a.u.)

C,0,-0.7473308164,-0.3289104568,3.0165699164  
C,0,-0.9166855152,1.0473864363,2.8340173146  
C,0,-2.0927826268,1.5642876443,2.293428432  
C,0,-3.0914072197,0.666823077,1.9127234651  
C,0,-2.9224135488,-0.7146159865,2.0735927805  
C,0,-1.7497664377,-1.2151393258,2.6396441134  
C,0,0.6001437326,-0.5645620015,3.6337274639  
C,0,1.2964859357,0.7818824412,3.4109344754  
H,0,-2.2322032135,2.6304622401,2.1304432054  
H,0,-1.6258494691,-2.2911652177,2.7369551587

### Dopaquinone cyclization;

**R** is reactant, **P** is product, **TS** is transition state structure,  $n$  is number of Au atoms included in the calculation.

**R**,  $n = 0$  ( $G_{298} = -703.856200$  a.u.)

C,0,-7.3346328857,-2.1414086349,-1.3837506135  
C,0,-6.3250905011,-1.4206131969,-2.1408257021  
C,0,-5.296439885,-0.8306802809,-1.4960987732  
C,0,-5.1304012929,-0.8781129815,-0.040645091  
C,0,-6.0339428047,-1.5269590222,0.7400082444  
C,0,-7.1738165857,-2.1949970826,0.157536658  
H,0,-6.4357157297,-1.3697193671,-3.2192086434  
H,0,-5.917792817,-1.5668241969,1.8196390482  
O,0,-8.0197276314,-2.8058244448,0.8139219727  
O,0,-8.300498885,-2.6985310816,-1.9001981444  
C,0,-3.9493762136,-0.1761865111,0.5413704144  
H,0,-3.9852807168,0.8805085541,0.2514472038  
H,0,-3.9900396148,-0.2240018865,1.6345895342

C,0,-0.3248545394,-0.5030193653,-0.6859705494  
C,0,-1.3598076547,-1.331559412,-0.451048196  
C,0,-2.6647672449,-0.792945954,-0.0857309338  
H,0,-1.8711445685,2.6068340688,-0.3491137921  
H,0,-1.2341181131,-2.4111114381,-0.4359770888  
O,0,-3.6142883506,-1.5354331705,0.1851587368  
O,0,-3.9957881067,1.1523885049,0.3037913623  
C,0,1.1078630581,-0.899616813,-0.7810791608  
H,0,1.2618903041,-1.9739463659,-0.6833147073  
H,0,1.5234667726,-0.5755961823,-1.7429182472  
C,0,1.7780089041,-0.1297273784,0.3843831948  
H,0,1.7713777677,-0.7637246163,1.2749684202  
N,0,0.97420431,1.0739688861,0.6485198916  
H,0,1.5004900101,1.9291245494,0.4761491303

C,0,-2.6174119806,-0.7705714612,0.0553384749  
 H,0,-2.5566980951,-0.65715679,-1.033949115  
 N,0,-2.5465285118,-2.1829398697,0.3795731654  
 H,0,-2.6050569678,-2.2811734322,1.3909856845  
 H,0,-1.6228653896,-2.5252887609,0.1315395813  
 H,0,-4.549578656,-0.280943831,-2.064882439  
 C,0,-1.4763317932,0.0486301573,0.6282624308  
 O,0,-0.6671285821,-0.362872364,1.4435024337  
 O,0,-1.4482540271,1.2967036821,0.1296028139  
 H,0,-0.7031724936,1.7742307826,0.5329244715

**TS**,  $n = 0$  ( $G_{298} = -703.832100$  a.u.)

C,0,-2.8406224553,0.7280833598,0.0236414638  
 C,0,-1.7335811887,1.5311334447,-0.2891283029  
 C,0,-0.5065168212,0.9649694598,-0.6612989563  
 C,0,-0.3248545394,-0.5030193653,-0.6859705494  
 C,0,-1.3598076547,-1.331559412,-0.451048196  
 C,0,-2.6647672449,-0.792945954,-0.0857309338  
 H,0,-1.8711445685,2.6068340688,-0.3491137921  
 H,0,-1.2341181131,-2.4111114381,-0.4359770888  
 O,0,-3.6142883506,-1.5354331705,0.1851587368  
 O,0,-3.9957881067,1.1523885049,0.3037913623  
 C,0,1.1078630581,-0.899616813,-0.7810791608  
 H,0,1.2618903041,-1.9739463659,-0.6833147073  
 H,0,1.5234667726,-0.5755961823,-1.7429182472  
 C,0,1.7780089041,-0.1297273784,0.3843831948  
 H,0,1.7713777677,-0.7637246163,1.2749684202  
 N,0,0.97420431,1.0739688861,0.6485198916  
 H,0,1.5004900101,1.9291245494,0.4761491303  
 H,0,0.5881552421,1.0913543299,1.5874287463  
 H,0,0.1078818445,1.5134179356,-1.37361985  
 C,0,3.2092196079,0.2349270541,0.0866249385  
 O,0,3.635468488,1.3762545954,0.0513015077  
 O,0,3.9456666763,-0.8549912074,-0.1493626338  
 H,0,4.8585609677,-0.5830221953,-0.347487714

**P**,  $n = 0$  ( $G_{298} = -703.888561$  a.u.)

C,0,-2.4084119465,-0.649530504,0.0040045397  
 C,0,-1.2631794739,-1.2554027501,-0.5116690156  
 C,0,-0.1229385632,-0.4715383981,-0.6624609715  
 C,0,-0.1146324823,0.8805217785,-0.3097919119  
 C,0,-1.2631677961,1.4817093744,0.191804115  
 C,0,-2.4124470673,0.7084221028,0.3515195631  
 H,0,-1.2818361137,-2.3091206133,-0.7725764405  
 H,0,-1.2806557695,2.5322263338,0.472419527  
 O,0,-3.6050446291,1.1898946556,0.8582842379  
 O,0,-3.5400860932,-1.4129559214,0.1758742858  
 C,0,1.2405918669,1.4449537223,-0.6230734012  
 H,0,1.2342896456,2.002919998,-1.5672183461  
 H,0,1.6429477829,2.1118698849,0.1431529299

H,0,0.5881552421,1.0913543299,1.5874287463  
 H,0,0.1078818445,1.5134179356,-1.37361985  
 C,0,3.2092196079,0.2349270541,0.0866249385  
 O,0,3.635468488,1.3762545954,0.0513015077  
 O,0,3.9456666763,-0.8549912074,-0.1493626338  
 H,0,4.8585609677,-0.5830221953,-0.347487714

**P**,  $n = 0$  ( $G_{298} = -703.888561$  a.u.)

C,0,-2.4084119465,-0.649530504,0.0040045397  
 C,0,-1.2631794739,-1.2554027501,-0.5116690156  
 C,0,-0.1229385632,-0.4715383981,-0.6624609715  
 C,0,-0.1146324823,0.8805217785,-0.3097919119  
 C,0,-1.2631677961,1.4817093744,0.191804115  
 C,0,-2.4124470673,0.7084221028,0.3515195631  
 H,0,-1.2818361137,-2.3091206133,-0.7725764405  
 H,0,-1.2806557695,2.5322263338,0.472419527  
 H,0,-2.2000784938,-1.3705496186,2.6747759132  
 O,0,-0.8096716138,-3.4073630442,1.7859118838  
 O,0,-0.4986920782,-3.5643709925,-0.9242950895  
 C,0,-3.2733088909,0.7442840883,1.2008688504  
 H,0,-3.5948185706,0.6856838646,2.2403293913  
 H,0,-2.8928600946,1.7533321822,1.0049747964  
 C,0,-4.4407626784,0.409917756,0.23704512  
 H,0,-5.0770643551,-0.3398707753,0.7153909831  
 N,0,-3.8720498379,-0.1631757383,-0.9900565706  
 H,0,-4.0079647009,0.4445424175,-1.7955244174  
 H,0,-4.2332261727,-1.0892326026,-1.1958646045  
 H,0,-1.7906096061,0.7677340103,-1.0176075258  
 C,0,-5.2969899809,1.6113918208,-0.0675764228  
 O,0,-5.4907503991,2.0529860605,-1.1872569051  
 O,0,-5.806361972,2.1398406702,1.0494432418  
 H,0,-6.3460885448,2.913686577,0.8124919589  
 Au,0,0.8409590037,-0.3248118218,-0.4265097656  
 Au,0,3.1025609385,0.7022966454,0.2430044448

**P**,  $n = 2$  ( $G_{298} = -974.911870$  a.u.)

C,0,1.9176729531,0.4964569807,-0.5933370841  
 C,0,2.3281931217,0.6361409378,0.7532599962  
 C,0,2.1322833738,1.8214124246,1.4553944112  
 C,0,1.554436841,2.8932870569,0.7767497899  
 C,0,1.1778089625,2.7957904285,-0.5768030361  
 C,0,1.3665061768,1.6069135705,-1.2712020801  
 C,0,2.5396869533,-0.7640063243,-1.1342933544  
 C,0,2.7997873315,-1.5463615937,0.1696514153  
 H,0,2.4369566637,1.9334841102,2.4915398381  
 H,0,1.1075391326,1.5496317451,-2.3238359583  
 H,0,3.4884524476,-0.5280363381,-1.6360842096  
 H,0,1.907161531,-2.1403651405,0.4174385454  
 H,0,1.920052912,-1.3296287115,-1.831283532  
 N,0,3.0387458149,-0.4957987408,1.1698746914

C,0,2.0820758207,0.1603117558,-0.7862723909  
 H,0,2.8760239976,0.2946976397,-1.5266507434  
 N,0,1.1168225173,-0.8544583394,-1.2176488048  
 H,0,1.4004430346,-1.7925530241,-0.9542218487  
 C,0,2.755024284,-0.2280385961,0.5139155597  
 O,0,2.4968815677,-1.2250055694,1.1685622512  
 O,0,3.7040314115,0.6569258581,0.8621979502  
 H,0,4.1095410625,0.365646546,1.6967594196  
 H,0,-3.5051076015,2.1257701698,1.0763478947  
 H,0,-4.2349452251,-0.8445527039,0.5401206108

**R**,  $n = 2$  ( $G_{298} = -974.897049$  a.u.)

C,0,-1.587706631,2.0123342369,-0.5015389116  
 C,0,-1.0315031067,2.0772514796,0.9319710442  
 C,0,0.4063059213,2.082104569,1.0897564147  
 C,0,1.2482551359,2.0537917995,0.0146857369  
 C,0,0.7133781584,2.0006133839,-1.33571283  
 C,0,-0.6157463213,1.922242672,-1.587372305  
 H,0,0.8001699271,2.1186498771,2.1024853308  
 H,0,1.416718058,2.0052390087,-2.1654616541  
 H,0,-1.0023953289,1.8828821207,-2.6015709054  
 O,0,-1.8206808152,2.2021902185,1.8817542251  
 O,0,-2.7981435939,2.1972750767,-0.6955233525  
 C,0,2.7381406254,2.0835383564,0.1970200544  
 H,0,3.1219653477,3.0077197599,-0.2504320898  
 H,0,2.9841967589,2.1140101147,1.2637221402  
 C,0,3.4931143737,0.9170238871,-0.4595777975  
 H,0,3.2060275409,0.8419014385,-1.514408352  
 N,0,3.1846111269,-0.3750895203,0.181181303  
 H,0,3.749911823,-1.1014712011,-0.2530778522  
 H,0,3.4776032177,-0.3397135594,1.1567050328  
 C,0,4.9866517896,1.1732206024,-0.4265494194  
 O,0,5.7863750567,0.4886058113,0.1879928081  
 O,0,5.3245121021,2.2376256799,-1.164289751  
 H,0,6.2879615636,2.3608294158,-1.1122801321  
 Au,0,1.0405998384,-0.8681679195,0.0743980219  
 Au,0,-1.5227720582,-0.8400184582,-0.0937415195

**TS**,  $n = 2$  ( $G_{298} = -974.861231$  a.u.)

C,0,-0.9015425906,-2.4979318806,-0.4304497262  
 C,0,-1.0980714202,-1.2689069192,-1.1595333439  
 C,0,-1.8474686034,-0.2180790967,-0.5676889974  
 C,0,-2.2481818682,-0.277335928,0.8510857786  
 C,0,-1.881040591,-1.3109238576,1.6376068289  
 C,0,-1.1508164417,-2.4476741274,1.0917240886  
 H,0,-0.9692074373,-1.28832469,-2.2388839109  
 C,0,-1.0907427092,3.2387554626,0.5751617807  
 C,0,-0.6627408436,3.210641647,-0.8782503869  
 C,0,0.5533030037,2.4922382124,-1.1999749046  
 C,0,1.5095668051,2.1244020814,-0.1689996832

H,0,4.981758054,-1.1716738813,0.9309695602  
 C,0,3.9740344066,-2.4794178643,0.0210537678  
 O,0,3.90208375,-3.5539438697,-0.5516894639  
 O,0,5.1417835991,-2.0434106086,0.5131151935  
 H,0,2.8589740567,-0.7842889441,2.1262147001  
 Au,0,-2.6323330283,-1.2350930431,0.3392356799  
 Au,0,-0.3221289828,-0.2012752929,-0.1031232805  
 O,0,1.3076325193,4.1027134056,1.3601177815  
 H,0,1.5968002021,4.0894044657,2.2831975325  
 O,0,0.604026936,3.8659292473,-1.2202588008  
 H,0,0.5491560918,4.6054828498,-0.5970238734

**R**,  $n = 4$  ( $G_{298} = -1245.961587$  a.u.)

Au,0,-0.8848895992,-0.8724259292,0.0407773725  
 Au,0,1.7046368002,0.1439886634,-0.4923842619  
 Au,0,1.383551842,-2.3688251565,0.2130713626  
 C,0,-2.8221148489,4.718146251,0.3238297107  
 O,0,-2.7117933585,5.8834179172,-0.0164801209  
 O,0,-3.8300052242,4.2417818628,1.0671888551  
 H,0,-4.4332428628,4.9730630137,1.2844727112

**P**,  $n = 4$  ( $G_{298} = -1245.968331$  a.u.)

C,0,2.8289882872,1.1694260795,1.0130302794  
 C,0,3.4397771303,1.5147738862,-0.1916620457  
 C,0,4.7461926291,1.1397485065,-0.48440474  
 C,0,5.4413537718,0.4014259475,0.4722354913  
 C,0,4.8422143887,0.060136003,1.6937849825  
 C,0,3.5309784015,0.4437271711,1.9692395881  
 C,0,1.4231887351,1.6858718384,1.027903409  
 C,0,1.2199444221,2.1074279278,-0.450889468  
 H,0,5.2266868962,1.3951582431,-1.4236651286  
 H,0,3.0736584508,0.1548015983,2.912449632  
 H,0,1.3070249133,2.5408565539,1.7071678851  
 H,0,0.6580874475,1.3174596809,-0.9776306635  
 H,0,0.6752804755,0.9351533334,1.3146571976  
 N,0,2.5717187756,2.2856169458,-1.0044849421  
 H,0,2.0398686534,4.2038552382,-0.9361289492  
 C,0,0.4234089621,3.3775461551,-0.5438206921  
 O,0,-0.7951750158,3.4420093929,-0.3559184114  
 O,0,1.1017773881,4.483178144,-0.8062478581  
 H,0,2.6175072644,2.0331054377,-1.9867049301  
 Au,0,-0.6298269446,-1.0154462187,-0.1904387892  
 Au,0,1.7890881062,-1.8903353433,-0.6287309627  
 Au,0,-3.275453118,-0.749408745,0.4386701893  
 Au,0,-1.9417720688,1.4500604994,0.0083905351  
 O,0,5.629961864,-0.6698320546,2.5595711673  
 H,0,5.1311352177,-0.8558573904,3.3659708805  
 O,0,6.7302895483,0.0119916859,0.1969664448  
 H,0,7.0644248783,-0.4895469771,0.9554539687

C,0,1.1497328602,2.2483956495,1.146332037  
 C,0,-0.1913909136,2.6453698433,1.5379004927  
 H,0,0.9427948626,2.662151233,-2.2061881568  
 H,0,1.8360966051,1.9755909801,1.9438314323  
 H,0,-0.3548708528,2.9410125081,2.5743422547  
 O,0,-1.3258059969,3.8796849593,-1.7224615231  
 O,0,-2.1455424735,3.8601941569,0.8911187539  
 C,0,2.7892427344,1.4750506935,-0.6342006554  
 H,0,2.5199652542,0.7795924095,-1.4407253603  
 H,0,3.4686536616,2.2035382899,-1.098581757  
 C,0,3.5739073513,0.7196296171,0.4511202461  
 H,0,2.8829198008,0.444611117,1.2608916418  
 N,0,4.7350771869,1.4724629815,0.9163256281  
 H,0,5.7092361012,0.1578338175,-0.0548197574  
 H,0,4.5708851005,2.4674437298,0.8097936649  
 C,0,4.0374064206,-0.6091537427,-0.0954580016  
 O,0,5.3297109032,-0.7137700149,-0.3486342091  
 O,0,3.282331938,-1.5639197467,-0.3098374179  
 H,0,4.8936916769,1.3020961139,1.9042171999  
 Au,0,0.9737329061,-1.3754740032,0.1081717536  
 Au,0,-0.5372006972,0.5027284844,-1.4152840393  
 Au,0,-1.6699542809,-1.7281657229,-0.0218323727  
 Au,0,-0.9251728242,0.5011154227,1.4005630595

**TS**,  $n = 4$  ( $G_{298} = -1245.922769$  a.u.)

C,0,2.8391004511,2.7521817358,-0.3615164468  
 C,0,1.7060826343,2.3323760228,-1.1468621794  
 C,0,0.3976061987,2.4031902992,-0.5869457023  
 C,0,0.1997593636,2.6928852698,0.8489763823  
 C,0,1.2584262533,2.881677511,1.6670559538  
 C,0,2.6209617778,2.8671087701,1.1587416959  
 H,0,1.8187261849,2.2875606635,-2.2272117601  
 H,0,1.1182222807,3.1326924266,2.7151845164  
 O,0,3.6006160869,3.0307682913,1.8919405091  
 O,0,3.9762093292,2.9721920147,-0.8131012469  
 C,0,-1.2203669122,2.9543349766,1.2155407522  
 H,0,-1.7544711832,2.0148736296,1.4273298434  
 H,0,-1.2783693746,3.5844764521,2.1059781157  
 C,0,-1.8520050219,3.6238764879,-0.0279087657  
 H,0,-2.4092067161,2.8549892868,-0.5863022216  
 N,0,-0.7568485314,4.0804538512,-0.8831996462  
 H,0,-0.3158787386,4.9321403999,-0.5402942484  
 H,0,-1.0263723756,4.1995463534,-1.8553941953  
 H,0,-0.4032917008,1.864969309,-1.0908409172  
 Au,0,-3.2303922347,0.2566563265,-0.1479773984  
 C,0,-1.6225274091,1.7102315835,3.0566606343  
 H,0,-1.6199065869,2.8042882571,3.0387275485  
 H,0,-1.7974467092,1.3831377032,4.0875982605  
 C,0,-0.2417521975,1.2042483202,2.6125920278  
 H,0,-0.1295815383,1.424351644,1.5356633

**R**,  $n = 6$  ( $G_{298} = -1517.039322$  a.u.)

C,0,-4.5892553409,0.2474342489,0.1918397489  
 C,0,-4.2507355804,-0.5770524401,1.4533709733  
 C,0,-3.2527967429,-0.042444765,2.3583347718  
 C,0,-2.6824762588,1.1772702878,2.1486330643  
 C,0,-3.0384665727,1.9598711381,0.9715875192  
 C,0,-3.9245017077,1.5251065289,0.0361447098  
 H,0,-3.0099319043,-0.6302673549,3.2406437141  
 H,0,-2.5716898556,2.9373713647,0.8625347488  
 H,0,-4.1795902112,2.129543947,-0.829235473  
 O,0,-4.8868644637,-1.6155076186,1.6775603408  
 O,0,-5.449076445,-0.1760264382,-0.5912456163  
 H,0,6.3608592031,1.1006487757,2.0466983122

**P**,  $n = 6$  ( $G_{298} = -1517.063620$  a.u.)

C,0,1.0617570462,-1.7049870777,2.3089737352  
 C,0,0.9297995282,-0.332699748,2.5097237773  
 C,0,2.0359920637,0.5124491047,2.5502120134  
 C,0,3.2970339699,-0.0504790184,2.366964614  
 C,0,3.4428039822,-1.4323198543,2.1689856185  
 C,0,2.3255804632,-2.2647802099,2.1392565919  
 C,0,-0.2912167291,-2.3463022801,2.2460107069  
 C,0,-1.2447453616,-1.1616920398,2.5312369465  
 H,0,1.9375406826,1.5836783014,2.7003316859  
 H,0,2.457578158,-3.3306226949,1.9682505452  
 H,0,-0.4245427315,-3.1531816816,2.9742929498  
 H,0,-1.9646858063,-1.043895253,1.7056337811  
 H,0,-0.4916712504,-2.7736337722,1.2521094886  
 N,0,-0.4247965164,0.0631066237,2.660665105  
 H,0,-1.2916426156,0.210263638,4.3479238305  
 C,0,-2.0670241823,-1.3791008392,3.7816222818  
 O,0,-2.8039604449,-2.3414673386,3.9436110612  
 O,0,-1.952368562,-0.4295997158,4.7156859119  
 H,0,-0.6881638607,0.7627556867,1.9577090499  
 Au,0,-1.9509211522,0.5474758161,-0.452197465  
 Au,0,-1.210220914,2.9859963908,0.4160057234  
 Au,0,-2.4376837661,-2.0316722441,-1.062680136  
 Au,0,0.1454803445,-1.2791401342,-1.1146008451  
 Au,0,0.7982653955,1.3962541171,-0.4171495429  
 Au,0,2.6797445311,-0.3752277259,-1.1697322029  
 O,0,4.7379957644,-1.8765498478,2.0045676344  
 H,0,4.7351726742,-2.8374604529,1.8987189605  
 O,0,4.3988456983,0.7712007092,2.3790486701  
 H,0,5.187181221,0.2240171608,2.246499179

N,0,-0.016534836,-0.2252462887,2.7836157928  
H,0,1.7404040519,0.3350590653,3.2293702374  
H,0,-0.5566509296,-0.5739848931,3.5716315034  
C,0,0.8965623413,1.9889622694,3.2339146446  
O,0,1.9992215991,1.264591353,3.4597984866  
O,0,0.8741834142,3.1914527993,3.4515138924  
H,0,-0.336709181,-0.7220827258,1.9521942419  
Au,0,0.5315584297,-1.6359426107,-0.3101955069  
Au,0,-2.182504554,-1.7130970324,-0.4838386223  
Au,0,3.1223396499,-1.313900806,0.3908665539  
Au,0,1.7709699585,0.9082397145,-0.2824015624  
Au,0,-1.0301221658,0.709373029,-0.8119004598  
Au,0,0.257264446,3.0649759597,-0.8710495943

**TS**,  $n = 6$  ( $G_{298} = -1517.004446$  a.u.)

C,0,-0.3201059375,-3.1089691975,2.1661739492  
C,0,0.8709635999,-3.2911008715,1.4466621418  
C,0,1.7508128733,-2.2212082146,1.2177498455  
C,0,1.5300250629,-0.9059493534,1.8629696234  
C,0,0.3796345256,-0.6570749809,2.5224267775  
C,0,-0.6138516044,-1.7039288453,2.7043606851  
H,0,1.0184339087,-4.2274432309,0.9154822364  
H,0,0.2038761646,0.2962724691,3.0168239555  
O,0,-1.6545273588,-1.5038145435,3.3458850353  
O,0,-1.2152396878,-3.9864983401,2.3272187789  
C,0,2.7259707865,-0.0058947288,1.8629825135  
H,0,2.6275755527,0.8030935802,1.1260952356  
H,0,2.837977683,0.4628240266,2.8460845646  
C,0,3.9271981341,-0.9031666631,1.5311130926  
H,0,4.0435854364,-0.9467833464,0.4376763823  
N,0,3.5624551776,-2.2443979397,1.9819748053  
H,0,3.5597164734,-2.3303693288,2.9972369164  
H,0,4.1306962851,-2.9816994127,1.5743077076  
H,0,2.2245849828,-2.1708240211,0.2340911386  
Au,0,-1.0446105509,3.1345351038,0.7387675241  
Au,0,-1.8765021536,0.609909498,0.3033535113  
Au,0,-2.5198182795,-1.9518065751,-0.2293595098  
Au,0,-0.1500963171,-1.1196025829,-1.2097780472  
Au,0,0.6743477556,1.5445944055,-0.5770044961  
Au,0,2.3242512977,-0.2044294686,-1.7791611414  
C,0,5.2232394007,-0.409501642,2.1131948518  
O,0,5.9100103975,-1.0280280933,2.9074110214  
O,0,5.5244641884,0.8088735212,1.6449985888

## § 9. CURRICULUM VITAE

Nikolina Kalčec was born on 5 February 1995 in Zagreb. After finishing high school in 2013, she continued her education at the Faculty of Chemical Engineering and Technology, University of Zagreb. She obtained her Bachelor's degree in Applied Chemistry in 2016, and graduated cum laude in 2018 and obtained the title of Master in Applied Chemistry. Since December 2019, Nikolina has been employed in the Analytical Toxicology and Mineral Metabolism Unit at the Institute for Medical Research and Occupational Health as a doctoral assistant on the Croatian Science Foundation project, "Safe-by-Design Approach for Development of Nano-Enabled-Delivery Systems to Target the Brain – SENDER", led by Prof. Ivana Vinković Vrček and Prof. Frances Separovic. That same year, she enrolled in doctoral studies in chemistry at the Department of Chemistry, Faculty of Science, Zagreb.

Nikolina has participated in 3 domestic and 6 international conferences delivering poster or oral presentations. She was involved in organizing the conference, "Nano2Clinic – Synergies for Clinical Translation of Nanotechnology in Cancer Therapies", supported by Cost Action CA17140 – Cancer nanomedicine – from the bench to the bedside, and the symposium "Synergy at the chemistry-nanotechnology interface 2022" supported by the Croatian Chemical Society. Nikolina was awarded a Short Term Scientific Mission (STSM) scholarship (COST action 17140), part of which she undertook at the Faculty of Medicine, University of Graz, Austria, in March 2020. In order to achieve the best possible collaboration with members of the project team, Nikolina spent 2 months at the Bio21 Institute, University of Melbourne, Australia. Additionally, she is the recipient of the City of Zagreb Scholarship for Excellence for the academic year 2017/2018. Nikolina is a member of the Croatian Chemical Society.



**List of publications:**

1. S. Inkret, M. Ćurlin, K. Smokrović, **N. Kalčec**, N. Peranić, N. Maltar-Strmečki, D. Domazet Jurašin, and M. Dutour Sikirić, *Materials (Basel)*. **16** (2023) 1764.
2. K. Ilić, **N. Kalčec**, L. Krce, I. Aviani, P. Turčić, I. Pavičić, and I. Vinković Vrček, *Chem. Biol. Interact.* **368** (2022) 110225.
3. E. Galić, K. Radić, N. Golub, D. Vitali Čepo, **N. Kalčec**, E. Vrček, and T. Vinković, *Int. J. Mol. Sci.* **23** (2022) 9128.
4. **N. Kalčec**, A. Ljulj, L. Božičević, V. Vrček, D. Marson, S. Pricl, F. Separovic, and I. Vinković Vrček, *Inorg. Chem.* **61** (2022) 10781–10791.
5. Ž. Debeljak, I. Vinković Vrček, N. Drinković, V. Micek, E. Galić, D. Gorup, M. Ćurlin, D. Mandić, A. Bandjak, B. Pem, **N. Kalčec**, K. Ilić, I. Pavicic, N. Gunday-Tureli, and E. Tureli. *Analyst* **147** (2022) 3201–3208.
6. K. Ilić, L. Krce, J. Rodriguez-Ramos, F. Rico, **N. Kalčec**, I. Aviani, P. Turčić, I. Pavičić, and I. Vinković Vrček, *J. Trace Elem. Med. Biol.* **73** (2022) 127004.
7. **N. Kalčec**, N. Peranić, R. Barbir, C.R. Hall, T.A. Smith, M.A. Sani, R. Frkanec, F. Separovic, and I. Vinković Vrček, *Spectrochim. Acta Part A Mol. Biomol. Spectrosc.* **268** (2022) 120707.
8. N. Novosel, **N. Kalčec**, I.D. Marion, I.Š. Rakić, Đ. Drobac, Ž. Marohnić, and M. Prester, *J. Magn. Magn. Mater.* **543** (2022) 168607.
9. R. Barbir, B. Pem, **N. Kalčec**, S. Kastner, K. Podlesnaia, A. Csáki, W. Fritzsche, and I. Vinković Vrček, *Langmuir* **37** (2021) 1991–2000.

**Conference contributions:**

1. **N. Kalčec**, A. Ljulj, L. Božičević, V. Vrček, D. Marson, S. Pricl, F. Separovic, R. Prassl, I. Vinković Vrček, *Transformations of L-DOPA during the synthesis of gold-based nanodelivery systems for LAT-1 targeting*, 2<sup>nd</sup> CA17140 STSM Virtual Conference, 23 February 2023 (**oral presentation**)
2. **N. Kalčec**, A. Ljulj, L. Božičević, B. Pem, V. Vrček, F. Separovic, I. Vinković Vrček, *Combined NMR and computational study of L-DOPA and dopamine oxidation upon*

- interaction with gold nanosurface*, Magnetic moments in Central Europe 2022, 1-4 June 2022, Primošten, Croatia (**poster presentation**)
3. K. Ilić, N. Drinković, Ž. Debeljak, V. Micek, **N. Kalčec**, I. Pavičić, E. Türeli, N. Günday Türeli, I. Vinković Vrček, *Design of novel nanoformulation to decrease cardiotoxicity of doxorubicin*, Final CA17140 COST Conference Cancer Nanomedicine – from the Bench to the Bedside, 2022, Rome, Italy (oral presentation)
  4. N. Peranić, **N. Kalčec**, K. Ilić, I. Vinković Vrček, *Blood brain barrier permeability of selenium nanoparticles*, 2022, Limasol, Cyprus (poster presentation)
  5. I. Mamić, M. Beus, N. Peranić, **N. Kalčec**, P. Turčić, I. Vinković Vrček, *Cellular model of Parkinson's disease for safety testing of gold-based nanodelivery system*, SynChemNano2022, 28 May 2022, Zagreb, Croatia (oral presentation)
  6. **N. Kalčec**, R. Frkanec, M. Šišić, T. Kurtović, I. Brizić, M. Ćurlin, L. Frkanec, L. Horvat, I. Vinković Vrček, *Different conjugation strategies of gold nanoparticles with anti-SARS-CoV-2 antibodies for ultrasensitive detection of coronavirus*, SynChemNano2022, 28 May 2022, Zagreb, Croatia (**oral presentation**)
  7. N. Peranić, **N. Kalčec**, K. Ilić, I. Vinković Vrček, *Biocompatibility assessment of selenium nanoparticles as potential drug delivery system*, SynChemNano2022, 28 May 2022, Zagreb, Croatia (oral presentation)
  8. T. Vinković, L. Galić, Z. Lončarić, B. Ravnjak, E. Galić, I. Vinković Vrček, **N. Kalčec**, *Biofortifikacija štira različitim kemijskim oblicima selena*, 56. hrvatski i 16. međunarodni simpozij agronoma, 2021, Osijek, Croatia (oral presentation)
  9. **N. Kalčec**, V. Vrček, B. Pem, L. Božičević, I. Vinković Vrček, *NMR study of interaction of l-dopa and dopamine with gold nanoparticles*, 27th Croatian Meeting of Chemists and Chemical Engineers, 5-8 October 2021, Veli Lošinj, Croatia (**poster presentation**)
  10. **N. Kalčec**, A. Ljulj, L. Božičević, B. Pem, V. Vrček, I. Vinković Vrček, *Oxidation of L-DOPA and dopamine during gold clusters formation: NMR and computational study*, The 18th European Symposium on Organic Reactivity, October 2021, Amsterdam, The Netherlands (**poster presentation**)
  11. **N. Kalčec**, K. Ilić, N. Drinković, V. Micek, E. Türeli, N. Günday Türeli, I. Pavičić, I. Vinković Vrček, *In vivo investigation of inflammatory response of different*

*doxorubicin formulations*, NanoInnovation 2021, 19-23 September 2021, Rome, Italy  
(poster presentation)

12. B. Pem, L. Božičević, **N. Kalčec**, A. Ljulj, V. Vrčec, I. Vinković Vrčec,  
*Computational study on the binding of L-dopa, dopamine and oxidised derivatives to gold nanoparticles*, NanoInnovation 2021, 19-23 September 2021, Rome, Italy  
(poster presentation)
13. R. Barbir, N. Drinković, V. Micek, E. Türeli, N. Günday Türeli, **N. Kalčec**, K. Ilić, B. Pem, I. Pavičić, P. Turčić, I. Vinković Vrčec, *Nanoformulations reduce cardiotoxicity of doxorubicin – in vivo animal study*, NanoInnovation 2021, 19-23 September 2021, Rome, Italy (poster presentation)
14. K. Radić, D. Vitali Čepo, N. Golub, J. Štimac, **N. Kalčec**, E. Vrčec, T. Vinković,  
*Gastrointestinal stability of selenium nanoparticles*, UNGAP All-workgroups meeting "Current challenges and future perspectives in oral drug absorption research", 2021, Leuven, Belgium (poster presentation)
15. K. Ilić, L. Krce, J. Rodriguez-Ramos, F. Rico, **N. Kalčec**, I. Aviani, I. Pavičić, I. Vinković Vrčec, *Immunotoxicity of nanomixture: joint action of silver and plastic nanoparticles*, EuroNanoForum 2021, 5-6 May 2021, Braga, Portugal (poster presentation)
16. **N. Kalčec**, I. Mamić, N. Peranić, I. Vinković Vrčec, *Fluorescence spectroscopic study on the interaction of dopamine and L-dopa with different selenium nanoparticles*, EuroNanoForum 2021, 5-6 May 2021, Braga, Portugal (poster presentation)
17. **N. Kalčec**, R. Frkanec, I. Vinković Vrčec, *Fluorescence spectroscopic study of the interaction of differently coated gold nanoparticles with dopamine and l-dopa*, The Faculty of Science PhD Student Symposium- 5th edition, 24-25 April 2021, Zagreb, Croatia (poster presentation)
18. K. Ilić, L. Krce, J. Rodriguez-Ramos, F. Rico, **N. Kalčec**, I. Aviani, I. Pavičić, I. Vinković Vrčec, *Assessment of silver nanoparticle (AgNP) suitability for use in polystyrene-based medical devices*, NanoTox 2021 Virtual Conference, 20-22 April 2021, Edinburgh, UK (poster presentation)
19. **N. Kalčec**, R. Frkanec, I. Vinković Vrčec, *Impact of serum albumin on binding ability of dopamine and L-dopa on differently coated gold nanoparticles*, NanoTox 2021 Virtual Conference, 20-22 April 2021, Edinburgh, UK (poster presentation)

20. K. Radić, D. Vitali Čepo, N. Golub, **N. Kalčec**, E. Galić, I. Vinković Vrček, T. Vinković, Primjena ekstrakta komine masline u biogenoj sintezi nanoselena, 18<sup>th</sup> Ružička days "Danas znanost – sutra industrija", 2022, Vukovar, Croatia (poster presentation)
21. E. Galić, N. Golub, K. Radić, D. Vitali Čepo, **N. Kalčec**, I. Vinković Vrček, T. Vinković, Primjena pektina iz kore mandarine (*C. reticulata*) u biogenoj sintezi selenovih nanočestica, 18<sup>th</sup> Ružička days "Danas znanost – sutra industrija", 2022, Vukovar, Croatia (poster presentation)